Quantitative Spectroscopic Studies of Wolf-Rayet Stars in Local Group Galaxies

Jay Brian Abbott

Thesis submitted for the Degree of Doctor of Philosophy
of the University of London

Department of Physics & Astronomy
UNIVERSITY COLLEGE LONDON

November 2003

ProQuest LLC
789 East Eisenhower Parkway
P.O. Box 1346
Ann Arbor, MI 48106-1346

ABSTRACT

With recent advances in astronomical instrumentation, individual massive stars in Local Group galaxies are now easily accessible to ground-based telescopes. We present deep, high quality images for two late-type spiral galaxies; NGC 300 and M 83, located beyond the Local Group at distances in excess of a Mpc. Through the use of narrow-band interference filters, utilizing the strong Wolf-Rayet (WR) emission lines, we have identified a large number of previously unknown WR stars revealing a significant increase in the known WR population of these galaxies, resulting in new catalogues. We have also used a number of modern ground-based optical telescopes with efficient multi-object spectrographs to obtain observations for a representative sample of known extra-galactic WR stars in M 33, M 31 and IC 10, significantly improving on existing data. These galaxies are members of the Local Group and span a metallicity range of approximately a factor of 10, providing us with a variety of environments in which to study individual WR stars. Our large sample has allowed us to re-examine a number of spectral morphologies and to asses their potential multiplicity. We have also re-evaluated the metallicity gradients for three spiral galaxies in which we have observed WR stars, M 33, M 31 and NGC 300 – the results of which are considered in later analysis.

For our sample of identified single WR stars we perform detailed, tailored analyses using the non-LTE code, CMFGEN, which assumes a spherically expanding, extended atmosphere subject to line blanketing. Fundamental stellar parameters are derived for each star and subsequently collated, permitting us to investigate the role that metallicity plays on the derived stellar properties for both WN and WC subtypes. The WN stars examined display little difference in the observed properties between the Galactic and LMC samples. Comparison of the single WN stars in the SMC suggest they have significantly

reduced mass-loss rates and increased luminosities, implying that WN stars display an observational mass-loss – metallicity relationship comparable to O-type stars (i.e. $\dot{M} \propto Z^{0.5-0.8}$). Results for our sample of extra-galactic WC stars appear somewhat less clear, with a range of derived mass-loss rates and luminosities for stars located in a variety of environments. Our results imply that early-type WC stars are relatively uniform and that their wind structure is inherently the same, as indicated through their constant observed line fluxes, after correcting them for distance, and their narrow range of derived properties. Our results call into question whether their mass-loss rates are enhanced with increasing metallicity or whether other factors are important; such as carbon and oxygen significantly aiding line driving and further accelerating the star's atmosphere. Further analysis of more high quality spectroscopic observations are required, for both subtypes of WR stars, located in as many extreme environments as possible to confirm our conclusions.

To Kate

ACKNOWLEDGEMENTS

There are a number of people I am indebted to for their help during my Ph.D. Firstly, I would like to thank my supervisor, Paul Crowther, for his help and guidance over the last three years. I would also like to thank Linda Smith who unselfishly and possibly painfully, read my entire thesis providing me with useful feedback. Gratitude must also be extended to Allan Willis for his financial support towards the end of my Ph.D. as well as Mike Barlow and Raman Prinja for their helpful comments and advice. Credit must also go to John Hillier for the generous use of code, CMFGEN, for which proved invaluable to my work and to Georges Meynet for the use of his evolutionary tracks.

I feel I must thank past and present members of A5 – Richard Norris, Sam Thompson, Dugan Witherick and Sam Searle – for their help, support, patience and friendship. Thanks to Adam Burnley, Fab Sidoli (a.k.a. 'Fabian'), Jo Fabbri and Ki-Won Lee for "putting up with me" and laughing at my jokes whilst out having a pint or three and to everyone else at UCL that I haven't already mentioned. I would also like to thank the staff at the observatory for making me feel welcome whenever I chose to work out there with special thanks to the ladies for generously keeping me full on tea and toast.

Special mention must go to Kate, for tolerating me during my moments of madness and for her unconditional support throughout my Ph.D. as well as her kindly making my lunch (and dinner!). Finally, huge thanks to my parents for their constant love and support.

"To alcohol! the cause of, and solution to, all of life's problems."

- Homer Simpson

"Only two things are infinite, the universe and human stupidity, and I'm not sure about the former."

- Albert Einstein

- (1879 – 1955).

Contents

List of Figures

List of Tables

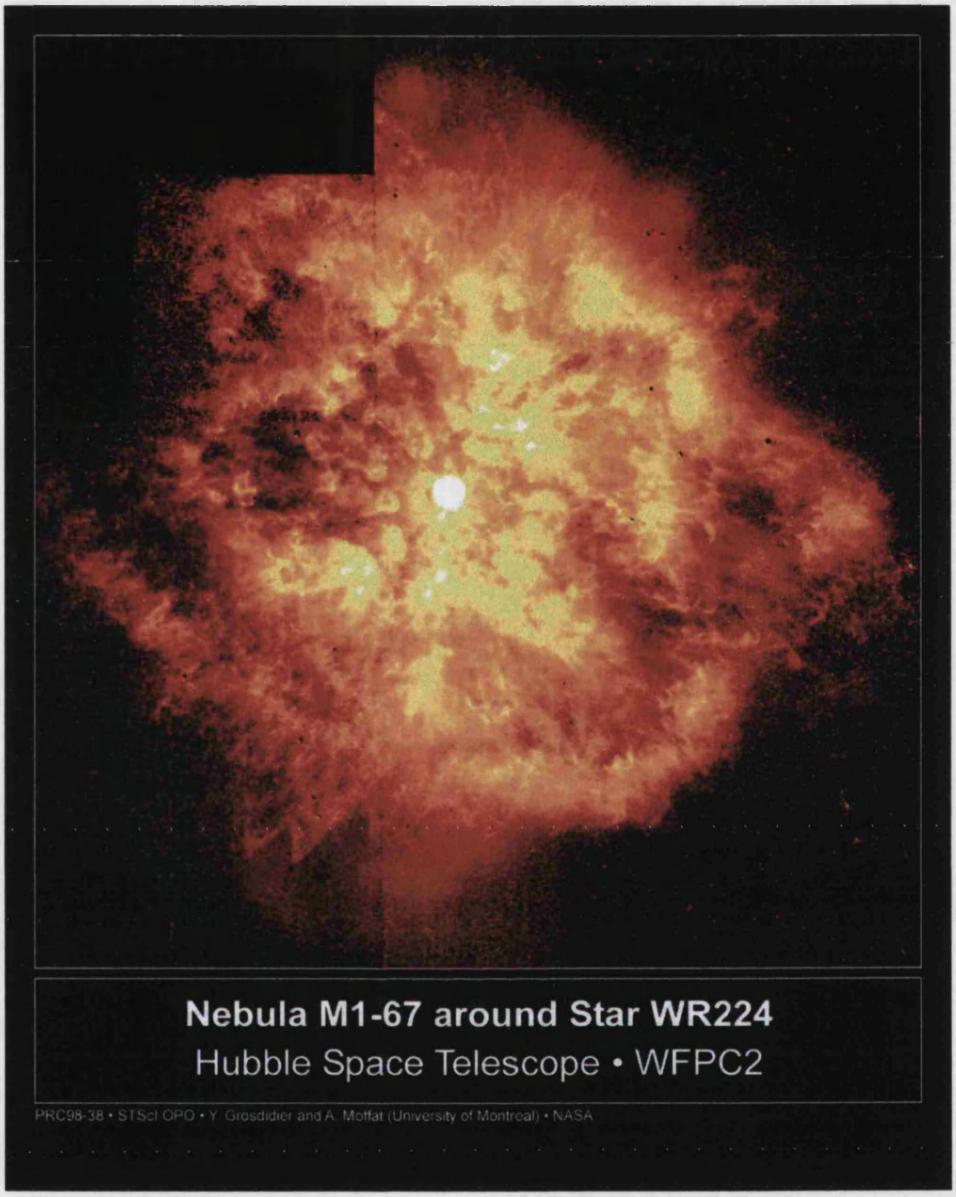

HST image of WR124 showing the dusty nebula known as M1-67 produced by its powerful stellar outflow. Credit: Y. Grosdidier (U. Montreal) et al., WFPC2, HST, NASA.

CHAPTER 1

Introduction

1.1 Massive Stars

Massive stars are one of the most instrumental factors in the evolution of the Universe. They provide an important source of chemical enrichment, kinetic energy and momentum into the surrounding interstellar medium (ISM) through their stellar winds. They provide feedback not just through their continuous stellar winds but also when they inevitably explode as supernova, suddenly enhancing the ISM's chemistry. They also shape their local environment as they are strong sources of ionizing radiation.

The exact lower mass boundary between a low-mass star (like the Sun) and a massive star is still debated and depends on which set of definitions are used. For this work we choose to delineate the boundary for a massive star if it's initial mass is greater than $8M_{\odot}$ (spectral types earlier than B3V). The reasons for this are, (i) for stars with initial masses above $8M_{\odot}$, there is no pre-main sequence phase as they are already burning hydrogen in their earliest stages of evolution (Palla & Stahler 1993); (ii) above this mass cut-off, stars emit Lyman continuum photons and (iii) this mass boundary provides a division between stars which end their lives as white dwarfs and those that will evolve to become Type II supernovae (Heger *et al.* 2003).

The number of massive stars within a cluster/association can be described from the Initial Mass Function (IMF), which characterizes the relative distribution of stars after their formation as a function of their initial mass. The IMF was was first estimated by Edwin E. Salpeter back in 1955, when he studied stars within the Solar Neighbourhood.

He parametrized stars in the range 0.4 – $10M_{\odot}$ by a power-law with an index, α = -2.35 (Salpeter 1955). The IMF can be measured by counting stars (as a function of their bolometric luminosity), and converting them into an IMF after considering the star formation history. This has been done for clusters and associations in both the Galaxy and the Magellanic Clouds and the IMF slope can still be essentially described by the Salpeter power-law, and so it is not believed to be affected by metallicity for massive stars (Massey 1998*b*). There is evidence that for low mass stars the IMF diverges from the Salpeter approximation and become much flatter. This distribution can then explain why we observe large numbers of low-mass stars and only a small number of massive stars in a given cluster/association; even though their numbers are small their impact, via their stellar wind, on the surrounding environment is substantial.

A stellar wind is a continuous, supersonic outflow of material from the surface of the star. This outflow of matter plays an important role on both the evolution of the star as well as the surrounding ISM. It is understood that these strong, stellar winds are driven through radiation pressure (see Chapter 3 for detailed discussion). The term *'stellar wind'* was originally coined by Parker (1960) in analogy with the solar wind, although observational evidence for stellar winds had long been identified. As the spectroscopic and photographic techniques improved at the end of 19th Century, a number of stars were soon identified to resemble 'novae' (i.e. they spectra contained emission lines), and the connection was soon made between stars with P–Cygni - type profiles and a bulk, outward expansion of material. It wasn't until the invent of space-borne observatories that real observational progress was made into stellar winds. Morton (1967), first reported to have obtained Far-Ultraviolet spectra of six stars in Orion, using an Aerobee rocket. This work identified significant evidence of mass-loss in massive, hot stars through P-Cygni profiles of C IV and Si IV. Much of our understanding today regarding stellar winds was made possible through the successful UV satellite, IUE, which launched in 1978 and continued for an amazing 18 years and 9 months.

We are able to observe the signatures of existing massive stars throughout the local universe, whilst they significantly contribute processed chemicals to the surrounding medium. We observe this feedback on many levels, from wind-blown bubbles (i.e. ring nebulae) around individual massive stars (Johnson & Hogg 1965), to superbubbles in nearby galaxies. These superbubbles occur when large star forming regions produce a number of supernova explosions which cause drastic changes in the kinematic and physical nature of

the interstellar medium producing large-scale outflows (Matsushita *et al.* 2000). Type II and Ib/Ic supernovae (SNe) are thought to be massive stars that follow a core collapse at the end of their lifetimes (Filippenko 1997). They provide yet another important source of chemical enrichment, contributing large quantities of iron-group elements into the ISM.

Massive stars and their trade mark signatures can be used as tracers of star formation, enabling astronomers to observe them in distant galaxies. Thankfully there are a number of tested observational tools available to detect massive star formation in galaxies without necessarily observing individual stars, and as a result allow star formation rates (SFR) to be estimated. Observational indicators include measuring Far-IR Luminosities; 21cm radio fluxes; optical Hα and He II λ4686 emission. All these observables indicate either current star formation and/or recent star formation where there is a population of evolved, massive stars. By understanding more about individual massive stars we are able to constrain the large number of parameters which are assumed in current population synthesis models.

1.1.1 OB Stars

Unlike low mass stars, massive stars spend little time on the main sequence and rapidly evolve. Although in terms of stellar lifetimes their existence is relatively brief, their impact and importance on the surrounding environment is huge.

Main Sequence (MS) massive stars can be categorized into two observational classes; O- and B-type stars. B stars (for this work we only discuss mid to early types) are formed within the mass range 8 – 18 $M_{\odot}$, they have high temperatures ($T_{eff} \simeq$ 20,000K), and weak stellar winds. Above this mass range stellar winds become much more significant. O stars are formed from the most massive stellar populations (initial mass > 18$M_{\odot}$) and are characterized by their strong UV radiation, even higher temperatures ($T_{eff} \simeq$ 30,000K), and highly ionized photospheric lines. Young O stars on the main sequence show little evidence for a stellar wind, except for a few extremely wind-sensitive lines such as He II λ4686 or Hα λ6563. For more compelling evidence UV data are required; here the most sensitive wind diagnostic is the resonance line of C IV at λ1550 (Walborn *et al.* 1985).

Modern spectral classifications for O stars were refined and catalogued by Walborn & Fitzpatrick (1990), who used a series of optical He I and He II absorption lines to define the spectral types O3-B0. This line ratio varied such that O3 stars were classified if He I was absent, due to its the ionizing radiation doubly ionizing all the helium. Since then due to a further understanding of massive stellar atmospheres and their evolution, Walborn *et al.*

(2002) re-classified the upper-end of the O star subtype to include O2–3.5. Their revised classification principally uses the N IV/N III emission-line ratio to discriminate between classes.

Spectroscopically B stars predominately display neutral hydrogen and helium absorption lines. Optically B stars are classified primarily using their photospheric absorption lines of Si II and Si III (Rountree & Sonneborn 1991), although there have been a number of studies (e.g. Smith Neubig & Bruhweiler 1997) utilizing UV wavelengths where there are a number of unsaturated, low-ionization (e.g. Si III, C II, Mg II) and high ionization (N V, Si IV, C IV) lines.

Main sequence B stars are widely used to measure present day chemical abundances in both Galactic clusters and field stars (e.g. Smartt *et al.* 1997), as their atmospheres are uncontaminated by products of nucleosynthesis. Observational results indicate that O star's hotter temperatures result in a higher energy radiation output and higher luminosities causing much higher mass-loss rates than B stars. These higher core temperatures and densities in O stars increase the rate of nuclear burning. It is also believed that their strong ionizing radiation is responsible for globally ionizing the ISM as their Lyman continuum fluxes are greater than the hydrogen recombination rate (Reynolds 1984). B stars can still be important in star forming regions, however, even though their UV fluxes are less than O stars, due to the shape of the IMF they are much more numerous. Observational studies still suggest they play a significant role in star forming regions, particularly at later stages when O stars have evolved (e.g. Garay *et al.* 2002; de Mello *et al.* 2000).

1.1.2 LBV Stars

S Doradus-type variables were first identified by Hubble & Sandage (1953) in M 31 and M 33, and as a result they were called as "Hubble-Sandage variables". This was later revised by Conti (1984) who renamed them more aptly as, "Luminous Blue Variables" (LBVs). These stars are in a brief ($\sim 10^5$yr) yet violent post-main sequence phase of evolution. They occupy the upper-right region of the Hertzsprung-Russell (HR) diagram which is void of normal, stable stars. This empirical luminosity limit, known as the Humprhreys-Davidson limit, was determined by studying the distribution of Galactic and LMC stars (Humphreys & Davidson 1979; Fitzpatrick & Garmany 1990). Beyond this boundary stars begin to exceed the Eddington limit and become unstable.

LBVs undergo both short-term micro-variations ($\sim$0.1 mag) in their quiescent state

(visual minimum), as well as the much longer (years), more irregular outbursts which are more violent (~1-2 mag). During these cycles their observed effective temperatures vary from, $T_{eff} \simeq$ 20,000-30,000K, when they cross the upper luminosity boundary, to $T_{eff} <$ 10,000K when their atmospheres are dense and extended. As a result of their ever changing, unstable nature there are no defining characteristics which enable us to spectroscopically classify LBVs. Their spectra do typically exhibit emission lines of H, He I Fe II and [Fe II], some of which are seen as P–Cygni profiles.

In evolutionary terms the LBV phase is very short, and as a result only 5 LBVs are known in the Galaxy, with a few tens known in other galaxies. P–Cygni and η Carinae are two of the most well studied LBVs in our Galaxy. Stahl *et al.* (1983) found that R127 (an Ofpe/WN star in the LMC) underwent an S Doradus-type eruption, suggesting a possible link between slash stars (see Section 1.1.3) and LBVs (maybe seen during their minimum phase). When they are observed at visual maximum their optically thick atmosphere changes their appearance such that they resemble an A supergiant or occasionally, an F-type hypergiant.

Theoretical work on the causes of the LBV phenomenon has been far more limited compared with the observational work to date. The exact cause of why LBVs undergo these instabilities is still not known, although it has been proposed that LBVs have a 'opacity-modified' Eddington limit (Humphreys & Davidson 1984) which could trigger the instabilities. Whatever the reason, it results in enhancing the outflow from the star, detaching the star's outer atmosphere. This extended atmosphere (or pseudo-photosphere) is in effect suspended through radiation pressure causing the observed oscillations. Even though the observed spectral appearance alters along with the luminosity and temperature, the bolometric luminosity essentially stays constant. The visual variations seen are due to the energy distribution shifting, which is driven by the instability (Humphreys & Davidson 1994). LBVs are important in the evolution of massive stars and are thought to be one of the progenitors of Wolf-Rayet stars (Maeder 1983).

1.1.3 Of/WN - Slash Stars

Walborn (1977) first reported a new class of hot, massive stars which displayed spectral characteristics of both emission line O stars, and late-type WN stars. This small subset of massive stars were soon given their own name, *'Slash Stars'*. Since Walborn's early work identifying this new breed of massive stars we have learnt more about this rather rare type

of transitional star. There are now two groups of slash stars, this division is based upon their spectral features but can be attributed to their stellar temperatures.

The first, hot group of slash stars, such as Melnick 42, are classified O3 If/WN (Walborn 1986). These stars have emission lines which are similar in strength to both O supergiants and late-type WN stars, although their spectra commonly display signatures of a hydrogen-rich envelope as well as intrinsic (weak) absorption lines (Crowther & Dessart 1998). In evolutionary terms this links them more closely to O supergiants than helium burning WN stars (see section 1.2.2 for further details).

The second, cooler set of slash stars were originally discussed by Walborn (1982), who coined the classification Ofpe/WN9 stars. More recently Smith, Crowther & Prinja (1994) and Crowther & Smith (1997) revised this class of slash stars to WN9–WN11, thus including these objects as an extension of the late-type WN phase, defined as having lower excitation. Their reasoning for this lay somewhat with the fact that unlike their O3 If/WN companions, photospheric absorption lines were absent from these stars.

1.2 Wolf-Rayet Stars

Wolf-Rayet (WR) stars are the highly evolved, (mostly) helium burning descendents of the most massive initial stellar populations. Their name is attributed to their co-discoverers, two French astronomers, C. J. E. Wolf and G. Rayet (1867). They made their discovery whilst observing stars in Cygnus. They observed the optical spectra from these objects by eye through a spectrometer and reported their peculiar findings. Compared with the spectra of most stars, the spectra of these 'strange' stars were dominated by strong, broad emission lines. Although many more WR stars were subsequently found visually, it was not until photographic efforts (e.g. Pickering 1890) that many more WR stars were identified. The source of these emitting atoms was unknown until Beals (1930) attributed them to highly ionized lines of helium, nitrogen and carbon. Since then we now know that the spectra of WR stars are a result of their strong, dense stellar winds, and that we are not actually seeing the surface (photosphere) of the 'hidden' central star. It is this rich, emission line spectrum that characterizes WR stars today and is useful in identifying them, even at large distances.

1.2.1 Classification Scheme

The spectra of WR stars can be divided into three distinct groups WN, WC, and WO, these classifications are based on their optical emission line spectrum, and discriminate whether we observed strong emission from nitrogen, carbon or oxygen. The spectra of WN-type stars are rich in helium and nitrogen emission lines and are (mostly) free of hydrogen. The spectra of WC stars typically contain broader emission lines compared with their WN counterparts, and are rich in carbon and helium. Nitrogen lines are absent from WC stars but instead we see an abundance of strong, dominant oxygen lines, this is because nitrogen is depleted very effectively during helium burning (see Section 1.2.5). The last, and somewhat rare group of WR stars are the WO subtype, these stars are not too dissimilar to WC stars, except that a range of highly ionized oxygen and carbon lines are prevalent. There is also another type of WR star which is rarely observed, and they are called WN/WC type. They are fundamentally transitional stars which are in some intermediate stage between WN and WC, so strangely we see strong nitrogen lines typical in a WN star but also strong carbon emission.

These three spectral classes are divided again into sub-classes, depending upon their emission line ratio from pre-defined lines of neighbouring ionizations, hence the classification is defined in some way by the star's ionization (caveats to this are discussed later in this work). The subclasses range from WN2–11 and WC4–9, with the lower numbers referring to the *'earlier'* stars in the sequence. Early work by Smith (1968) calculated a decisive relationship to help unify the classification of WN stars, principally using emission line ratios of He I/He II, this classification scheme was later extended to include lower excitation objects and hence *'later'* WN status (Smith, Crowther & Prinja 1994). Finally the WN classification scheme was revised by Smith, Shara & Moffat (1996) to include secondary and tertiary criteria in an attempt to more accurately classify WN stars, these criteria mainly included line ratios of N V/N III. As mentioned, WC classifications range from WC4–9, these were originally devised by Smith, Shara & Moffat (1990), and were later extended by Crowther, de Marco & Barlow (1998).

Smith, Shara & Moffat (1996) also formulated a method to discriminate WN stars with definite signs of hydrogen in their atmosphere, labelled 'h', and those with only a marginal hydrogen content, labelled '(h)'. This classification scheme identified hydrogen if the (H+He) lines, λ4340 and/or λ4861, clearly exceed the height of a line drawn between

the peaks of the pure He II lines, $\lambda\lambda\lambda$4200,4541,5411. These classifications were quantified by two formula described by

$$\lambda 4861/\sqrt{\lambda 4541 \times \lambda 5411} - 1 \tag{1.1}$$

$$\lambda 4340/\sqrt{\lambda 4200 \times \lambda 4541} - 1 \tag{1.2}$$

where stars with $H^+/He^{++} > 0.5$, are classified as containing significant quantities of hydrogen, whereas stars with measured $H^+/He^{++} < 0.5$, are only classified as having a marginal hydrogen content, and finally, for completeness stars with no hydrogen are labelled 'o', when the H/He ratio was zero.

1.2.2 Non-Rotating Evolutionary Models

It is now commonly accepted that WR stars are the highly evolved descendants of the most massive O stars initially formed. This was not always the case. Until the work by Conti (1976) there were three distinct types of spectral classification for evolved massive stars, all of which displayed emission lines, Of stars; WR stars; and P–Cygni stars, all thought to be separate kinds of objects. Conti's work recognized that they all appeared to under-go a similar physical phenomenon that connected them in evolutionary terms – stellar winds. It was proposed that a massive O star evolved such that,

$$O \rightarrow Of \rightarrow WR$$

Today this fundamental evolutionary sequence is known as the *"Conti Scenario"*. Since then, with help from both observational and theoretical work, this evolutionary sequence has been refined. There are many factors that affect the evolution of a massive star most notably; mass-loss, surface chemistries, initial mass, and mixing, all of which are predicted to vary with metallicity.

There have been a number of evolutionary tracks calculated for massive stars, notably those by Meynet *et al.* (1994), the results of which will be discussed here. The effect of metallicity plays a pivotal role not just in massive stars but also in the evolution of WR stars. Theory expects a correlation between the initial metallicity at which a WR star is formed and the rate at which it loses material during its WR lifetime - an affect which is yet to be determined through direct observational evidence. Other fundamental parameters are also indirectly effected by metallicity, again as a consequence of mass-loss. For example,

a WR star with an initial mass of $85M_{\odot}$ at solar metallicity, is predicted to live for a factor of ~2 longer than a star with the same initial mass formed in the SMC (Meynet *et al.* 1994). Non-rotating evolutionary models also predict that when comparing WR stars located in low metallicity environments to WR stars formed at higher metallicities, they have: (i) increased luminosities; (ii) their surface abundances are generally higher (i.e. they tend to enter the WR phase later in their lifetime); (iii) the ratio of binary/single WRs formed increase. It is still uncertain whether all of these trends are seen observationally.

Below is the evolutionary sequence for five different stars with a range of initial masses, showing their different transitional phases as they evolve. These sequences were inferred from the evolutionary models by Meynet *et al.* (1994) calculated for massive stars at solar metallicities. Its worth noting that at each stage in the sequence the lifetimes vary wildly between initial masses. Table 1.1 shows the lifetimes during different WR stages as well as the total WR lifetime calculated from these evolutionary tracks (Meynet *et al.* 1994).

120 $M_{\odot}$:	O →	BSG →	WNL →	WNE →	WCE →	WO		
85 $M_{\odot}$:	O →	BSG →	WNL →	WNE →	WCL →	WCE →	WO	
60 $M_{\odot}$:	O →	BSG →	LBV →	WNL →	WNE →	WCL →	WCE →	WO
40 $M_{\odot}$:	O →	BSG →	RSG →	WNL →	WCE →	WO		
25 $M_{\odot}$:	O →	BSG →	RSG					

The notation used in the evolutionary sequence: O, is simply a young O dwarf or main sequence O star, BSG is a Blue Supergiant, RSG is a Red Supergiant, LBV is a Luminous Blue Variable, with the various early and late WR phases indicated. An important point to note from these evolutionary models is that, at solar metallicities, only a star with an initial mass of at least of $40M_{\odot}$ will evolve to become a WR star during its lifetime.

An important stage in massive stellar evolution is the supergiant phase. As a massive star evolves its hydrogen core is depleted through ongoing nucleosynthesis. Eventually the hydrogen fuel is exhausted and the temperatures are insufficient to ignite helium burning in the core (temperature for He burning $T \simeq 2 \times 10^8$K; Maeder 1983). As the fusion rate decreases the amount of energy generated declines. This causes the core to contract, converting gravitational energy into thermal energy allowing the surrounding shell temperature to increase. This rapid rise in temperature triggers hydrogen shell burning, and as a result the shell burning suddenly generates more energy which causes

Table 1.1: Evolutionary predictions for WR star lifetimes (in units of 10^5 years) calculated at solar metallicity with standard and twice standard mass-loss rates (Maeder & Meynet 1994).

Initial Mass	τ(WNL)	τ(WNE)	τ(WC)	τ(WR)
Standard mass-loss rates				
$120M_\odot$	4.422	0.000	3.008	7.430
$85M_\odot$	1.772	0.004	2.232	4.008
$60M_\odot$	1.406	0.162	2.654	4.222
$40M_\odot$	0.266	0.458	1.851	2.575
2 $\times$ Standard mass-loss rates				
$120M_\odot$	11.504	4.395	3.687	19.586
$85M_\odot$	2.818	0.149	5.552	8.520
$60M_\odot$	0.789	0.171	4.171	5.130
$40M_\odot$	0.336	0.525	4.581	5.443

an expansion of the stellar radius and an increase in the luminosity. As the outer envelope expands its temperature decreases moving it redward along the Hertzsprung-Russell (HR) diagram (see Section 1.2.4). Spectroscopically these stars appear to be K- to M-type, observational studies have found that the mean spectral type changes with metallicity, appearing later at higher metallicities (Elias, Frogel & Humphreys 1985).

1.2.3 Rotating Evolutionary Models

The effects of rotation on the evolutionary lifetime of a massive star have been studied in a series of papers (e.g. Meynet & Maeder 2000), continuing their earlier work described in Section 1.2.2. This work has recently been extended to study the effects of rotation on WR stars in a paper by Meynet & Maeder (2003). Their revised evolutionary grid of models found that compared with non-rotating models; (i) their WR lifetimes were enhanced (typically by a factor of 2); (ii) stars enter the WR phase earlier and as a result they still have a large hydrogen-rich envelope, this notably increases the time that a star spends in the WNL phase; (iii) the transitional WN/WC phase where both H- and He-burning products are seen at the surface of the star is also predicted in the rotating models

Table 1.2: Rotating evolutionary predictions for WR star lifetimes (in units of 10^5 years) calculated at solar metallicity (Meynet & Maeder 2003). These models assumed an initial rotational velocity, $v_{ini} = 300\text{kms}^{-1}$, as well as the proposed mass-loss rates by Nugis & Lamers (2000).

Initial Mass	τ(WNL)	τ(WNE)	τ(WN/WCE)	τ(WC)	τ(WR)
$120M_\odot$	10.402	0.706	0.010	2.851	13.969
$85M_\odot$	10.707	1.263	0.065	2.015	14.050
$60M_\odot$	4.489	0.562	0.202	2.274	7.527
$40M_\odot$	1.478	0.000	0.447	1.745	3.670
$25M_\odot$	2.068	0.000	0.000	0.000	2.068

(although not in the most massive stars as mass-loss is too rapid); (iv) the minimum initial mass for a star to evolve to the WR phase has been reduced from $37M_\odot$ to $22M_\odot$ when rotating at an initial velocity, $v_{ini} = 300\text{kms}^{-1}$. It is clear to see that rotation is an essential ingredient when considering evolutionary models for massive stars.

To highlight the improvements made with the inclusion of rotation we have listed the revised WR lifetimes in Table 1.2, the main differences are that the models predict that stars will enter the WR phase earlier extending the WNL phase. Importantly, the new models also predict the (modest) existence of the intermediate WN/WCE phase which have been widely observed but until now not predicted. By including rotation into the evolutionary model calculations it permits mixing within the star causing both H and He burning products to be simultaneously observed in the star's atmosphere, which characterizes these stars. In effect, the inclusion of mixing produces a shallower chemical gradient inside the star. For the $120M_\odot$ star the rapid mass-loss removes the outer envelope which reduces the time spent as a WN/WCE star. The effects of rotation on current evolutionary models have been substantial in bridging the gap between observations and theory, we now await a large grid of models calculated at a variety of metallicities and velocities before we can fully test these exciting results.

There has long been a discrepancy between the observed Blue to Red supergiant (B/R) ratio, and the theoretically predicted ratio. For example, the B/R ratio observed for the SMC cluster NGC 330 was found to be between 0.5 – 0.8 (Langer & Maeder 1995),

subsequent IR observational studies did little to alter this ratio (e.g. Kucinskas *et al.* 2000). Previously determined non-rotational models predict stars to become RSGs at the end of the He-burning phase. At SMC metallicities these non-rotational models predict B/R $\simeq$ 47. The inclusion of rotation into theoretical models decrease the B/R ratio with increasing rotational velocities, favouring the RSG phase and reducing the BSG lifetime. The rotational models by Maeder & Meynet (2001) found that for calculations with an average rotational velocity of $\bar{v} = 200\text{kms}^{-1}$, the predicted B/R ratio was $\sim$0.6, well in agreement with observed values.

1.2.4 The Hertzsprung-Russell Diagram

The Hertzsprung-Russell (HR) Diagram was first drawn up by Ejnar Hertzsprung in 1911, and later independently by Henry Norris Russell in 1913. Their two-dimensional plot shows how the luminosity of a star varies with it's surface temperature. When these observational parameters are plotted the majority of stars lie along a diagonal band which is now known as the main sequence (MS), this stage represents a significant phase in which a star still burns hydrogen at its core. This diagram became the foundation for what is now known as one of the most important, fundamental plots in stellar astrophysics, as it maps out the evolution of a star during it's lifetime.

Figure 1.1 shows the upper region of a theoretical HR diagram, representing a cluster (or association) of stars formed at the same time, and so we are effectively seeing a snapshot of stars at different ages in their evolution with a range of stellar masses. The figure shows stars with hydrogen (and the earliest stages of helium) core-burning, such that the WR phase is truncated.

For the most part, the majority of stars spend their life burning hydrogen and appear on the HR diagram close to (or on) the main sequence. A 'typical' high mass star will then evolve off the MS and move redward (or cooler) on the HR diagram, this occurs when the central hydrogen burning core becomes depleted. As this happens the star expands and as a consequence the star becomes more luminous and cooler. Because Figure 1.1 only shows the theoretical scenario up to an age of 10 Myr, we only see the evolution of high mass stars. On these timescales the lower mass stars are either, still burning hydrogen on the MS or are yet to reach the MS, and are still embedded in their dusty shells as a proto-star. So for the stars in Figure 1.1, once a high mass star has evolved to become a RSG their atmospheres become extended and they lose their outer shells through dense, slow stellar

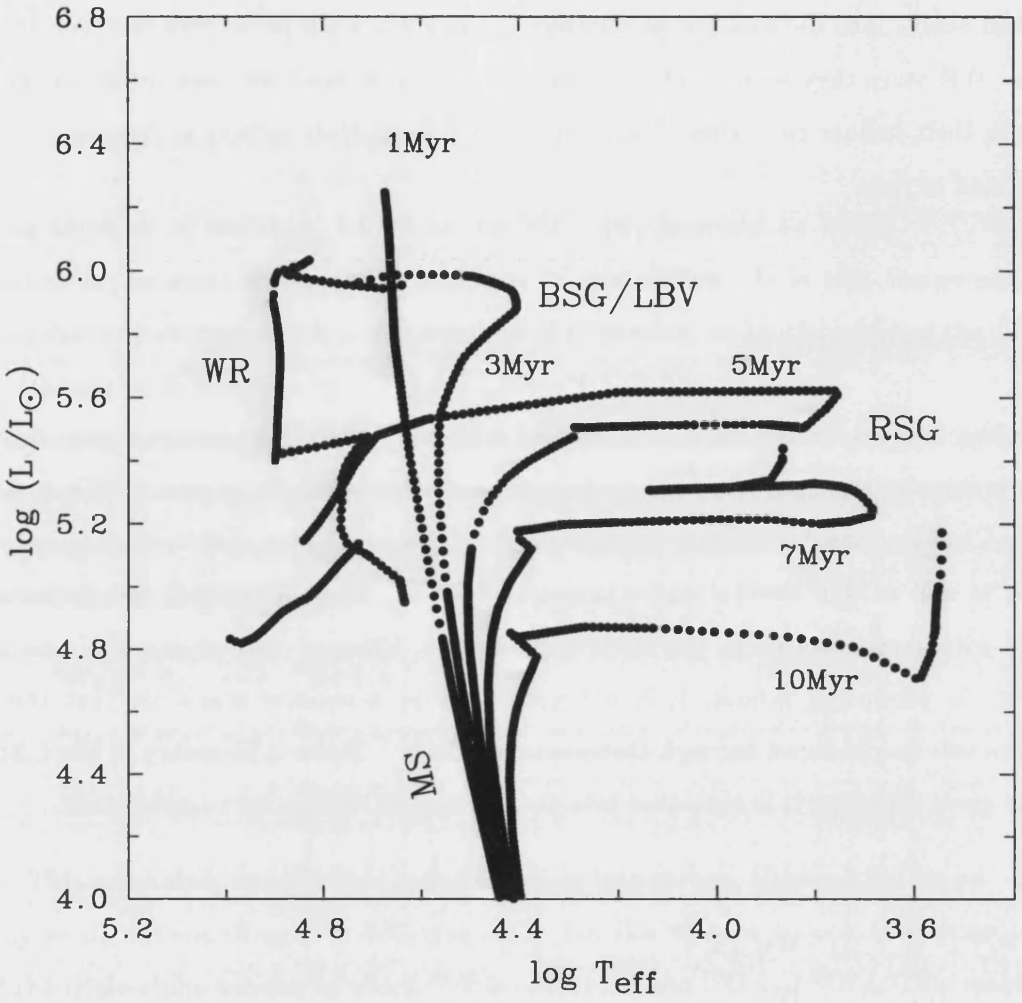

Figure 1.1: The upper regime of the Hertzsprung-Russell Diagram. The figure shows the same stellar populations at a variety of different ages, during both hydrogen and the earliest stages of helium core burning. The upper section of the main sequence (MS) is shown, and a number of evolutionary stages are also indicated, including the Blue Supergiants (BSG), the Luminous Blue Variables (LBV), the relatively cooler Red Supergiants (RSG), as well as the beginning of a Wolf-Rayet (WR) star's lifetime.

winds. In doing this they expose their cores moving blueward (or hotter) across the HR diagram entering the BSG/LBV and/or the WR phase. This phase is truncated for the highest mass O stars, such that they after they evolve off the MS, become a BSG/LBV and then evolve into the WR phase, without entering the RSG phase. By the time they become WR stars they soon reach core temperatures that are high (and dense) enough to ignite their helium rich cores where through nuclosynethsis helium is processed into carbon and oxygen.

1.2.5 Nucleosynthesis

Unlike the Sun where hydrogen is converted into helium via the proton-proton chain reaction, massive stars produce helium through the carbon-nitrogen-oxygen (CNO) cycle. For the CNO cycle to dominate it requires that trace elements of carbon and nitrogen are present as well as high internal stellar temperatures, such that the reaction rate increases rapidly with temperature. In the CNO cycle carbon, nitrogen and oxygen are used as catalysts in producing helium, it is not until later in a massive star's life that these elements will be produced through thermonuclear fusion. Below a summary of the CNO cycle is given although it is seperated into the CN and NO cycles for completeness.

$$\begin{aligned}
^{12}C + ^{1}H &\longrightarrow {}^{13}N + \gamma \\
^{13}N &\longrightarrow {}^{13}C + e^{+} + v_e \\
^{13}C + ^{1}H &\longrightarrow {}^{14}N + \gamma \\
^{14}N + ^{1}H &\longrightarrow {}^{15}O + \gamma \\
^{15}O &\longrightarrow {}^{15}N + e^{+} + v_e \\
^{15}N + ^{1}H &\longrightarrow {}^{4}He + ^{12}C \\
^{15}N + p &\longrightarrow {}^{16}O + \gamma
\end{aligned} \tag{1.3}$$

The timescale for the CN cycle is mainly dominated by the fourth reaction shown above (i.e. $^{14}N + ^{1}H \rightarrow ^{15}O + \gamma$), as this reaction is the slowest and can typically last on the order of a million years.

$$\begin{aligned} {}^{16}O + p &\longrightarrow {}^{17}F + \gamma \\ {}^{17}F &\longrightarrow {}^{17}O + e^{+} + v_e \\ {}^{17}O + p &\longrightarrow {}^{14}N + {}^{4}He \end{aligned} \tag{1.4}$$

This sequence of reactions, known as the NO cycle, produces an excess of ^{14}N as this isotope is the most stable and is resistant to destruction. It is this temporary over-abundance of nitrogen which is characteristic of H-burning, and is the origin of the nitrogen enrichment in WN stars.

Once the abundance of helium increases and the internal temperatures are significantly increased then the conditions are such that carbon will be produced through the triple alpha process. ^{12}C is the main product during this process, below the nuclear reactions for helium burning are shown:

$$\begin{aligned} {}^{4}He + {}^{4}He &\longleftrightarrow {}^{8}Be + \gamma \\ {}^{8}Be + {}^{4}He &\longrightarrow {}^{12}C + \gamma \\ {}^{12}C + {}^{4}He &\longrightarrow {}^{16}O + \gamma \end{aligned} \tag{1.5}$$

This is the main reaction that converts helium into carbon, although it does not explain why we do not see nitrogen in WC-type stars. For this we have to look at another branch of the triple-alpha process in which ^{14}N is converted into ^{18}O and ^{22}Ne. This reaction of ^{14}N is highly resonant (Maeder 1983) and so the C/N and O/N drastically and suddenly increase as nitrogen is rapidly depleted. We show the reactions that produce both ^{18}O and ^{22}Ne through the destruction of ^{14}N:

$$\begin{aligned} {}^{14}N + {}^{4}He &\longrightarrow {}^{18}O + e^{+} + v_e \\ {}^{18}O + {}^{4}He &\longrightarrow {}^{22}Ne + \gamma \\ {}^{22}Ne + {}^{4}He &\longrightarrow {}^{25}Mg + n \\ {}^{22}Ne + {}^{4}He &\longrightarrow {}^{26}Mg + \gamma \end{aligned} \tag{1.6}$$

This sits well with the current evolution theory of WR stars and can also explain why we see the (rare) intermediate WNE/WC stars. These objects are undergoing the nuclear reactions described in Equations 1.6 and 1.7 but due to mixing have slowed the rate at which ^{14}N is destroyed.

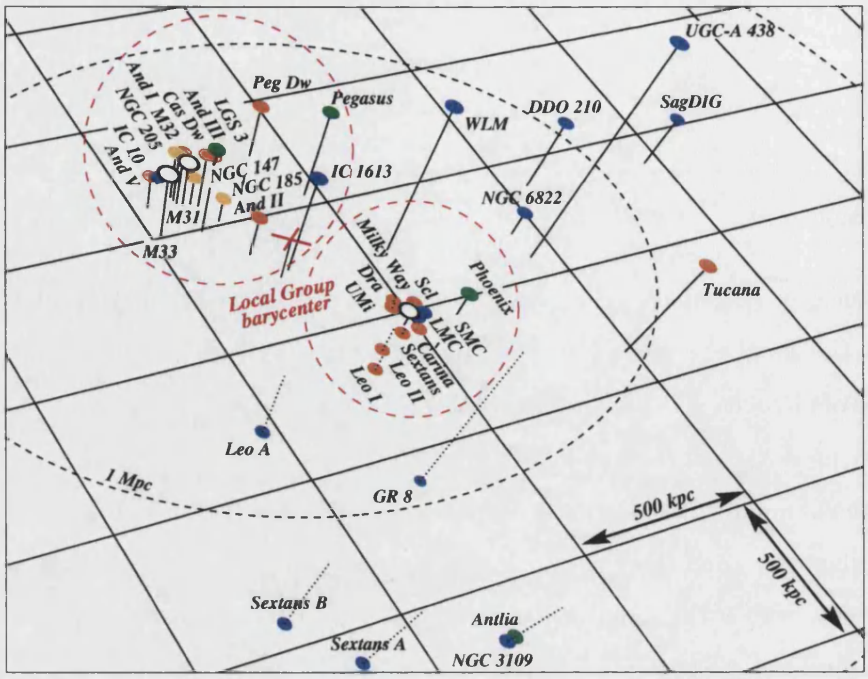

Figure 1.2: A scaled, three-dimensional map of the Local Group taken from Grebel (1999). The underlying grid is parallel to the plane of the galaxy. The three large spiral galaxies in our Local Group are shown (open symbols), as well as dwarf ellipticals and dwarf spheroidals (orange and green symbols respectively). The dwarf irregular galaxies are also shown (blue symbols). The main point that this Figure highlights is a morphological segregation, with clear evidence that the dwarf ellipticals and spheroidals are focused around the larger spirals.

1.3 The Local Group Galaxies

The WR population in the solar neighbourhood has been well studied with ground-based facilities and there have been a number of detailed studies of individual Galactic WR stars (e.g. Dessart *et al.* 2000), although current numbers are not believed to be final as observational studies have been hampered due to the large extinction in the Galactic plane. Things are slightly better for both Magellanic Clouds, as deep imaging has surveyed these galaxies to below the detection limit, even for the weak lined WN stars. These studies have revealed a number of WR stars, and again as with the Milky Way a number of these objects have been analyzed in detail (e.g. Crowther 2000; Crowther *et al.* 2002), although beyond our nearest galactic neighbours surveys have been limited and analysis

of individual stars rare. A summary of the known WR populations in nearby galaxies is given in Table 1.3. NGC 300 is included although strictly it is not a member of the Local Group, but in fact a member of the nearby Sculptor Group, but is within the viable limits such that ground-based detections are possible.

Table 1.3: List of known WR population in the Local Group galaxies. The abundances were all taken from Kennicutt *et al.* (1998) and references therein, apart from the SMC and the Milky Way, where the values from Russell & Dopita (1990) and Esteban & Peimbert (1995) are shown. These (approximate) abundances were all determined from H II regions.

Galaxy	Distance (kpc)	Abundance 12+log(O/H)	WRs	WC/WN	References
Milky Way	< 3	8.70	227	1.50	12
LMC	50	8.50	135	0.23	3,10
SMC	63	8.13	11	0.12	1,9
NGC 6822	530	8.14	4	0.00	2,7
IC 1613	766	7.86	1	1.00	2,7
M 31	796	8.98	49	0.67	4,5,7,8
IC 10	820	8.20	15	2.00	6,7
M 33	843	8.82	141	0.44	2,7
NGC 300	2188	8.35	32	1.50	11

References – [1]Azzopardi & Breysacher (1979); [2]Armandroff & Massey (1985); [3]Breysacher *et al.* (1999); [4]Bransford *et al.* (1999); [5]Galarza *et al.* (1999); [6]Massey & Armandroff (1995); [7]Massey & Johnson (1998); [8]Moffat & Shara (1987); [9]Morgan *et al.* (1991); [10]Massey *et al.* (2000); [11]Schild & Testor (1992); [12] van der Hucht (2001).

Figure 1.2 shows a scaled, three-dimensional map of the Local Group taken from Grebel (1999). It shows their spatial distribution within the local universe as well as their galaxy classifications. The three large spiral galaxies in our Local Group are shown, as well as dwarf ellipticals, dwarf spheroidals, and dwarf irregulars. The main point that this Figure highlights is a morphological segregation, with clear evidence that the dwarf ellipticals and spheroidals are focused around the larger spirals.

This work in part probes the WR populations in a number of these galaxies and beyond where surveys have been limited or non-existent. As well as finding candidate

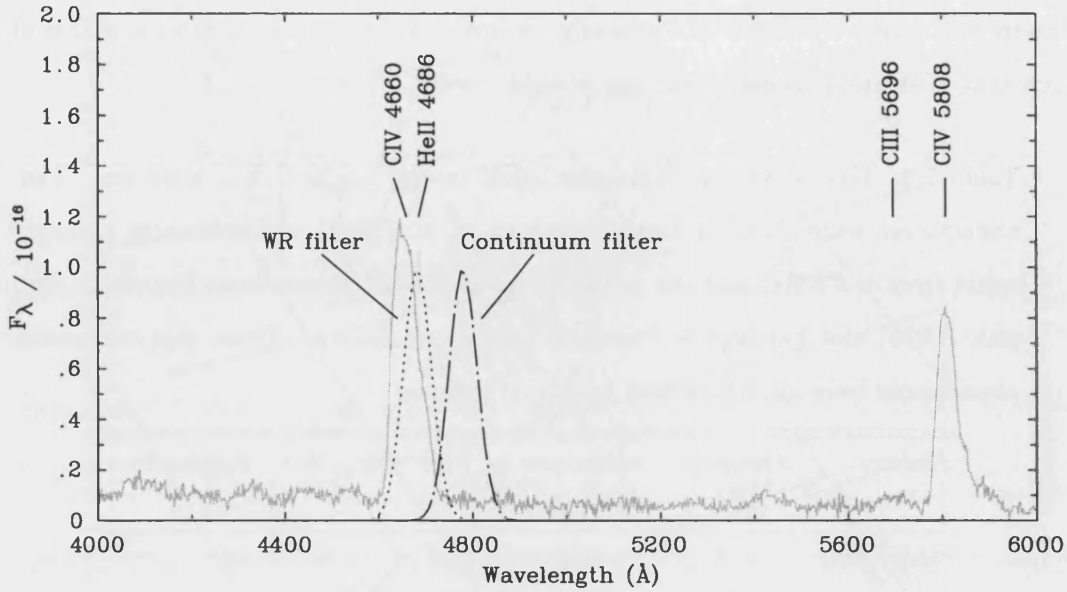

Figure 1.3: A spectrum of a faint WCE star in NGC 300 (WR29, $\text{mag}_V = 21.61$), showing the position and width of the interference filters used to identify it as a WR candidate. The *'WR filter'* (dotted line) is situated where there are known WR emission features and the *'continuum filter'* (dot-dashed line) is situated in a region relatively free of emission. The relatively large excess in flux between these two filters highlights the potential method for discovering candidate WR stars.

WR stars we also concentrate on individual 'single' stars and attempt to determine their stellar parameters from which we can learn more about their fundamental properties in a number of different environments.

1.3.1 Detection Methods

Beyond the Milky Way there have been a number of surveys to identify WR stars. The majority of these surveys use the well tested method of observing large regions of galaxies through interference filters. There have been previous WR filter systems that have successfully identified candidate WR stars within large stellar populations (e.g. Smith 1968), although more recently a more sophisticated series of narrow-band photometric systems

have been developed (e.g. Royer, Vreux & Manfroid 1998). These methods involve two (or more) specially designed narrow-band filters centered at 4686 Å and 4781 Å, with a modest band width of $\sim$ 70 Å. The filters are centered on these regions to match known, strong WR emission features, and a region of relatively free emission. For WC stars, the former filter will contain emission from the blended feature of He II λ4686, C III λ4650, and C IV λ4660, for WN stars, it will predominately include He II λ4686 with some minor contribution from N III λ4640. From observations taken through these filters it is possible to distinguish objects that appear to have an excess of flux in the *'WR filter'*, and that would otherwise appear a perfectly normal star through broad-band photometry. There are limitations with this technique, for instance a foreground (cool) star could mimic He II λ4686 emission if absorption lines were observed in the *'Continuum filter'*.

A schematic of this technique is shown in Figure 1.3; it shows a faint WC star (NGC 300-WR29, m_V=21.61) with the two filters over-plotted to illustrate their position with respect to the strong WR emission. The *'WR filter'* is shown in red, and the *'continuum filter'* is shown in blue. The large excess in flux between the two filters indicates a potential WR star. This technique was used to find candidate WR stars in NGC 300, the results of which are described in Section 2.5. Follow-up spectroscopy successfully confirmed that NGC 300-WR29 was indeed a WR star. WR stars observed at different radial velocities within the Local Group will still be detected using this method due to the large intrinsic widths of WR star emission lines.

1.4 Metallicity Effects Within the Local Group

The Local Group is an ideal laboratory for testing the theories of massive stellar evolution, as the metallicity range spans a factor of ten. Even though the massive stellar content is still not fully known for all the Local Group galaxies we have now obtained enough data to test current evolutionary models. By comparing a number of measured observables for different galaxies we can test the effects of metallicity on massive stellar populations. In this section we discuss both current observed trends and evolutionary predictions.

The effect of metallicity plays a pivotal role in the evolution of massive stars, as it is predicted that a massive-star is heavily influenced by mass-loss throughout its life. Since it is believed that these stellar winds are driven by radiation pressure in optically thick lines of highly ionized metals, we should expect that their properties (e.g. $\dot{M}$, v_∞) are sensitive to

metallicity variations. As previously discussed theoretical predictions expect a correlation between the initial metallicity in which a WR star is formed and the rate at which it loses material during its WR lifetime - an effect which is yet to be determined through direct observational evidence. It is unclear as to whether this effect will be observed for both WN and WC-type stars. Other fundamental parameters are also thought to indirectly be effected by metallicity, again as a consequence of mass-loss.

1.4.1 The WC/WN Ratio

It is predicted that the metallicity plays an important role in defining the initial mass required to form a WR star. So because WR stars are formed from massive stars within initial stellar populations, only the most massive of those stars will evolve to become WC stars. As a result stellar evolution theory suggests that the WC/WN ratio should be sensitive to the surrounding metallicity, and can be used as a excellent indicator of massive stellar evolution. Massey & Johnson (1998) first tested whether this ratio was sensitive to metallicity by plotting the current observed WC/WN ratios against the respective metallicity for a number of our Local Group galaxies. These results are reproduced in Figure 1.4, the metallicity in this plot is taken from oxygen abundance calculations. The H II region oxygen abundance is used to indicate the metallicity.

The WC/WN ratio versus metallicity plot by Massey & Johnson (1998) has emerged as a potentially useful indicator for astronomers working on WR stars in and around the Local Group. Almost all the galaxies plotted in Figure 1.4 follow the expected trend, where the WC/WN ratio increases linearly with increasing metallicity. This trend is well correlated apart from our own galaxy, the Milky Way, and IC 10. For the Milky Way it can be reasoned that our numbers for both the WC and WN stars are incomplete. Most of the known WR stars in the solar neighbourhood were found as part of the Henry Draper catalogue, and when considering factors such as extinction a typical WN star could easily be below the completeness limit. Meynet & Maeder (2003) recently compared their theoretical WC/WN number ratios for both non-rotating and rotating models. Their recent rotating models predict a reduced ratio, more in line with the observed trend seen for the other galaxies.

The unusually large WC/WN ratio in IC 10 (WC/WN $\approx$ 2) has baffled astronomers for many years now, surprisingly it has a metallicity similar to that of the SMC but with a WC/WN ratio twenty times larger (Lequeux *et al.* 1979). There are many possibilities

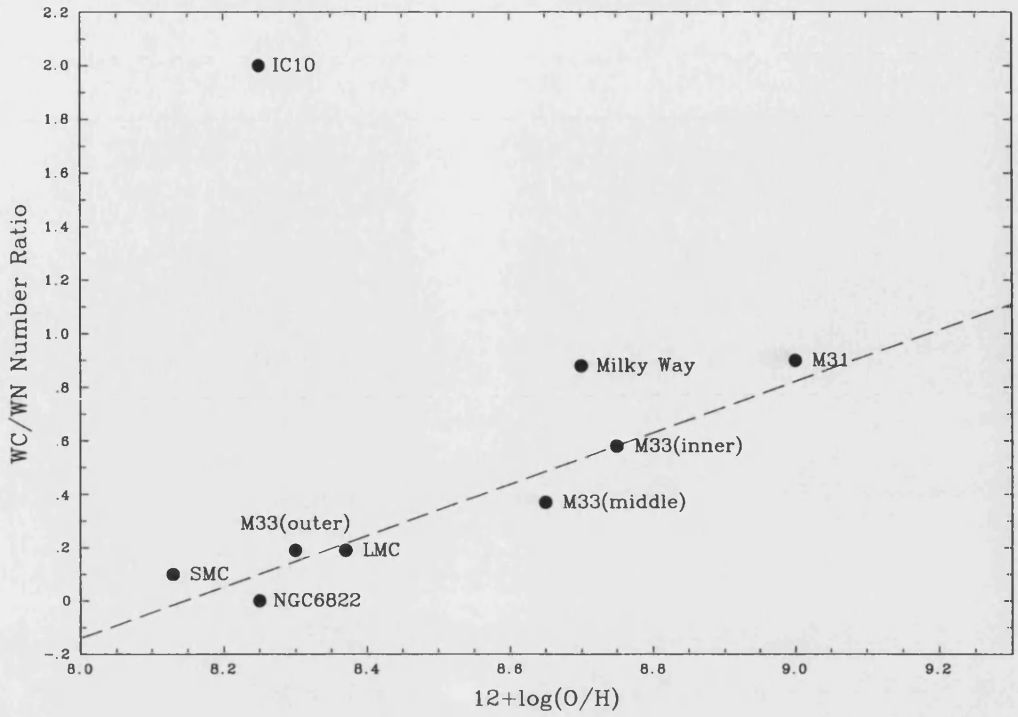

Figure 1.4: WC/WN ratio versus oxygen abundance for Local Group galaxies reproduced from Massey & Johnson (1998). The dashed line is a least-squared fit to the points (ignoring IC 10 and the Milky Way).

as to why this may be the case, and an attempt to answer this is given later in this thesis (see Section 6). Apart from the exception of IC 10 the other Local Group galaxies studied seem to follow a tight correlation between the WC/WN ratio and metallicity; increasing towards higher metallicities. This trend can be explained as we do not expect to see as many WC stars at lower metallicity due to those stars that do enter the WR phase evolving with considerably weaker winds than those at higher metallicity.

1.4.2 The RSG/WR Ratio

Not only do evolutionary models predict the WC/WN ratio to be sensitive to metallicity but we also expect the observed O/WR number ratio to vary with metallicity, and as a consequence the RSG/WR ratio to also be sensitive to metallicity variations. This is achievable with modern evolutionary models, and as expected this number ratio is predicted to decrease with increasing metallicity, as the initial mass required to form a WR sharply increases. Again, comparing the most recent rotational models (Meynet &

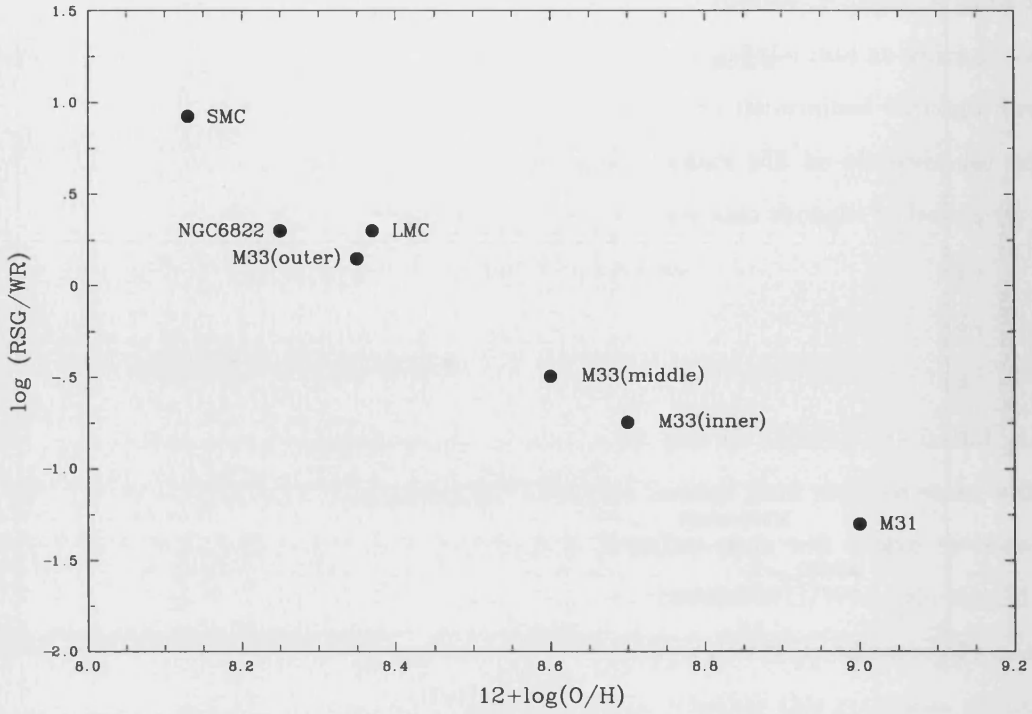

Figure 1.5: Log (RSG/WR) ratio versus oxygen abundance for Local Group galaxies reproduced from Massey (2002).

Maeder 2003) to previous non-rotating models (Meynet *et al.* 1994), the rotational models favour the observed number ratios. We await more evolutionary grids calculated at a variety of metallicities before a full comparison can be made.

This theory was observationally tested recently by Massey (2002), who undertook deep photometric surveys of both the Magellanic Clouds. From these results he was able to re-determine the observed RSG/WR ratio (instead of the O/WR ratio, although the same effect should still be observed) for a number of Local Group galaxies. He excludes RSGs with $M_{bol} > -7.5$ to avoid intermediate-mass AGB stars, as well as only including RSGs that lie in same areas for which there have been complete WR surveys. We have reproduced these results in Figure 1.5. It appears that observationally there is a trend for the RSG/WR number ratio to scale with metallicity. Unfortunately current evolutionary models fail to match this trend, as we see a reduction in the RSG/WR number at ~LMC metallicity (Massey 2003).

CHAPTER 2

Observations of Wolf-Rayet Stars in Nearby Galaxies

This chapter consolidates all the observations and techniques used to study individual Wolf-Rayet stars in the Local Group and beyond. Previous attempts to resolve single WR stars within the Local Group have proven difficult; the quality, resolution and the signal-to-noise of the spectra obtained from these studies have been poor. In comparison, recent instrumental improvements at 4-metre telescopes (e.g. CFHT-MOS) as well as a number of new instruments at 8-metre telescopes (e.g. Gemini-GMOS) offers the possibility of observing many WR stars simultaneously, increasing the exposure time by an order of magnitude over standard (single) long-slit spectroscopy thereby delivering spectra with a signal-to-noise ratio sufficiently high to permit a detailed quantitative spectroscopic analysis. We now have the opportunity to study massive stars in a number of different environments which enables us to try to answer some of the fundamental questions still surrounding massive stars and their evolution.

2.1 M 33

Detailed studies of WR stars nearby in the Solar neighbourhood and the Magellanic Clouds have been numerous (e.g. De Marco *et al.* 2000; Hillier & Miller 1998; Dessart *et al.* 2000). Beyond the Magellanic Clouds detailed spectroscopic studies of WR stars have been limited, and the quality of data obtained poor. In this work we study the Wolf-Rayet population of the late-type spiral (Sc) galaxy M 33 (NGC 598). M 33 is an ideal

candidate galaxy to continue with these detailed studies, as it contains a large number of known WR stars, it is nearby, with a well determined distance, a low extinction, and is viewed at a low inclination.

2.1.1 Previous Work

The early work on M 33 by Wray & Corso (1972) using interference filters of He II and C III led to 25 WR candidates, of which 22 were spectroscopically confirmed (Boksenberg, Willis & Searle 1977; Conti & Massey 1981). A further 15 WR stars – mainly serendipitously discovered while studying H II regions – were found by Conti & Massey (1981). There have been numerous subsequent studies notably by Massey & Conti (1983), Massey *et al.* (1987*b*) and Willis, Schild & Smith (1992). Most recently there was a deep CCD survey of M 33 by Massey & Johnson (1998) who found a further 22 new spectroscopically confirmed WR stars, bringing the total number of known WRs in M 33 to 141.

Until now the quality, resolution and the signal-to-noise of the spectra obtained from these studies have been poor, allowing only determination of their spectral types and measurement of the line strengths from the strongest features. In only two cases have individual WR stars been studied in detail (Smith *et al.* 1995; Crowther *et al.* 1997). In comparison, recent instrumental improvements at 4-metre telescopes (e.g. CFHT-MOS) offers the possibility of observing many WR stars simultaneously, increasing the exposure time by an order of magnitude over standard (single) long-slit spectroscopy, thereby delivering spectra with a signal-to-noise ratio sufficiently high to permit a detailed quantitative spectroscopic analysis. We have observed a relatively large sample of known WRs in M 33 and obtained a new, improved dataset suitable for detailed analysis.

2.1.2 CFHT-MOS Observations of Wolf-Rayet Stars in M 33

This study uses data taken with the Multi-Object Spectrograph (MOS) on the 3.6-metre Canada-France-Hawaii Telescope (CFHT) between 1–2 September 2000 and 17–19 October 2001. 50 WR stars were observed in four-fields (see Table 2.1), sampling approximately a third of the known WR content of M 33. Each field encompassed an area of approximately $9.5'$x$9.5'$ with a scale of $0.28''$/pixel. Figure 2.2 shows the location for each of the four fields, superimposed in an archival 40s V-band CFH12K MOSAIC image from 7 Aug 2000.

All program stars were spectroscopically observed with MOS using the 2048 x 4500 EEV1 CCD with 13.5μm pixels. Multiple exposures were taken using integration times

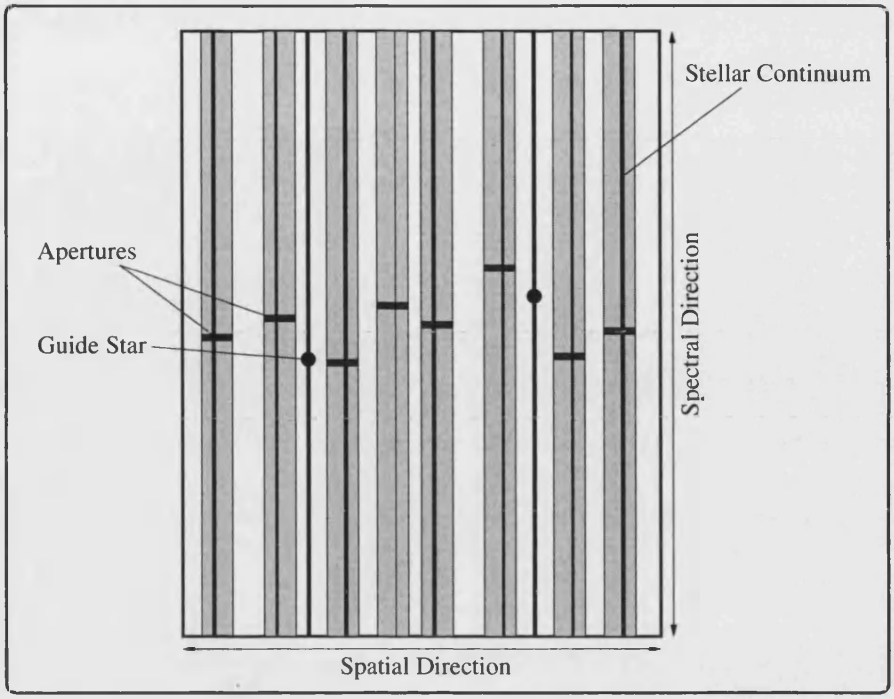

Figure 2.1: Schematic showing the data format from a Multi-Object Spectrograph. Each aperture is cut to produce a unique mask for the target field.

of 1800 sec. Individual masks were designed to include the maximum number of WRs possible for each field, attention was given such that the slit positions did not overlap in the spatial direction. Slits within each mask were cut to an aperture width of 1.5″. The wavelength coverage obtained for each object depends on the vertical position of the slit on the mask, but typically we aimed for spectroscopic coverage of $\lambda\lambda$3800-7000 for all our target stars.

Data from a Multi-Object Spectrograph are taken through a number of narrow apertures (or *'slitlets'*) spatially positioned to observed a number of objects at once. Each of these apertures are cut using a laser to produce a series of tiny slits which in turn make a unique mask for the target field. The slit positions are decided on using primary observations taken to identify the location of each object. Figure 2.1 is a schematic showing the data format for a *generic* Multiple-Object Spectrograph, each observation is in essence a series of smaller, long-slit observations acquired simultaneously. There also one or two bright guide stars that are concurrently observed within the field, these are used to help track the fainter objects.

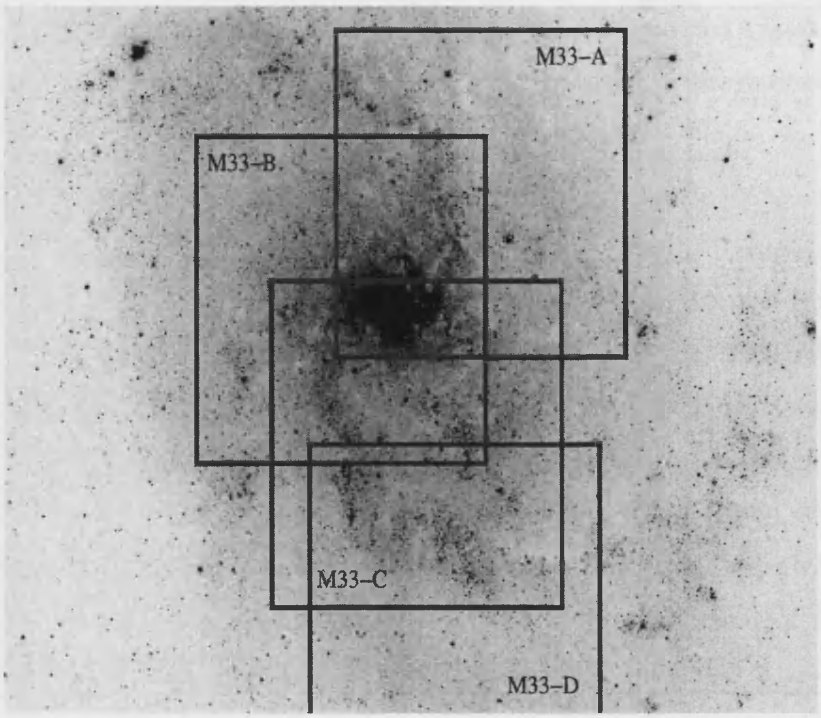

Figure 2.2: The four observed fields for M 33 are shown, the coordinates can be found in Table 2.1. In this figure north is up and east is to the left. The field of view for each field is 9.5′x9.5′.

The data were reduced and extracted using standard IRAF[1] procedures modifying them for our data format. The majority of the packages used for the reduction are found under *twodspec.apextract*. After the data were bias subtracted, they were flat field corrected using a normalized flat field. For MOS data this stage primarily involves defining each aperture, after which they are traced to account for any non-linearity, and finally a high order spline is fitted to match the response across the chip. This gives a normalized flat-field with each aperture containing any small scale pixel-to-pixel variations. The next procedure was to clean any cosmic rays from each image, for this we used the *kappa.bclean* package under IRAF. The extraction stage uses the apertures that were previously defined whilst normalizing the flat-fields, this was one of the most challenging tasks as some of the stars observed in our sample had extremely weak continuum which meant that tracing the star was very difficult. For some of the fainter objects increasing the number of

[1] IRAF is distributed by the National Optical Astronomy Observatories, which is operated by the Association of Universities for Research in Astronomy, Inc., under agreement with the National Science Foundation.

Table 2.1: Observed log for the four fields for M33, including the central coordinates for each field.

Field	Position (2000)		Epoch
	α	δ	
M33-A	01 33 36.89	+30 42 38.4	Aug. 2000
M33-B	01 33 59.70	+30 39 27.1	Oct. 2001
M33-C	01 33 45.21	+30 35 31.4	Aug. 2000
M33-D	01 33 41.92	+30 31 18.0	Oct. 2001

summed rows between each trace step helped with its extraction. Once the data were one-dimensional they were wavelength calibrated under FIGARO Shortridge *et al.* (1999) using the standard packages. Where possible the sky was subtracted using local sky regions within the slit, although due to crowding and the need to use narrow apertures this was at times impossible. In these cases where there were no (or highly variable) local sky regions, we used observations of nearby sky taken through separate slits for these purposes. The sky was then subtracted using DIPSO (Howarth et al. 1998) after a scaling factor was applied, this was calculated from the number of pixels summed in the extraction. We checked this method by extracting and locally sky subtracting a star within IRAF, and comparing the result with a sky subtraction made using a scaled, generic nearby sky region. Apart from the absolute levels differing slightly the main sky features were largely removed.

Given the large distance to M33, there were often large variations in the sky background across individual slits, which were imperfectly subtracted. For example, a 1.5″ slit width corresponds to a spatial scale of ~6pc at a distance of 816kpc. These strong OH sky emission features were particularly problematic at wavelengths redward of $\sim \lambda 6000$. Fringing is also common long-ward of $\sim \lambda 6800$. In addition, the final data were not absolute flux calibrated. This was due to the fact that the standard stars were observed through a much larger slit width, such that the effects of differential, atmospheric refraction altered the shape of the WR star's continuum. The effects of possible contamination from nearby objects is an observational challenge, especially at relatively large distances such as M33. Added to the fact that the majority of WR stars are located in crowded regions containing large stellar populations, the task of obtaining uncontaminated WR spectra is made very difficult.

Tables 2.1.2 and 2.1.2 list the Wolf-Rayet stars observed in all four fields. Their M33-WR number (column 1) and continuum magnitudes (column 4) are taken from Massey & Johnson (1998), the latter relating to narrow band filters with a central wavelength of λ4750. In general, we shall refer to individual stars by their discovery reference, listed in column 2. The de-projected galactocentric distances for each star are also shown (column 3), and are expressed as a fraction of the Holmberg radius[2] ($\rho_0 = 25'$). Figures A.1 - A.7 show all the WN and WC stars taken from our observed sample.

2.2 Notes on Individual Stars

Revised spectral types are listed in the tables together with their previous classifications. We follow the classification schemes devised by Smith, Shara & Moffat (1996) and Crowther, de Marco & Barlow (1998) for WN and WC stars respectively. Unfortunately, due to unreliable sky subtraction we were unable to use the primary criteria of He II/He I, to distinguish between WN subtypes. This meant that the three-dimensional classification scheme calculated by Smith, Shara & Moffat (1996) was reduced to two-dimensions relying on the ratios of the weak-lined N III-V emission lines. All of the previous classifications (taken from Table 9 of Massey & Johnson (1998) and references therein) are in relatively good agreement.

Overall, our sample revealed a majority of early-types amongst both WN and WC stars: WN3–5 accounted for 55% of the WN sample, whilst WC4–6 stars represented 90% of the WC sample. Our datasets extended sufficiently blueward to potentially identify WO stars, predomaintely searching for highly ionized oxygen lines, such as O VI $\lambda\lambda$3811,3834. From our sample none were classified as WO types. To date, late WC (WC8-9) subtypes remain exclusive to the inner Milky Way and M31. We generally refine previous spectral types, details of which are given for notable individual stars.

[2]The Holmberg radius is defined as the radius of a galaxy at which the surface brightness is 26.6 mag arcsec^{-2}, this method was developed by Holmberg in 1958 to estimate the actual dimensions of the major and minor axes of a galaxy regardless of its orientation.

Table 2.2: List of WN stars and candidates observed with CFHT-MOS. Star identifications are: AM = Armandroff & Massey (1985); MC = Massey & Conti (1983); W&C = Wray & Corso (1972); MCA = Massey *et al.* (1987*b*); OB = Massey *et al.* (1995); UIT = Massey *et al.* (1996); HS-B = Humphreys & Sandage (1980) blue star; MJ = Massey & Johnson (1998); NGC 595-WR# = Drissen, Moffat & Shara (1990). The M33-WR# assigned to each star and the previous spectral classification relates to that given by Massey & Johnson (1998).

M33		Position (2000)					Spectral Type		
WR#	Alias	α	δ	ρ	m_{cont}	Fld	Previous		New
42	AM3,NGC595-5,UIT118	01 33 32.80	+30 41 46.2	0.32	18.1	A	WNL	4)	WN8
49	CM6,AM6,MC32,NGC595-WR1,UIT126	01 33 34.22	+30 41 38.1	0.30	18.1	A	WNL	4)	WN8
—	NGC595-WR9	01 33 33.83	+30 41 29.7[a]	0.30	—	A	—	–	WN8
50	MJ-G13	01 33 34.24	+30 33 47.5	0.29	20.7	C	WN	6)	WN5
54	MCA5	01 33 37.30	+30 35 27.2	0.22	20.9	C	WN	1)	WN4
56	W&C4,MC36	01 33 39.27	+30 35 54.9	0.19	19.6	C	WN	8)	WN4-5
59	W&C5,MC37	01 33 39.92	+30 31 38.4	0.33	19.1	D	WN	8)	WN4-5
60	MJ-G3	01 33 40.01	+30 31 21.3	0.35	19.4	D	WN	6)	WN5-6+abs
74	MCA8	01 33 43.30	+30 44 50.7	0.30	21.1	A	WN	1)	WN4

Table continued on next page .....

[a]Coordinates from HST/WFPC2 images, kindly supplied by Laurent Drissen (Univ. Laval).

M33		Position (2000)					Spectral Type		
WR#	Alias	α	δ	ρ	m_{cont}	Fld	Previous		New
77	OB66-25,UIT184,HS-B205	01 33 44.65	+30 44 36.8	0.28	18.4	A	WN8	5,6)	Of
78	MCA9	01 33 45.21	+30 38 41.1	0.08	20.1	B	WN	1)	WN8
80	W&C11,MC46	01 33 45.98	+30 36 02.4	0.15	20.1	C	WN	1)	WN4-5
83	W&C13,MC48	01 33 46.77	+30 33 34.4	0.26	20.1	C+D	WN/CE	2,7)	WN/WCE
86	MJ-G8	01 33 47.81	+30 33 38.0	0.26	19.6	C+D	WN	6)	WN3-4
91	MJ-G9	01 33 50.18	+30 33 42.4	0.26	22.3	C	WN	6)	WN3
103	MJ-X15,UIT236	01 33 53.58	+30 38 51.5	0.06	17.8	B	Ofpe/WN9	3,6)	WN9
106	OB6-5	01 33 54.83	+30 32 22.7	0.35	17.9	D	WN8	5)	WN9
122	UIT289	01 34 02.24	+30 37 49.5	0.22	18.5	B	WN4	3)	WN4+abs?
43A	MJ-G1	01 33 33.19	+30 33 43.4	0.30	19.3	C+D	Cand WN	6)	Not WR
55A	MJ-C21	01 33 38.39	+30 43 02.1	0.29	19.7	A	Cand WN	6)	Not WR
118	MJ-X16	01 34 00.55	+30 38 09.1	0.18	20.1	B	WN	6)	Not WR?

(1) Massey, Conti & Armandroff (1987*a*); (2) Willis, Schild & Smith (1992); (3) Massey *et al.* (1996); (4) Armandroff & Massey (1991); (5) Massey *et al.* (1995); (6) Massey & Johnson (1998); (7) Schild, Smith & Willis (1990); (8) Massey & Conti (1983).

Table 2.3: List of WC stars observed with CFHT-MOS. Star identifications are as in Table 2.1.2.

M33		Position (2000)					Spectral Type		
WR#	Alias	α	δ	ρ	m_{cont}	Fld	Previous		New
38	MC26,AM1	01 33 26.64	+30 40 40.5	0.39	21.8	A	WC5-6	4)	WC6
45	MC29,AM5,NGC595-3	01 33 33.28	+30 41 29.8	0.31	19.7	A	WC	4)	WC6
52	MC33,AM8	01 33 35.45	+30 42 20.4	0.30	20.4	A	WC	4)	WC4
55	W&C3,MC35	01 33 38.16	+30 31 12.6	0.35	21.0	D	WC	8)	WC6
61	MC39,AM9	01 33 40.05	+30 42 38.8	0.25	20.0	A	WC4-5	4)	WC5+abs
62	W&C8,MC42	01 33 40.16	+30 31 34.5	0.34	19.7	D	WC4-5	4)	WC4
63	W&C9,MC40	01 33 40.18	+30 35 51.8	0.18	19.1	C	WC	8)	WC4
69	W&C10,MC43,AM13 .	01 33 41.81	+30 41 55.0	0.20	20.6	A	WC6-7	4)	WC7
71	MC44	01 33 42.50	+30 33 14.6	0.27	18.7	C+D	WC4-5	7)	WC5
73	MJ-C4	01 33 43.19	+30 39 00.5	0.11	18.6	B	WC	6)	WC4-5
76	MC45	01 33 44.34	+30 38 44.5	0.09	—	B	WC	8)	WC4
82	W&C12,MC47	01 33 46.54	+30 37 00.3	0.11	20.9	B	WC	8)	WC6
84	MC49	01 33 47.14	+30 37 02.5	0.11	21.0	B	WC	8)	WC6

Table continued on next page .....

M33		Position (2000)					Spectral Type		
WR#	Alias	α	δ	ρ	m_{cont}	Fld	Previous		New
89	W&C12,MC52	01 33 50.06	+30 38 56.2	0.03	20.1	B	WC	8)	WC7+abs
92	W&C16,MC53	01 33 50.18	+30 41 35.1	0.09	19.1:	A	WC4-5	2,7)	WC6
94	W&C17,MC54	01 33 51.27	+30 38 11.7	0.07	18.5	B	WCE	6,8)	WC7+abs
95	W&C19,MC55	01 33 51.82	+30 33 28.3	0.28	21.1	C+D	WC	4)	WC6
96	W&C18,MC56	01 33 51.99	+30 40 23.5	0.03	21.4	B	WC	8)	WC4+abs
99	MC57	01 33 52.67	+30 45 02.0	0.24	20.8	A	WC	4)	WC4
105	W&C21,MC60,AM14	01 33 54.40	+30 34 53.0	0.24	21.6	C	WC	4)	WC6
110	MC61,AM16	01 33 56.21	+30 32 41.5	0.35	21.3	D	WC	4)	WC5
111	W&C23,MC62,AM17	01 33 56.36	+30 34 55.5	0.26	20.9	C	WC	4)	WC5
116	MC65,AM19	01 33 59.27	+30 33 38.0	0.34	20.0	C	WC6	2)	WC6
120	MJ-X19	01 34 01.29	+30 40 04.3	0.15	17.9	B	WCL	6)	WC6-7+abs
121	MJ-X9	01 34 01.74	+30 36 19.8	0.26	19.0	C	WNL?+abs	6)	WC4+abs
125	W&C25,MC68	01 34 09.09	+30 39 06.8	0.28	—	B	WC	4)	WC6
129	MC70	01 34 16.28	+30 36 46.8	0.45	19.1:	B	WC	4)	WC5

(1) Massey, Conti & Armandroff (1987*a*); (2) Willis, Schild & Smith (1992); (3) Massey *et al.* (1996); (4) Armandroff & Massey (1991); (5) Massey *et al.* (1995); (6) Massey & Johnson (1998); (7) Schild, Smith & Willis (1990); (8) Massey & Conti (1983).

2.2.1 WN stars

2.2.1.1 NGC595-WR9 (WN8)

NGC595-WR9 (Drissen, Moffat & Shara 1990) is not M33-WR47 (MC31) as listed by Massey & Johnson (1998), but is newly confirmed as a WNL star here, supporting the earlier photometric classification. This object is located in the giant H II region NGC 595 and as a result its spectrum is heavily contaminated by nebular emission lines, this is also the case for the other WR stars in NGC 595 (NGC595-WR1, NGC595-WR3 and NGC595-WR5).

2.2.1.2 MC37 (M33-WR59, WN4–5)

MC37 (Massey & Conti 1983) has unusually broad emission lines (i.e. FWHM(He II) $\sim$ 70Å) compared with other WNE stars of a similar spectral type (i.e. MC36 – FWHM(He II) $\sim$ 30Å) indicating a large terminal wind velocity for this star.

2.2.1.3 MJ-G3 (M33-WR60, WN5–6+abs)

This early-type WN star was revised to WN5-6+abs, although the emission lines appear weak and the spectrum is dominated by a broad absorption component from either a companion or a chance line-of-sight star.

2.2.1.4 MCA8 (M33-WR74, WN4)

Our spectrum for MCA8 (Massey et al. 1987), differs from that originally published by Massey et al. (1987), their spectrum shows a weak He II λ4686 emission line as well as He I λ4471 which appears approximately equal strength. Whereas our observations show a typical, strong-lined early-type WN star with well resolved N V emission lines and an absence of He I λ4471.

2.2.1.5 MJ-G8 (M33-WR86, WN3–4)

This weak-lined WN star was identified by Massey & Johnson (1998) during their deep imaging survey of M 33. From our observations we have simply refined its spectral type to WN3-4.

2.2.1.6 MJ-G9 (M33-WR91, WN3)

Our observations of MJ-G9 (Massey & Johnson 1998) show a early-type WN star (WN3) due to the absence of N IV λ4057 and the presence of strong N V $\lambda\lambda$4604-4620. MJ-G9 also suffers from nebular contamination.

2.2.1.7 OB6-5 (M33-WR106, WN9)

This noisy spectrum contains He II λ4686 emission as well as a weak (tentative) detection of N II λ3995 emission. As a result we have refined the spectral classification slightly from WN8 to WN9.

2.2.1.8 UIT289 (M33-WR122, WN4+abs)

The most notable feature about this star is that the emission lines appear very weak, in contrast to the strong absorption lines. Even though the emission features are weak we tentatively classify UIT289 (Massey *et al.* 1996) as WN4+abs, due to the weak detection of N V. This is in agreement with the previous WN4 classification given by Massey *et al.* (1996).

2.2.2 WN/CE stars

2.2.2.1 MC48 (M33-WR83, WN/CE)

This is the only WN/CE star is our sample and its broad-lined spectrum contains both strong C IV λ5808 and nebular emission.

2.2.3 WC stars

2.2.3.1 MC33 (M33-WR52, WC4)

We have refined the spectral type for MC33 (Massey & Conti 1983) from WC to WC4. This star also interestingly appears to display weak C IV λ5471 emission.

2.2.3.2 MJ-C21 (M33-WR55A)

MJ-C21 (Massey & Johnson 1998) was another WN candidate found not to be genuine from our observations.

2.2.3.3 MC39 (M33-WR61, WC5+abs)

There is very little unusual about this 'typical' WC5 star, except that it appears to have faint signatures of absorption lines in its spectrum.

2.2.3.4 MC42 (M33-WR62, WC4)

MC42 (Massey & Conti 1983) is a broad-lined (FWHM(C IV) $\sim$ 70Å) WCE star which also shows strong nebular emission lines. Its spectrum closely resembles MC57 (M33-WR99), another WC4 star which has similar line widths and also shows strong nebular emission.

2.2.3.5 MC44 (M33-WR71, WC4)

The line profiles for MC44 (Massey & Conti 1983) show a strange morphology, especially for C IV λ5808. This could simply be an artifact of a incorrect sky subtraction. In fact it seems that some nebular lines have been over-estimated during the sky subtraction.

2.2.3.6 MC45 (M33-WR76, WC4)

MC45 (Massey & Conti 1983) was first identified by Wampler (1982) who labelled it Anon. 1. Wampler (1982) remarked that this star, which appeared as an unmarked object on the Wray & Corso (1972) identification plate, was bright in the λ4670 filter plate. Subsequent spectroscopy by Wampler (1982) identified Anon. 1 as a WC5 star, and appears very similar to our spectrum, with weak WR emission lines and strong nebular lines.

2.2.3.7 MC52 (M33-WR89, WC7+abs)

The spectrum for this late-type WC star has weak C IV λ5808 emission and is clearly contaminated by a hot OB star, with a series of narrow Balmer absorption lines present.

2.2.3.8 MC53 (M33-WR92, WC6)

MC53 (Massey & Conti 1983) is a narrow-lined WC star (i.e. FHWM(C IV) $\sim$ 30Å) where He II λ4686 is resolvable from the usually blended C III-IV λ4650 emission feature. C IV λ5471 also appears very weak. We revise the earlier classification of WC4–5 (Schild, Smith & Willis 1990) to a somewhat later WC6.

2.2.3.9 MC54 (M33-WR94, WC7+abs)

MC54 (Massey & Conti 1983) was noted by Massey & Johnson (1998) to be located NE of a brighter star, and its spectrum reflects this, as it is heavily dominated by strong Balmer absorption lines, with weak WR emission features. We revise the classification for this star from WCE (Massey & Johnson 1998) to WC7+abs.

2.2.3.10 AM14 (M33-WR105, WC6)

AM14 (Armandroff & Massey 1985) is relatively faint (V $\sim$ 21.3 mag) compared with other early-type WC stars in M 33. The overall emission line strength for AM14 is also weaker.

2.2.3.11 AM16 (M33-WR110, WC5)

The emission line strength for AM16 (Armandroff & Massey 1985) was very large for this WC5 star (i.e. log EW(C IV) $\sim$ 2000Å), potentially indicating that it does not suffer from contamination.

2.2.3.12 AM17 (M33-WR111, WC5)

This early-type WC star is similar to AM16 (Armandroff & Massey 1985), in that it has very strong, broad emission lines (i.e. log EW(C IV) $\sim$ 2000Å). O III-V λ5590 also appears unusually strong in AM17.

2.2.3.13 MJ-X9 (M33-WR121, WC4+abs)

We obtain WC4+abs for MJ-X9 (Massey & Johnson 1998), versus WNL?+abs from Massey & Johnson (1998), although only blue optical datasets were available to the earlier study. This star has exceptionally broad emission lines, plus an unusual morphology in the λ4660 region. We also detect clear Balmer absorption lines in its optical spectrum.

2.2.3.14 MC70 (M33-WR129, WC5)

Comparing the original spectra published for MC70 by Massey & Conti (1983), we find that instead of a spectrum heavily dominated by what appears to be nebular emission, we see a clean, well resolved early-type WC star. The widths for MC70 (Massey & Conti 1983) tend to be somewhat narrower compared with other WC4–5 stars in M 33.

2.2.4 Other stars

2.2.4.1 MJ-G1 (M33-WR43A)

MJ-G1 was identified as a WN candidate by Massey & Johnson (1998), although our observations did not confirm this. However, our observations for this star did find the presence of strong Hα emission.

2.2.4.2 OB6-25 (M33-WR77, Of)

We propose an Of spectral type for OB66-25 from Massey *et al.* (1996), alias HS-B205, Humphreys & Sandage (1980), rather than WN8 due to the weak He II λ4686 and N III $\lambda\lambda$4634-41 emission plus He II $\lambda\lambda$4542,5411 absorption. The spectrum for this star also contains strong nebular emission.

2.2.4.3 MJ-X16 (M33-WR118)

Our spectrum of MJ-X16 differs from that published by (Massey & Johnson 1998) in the sense that their weak, broad He II 4686 emission was not confirmed by our spectroscopy.

2.2.5 Photometry, distance and reddening to M 33

There have been a number of magnitudes quoted for the WR population in M 33 (e.g. Massey & Conti 1983; Drissen *et al.* 1990; Armandroff & Massey 1991; Massey & Johnson 1998), the majority of these magnitudes are quoted as 'continuum magnitudes'. Unfortunately the definitions for these continuum magnitudes vary between authors. For completeness we have listed the continuum magnitudes (equivalent to "AB" magnitudes at λ4750) calculated by Massey & Johnson (1998) in Table 2.2. For our purposes we have determined broad-band Johnson V and B magnitudes for our sample of apparent single WC stars in M 33; from two sources, archival HST WFPC2 images[3], where these were available. Photometry was performed on HST F555W images using the HSTPHOT package (Dolphin 2000), this procedure is similar to DAOPHOT but is fine-tuned for WFPC2 images, including corrections for QE variations, accurate PSF determinations, contamination as well as geometric and aperture corrections. We also obtained broad-band Johnson V and B magnitudes from archival CFHT-12K images[4]taken in August 2000 (see image;

[3]Credit: HST photometry was performed by L. Drissen (Univ. Laval).

[4]Credit: CFHT photometry was performed by P. Crowther (UCL).

Fig 2.2). Photometry was obtained using the DAOPHOT software package under IRAF, using nearby field stars observed by Macri *et al.* (2001) as photometric standards. Overall the HST photometry resulted in systematically fainter magnitudes for all but five WC stars, these variations were typically ~0.4 mag. These significant discrepancies are largely due to crowding, in which accurate sky subtraction is made difficult using ground-based observations. Photometry calculated from HST images were used in preference and are shown in Tables 2.4 and 2.5, unfortunately HST images were unavailable for a number of WR stars in our sample and so we use ground-based photometry taken from CHFT-12K.

M 33 is used as a primary indicator to calibrate extragalactic distance scales and to constrain the Hubble constant (H_0), and as a result its distance has been well studied (e.g. Kennicutt, Stetson, Saha, Kelson, Rawson, Sakai, Madore, Mould, Freedman, Bresolin, Ferrarese, Ford, Gibson, Graham, Han, Harding, Hoessel, Huchra, Hughes, Illingworth, Macri, Phelps, Silbermann, Turner & Wood 1998; Freedman, Wilson & Madore 1991). We chose to use a distance modulus of $(m - M)_0 = 24.56$ (corresponding to 816 kpc), obtained by Freedman *et al.* (2001) using revised Cepheid distances.

The reddening towards M 33 was examined by Sandage & Johnson (1974), Humphreys (1980), Johnson & Joner (1987) and more recently by Massey *et al.* (1995) and Massey (1998*a*). Massey *et al.* (1995) acquired a large sample of photometric observations for hot, luminous stars in a number of Local Group galaxies including M 33. They concluded for M 33 that the typical colour excess is $E_{B-V} \approx 0.16$; they also found that there is still a scatter of colour excesses amongst OB associations within the galaxy ranging from 0.06 – 0.33. These values, as well the the average reddening determined by Massey *et al.* (1995) are also consistent with those inferred by the earlier studies mentioned above.

As discussed in Section 2.1.2, our spectra could not be reliably flux calibrated and so accurate reddenings could not be determined for each star. For our purposes we have used a nominal value of $E_{B-V} = 0.15$, after taking the previous published values into consideration we feel that this is a representative value for M 33. Absolute magnitudes resulted from these 'generic' reddening. This approach is far from ideal. Nevertheless, an uncertainty of ± 0.1 mag in E_{B-V}, amounts to an uncertainty of 30% in luminosity.

Table 2.4: List of ground-based CFHT photometry for the WC stars in M 33 and where possible, space-based HST broad-band photometry.

M33-	HST			CFHT	
WR#	F336W	F439W	F555W	V	B
38	——	——	20.895	21.03	20.68
45	——	——	——	19.43	——
52	19.373	20.620	20.622	20.16	——
55	——	——	——	19.98	——
61	19.373	20.660	20.583	20.01	——
62	18.308	19.694	——	19.81	——
63	——	——	——	19.36	——
69	19.752	20.841	——	20.49	20.60
71	——	——	——	18.89	——
73	——	——	18.757	18.67	——
76	——	——	——	17.97	——
82	——	——	——	20.46	20.40:
84	——	——	——	20.48	——
89	18.418	19.635	19.739	19.83	——
92	——	——	——	19.50	——
94	——	——	20.550	18.83	——
95	——	——	21.165	20.75	——
96	20.388	21.507	21.298	21.02	——
99	19.440	20.670	20.423	20.55	——
105	——	——	21.264	21.56	21.71
110	——	——	21.278	20.79	20.88
111	——	——	20.576	20.73	20.36
116	18.435	19.634	19.661	19.61	19.41
120	——	——	——	18.22	——
121	17.961	19.230	19.084	18.04	——
125	19.029	20.339	20.542	19.94	——
129	18.720	19.940	19.935	19.87	19.77

Table 2.5: List of both HST and CFHT photometry for the WN stars in M 33, as well as three previous WN candidates identified by Massey & Johnson (1998).

M33-	HST			CFHT	
WR#	F336W	F439W	F555W	V	B
42	——	——	——	18.23	17.97
49	——	——	——	16.91	——
50	——	——	——	19.50	——
54	——	——	——	21.46	20.92
56	——	——	——	19.74	——
59	18.290	19.649	——	>18.60	——
60	——	——	——	19.74	——
74	20.527:	21.953:	——	21.18	20.75
77	——	——	——	18.54	——
78	——	——	20.561	20.66	——
80	——	——	——	20.57	19.84
83	——	——	——	19.40	19.60:
86	——	——	——	20.08	——
91	——	——	22.177	21.64	22.80:
103	16.437	18.050	18.198	18.08	——
106	16.858	——	18.187	18.62	——
122	17.982	19.477	20.128:	18.69	——
43A	——	——	——	19.57	——
55A	19.649	18.982	18.691	18.09	——
118	19.542	20.732	20.538	19.98	——

2.3 M 31

Observationally, M 31 is a more challenging target to study large stellar populations. Its large angular size and high inclination restricts the use of current multi-object spectrographs. Despite these limitations it proves an important laboratory for probing massive stars, as it is the largest and most metal-rich galaxy in our galactic neighbourhood.

2.3.1 Previous Work

The earliest searches for WR stars in M 31 were performed by Moffat & Shara (1983) using interference filters centred on strong WR emission lines. Their detection method

scanned approximately two thirds of M 31 using a series of narrow-band photographic plates centred on λ4670 to identify potential WR emission, and a number of broad-band B plates centered on $\sim$ λ4500 which served as continuum magnitudes. Their surveys uncovered 21 WR candidates of which 17 were later spectroscopically confirmed as bona-fide WR stars. This work was later extended by Moffat & Shara (1987), where they added a further 16 WR candidates using an imaging tube. Unfortunately these early studies only identified strong-lined WR stars.

Subsequently, there were further studies by a number of different groups (e.g. Massey *et al.* 1986; Armandroff & Massey 1991; Willis *et al.* 1992) who spectroscopically confirmed the majority of these WR stars. More recently work by Massey & Johnson (1998) increased the number of known WRs in M 31 to 48, with a few remaining candidates. This number is very low when compared with the number of known WRs in our galaxy (227; van der Hucht 2001), although this can be partly explained by the fact that the majority of these surveys have not identified a potentially large population of faint (weak-lined) WR stars, and that observational work has been hampered further due to the low inclination of the galaxy. There has also been recent observational evidence by Williams (2003) to suggest that the star formation rate in M 31 has been low over the past 100 Myr.

Apart from the work by Smartt *et al.* (2001*a*), very little analysis has been carried out on the WR population in M 31. This is mainly due to the poor quality of data achieved, such that beyond spectral classification and equivalent width measurements very little analysis was possible (e.g. Schild, Smith & Willis 1990; Willis, Schild & Smith 1992). We have obtained high resolution spectra with a good signal-to-noise such that a qualitative and quantitative analysis may be performed enabling us accurately determine stellar parameters. Unfortunately our sample is small but importantly we have data for both a WCL and a WO star, both of which are rare in themselves.

2.3.2 WHT-ISIS Observations of Wolf-Rayet Stars in M 31

Long-slit spectra of our WR stars in M 31 were observed using the ISIS double-armed spectrograph on the the 4.2-metre William Herschel Telescope. Figure 2.3 shows a schematic of a generic long-slit spectrograph such that a comparison can be made with a Multi-Object Spectrograph described in Section 2.1.2. Observations were made on two separate occasions, as we lost one and a half nights on our first observing run due to technical difficulties. The first set of observations were made on 3rd August 2002, with the other

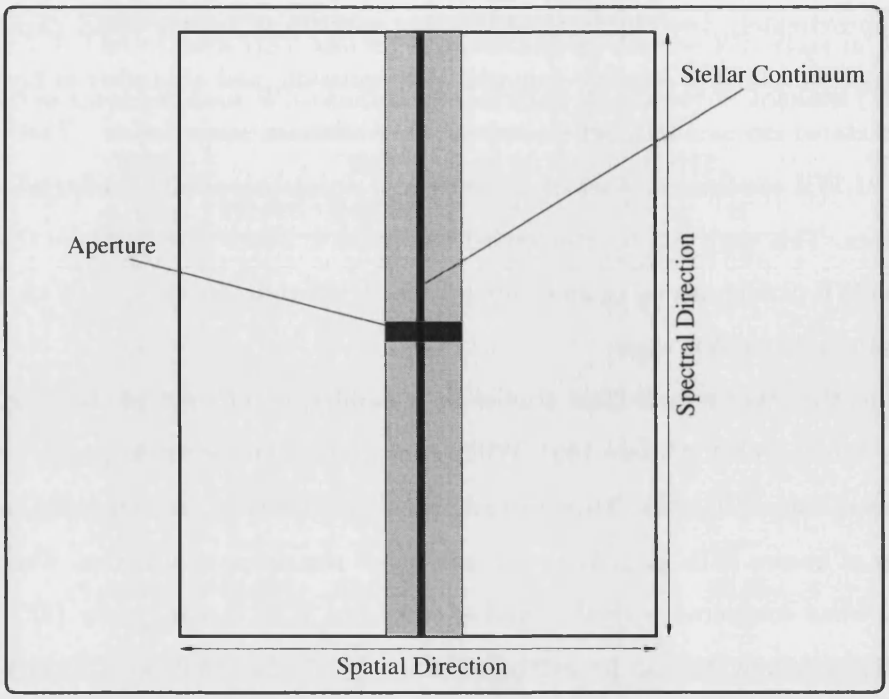

Figure 2.3: Schematic showing the data format for a generic long-slit spectrograph such that a comparison can be made with that of a Multi-Object Spectrograph (see Fig 2.1). The aperture width can vary depending on the object that is being observed.

set being made on 28th November 2002, unfortunately the second observing run ended prematurely due to bad weather. A list of observations is given in Table 2.6, all of these stars were observed on the 3rd August, except for OB48-WR1 which was obtained on the 28th November. Its important to note that long-slit observations were made in preference over using a Multi-Object Spectrograph due to the large angular separation between objects in M31, this is again another factor as to why observational studies in M31 have been restricted.

Our observational setup used the 6100 beam splitting dichroic such that light was simultaneously observed through both the blue and red channels. For the red arm we used the R300R grating along with the 4700 x 2148 MARCONI CCD (13.5μm pixels), whilst on the ISIS blue arm we used the R316B grating with the 4096 x 2048 EEV12 CCD (13.5μm pixels). This setup gave us continuous wavelength coverage from $\lambda\lambda$3500-9000, and dispersions of 0.84 Å/pix and 0.86 Å/pix for the red and blue arms respectively. Each target was observed through a 1″ slit, giving us a 3 pixel spectral resolution of 3Å. For our

Table 2.6: Observational target list of WR stars in M31, showing their coordinates, continuum magnitudes, galactocentric distance, and spectral classifications. These parameters were taken from Table 10, Massey & Johnson (1998). Star identifications are: MS = Moffat & Shara (1983); OB = Massey *et al.* (1986); IT = Moffat & Shara (1987). The OB associations designations are from van den Bergh (1964).

	Position (2000)				Spectral Type	
Alias	α	δ	ρ	m_{cont}	Previous	New
MS5	00 42 34.40	+41 30 22.2	0.62	—	WC7-8	WC8
MS12	00 40 19.46	+40 52 24.8	0.63	—	WC	WO4
MS21	00 39 11.00	+40 38 16.6	0.88	—	WCE	WC6
OB48-WR1,IT 5-01	00 44 55.54	+41 31 04.2	0.70	20.7	WC6-7	WC6

observations of the (faint) WR stars in M31 a slow readout speed was used in preference to reduce the readout noise. Exposure times were typically 2 x 3000s, although MS5 was only observed for 2 x 2400s owing to the fact that it was somewhat brighter than the other WR stars. The standard star BD+25 4655 was also observed with a 60s exposure, using an identical setup as described, immediately prior to the observations of the WR stars and was chosen due to its similar airmass.

The data were reduced and extracted using standard longslit packages under IRAF, using the standard data reduction procedures under *twodspec.longslit.* Once the spectra had been bias subtracted, they were flat field corrected using a normalized flat field taken with the internal quartz lamp. Next they were then cosmic ray cleaned, again using *kappa.bclean* package whilst still under IRAF, and finally extracted, making sure that the sky was consistently subtracted during this stage. It was then both wavelength and flux calibrated using the standard, well documented FIGARO packages (Shortridge *et al.* 1999). Telluric corrections were also made using the standard star BD+25 4655 to determine the strong absorption features. A sky subtraction was achieved using local sky regions within the slit.

The data were flux calibrated and checked for consistency between objects and different exposures, and the final flux calibrated standard star was also in excellent agreement with published values. During the observing run we also observed a number of well studied

Galactic WR stars. As an extra check we also compared these calibrated spectra against previously obtained spectra from independent sources and found excellent agreement. This gives us confidence in our absolute flux levels for our sample of stars and as a result we have calculated narrow-band v magnitudes for all four WR stars observed in M 31 (see Table 2.7). Figure B.1 shows the calibrated spectra for our four WR stars in M 31; we only show the region between $\lambda\lambda$4000-7000 to highlight the strong WR emission lines.

2.3.3 Notes on Individual Stars

2.3.3.1 MS5 (WC8)

MS5 (Moffat & Shara 1983) is a bright, weak-lined WC8 star. It has narrow emission lines (i.e. FWHM(CIV) $\sim$ 30Å), typical for late-type WC stars.

2.3.3.2 MS12 (WO4)

Using the classification scheme by Crowther, de Marco & Barlow (1998) we have revised the spectral classification for MS12 (Moffat & Shara 1983). We obtain WO4 for MS 12 owing to the presence of highly ionized oxygen lines. Its spectrum predominately resembles a broad-lined WC4 star, although O IV λ3412 and O VI λ3834 appear strong and resemble an early WO-type.

2.3.3.3 MS21 (WC6)

MS21 (Moffat & Shara 1983) looks like a typical WC6 star and is almost identical to another WC6 star in M 33, MC26 (Massey & Conti 1983), as it has extremely similar line strengths and line widths. We refine the spectral classification for MS21 from WCE (Massey & Johnson 1998) to WC6.

2.3.3.4 OB48-WR1 (WC6)

We classify OB48-WR1 (Massey *et al.* 1986) as another WC6 star, in agreement with that found by Massey *et al.* (1987*a*). Compared with MS21 its line strength is somewhat weaker.

Table 2.7: Observed spectrophotometry of WC stars in M31, both narrow-band v and broad-band V magnitudes are shown. Our calculated absolute magnitudes are also shown, assuming a distance of 752Kpc, along with the derived reddenings.

Star	Spectral Type	m_v (mag)	m_V (mag)	E_{B-V}	M_V (mag)
MS5	WC8	18.82	18.82	0.26	-6.37
MS12	WO4	20.41	19.83	0.42	-5.85
MS21	WC6	21.15	20.73	0.43	-4.98
OB48-WR1	WC6	19.46	19.23	0.34	-6.21

2.3.4 Photometry, distance and reddening to M 31

Table 2.6 lists our observed WR targets in M31; it also contains coordinates, continuum magnitudes, galactocentric distances, ρ (as a fraction of the Holmberg radius), and spectral classification, all taken from the work by Massey & Johnson (1998). It can be seen that in most cases very little is known about most of the WR stars in M31. The spectral classification have been refined with no noticeable changes, except for MS12 which has been revised from WC to WO4. MS5 was also confirmed as a rare, late-type WC8 star.

We are confident that we achieved an accurate flux calibration for our dataset, as a result we derived spectrophotometric narrow-band and broad-band V magnitudes (see Table 2.7). Apart from OB48-WR1 there is no published photometry for any of the WR stars in our sample. Massey *et al.* (1986) measured OB48-WR1 to have a continuum magnitude (equivalent to "AB" magnitudes at λ4750) of 20.7. We found, from our narrow-band v magnitude (equivalent to λ5160), that OB48-WR1 is somewhat brighter at 19.46. From the line strength of the C III λ5696 and C IV λ5808 MS5 looks like is either in a multiple system, or that the continuum has been diluted by another nearby star. This theory is supported by the fact that is significantly brighter than the other three WR stars in our sample, and that even for a WCL star, the equivalent widths measured for MS5 are low.

The distance to our nearest spiral galaxy, M31 has been well studied and is used as a primary distance indicator (e.g. Freedman *et al.* 1991; Holland 1998). The distance has been measured using a number of different methods although the most commonly used method is using observations of Cepheids. This method was used during an extensive

study of many of the local group galaxies as part of one of the Hubble Space Telescope Key Projects (see Kennicutt *et al.* 1998). Original observations suggested a distance to M 31 of (m - M) = 24.42 (D = 796kpc), these observation have since been revised (Freedman *et al.* 2001), and after the refinements were included, the distance was finally determined as (m - M) = 24.38 (D = 752kpc). It is this distance of 752kpc that is adopted for all our calculations.

The reddenings towards our objects were independently obtained from the model fits to the calibrated spectra, de-reddening our observations until the flux distribution matches the theoretical model. Massey *et al.* (1995) observed a large sample of stars situated in crowded regions within M 31. They used their photometric and spectroscopic results to infer a reddening towards each observed field. Although unlike M 33 and NGC 6822, the reddening towards M 31 did not agree between the spectroscopic and photometric set of results. They conclude that the reddening in M 31 is peculiar, with an average value of $E_{B-V} = 0.16 \pm 0.01$, they also found that the average reddening also varied between a number of OB associations ranging from $E_{B-V} = 0.14 - 0.23$. We suggest that from our spectroscopic observations that the reddening towards our objects is in fact larger. This is not surprising considering the high inclination of the galaxy, and may (partly) explain why such a variable reddening was noted by Massey *et al.* (1995).

This variable reddening was also reported by other authors, Barmby *et al.* (2000) observed a substantial number of globular clusters in M 31. They found that from the distribution of 221 reliable reddenings, the average was $E_{B-V} = 0.22$. It must be added that there was still a huge range of reddenings within their sample, the largest reliable reddening as high as $E_{B-V} = 1.38$ (globular cluster 037-B327), although this was an extreme case. We are confident that our assumed reddenings are well within previously determined values.

2.4 IC 10

"IC 10 is one of the most curious objects in the sky"
- Hubble (1936)

This quote by Edwin Hubble describing IC 10 has turned out to be almost prophetic as the mysteries of IC 10 have puzzled astronomers for decades - this work has attempted to

help resolve at least part of the questions surrounding IC 10. One reason this nearby dwarf irregular galaxy has proven so interesting is its extraordinarily high star formation rate. There have been numerous different studies suggesting that IC 10 has recently under-gone an intense burst of activity. This evidence for a unusually high star formation rate is inferred from its large population of H II regions (Hodge & Lee 1990), its observed non-thermal radio continuum (Yang & Skillman 1993), its large far-IR luminosity (Melisse & Israel 1994), and more directly from its high surface density of massive stars (Massey & Armandroff 1995). Later observations by Massey & Johnson (1998) also found an unusually high WR population; not only were there a surprising number of WR stars, but the observed WC/WN ratio was also remarkably high. This is especially odd considering that metallicity studies have indicated that IC 10 has a metallicity similar to that of the SMC ($\sim 0.2 Z_{\odot}$), yet its WC/WN ratio was higher than any other Local Group galaxy studied. This work will re-address this issue through new, high-resolution spectroscopy.

2.4.1 Previous Work

Previous observational programs to study the massive star content in IC 10 have been hampered due to the low inclination towards the galactic plane, and hence the large interstellar reddening (see Section 2.4.3). The first narrow-band surveys by Massey, Armandroff & Conti (1992) found 16 'significant' candidate WR stars, this number was later increased when another, more thorough, survey by Royer *et al.* (2001) detected a further 13 new WR stars, more importantly they claimed that three of these were WC9 stars. Given the metallicity of IC 10 (12+log(O/H) = 8.19; Lee *et al.* 2003) this was very surprising considering that previously the only WC9 stars to be identified were located in the Solar neighbourhood where the metallicity is approximately solar. Not only this but in other detailed surveys of both Magellanic Clouds where the metallicities are much lower, the only WC stars found are that of early type WC4–5. This speculation of WC9 stars added to the curious nature of IC 10. Most recently the WR content was again examined with the use of narrow-band photometry by Massey & Holmes (2002). They obtained deep exposures of IC 10 and claimed to have found a large number of objects with significant He II λ4686 emission, which they infer are the currently large unidentified WN population which would alter the WC/WN ratio to a more sensible value.

2.4.2 Gemini-GMOS Observations of Wolf-Rayet Stars in IC 10

Due to the very limited number of spectroscopically confirmed WR stars we undertook an observational programme to observe almost all the known WR population in IC 10. This was achieved using the Gemini Multi-Object Spectrograph (GMOS) on the 8-metre Gemini-North telescope between 21st December 2001-16th January 2002. The observational procedure is very similar to that described in Section 2.1.2. After deciding on the location of the target stars, two masks were made, encompassing ~15 WR candidates in each field, there was a slight over-lap of the fields. The coordinates for these fields are given in Table 2.8.

The GMOS instrument consists of three 2048 x 4608 EEV CCDs with 13.5μm pixels, they are aligned in the dispersion plane to give a total detector area of 6144 x 4608 pixels. The three CCDs are positioned with only a narrow gap of 0.5mm between each detector. Each "slitlet" within the masks were cut to a 1″ width, and in conjunction with the B600 grating we achieved a 2 pixel spectral resolution of 5Å. Multiple exposures were taken for both fields of 5 x 3600sec and 4 x 3600sec for fields A and B respectively. Where possible spare slilets were made to observe 'blank' sky regions or nearby H II regions. The total wavelength coverage achieved differed wildly depending on the vertical (or spectral) direction within the mask, although with our grating centered around λ5600, we aimed to observe a spectroscopic coverage of $\lambda\lambda$4000-7000. Failing this we aimed to at least include both strong, distinguishing WR features around λ4686 and λ5808 for classification purposes.

The data reduction was achieved using the Gemini pipeline package *gemini.gmos* written and supported under IRAF. This package is specific to GMOS data and as a result it converts the data into a multi-extension format (MEF). Our method of reduction followed standard procedures within the pipeline; bias subtraction, flat field correction. After this we extracted the (partly) reduced image and cosmic ray cleaned them using *kappa.bclean* package under IRAF, as the current version for the reduction does not support this option. Once they had been cleaned they were replaced into their original format. The wavelength and extraction stages within the pipeline package vary from other Multi-Object Spectrograph reduction packages, as each slitlet is automatically cut into yet more file extensions. Now each 2-D spectrum is wavelength calibrated using the observed internal CuAr arc lamp, the next interactive stage sky subtracts each spectra before the data is

Table 2.8: Observed log for the two fields for IC 10, including the central coordinates for each field.

Field	Position (2000)		Epoch
	α	δ	
IC10-A	00 20 28	+59 17 40	Dec. '01/Jan. '02
IC10-B	00 20 14	+59 18 25	Dec. '01/Jan. '02

finally extracted. At this stage the data were converted into single extension files and flux calibrated using standard IRAF packages under *noao.onedspec*. The flux calibration used a 60 sec exposure of the standard star G191-B2B. We are confident that our flux calibration was accurate as our spectrophotometry agrees well with previously published narrow-band photometry.

Unfortunately due to the small spatial scales between each WR star in IC 10 we were unable to observe all 28 candidates with GMOS. Subsequently a small sample of known WR stars were included in our observing run at the 3.6-metre CFHT on 18th October 2001, using MOS. Full details of the instrument and data reduction can be found in Section 2.1.2. To summarise, we used the 2048 x 4500 EEV1 CCD with 13.5μm pixels, each slit was cut to a width of 1.5″, which gave as a spectral resolution of 7Å with the B600 grating. Three exposures were taken using integration times of 1200 secs. We were unable to flux calibrate the data for reasons outlined in Section 2.1.2.

Between both datasets we observed 27 of the 28 WR candidates (15 from Massey & Armandroff (1995) and 13 from Royer *et al.* (2001)), with 24 in our GMOS dataset and 17 observed with CFHT. The one candidate that we failed to observe was WR15 from Massey & Armandroff (1995), although the classification of this star was confidently assigned spectroscopically by Massey & Armandroff (1995).

2.4.3 Photometry, distance and reddening to IC 10

We use the photometric observations taken from Royer *et al.* (2001), in which their photometric filter system centres on λ_c=5055, with a FWHM=51Å, this is close the to narrow-band v WR filter devised by Smith (1968). For the few cases where we do not have photometric observations for our candidate WR stars we quote spectrophotometric values. These values agree exceptionally well with those by Royer *et al.* (2001), to within

~0.1 mag, and are listed in Table 2.9. For consistency we have also shown the broad-band V magnitudes calculated from HST WFPC2 images taken through the F555W filter, presented by Crowther *et al.* (2003).

Due to the low inclination of IC 10 within the Galactic plane (l, b = 119°,-3°) the observed interstellar reddening is very high. This has hampered observational studies of this galaxy in the past, especially in the optical regime and is one of the reasons that previous observational programmes have been limited. There have been a number of published values for the fore-ground reddening, with estimates ranging from E_{B-V} = 0.77 - 0.91 (Richer *et al.* 2001; Lee *et al.* 2003). IC 10 also contains high quantities of internal dust (Richer *et al.* 2001) which explains the variety of published reddenings for this galaxy. As our observations for the WR population within IC 10 are accurately flux calibrated, when we model these results we are able to obtain individual reddenings towards each WR star (see Section 6.5). We also calculate less accurate reddenings from the photometry which is listed in Table 2.9. Here we quote the published values by Royer *et al.* (2001), which by their notation relates to $c_1 - c_2$, but is equivalent to $(v - r)$. We calculate the interstellar reddening, E_{b-v} assuming an intrinsic colour of $(v-r)_0$ = -0.2 mag, and taking into account $E_{b-v} \sim E_{v-r}$ using a standard extinction law.

As with the reddening determinations (and as a result of the variable reddening), the distances calculated for IC 10 have also varied. In recent years this variation has narrowed somewhat to approximately 700kpc. Kennicutt, Stetson, Saha, Kelson, Rawson, Sakai, Madore, Mould, Freedman, Bresolin, Ferrarese, Ford, Gibson, Graham, Han, Harding, Hoessel, Huchra, Hughes, Illingworth, Macri, Phelps, Silbermann, Turner & Wood (1998) determined the distances to a number of Local Group Galaxies using a variety of methods. Using the period-luminosity relation for Cepheids they calculated a (m - M) = 24.57 (D = 820kpc). Sakai *et al.* (1999) then published a much lower value for the distance to IC 10, they quote (m - M) = 24.1 (D = 660kpc) using Cepheid variables, and (m - M) = 23.50 (D = 500kpc) using the tip of the RGB. More recently near-IR photometric observations by Borissova *et al.* (2000) re-evaluated the distance to IC 10 with respect to IC 1613 as this distance is known more accurately. They calculate a distance of (m - M) = 23.86 (D = 590kpc). It is this distance that we will adopt for our studies of WR stars in IC 10, as we feel that considering the high foreground reddening and variable dust content, near-IR studies are more favourable.

Table 2.9 also lists absolute magnitudes using the narrow-band photometry from Royer

et al. (2001), assuming a distance; D = 590kpc. Our reddenings are a little uncertain but agree with previous studies and compare with other WR stars in the Local Group (van der Hucht 2001).

2.4.4 New Wolf-Rayet Catalogue

We revise the known WR population in IC 10, including WR stars previously identified and observed by Massey, Armandroff & Conti (1992), referred to as [MAC92]# and Royer *et al.* (2001), referred to as RSMV#. Table 2.9 list 26 WR stars, all of which have been spectroscopically confirmed, in IC 10. Where high spatial resolution (via HST WFPC2 imaging) reveals multiple components we indicate these components with A, B etc, this nomenclature is recommended to avoid confusion.

Generally we refine spectral classifications, except for [MAC92]5, which we revise from WN to a rare WN/CE intermediate type WR star. This revised classification helps explain the discrepancies between the two authors for this star - Massey, Armandroff & Conti (1992) reported a WN star, from spectroscopic observations - whereas narrow-band photometry presented by Royer *et al.* (2001) identified an early-type WC star. Also our GMOS spectroscopy did not reveal two WR candidates identified by Massey, Armandroff & Conti (1992); [MAC92]3 and [MAC92]16 to be genuine WR stars.

Our dataset also includes spectroscopic observations of the 13 WR candidates identified photometrically by Royer *et al.* (2001). Ten of these candidates were observed with Gemini-GMOS, whilst the remainder (RSMV 1, 10 and 11) were observed using CFHT-MOS. We reveal that 9 of these candidates are bona-fide WR stars, while the three potential WC9 stars identified (RSMV 1, 3 and 7), plus the WC candidate RSMV 4 were all found not to be genuine WR stars.

Recently, Massey & Holmes (2002) spectroscopically confirmed two new emission line stars in IC 10. Crowther *et al.* (2003) argue against the debatable WR nature for their WR24. They discuss the fact that the published spectrum for this star closely resembles a O3IfWN star, like Melnick 42 in the LMC, especially as it has a lower line strength and similar FWHM as Melnick 42. Massey & Holmes (2002) also pointed out that this star was bright and as such indicated a WN star. Inspection of HST/WFPC2 F555W images in fact reveals three separate sources all within 1″ from the central coordinates listed by Massey & Holmes (2002), such that a ground-based telescope would be unable to clearly resolve all three components. The brightest of the three (labelled A; see Appendix C.1) signifi-

Table 2.9: Spectroscopically confirmed Wolf-Rayet stars in IC 10, plus Of/WN candidates, from catalogues of Massey et al. (1992, [MAC92]#), Royer et al. (2001, RSMV#) or Massey & Holmes (2002). Broad-band V and narrow-band v magnitudes are taken from archival WFPC2 imaging and Royer et al. (their c1), respectively, except those in parenthesis, which are obtained from GMOS spectrophotometry. See text for determination of absolute magnitudes. Line equivalent widths (W_λ) and FWHM refer to He II λ4686 for WN stars, and C III $\lambda\lambda$4647–50/He II λ4686 plus C IV $\lambda\lambda$5801–12 for WC stars.

Name	Position (2000)		m_V	m_v	E_{b-v}	M_v	Spectral Type		GMOS
#	α	δ	mag	mag	mag	mag	Old	New	Field
[MAC92]1	00 19 56.97	+59 17 08.0	—	22.0	1.02	−6.0	WC	WC4-5+abs	Can,MOS
[MAC92]2	00 19 59.65	+59 16 55.3	—	21.7	1.17	−7.0	WC	WC4	Can,MOS
RSMV 6	00 20 03.02	+59 18 27.4	(22.5)	22.8	1.22	−6.1	WC	WC4	Can
RSMV 5	00 20 04.24	+59 18 06.6	(22.0)	22.4	1.44	−7.4	WC	WC4–5+abs	Can,MOS
[MAC92]4	00 20 11.55	+59 18 58.3	(20.1)	20.3	1.26	−8.7	WC	WC4–5	Can
[MAC92]5	00 20 12.85	+59 20 08.5	(22.4)	23.2	1.14	−5.3	WN	WNE/C4	UK,Can
RSMV 13	00 20 15.62	+59 17 22.2	(23.8)	(24.0)	(0.7:)	−2.8:	WN	WN5	UK
RSMV 9	00 20 20.33	+59 18 40.2	(22.0)	21.6	1.16	−7.0	WN7	WNE+abs	UK
RSMV 8	00 20 20.56	+59 18 37.8	(20.8)	20.8	1.11	−7.6	WN8–9	WN10	Can
[MAC92]7	00 20 21.87	+59 17 41.5	(19.4)	19.6	1.01	−8.4	WC	WC4–5+abs	Can
[MAC92]9	00 20 22.60	+59 18 47.26	23.1	(23.9)	(0.8:)	−3.2:	WN	WN3	UK
RSMV 11	00 20 22.68	+59 17 53.91	22.8	—	—	—	WC	WC4	MOS
[MAC92]10	00 20 23.36	+59 17 42.6	(20.9)	22.2	0.98	−5.7	WC6–7	WC7	Can
RSMV 12	00 20 25.61	+59 16 48.60	22.7	(23.8)	(1.3:)	−5.4:	WN	WNE	Can
[MAC92]12	00 20 26.17	+59 17 26.90	21.9	22.0	1.0[a]	−6.0	WC	WC4+a	UK

Table continued on next page .....

Name	Position (2000)		m_V	m_v	E_{b-v}	M_v	Spectral Type		GMOS
#	α	δ	mag	mag	mag	mag	Old	New	Field
RSMV 10	00 20 26.48	+59 17 05.32	22.9	—	—	—	WC	WC4	MOS
[MAC92] 13-A	00 20 26.63	+59 17 33.20	20.8	21.4	1.03	−6.7	WC	WC5–6	Can
[MAC92] 13-B	00 20 26.62	+59 17 33.40	23.1	—	—	—			
[MAC92] 14-A	00 20 26.87	+59 17 20.21	20.7	21.4	1.0[a]	−6.6	WC	WC5	UK
[MAC92] 14-B	00 20 26.91	+59 17 20.34	22.4	—	—	—			
[MAC92] 15	00 20 27.03	+59 18 18.6	—	23.3	1.05	−4.9	WC6–7		
[MAC92] 24-A	00 20 27.67	+59 17 37.7	18.8	—	—	—	WN	WN+OB?	
[MAC92] 24-B	00 20 27.82	+59 17 37.5	21.3	—	—	—			
[MAC92] 24-C	00 20 27.75	+59 17 36.3	22.0	—	—	—			
RSMV 2-A	00 20 28.00	+59 17 14.63	21.4	22.4	1.24	−6.5	WN7–8	WN7–8	UK
RSMV 2-B	00 20 28.04	+59 17 14.87	25.1	—	—	—			
[MAC92] 17-A	00 20 29.05	+59 16 52.3	22.5	—	—	—	WN	WNE+OB	Can
[MAC92] 17-B	00 20 28.98	+59 16 51.9	22.2	—	—	—			
[MAC92] 19-A	00 20 31.01	+59 19 04.53	22.6	23.3	1.32	−6.0	WNE	WN4	UK,Can
[MAC92] 19-B	00 20 31.01	+59 19 05.25	24.0	—	—	—			
[MAC92] 23	00 20 32.79	+59 17 16.4	—	—	—	—	WN7–8		
[MAC92] 20	00 20 34.46	+59 17 14.71	22.0	(22.8)	(0.7:)	−3.9:	WC	WC5	UK
[MAC92] 21	00 20 41.64	+59 16 25.3	—	23.4	0.76	−3.6	WN	WN4	UK

(*a*): Set at E_{b-v}=1.0 due to severe contamination of ground based photometry by nearby red stars (see text).

cantly contributes to the observed continuum (V$\sim$19.8 mag). To confuse the prospect of identifying the individual WR component for WR24, all three sources have U–V colours that are consistent with early-type stars. Due to the severe crowding in the vicinity of this star (with two more bright sources both located within 2″), considering both imaging and spectroscopy, we conclude the object is either a WN+OB binary, or a WN star which is contaminated from a cluster of OB stars.

Finding charts for all confirmed WR stars, published in Crowther *et al.* (2003), are presented in Appendix C. They include ground-based, He II λ4686 narrow-band imaging from the 4-metre WHT[5] telescope, and space-based, HST WFPC2 images, which are used to resolve several WR stars into multiple components, A and B.

2.5 NGC 300

To-date, the majority of observational studies searching for WR stars in the Local Group have been focused on the Milky Way, Magellanic Clouds, M 33 and M 31. These discoveries all used 2-4m class facilities, and constrained the viability of observational studies beyond the Local Group. However, with the availability of modern 8m class telescopes it is now possible to obtain deep, high resolution images of galaxies beyond the Local Group allowing us not only to identify new WR populations, but to study them in detail.

2.5.1 Previous Work

NGC 300 is a late-type spiral (Sc) located in the nearby Sculptor Group of galaxies. As with the Local Group, observations suggest that the smaller members of the Sculptor Group are concentrated in several spatially separated loose groups around the larger spirals, NGC 300, NGC 253, and NGC 7793 (Karachentsev *et al.* 2003). In fact there are often references to NGC 300 being the Sculptor Group's counterpart to M 33, both are large, late-type spirals, that are orientated at low inclinations. Unlike M 33, where numerous observational studies have identified possible WR candidates, spectroscopically confirming 141 (Massey & Johnson 1998), the known WR population in NGC 300 is less clear.

The earliest signatures of WR stars in NGC 300 were recorded by D'Odorico, Rosa & Wampler (1983) who detected two WR stars whilst studying 16 H II regions. In the same year another study of H II regions in the Sculptor Group also remarked that from their

[5]WHT images kindly provided by P. Royer (Univ. Liège)

sample (also totalling 16) two H II regions displayed broad He II λ4686 emission - indicative of WR stars (Webster & Smith 1983). Later a further four WR stars were identified by Deharveng *et al.* (1988) while cataloging 176 H II regions within NGC 300. These independent findings clearly signalled a hidden WR population, although a systematic survey to target individual WR stars within NGC 300 was not undertaken until the work by Schild & Testor (1991). By using the well tested method of interference filters they were able to identify a number of WR candidates, three of the most obvious candidates were spectroscopically confirmed. This survey was later extended, confirming a further 10 previously undetected WR stars. Breysacher *et al.* (1997), found a further six WR stars located in five associations within NGC 300, again using the technique of interference filters. Finally, Bresolin *et al.* (2002) inadvertently discovered a late-type WN star in NGC 300 while spectroscopically surveying blue supergiants, increasing the total known WR population in NGC 300 to 22.

2.5.2 VLT-FORS2 Observations of Wolf-Rayet Stars in NGC 300

The majority of the previous studies have mainly focused around H II regions and associations. We have undertaken a deep narrow-band survey of NGC 300 using VLT-FORS2. Observations were taken with the VLT UT2 (Kueyen) telescope, using the Focal Reduced/Low Dispersion Spectrograph #2 (FORS2) between September 2nd-3rd 2000. Even though the conditions were photometric the two nights suffered from variable seeing conditions, ranging from 0.6 – 3.5″. Best attempts where subsequently made to alter the observing mode between imaging and spectroscopy during these highly variable conditions.

In imaging mode the standard collimator was used achieving a field-of-view of 6.8′ x 6.8′ with a scale of 0.2″/pixel. All observations were taken using the 2048 x 2048 Tektronix CCD with 24μm pixels. Imaging mode was favoured during spells of good seeing, typically 0.8″, unfortunately our field-of-view only permitted partial coverage of the galaxy losing the extreme west edge of the galaxy. NGC 300 was observed through two interference filters, the first centred at 4684 Å, and the second centred at 4781 Å, these filters had band widths of 66 Å and 68 Å respectively. As discussed in section 1.3.1, these filters are located to match known, strong WR emission features, and a region of relatively free emission. Two 600sec exposures were obtained through both narrow-band filters, centred at α: 0 h 54 m 59.0 s and δ: –37° 40′ 59″ (2000). Two more sets of images were also taken through broad-band Bessel B and V filters, typically with shorter exposure times of 120sec.

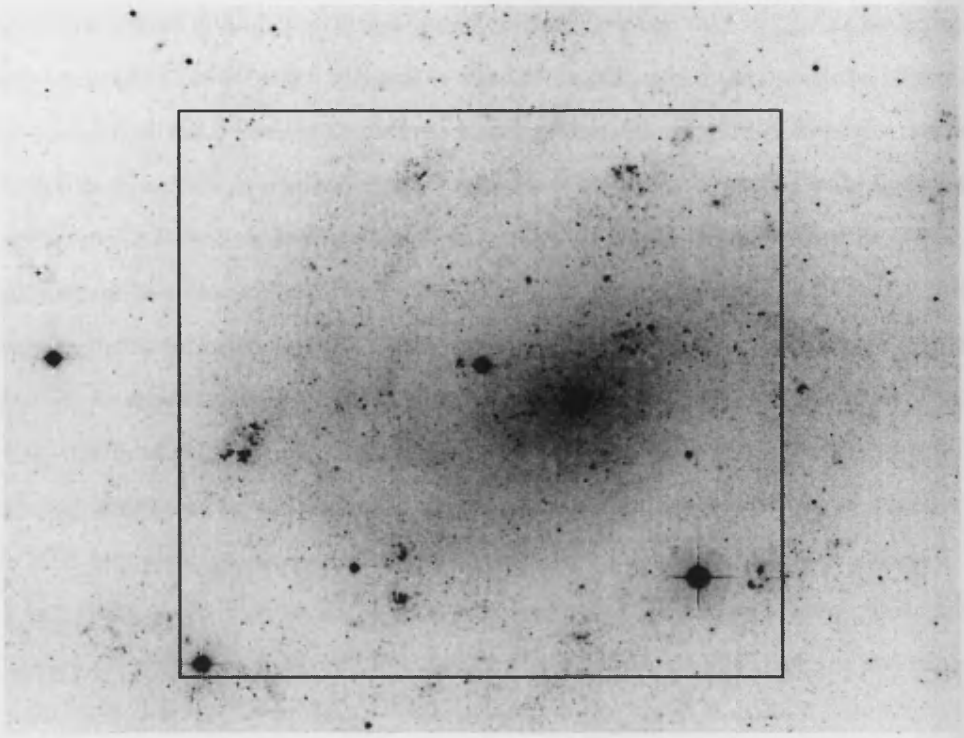

Figure 2.4: Zoomed in R-band image of NGC 300 taken with the ESO 2.2m WFI (see `http://www.eso.org/outreach/press-rel/pr-2002/phot-18-02.html`). The VLT-FORS2, 6.8′ x 6.8′ field-of-view is also shown. North is up and east is to the left.

Unfortunately due to moderate seeing conditions only one V-band image was suitable for measuring stellar magnitudes. Furthermore, it was slightly offset with respect to our other images which resulted in eight WR candidates lacking observed, m_V, magnitudes. This restriction meant that magnitudes were only obtained for WR candidates located east of 00 h 54 m 46.7 s. Figure 2.4 shows an archival ESO R-band image of NGC 300 taken with the 2.2m Wide Field Imager (WFI)[6], the observed VLT-FORS2 field is outlined. Figure 2.5 contains a typical FORS2 V-band image of NGC 300, showing the relevant finding charts, which can be found in appendix D.

Standard IRAF packages were used under CCDPROC to trim, bias subtract and flat field the images. Our photometry was obtained using the DAOPHOT software package, and converted into absolute fluxes using standard field stars in NGC 300 given by Pietrzyński *et al.* (2002).

[6]Kindly provided by Mischa Schirmer; ESO.

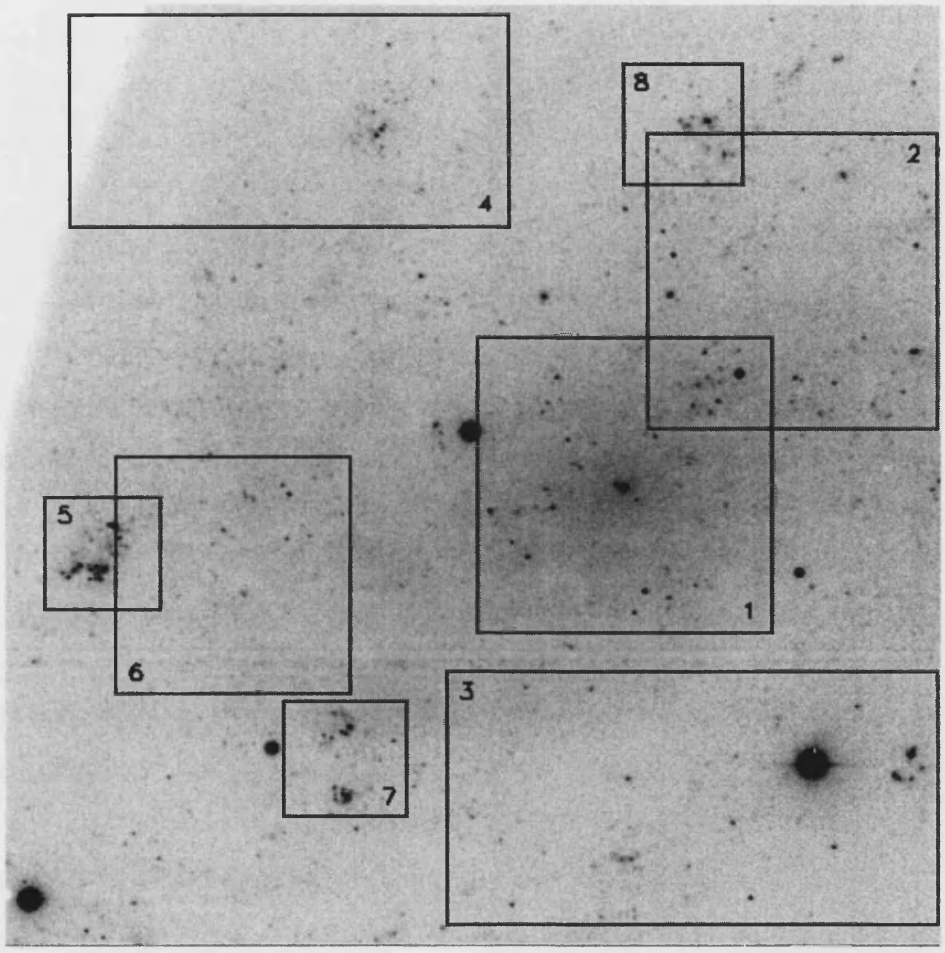

Figure 2.5: V-band image of NGC300 taken with VLT-FORS2 covering a field-of-view of 6.8′x6.8′. The location of the finding charts are shown, the numbers relate to the order in which they appear in Appendix D. North is up and east is to the left.

Spectroscopic[7] observations were taken for a select number of WR candidates directly following the narrow-band imaging, as narrow-band photometry was not available before the observing run. FORS2 was used in long slit mode (LSS), using the 300V grating and the GG435 filter. Targets were observed through a 1.0″ slit giving a spectral coverage of $\lambda\lambda$3500 – 8970 at a dispersion of 1.7 Å/pixel. Exposure times of 1800sec were used to observe eight targets, where possible two objects were simultaneously placed within the slit using the FORS Instrument Mask Simulator (FIMS) software to adjust the position angle. Two standard stars, Fiege 110 and LTT 1788, were observed using the same observational setup but with shorter exposure times, allowing an accurate relative flux calibration. These standards where then absolute flux calibrated by convolving their spectra with narrow-band *b* and *v* filters (Smith 1968), which are approximated to our continuum filter at 4684 Å. Spectroscopic observations were also made for three more stars but at a higher resolution. These were made with the same filter but using the 600R grating, this gave a shorter spectral coverage of $\lambda\lambda$5330 – 7540, at a dispersion of 0.7 Å/pixel. Exposure times of 1800sec were also used, and the same standards were observed as before but under the revised configuration. The data were bias subtracted, flat-field corrected, extracted, and both wavelength and flux calibrated using standard FIGARO (Shortridge *et al.* 1999) procedures. The flux calibrated, low dispersion FORS2 spectra can be found in Figures D.9 and D.10. We obtained spectra of four WC stars in NGC 300, previously identified by Schild & Testor (1992) and Schild & Testor (1991), and four newly identified WR stars in NGC 300.

From our improved spectra we have revised a number of previously determined spectral classifications. #24, alias WR11 (Schild & Testor 1992) had earlier been assigned as a WC5, we refine this to WC4 as C III λ5696 is very weak, and the $W_\lambda(\lambda5696)/W_\lambda(\lambda\lambda5801\text{-}12)$ ratio indicates a WC4 star (Crowther *et al.* 1998). We also revise the original classification of #29, alias WR3 (Schild & Testor 1991), from WC4-5 to WC5, due to the positive, but weak detection of C III λ5696, we also identify a weak signature of O III-V λ5592. The same revision was also made for #40, alias WR6 (Schild & Testor 1992), which we revised from WC4-6 to WC5, for the same reasons as described above for #29, although comparing the emission line strengths for these two stars, we find #29 is probably single (e.g. $W_\lambda(\lambda\lambda5801\text{-}12)\sim800$ Å, comparable with known single Galactic and LMC WCE stars).

[7]Credit: Spectroscopic reductions and observations of NGC 300 were made by P. Crowther (UCL).

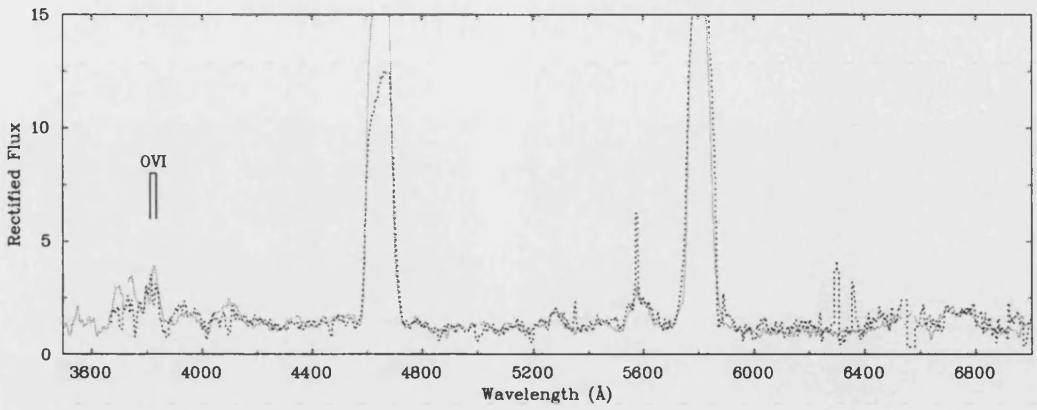

Figure 2.6: Plot showing the rectified spectrum of a WO4 star, MS12 (solid), in M 31, and the WR star NGC300-#48 (dotted), in NGC 300. Their optical spectra are extremely similar, plus there is strong evidence of O VI $\lambda\lambda$3811,3834 emission in NGC300-#48 and as such is re-classified as WO4.

Finally, we amend the classification of #48, alias WR13 (Schild & Testor 1992), which was originally classified as a WO4 by Breysacher *et al.* (1997), due to the broad C IV $\lambda\lambda$5801-12 detected, but latter re-classified WC4 by (Schild *et al.* 2003). Although on re-investigation of our improved spectroscopic observations we re-adjust this classification for #48 back to WO4, due to the detection of O VI $\lambda\lambda$3811-34 which are present in WO stars (see Fig. 2.6). Willis *et al.* (1992) discussed the problems with classifying WC stars from FWHM measurements alone. We also suspect that #48 is also single since $W_\lambda(\lambda\lambda 5801\text{-}12) \sim 1500$ Å.

Our observations also confirm four new WR stars, two WC stars and two WN stars, all of which were identified from our imaging survey. Both the newly found WC stars, #1 and #22 have broad emission lines but were classified WC4 owing to the absence of C III λ5696, and weak detection of O IV $\lambda\lambda$3811-34. The WN stars are both early-type, due to presence of N V and weak/absent detection of N III. We use the 'modified', (two-dimensional) WN classification scheme devised by Smith *et al.* (1996) to classify #9 as WN4-5 and #30 as WN3-4.

2.5.3 Photometry, distance and reddening to NGC 300

Due to the limited number of observational studies previously undertaken of NGC 300, there are very few published photometric observations of WR stars. We have obtained

Table 2.10: List of colour excesses towards the H II regions in NGC 300, determined using the C(Hβ) values (expect for the data by Christensen, Petersen & Gammelgaard 1997).

Number H II	E_{B-V}			References
Regions	Average	Min	Max	
6	0.47	0.21	0.58	1
15	0.32	0.22	0.59	2
12	0.17	0.08	0.25	3
42	0.28	0.03	0.59	4
15	0.30	0.14	0.55	5

References – [1]Pagel *et al.* (1979); [2]D'Odorico *et al.* (1983), [3]Webster & Smith (1983), [4]Deharveng *et al.* (1988) [5]Christensen, Petersen & Gammelgaard (1997)

a series of calibrated narrow-band observations surveying a large region of NGC 300 to include the two bright H II regions Deh 53 and 137 (Deharveng *et al.* 1988). Table 2.11 lists the narrow-band photometry[8] for all WR candidates in NGC 300, our sample is complete for the central regions out to a Holmberg radius of $\rho_0 > 0.4 - 0.5$ (where $\rho_0 = 9.75' \sim 5.75$ kpc). These magnitudes were used in identifying our WR candidates (see section 2.11).

Distance estimates have varied; early determinations by Graham (1984) using Cepheids calculated a distance modulus, (m - M)$_0$ = 26.09 (1.65 Mpc). Later, Richer *et al.* (1985) found a similar value, (m - M)$_0$ = 25.87 (1.49 Mpc) using carbon stars as distance indicators. More recently, Kennicutt *et al.* (1998) undertook a detailed survey for a number of nearby galaxies utilizing the excellent facilities offered with the HST to determine accurate distances. Comparing their distance modulus estimated by Cepheids, (m - M)$_0$ = 26.70 (2.19 Mpc), with previously determined values they found a significantly larger distance. These observations were later revised by Freedman *et al.* (2001), who refined the distance modulus to, (m - M)$_0$ = 26.53, this distance of 2.02 Mpc is used throughout this work.

The reddening towards NGC 300 is highly variable and published values range widely. This can be seen from the reddening determinations listed in Table 2.10, which were calculated using observed C(Hβ) determinations, assuming E_{B-V} = C(Hβ)/1.46 (Pottasch

[8]Credit: Photometric calibration and measurements were made by H. Schild.

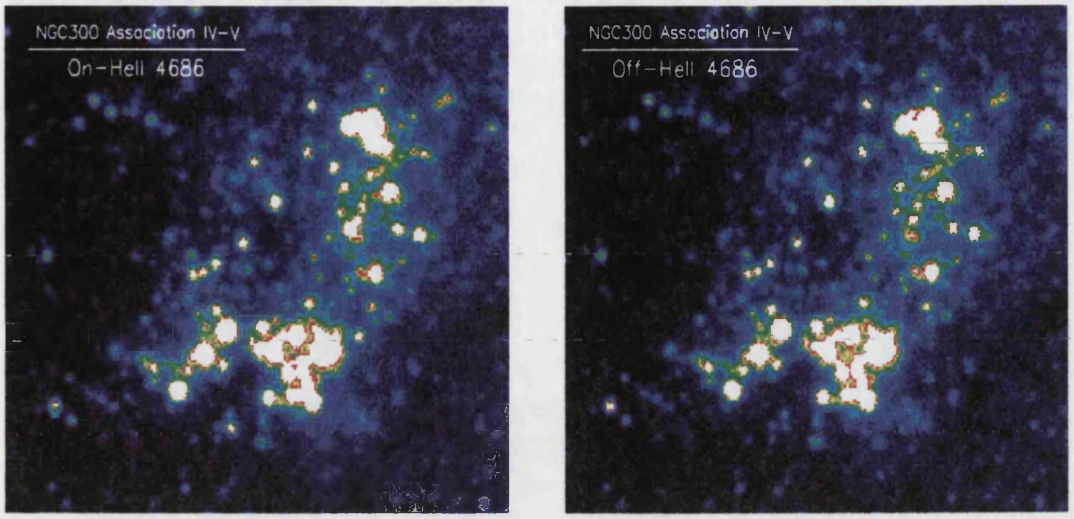

Figure 2.7: A small region of our VLT-FORS2 observations showing two OB associations (Association IV-V) in NGC 300. Images taken through both on and off-He II filters are shown. Each field shown is approximately 47″x 40″. The orientation is north is up and east to the left.

1984). Table 2.10 listed both the averaged determined colour excesses as well as the minimum and maximum calculated values. Bresolin *et al.* (2002) also found the colour excess towards a late-type WN star in NGC 300 to be, $E_{B-V} = 0.06$, which agrees with H II region determinations.

2.5.4 New Wolf-Rayet Catalogue

Once we had obtained accurate photometry for all the stars within our exposures, in both filters, we then used these results to identify possible WR star candidates. First a difference image was made after subtracting the λ4684 (He II) frame from the λ4781 (continuum) frame. This then presented us with a number of likely sources, we then reduced the number of possible candidates using the selection criteria; that their appearance is like that of a stellar source, and that their peak intensity is at least 6σ. Once our candidates had been identified their photometry measured through both filters were compared to check whether our technique has identified previously determined WR stars and for us to accurately measure the excess in flux.

Figure 2.7 identifies two bright OB associations (Association IV-V, Breysacher *et al.* 1997) which are located in the eastern section of NGC 300. Both images show the same

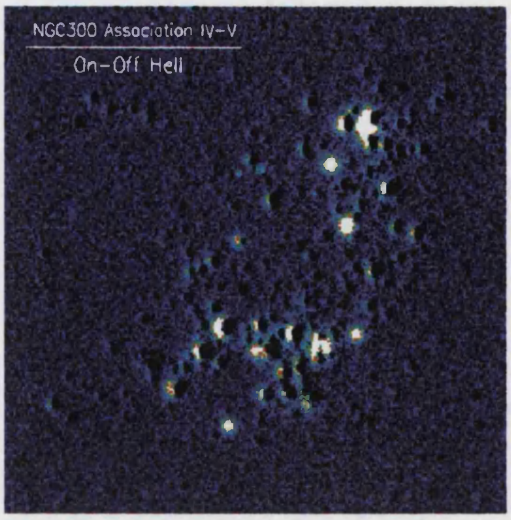

Figure 2.8: Difference between on- and off-He II observations taken with VLT-FORS2. Regions with an excess of flux are WR candidates. The field size and orientation is the same as 2.7.

region, covering a field-of-view of $\sim 47''$x $40''$, taken through the two narrow-band filters. A simple visual inspection of both images does not easily identify many potential WR stars, and it is only when a difference image is made between these two frames that the resulting image clearly uncovers stars with a large excess of flux through the λ4684 filter (see Figure 2.8).

We present a new catalogue of WR stars in NGC 300 which were identified from our narrow-band images in Table 2.11. This table lists our narrow-band photometry, and where available our V-band photometry, previously published spectral types, which are revised from our spectroscopy in a few cases (see Section 6.6). We also list any associated H II regions taken from Deharveng *et al.* (1988).

Figure 2.9 shows the λ4781 continuum magnitude and λ4684 excess magnitudes for stars that met our WR selection criteria. There are three stars which are listed in our WR catalogue that are not shown in Figure 2.9, #1, which was located on the edge of our images, and #37 and #57, both of which were severely blended. This figure clearly shows shows the separation between visual faint WC and WNE stars which also have characteristically large λ4684 excesses, and the visual bright WNL (and WR binaries), which are observed with small λ4684 excesses. *Approximate* equivalent widths are also shown in Figure 2.9, and were estimated from optical spectroscopy obtained. This method

Table 2.11: List of known Wolf-Rayet stars and our new candidates in the central regions of NGC 300. Outside of observed field there are two other WR stars known – WR8 (WN) in Deh 30 from Schild & Testor (1992) and a WC in Deh 24 from D'Odorico *et al.* (1983). Deprojected galactocentric distances are also shown and expressed as a fraction of the Holmberg radius (ρ_0=9.75′ $\simeq$ 5.75 kpc).

	RA (J2000)	Dec (J2000)	m_{4684}	$m_{4781} - m_{4684}$	m_V	ρ/ρ_0	Deh[4)]	Spect Type	ST[1)]	Brey[2)]	Remark
1	0 54 41.7	−37 38 39.0	out	out	out	0.44	48	WC4			5)
2	0 54 42.37	−37 43 7.3	18.93	1.02	out	0.33	53b	WC4	WR 10		
3	0 54 42.61	−37 40 28.5	21.88	1.25	out	0.25					
4	0 54 42.78	−37 43 1.8	17.88	0.25	out	0.32	53c	WN			4)
5	0 54 43.53	−37 39 49.9	20.52	2.09	out	0.28	54				
6	0 54 44.75	−37 42 40.0	19.03	0.13	out	0.26		WN11			3)
7	0 54 45.22	−37 38 48.0	19.71	0.14	out	0.37	61				
8	0 54 45.28	−37 38 47.0	20.22	0.24	out	0.37	61				
9	0 54 47.69	−37 42 45.3	20.26	0.58	20.62	0.24		WN4–5			5)
10	0 54 50.21	−37 40 29.7	19.68	0.52	20.04	0.10	76a				
11	0 54 50.22	−37 38 24.1	18.51	0.44	18.79	0.37	77	WC+WN	WR 9	I-1	
12	0 54 50.53	−37 38 26.7	20.87	1.57	22.12	0.36	77			I-2	
13	0 54 50.57	−37 38 13.2	20.54	0.29	20.58	0.39					
14	0 54 50.62	−37 40 21.7	20.39	1.49	21.64	0.11	76b	WC4-6	WR 1		
15	0 54 50.91	−37 38 30.0	20.35	0.16	20.41	0.35	79				
16	0 54 51.00	−37 38 26.1	20.10	0.10	20.27	0.36	79				
17	0 54 51.31	−37 38 26.3	22.50	0.14	weak	0.36	79				

Table continued on next page .....

	RA (J2000)	Dec (J2000)	m_{4684}	$m_{4781} - m_{4684}$	m_V	ρ/ρ_0	Deh[4)]	Spect Type	ST[1)]	Brey[2)]	Remark
18	0 54 51.65	−37 39 39.2	19.11	0.10	18.79	0.19	84				
19	0 54 51.89	−37 39 11.5	20.20	0.08	19.24	0.25					
20	0 54 52.59	−37 41 49.1	18.54	0.11	17.57	0.11	85				
21	0 54 52.93	−37 38 38.3	20.85	0.12	20.97	0.32					
22	0 54 53.09	−37 43 34.0	20.98	1.16	21.71	0.35	87	WC4			5)
23	0 54 53.11	−37 43 47.3	19.72	0.08	19.71	0.38	88				
24	0 54 53.80	−37 43 47.2	20.00	1.55	21.34	0.38	90	WC5	WR 11		
25	0 54 54.57	−37 41 54.7	20.28	0.09	20.27	0.13					
26	0 54 55.67	−37 40 25.1	20.12	0.08	20.10	0.09					
27	0 54 55.99	−37 40 17.6	20.39	0.15	20.47	0.11	96				
28	0 54 56.45	−37 40 35.1	20.55	1.90	22.05	0.09	98	WNE	WR 2		
29	0 54 56.76	−37 40 44.0	19.71	2.58	21.61	0.08	98	WC4-5	WR 3		
30	0 54 58.95	−37 43 58.7	21.24	1.31	22.01	0.44	107	WN			5)
31	0 55 0.65	−37 38 51.5	20.74	1.68	22.14	0.31					
32	0 55 2.33	−37 38 27.4	18.84	0.08	18.84	0.37	115				
33	0 55 2.88	−37 43 16.0	21.28	1.02	21.51	0.40				II-1	
34	0 55 3.34	−37 42 42.0	20.36	1.97	21.87	0.35		WC5-6	WR 12	III-1	
35	0 55 3.55	−37 42 49.4	19.06	0.09	18.82	0.36					
36	0 55 3.64	−37 43 20.0	18.06	0.13	17.97	0.42					
37	0 55 3.75	−37 42 51.6	blend	2.0	18.56	0.37					

Table continued on next page .....

	RA (J2000)	Dec (J2000)	m_{4684}	$m_{4781} - m_{4684}$	m_V	ρ/ρ_0	Deh[4)]	Spect Type	ST[1)]	Brey[2)]	Remark
38	0 55 4.09	−37 43 18.9	19.07	0.64	19.53	0.43		WN9-10	WR 7	II-2	
39	0 55 4.17	−37 43 16.6	20.05	0.08	19.99	0.42					
40	0 55 5.69	−37 41 13.4	20.13	1.68	21.56	0.28		WCE	WR 6		
41	0 55 9.98	−37 42 12.5	21.64	0.95	22.44	0.43					
42	0 55 11.03	−37 37 55.5	22.02	0.56	22.39	0.52					
43	0 55 12.07	−37 41 21.9	19.84	0.12	19.83	0.42	137d				
44	0 55 12.19	−37 41 19.7	17.71	0.19	17.80	0.42	137d				
45	0 55 12.21	−37 41 20.4	18.55	0.40	18.79	0.42	137d			IV-1	
46	0 55 12.32	−37 41 38.4	20.53	1.89	21.69	0.44	137a	WC4-5		V-1	
47	0 55 12.41	−37 41 29.0	19.68	2.95	21.19	0.43	137b	WC5-6	WR 5	IV-2	
48	0 55 12.54	−37 41 23.6	20.23	3.31	21.87	0.43	137b	WC4	WR 13	IV-3	
49	0 55 12.58	−37 41 39.5	18.46	0.31	18.85	0.45	137a	WN7	WR 4	V-2	
50	0 55 12.65	−37 41 38.5	19.62	0.18	19.73	0.45	137a				
51	0 55 12.72	−37 41 44.6	blend	0.7	20.38	0.45	137a				
52	0 55 13.18	−37 38 1.4	22.16	0.5	22.74	0.54					
53	0 55 13.23	−37 41 39.8	20.63	1.12	21.54	0.46		WN4-6		V-3	
54	0 55 13.36	−37 41 30.3	20.22	0.30	20.39	0.46					
55	0 55 13.47	−37 41 46.3	20.64	1.87	22.30	0.47		WN4-5		V-4	
56	0 55 13.51	−37 41 37.9	17.73	0.11	17.68	0.46	137c				
57	0 55 13.61	−37 41 32.0	20.31	0.11	20.34	0.46					
58	0 55 13.93	−37 41 43.2	18.82	0.08	18.75	0.48	137c				

[1)]: Schild & Testor (1991, 1992), Testor & Schild (1993); [2)]: Breysacher et al. (1997); [3)]: Bresolin et al. (2002ab); [4)]: Deharveng et al. (1988); [5)]: This work

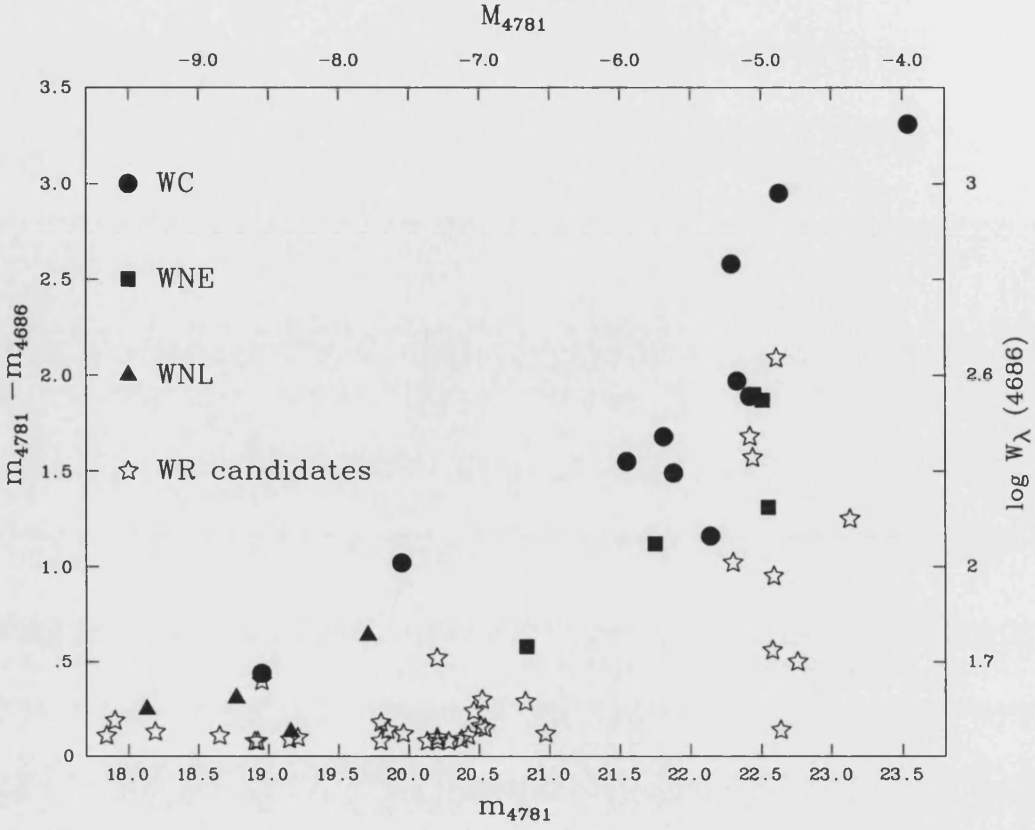

Figure 2.9: Comparison between λ4781 continuum magnitudes and candidate WR stars with an excess of flux in λ4684 (open stars). Stars with known spectroscopic classifications are shown (filled symbols), the key is presented in the figure. The *approximately* determined equivalent widths and absolute magnitudes are also shown (see discussion in text).

of determining WR stars and their subtypes could be very useful in identifying new WR populations in distant galaxies, or where visual extinctions are large, in which spectroscopic studies would be very difficult, even with 8-10m telescopes.

2.6 M 83

We extend this technique of detecting WR candidates to the metal-rich, late-type, barred spiral (SBc) galaxy M 83 (NGC 5236). Recently, Karachentsev *et al.* (2002) confirmed that both Cen A and M 83 form the centre of two spatially separated groups, each with their own number of smaller members. M 83 is an excellent candidate to uncover new WR stars;

it appears almost face-on, there are signs of intense star-forming activity, and there are a large numbers of known, activity H II regions.

2.6.1 Previous Work

As a galaxy M 83 has been well studied, from the X-rays (e.g. Soria & Wu 2002) to the radio (e.g. Israel & Baas 2001), although very little work has studied the massive star content of this large, metal-rich spiral. Signatures of WR stars have been detected in M 83 via spectroscopic studies of H II regions. Rosa & D'Odorico (1986) reported that from a survey of 8 H II regions, three showed signs of WR emission. Bresolin & Kennicutt (2002) also found possible evidence for WR stars in five H II regions. This prompted Rosa & Richter (1988) to undertake a narrow-band survey of M 83 in the search for WR stars, and strangely they reported that there was no conclusive evidence for the presence of WR stars in M 83.

The distance to M 83 had previously only been determined using unconventional methods, such as measuring distances by expanding photosphere method for Type II supernovae (Schmidt *et al.* 1994), or the method of surface brightness fluctuations (Jerjen *et al.* 2000). There had been efforts to observe the companion galaxy to M 83, NGC 5253, using more traditional methods via Cepheids, Freedman *et al.* (2001) estimated the distance modulus of NGC 5253, (m - M)$_0$ = 27.54 (D = 3.2Mpc). Until recently there were no modern determinations of the distance to M 83, Thim *et al.* (2003) observed a number of Cepheids using the 8-metre VLT to independently derive a distance modulus of (m - M)$_0$ = 28.25 (D = 4.5 Mpc).

The chemical abundance across M 83 was first investigated by Dufour *et al.* (1980), they claimed that the metallicity of M 83 was super-solar. Their results were based on differential analysis of theoretical models of both [O II] and [O III] lines, and found that the central regions of M 83 were 4-5 $Z_\odot$. A similar conclusion was found by (Webster & Smith 1983) although their results predicted a much sharper gradient. These results were later re-analyzed by Vila-Costas & Edmunds (1992), they revised the abundance for the central region to be somewhat lower, $12+log(O/H) = 9.24$ ($\sim$2.2 $Z_\odot$), a similar conclusion was also found by Zaritsky *et al.* (1994). According to Pilyugin (2001), the tradidational R_{23} method significantly over-estimates the abundance of O/H (see Section 4.1 for a more complete description). Hence this method would also reduce current metallicity gradients for M 83. Optical spectroscopy of a number of H II regions in M 83 were obtained by

Table 2.12: Central coordinates for the four observed fields for M 83.

Field	Position (2000)	
	α	δ
M83-A	13 37 10.9	-29 49 30.0
M83-B	13 36 49.0	-29 49 30.0
M83-C	13 37 11.1	-29 54 31.7
M83-D	13 36 49.0	-29 54 29.9

Bresolin & Kennicutt (2002), their evaluation of these H II regions indicated a metallicity in the central regions of $\sim$1.8 – 2.4 $Z_{\odot}$, employing the calibrations by McGaugh (1991) and Edmunds (1989). They also found a relatively shallow metallicity gradient across the galaxy, although their results provide limited radial coverage.

2.6.2 VLT-FORS2 Observations of Wolf-Rayet Stars in M 83

Previous studies have focused around H II regions, we have undertaken a deep narrow-band survey of M 83 using VLT-FORS2. Observations were made with the VLT UT4 (Yepun) telescope, using the Focal Reduced/Low Dispersion Spectrograph #2 (FORS2) over a number of dates spanning April 21st 2002 - June 3rd 2002. Conditions during the observations were photometric and the seeing was stable with typical seeing of 0.6″.

The detectors on FORS2 were recently upgraded, and replaced with two red-optimised 1024 x 2048 MIT CCDs with 15μm pixels. Using the standard collimator this configuration gave a total field-of-view of 7.0′ x 6.6′ with a scale of 0.126″/pixel. This only gave us partial coverage of M 83, and so we were required to observe four separate fields to encompass the entire galaxy, these positions are listed in Table 2.12. Our primary aim was to identify WR candidates in M 83 and image a large sample of H II regions to constrain the metallicity across the galaxy. M 83 was observed through four interference filters, two focused around He II λ4686 and two focused around Hα λ6563, the first set were centred at 4684 Å, and 4781 Å, these filters had band widths of 66 Å and 68 Å respectively. The second set of filters were centred at 6563 Å, and 6665 Å, these filters had band widths of 61 Å and 65 Å respectively. Our method for identifying new WR candidates is identical as described in section 2.5.4, where we locate a narrow-band filter to match known, strong WR emission features for both WN and WC types, and a second filter where WR stars

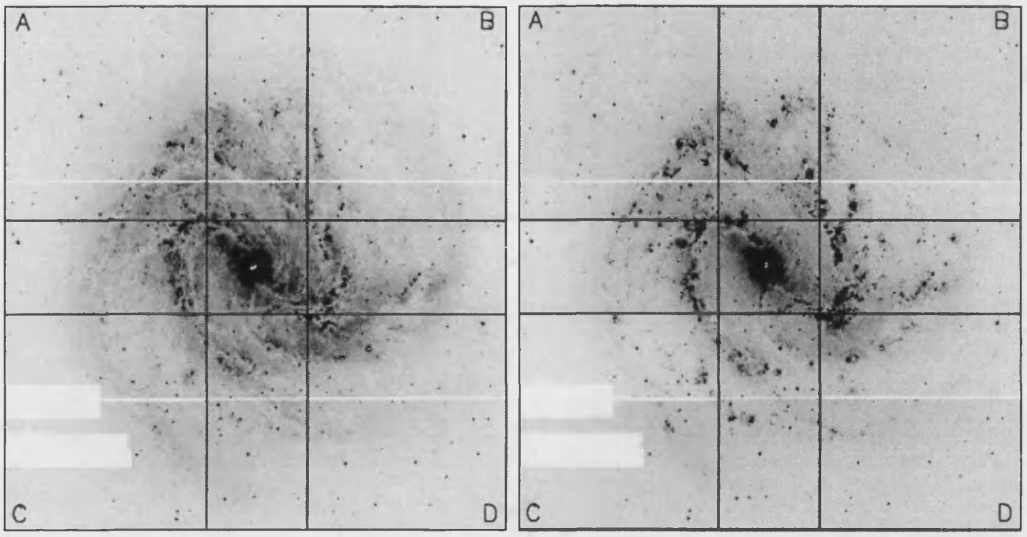

Figure 2.10: VLT-FORS2 composite image of M 83 taken through two interference filters centred at He II λ4686 (left) and Hα λ6563 (right). The position of the four observed fields in M 83 are shown, with a total field-of-view of 11.5' x 12.0'. Two bright stars are masked in the lower left corner. North is up and east is to the left.

are relatively free of emission. This practice was repeated for identifying regions that contain large excesses of Hα emission and are potential H II regions. Exposure times for the on-off He II filters were 1800sec and for the on-off Hα filters both sets were imaged with 600sec and 60sec exposure times, with the aim to imaging both bright and faint H II regions. M 83 was also imaged through a broad-band Bessel B filter, typically with shorter exposure times of 120sec.

Figure 2.10 shows two VLT-FORS2 composite images of M 83 taken through two interference filters centred at He II λ4686 and Hα λ6563. The position of the four observed fields in M 83 are shown, with a total field-of-view of 11.5′ x 12.0′. The images were reduced using standard IRAF packages to trim, bias subtract and flat field the images. Photometry has not yet been obtained for the data[9].

2.6.3 Catalogue of Wolf-Rayet Candidates

Even though the data have not (yet) been calibrated, the reduced images were sufficient to identify potential WR candidates by producing a difference image between the on-

[9]Note: This particular study is still work in progress.

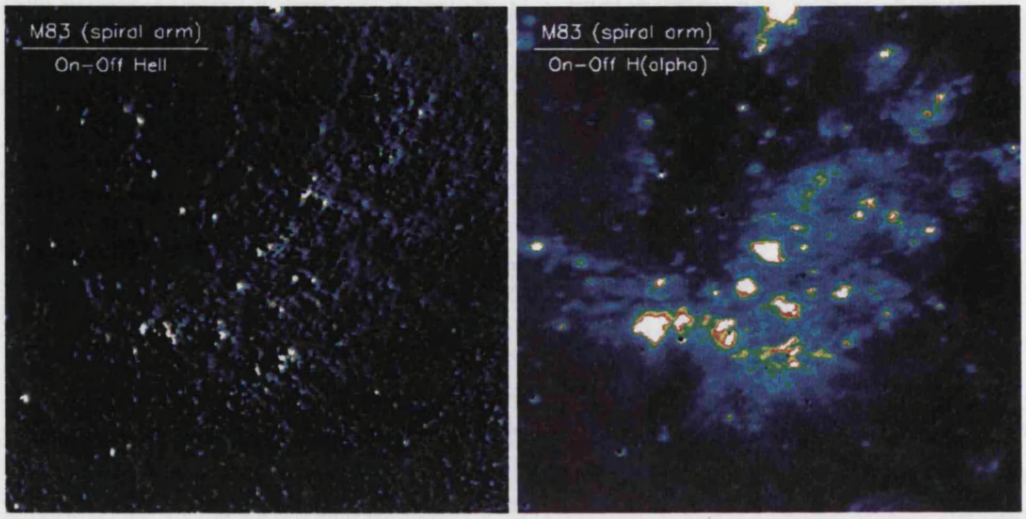

Figure 2.11: Difference images between on- and off-He II (left) and Hα (right) taken with VLT-FORS2. These observations show a section of the lower right spiral arm in M 83, covering a field-of-view of 115″ x 120″. WR candidates are identified as having an excess of He II emission, they are predominately located in a large H II region. North is up and east is to the left.

and off-He II. This procedure can be greatly improved after correcting for differences in the PSF between the two sets of images. After careful inspection of the images we have identified over 330 WR candidates[10] in M 83.

Figure 2.11 highlights the abundance of WR stars in M 83. It shows a 115″ x 120″ field-of-view located in the lower right spiral arm of the galaxy. Also shown is the difference between on- and off-Hα; the majority of the WR candidates detected are located within this large H II region. Our survey has also identified a number of field WR stars. Table 2.13 shows a sample of the full catalogue listing the Wolf-Rayet candidates in M 83 (column 1), the field and chip where each candidate was identified (column 2). Its also contains their coordinates (columns 3 and 4) and a rough measure of their peak intensity (in counts; column 6) in the He II λ4686 filter and the excess once the continuum filter had been subtracted (column 7). Column 5 details whether there was any Hα emission associated with the candidate WR star, to help discriminate whether it is located in a H II region or whether its a field star.

Recently a spectroscopic follow-up was preformed for a number of our WR candidates,

[10]Credit: WR candidates were identified by H. Schild

Table 2.13: List of Wolf-Rayet candidates in M83 identified from our narrow-band imaging survey. As well as their coordinates, we also list a rough measure of their peak intensity in the He II λ4686 filter (in counts) and the excess of He II once the continuum had been subtracted.

#	Field/Chip	α (2000)	δ (2000)	Hα Assoc.	He II	He II - Cont.
01	A1	13:36:55.15	-29:49:50.5	no	800	500
02	A1	13:36:55.31	-29:48:10.0	diffuse	700	300
03	A1	13:36:55.35	-29:49:47.6	no	500	730
04	A1	13:36:55.85	-29:47:47.5	no	400	250
05	A1	13:36:56.00	-29:49:53.8	strong H II	3500	1900
06	A1	13:36:56.22	-29:49:33.1	no	800	900
07	A1	13:36:58.55	-29:48:12.0	no	1200	700
08	A1	13:36:58.74	-29:48:06.3	strong H II	7000	2200
09	A1	13:37:00.28	-29:48:04.2	strong H II	2600	900
10	A1	13:37:02.49	-29:48:27.4		600	700
11	A1	13:37:02.68	-29:49:40.9	v. strong	21000	5400
12	A1	13:37:02.84	-29:49:15.3	no	900	1100
13	A1	13:37:04.39	-29:48:26.9	weak	2200	700
14	A1	13:37:04.56	-29:49:21.8	no	1200	900
15	A1	13:37:05.34	-29:48:20.4	strong	4000	1500
16	A1	13:37:05.53	-29:48:19.9	diffuse	1200	800
17	A1	13:37:06.36	-29:49:03.7	weak	2300	1100
18	A1	13:37:07.35	-29:49:39.2	yes-CH II	1500	900
19	A1	13:37:07.68	-29:49:13.9	v. strong	16000	3600
20	A1	13:37:07.76	-29:49:18.1	no	1000	1200
21	A1	13:37:08.55	-29:49:06.5	diffuse	6000	3000
22	A1	13:37:09.15	-29:49:20.6	diffuse	1000	500
23	A1	13:37:09.63	-29:49:56.4	no	200	535

NOTE. – Table 2.13 is presented in its entirety in Appendix E. A portion is shown here for guidance on its content.

again using VLT-FORS2 (Proposal ID: 071.B-0089). Early results indicate that a high percentage of the candidates are bona-fide WR stars (private communication: P. Crowther (UCL)). Importantly, not only are there a large number of WR stars but of this sample we find a considerable number of WC stars, of which a large proportion are late-type WCs

- as would be expected in a metal-rich environment.

CHAPTER 3

Modelling Stellar Atmospheres

In this chapter, we first introduce the basic concepts of a model atmosphere and then describe the physics of stellar winds, before turning to models appropriate to WR stars.

The spectra of Wolf-Rayet stars contain a rich plethora of emission lines from a number of chemically enriched elements, such that methods to interpret them have proven very difficult, with so many complexities involved in prescribing computational models. If we can accurately, and consistently model the spectra of WR stars, and deduce their fundamental parameters then we can learn a great deal about the evolution, of not just WR stars but massive stars in general. For most low-mass, cool stars (i.e. the Sun) plane-parallel, line blanketed models atmospheres calculated in local thermodynamic equilibrium (LTE) have proven successful (e.g. Ahmad & Jeffery 2003; Paunzen *et al.* 1999). Unfortunately for hot stars LTE assumptions are inadequate, for reasons which will be explained later, and more complex methods of determining their atmospheres are required.

3.1 Physical Ingredients of a Model Atmosphere

Here we give an overview behind the physical concepts of a stellar atmosphere, including mathematical equations that describe the 'macro-scopic' variables that occur in a generic stellar atmosphere. When the atmospheres of hot stars are discussed it is important to first clarify the difference between the photosphere of a star and its actual wind. The photospheric region is located deep at the base of the star's atmosphere and can be considered the region between the star's 'surface' and its extended atmosphere. It is considered static, due to the fact that the velocities are very small, even below the

local sound speed. Compared with the large extended stellar wind, the photosphere is radially small. Mathematically the photosphere can be characterised through hydrostatic and radiative equilibrium. These terms simply describe the gradient of the total pressure across the photosphere which is balanced by the local gravitational acceleration (which due to its small radial extent is considered as constant). For a spherically symmetric star with a static atmosphere this can be written as:

$$\frac{dP}{dR} = -\frac{\rho G M_*}{R^2} \approx -\frac{\rho G M_*}{R_*^2} \equiv -\rho g \tag{3.1}$$

where P is the total pressure (which is made up of the gas pressure, P_{gas}, the radiation pressure, P_{rad}, and the turbulent pressure, P_{turb}), and is expressed as a function of R, the photospheric radius, and M_* the stellar mass. R_* is the stellar radius, g is the gravitational acceleration, and ρ is the mass density. Unlike the Sun and its corona, the effects of gas pressure are negligible in hot star winds (except at the base), due to the extreme temperatures required before the force from gas pressures can drive the wind beyond the sonic point.

Radiative equilibrium states that only energy produced through nuclear reactions deep in the interior diffuse outward towards the star's surface and appears as observable radiation. In other words, the total radiation energy per unit volume of the stellar photosphere is equal to the total radiation energy emitted per unit volume, and that there is no creation of energy within the atmosphere. The equation of radiative equilibrium can be expressed as:

$$\int_0^\infty (\chi_\nu J_\nu - \eta_\nu) d\nu = 0 \tag{3.2}$$

where χ_ν is the extinction coefficient, η_ν is the emission coefficient, and J_ν is the mean intensity of the radiation as a function of frequency, ν – these terms will be discussed in more detail later in the text. The above equations assume that the stars are conventionally stable, which is accurate for hot, early-type stars but not the case for cool stars like our Sun where magnetic processes are also important. Equation 3.2 can then be used to express how the radiative energy interacts with the surrounding matter and is known as the 'radiative transfer equation', which is described as:

$$\left(\frac{1}{c}\frac{\partial}{\partial t} + n.\nabla\right) I(\nu, r, n, t) = \eta(\nu, r, n, t) - \chi(\nu, r, n, t) I(\nu, r, n, t) \tag{3.3}$$

where we now describe the radiation as the specific intensity transported by radiation I. More accurately, the specific intensity is dependent on the frequency, per unit solid

angle, per unit area, per time interval. In thermodynamic equilibrium, the intensity can be described by the Planck function (i.e. a black body). Now it becomes clear how the absorption and emission coefficients relate back to the radiative transfer equation. χ_ν, the absorption coefficient and η_ν, the emission coefficient both take into account various processes to form the spectral lines in the wind. These processes are described in detail in each term of the equations, with contributions of bound-bound transitions, bound-free transitions, free-free absorption, and electron scattering. The absorption coefficient can be expressed as

$$\begin{aligned}\chi_\nu &= \sum_i \sum_{j>i} [n_i - g_i/g_j n_j]\sigma_{ij}(\nu) \\ &+ \sum_i (n_i - n_i^* e^{-h\nu/kT})\sigma_{i\kappa}(\nu) \\ &+ \sum_\kappa n_e n_\kappa \sigma_{\kappa\kappa}(\nu, T)(1 - e^{-h\nu/kT}) + n_e \sigma_e \end{aligned} \tag{3.4}$$

and the emission coefficient can be expressed as

$$\begin{aligned}\eta_\nu &= \frac{2h\nu^3}{c^2}\left(\sum_i \sum_{j>i} n_j (g_i/g_j)\sigma_{ij}(\nu)\right. \\ &+ \sum_i (n_i^* \sigma_{i\kappa}(\nu) e^{-h\nu/kT}) \\ &+ \left.\sum_\kappa n_e n_\kappa \sigma_{\kappa\kappa}(\nu, T) e^{-h\nu/kT}\right) \end{aligned} \tag{3.5}$$

where n_i is the population density of state i (or to a transitional state j), whilst g_i is its corresponding statistical weight. n^* describes the population as if it where in statistical equilibrium (i.e. in LTE), σ is the cross section of the atom at frequency ν, and the κ term accounts for the continuum. These terms are consistent for both the absorption and emission coefficients. Equations 3.2 – 3.5 are taken from Hubeny (1999) in which they are discussed in greater detail.

3.2 The Physics of Stellar Winds

In this section we discuss the physics of stellar winds, as opposed to stellar atmospheres. We are essentially describing the physical regions of a star, focusing on the theories behind how these huge quantities of matter are accelerated away from the central star. A stellar wind is the large, continuous outflow of material from a star that is travelling at

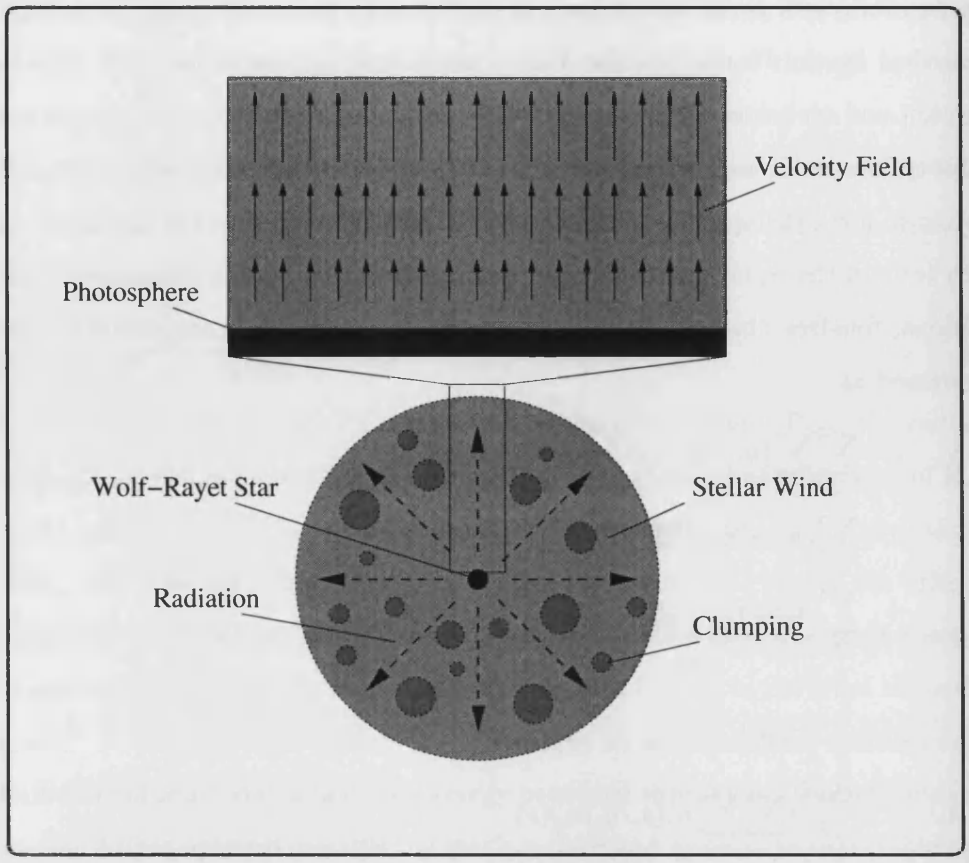

Figure 3.1: Schematic illustration of a Wolf-Rayet star (not to scale), showing the star's extended atmosphere. The velocity gradient within the wind is shown as well is clumping the the stellar wind.

supersonic speeds. Most stars eject material, although not all on the same scale. For instance, the Sun has a solar wind, but this is transparent and weak. On the other hand massive (hot) stars have dense wind that become opaque to certain wavelengths of the star's radiation. Figure 3.1 shows a simple schematic to illustrate the basic concept of a stellar wind observed in a WR star. Although not to scale important points to note are; (i) compared with the radial extent of the star, the wind is huge, (ii) within the wind inhomogeneities exist in the form of clumping, (iii) there exists a velocity gradient that increases with distant from the star.

3.2.1 Radiative Forces

The current accepted theory as to what accelerates a stellar wind is radiative driving processes, in which momentum is gained through line scattering – this was first recognised almost 80 years ago by Milne (1926). Mathematically, stellar winds can be characterised by two (global) parameters, the mass-loss rate and the terminal wind velocity. If the wind is stationary and spherically symmetric, then the mass-loss is related to the density and velocity within the wind via the equation of mass continuity.

$$\dot{M} = 4\pi r^2 \rho(r) v(r) \tag{3.6}$$

The simplest way to describe the radiative force is by the scattering of free electrons (sometimes referred to as a grey scattering). This process does not effect the star's luminosity so the radiative flux energy can be expressed as $L/4\pi r^2$, where r is the star's radius. Dividing this by the speed of light, c, gives the radiative momentum of flux, $L/4\pi r^2 c$. The probability that material in the wind will intercept the flux is now described as a condition of the absorption coefficient (see Equation 3.4) and relates to the interaction cross section per unit mass, more commonly referred to as the opacity.

The opacity is straight forward when considering electron scattering as it simply becomes a constant, $\kappa_e = \sigma_e/\mu_e$, where σ_e is the classical Thompson cross section and μ_e is the mean atomic mass per free electron, which varies as a function of mass and mass fraction of hydrogen. Combining the opacity of the wind as well as its radiative momentum flux gives an equation describing the radiative acceleration in the wind due to free-electron scattering:

$$g_e(r) = \frac{\kappa_e L}{4\pi r^2 c} \tag{3.7}$$

The radiative acceleration can then be compared with the star's gravitational acceleration, which is simply GM/r^2, where M is the star's mass and G is the gravitational constant. This now means that the r^2 term can be replaced to give a ratio between the luminosity and mass, this ratio is called the Eddington parameter, and describes the maximum possible luminosity a star might possess before the radiative forces become strong enough to make the stars unstable and ultimately destroy the star.

$$\Gamma_e = \frac{\kappa_e L}{4\pi G M c} \tag{3.8}$$

For low mass stars such as the Sun this ratio is very small (or order 2×10^{-5}), but for hotter, more massive stars this ratio can reach $\sim$0.5. When a star reaches the Eddington limit it starts to become unbound and unstable (i.e where Γ_e tends towards 1).

Unfortunately the radiative acceleration from free electrons alone is not enough to drive the stellar wind of a massive star. In fact the opacity due to the C IV λ1550 line can reach approximately 10^6 times that due to electron scattering (Lamers & Cassinelli 1999). So we must look elsewhere for a second source of radiative acceleration. This extra source of acceleration comes from 'line scattering' of free electrons. This method of providing a radiative force proves much more efficient for two reasons. Firstly, line scattering has a resonant nature. Bound electrons travelling between two discrete energy levels can amplify the interaction cross section with photons of the correct energy. Secondly, and importantly, the atmosphere is expanding away from the central star and so the outer regions, via the Doppler effect, redshift the local line resonance. This then allows the line to resonate with the flux that was previously unattenuated and with higher energies.

To solve the equations of radiative acceleration for line scattering requires a full evaluation over a non-local spatial integral. Thankfully this can be greatly simplified using the 'Sobolev Approximation' (Sobolev 1960), in which the equation for radiative transfer are solved such that the interaction region is infinitely narrow. The assumption is then made that the profile function, ϕ, can be treated as a delta-function. This hugely simplifies the problem as we need not integrate the density over distance. We only need to consider the *local* density and velocity gradient at any given radius. The optical depth of radiation at a given line resonance can now be expressed as a fraction of a *Sobolev length*, $l_{Sob} = v_{th}/(dv/dr)$ (which is now dependent on the velocity gradient and thermal broadening of the line).

$$\tau = \frac{\kappa \rho v_{th}}{dv/dr} \tag{3.9}$$

where κ is the line opacity and ρ is the local density. Integration of this equation leads to a solution which can then be re-introduced to give expressions for the optically thin and thick line accelerations.

Considering the optically thin (point source) limit for a line with a certain frequency, ν_0, it will be unable to absorb all the flux emitted from the stellar source. Instead, it is directly connected to the number of absorbing particles per unit volume and can be

written as

$$g_{thin} = \frac{\kappa v_{th} \nu_0 L_\nu}{4\pi r^2 c^2} \approx g_e \frac{\kappa}{\kappa_e} \frac{v_{th}}{c} \tag{3.10}$$

where κ is the opacity. The second approximation assumes that the line frequency is close to the peak of the flux such that, $\nu_0 L_\nu \approx L$.

The optically thick limit for a line (where $\tau \gg 1$) *all* the flux (close to ν_0) will be absorbed and is dependent on the optically thin result, such that it can be described by

$$g_{thick} \simeq \frac{g_{thin}}{\tau} = \frac{L}{4\pi r^2 \rho c^2} \frac{dv}{dr} \tag{3.11}$$

where τ is the optical depth in the wind. Combining the equations for the optically thin (Eqn. 3.10) and optically thick (Eqn. 3.11) line acceleration it is possible to derive an equation for the general line acceleration in the wind which provides a method to calculate the total line force by simply summing all the lines forces from all individual lines.

$$g_{line} \simeq g_{thin} \left(\frac{1 - e^{-\tau}}{\tau} \right) \tag{3.12}$$

These equations account for the Sobolev approximation and assume that the radiating source is emitted from the stellar photosphere in a radial direction, and does not account for diffuse line radiation as a result of multiple line scatterings. Improvements have since been made, for example, the finite disk correction (Owocki & Puls 2002), which accounts for the fact the the star is *not* a point source, an approximation which is inaccurate close to the star.

3.2.2 CAK Formalism

The early work on radiation driven wind theory by Castor, Abbott & Klein (1975) (CAK) still forms the foundation for today's modern theoretical work in stellar winds. Several authors have refined their work since (e.g. Abbott 1982; Kudritzki *et al.* 1989). However, their original formalism still proves significant in theoretical aspects of radiation driven stellar winds.

CAK theory predicts that the line acceleration is expressed in terms of the radiative force due to electron scattering times the *force multiplier*, $M(t)$, which is parameterised by

$$M(t) = kt^{-\alpha} \left(\frac{n_e}{W} \right)^{\delta} \tag{3.13}$$

where k, α and δ are the force multiplier parameters and W is the geometrical dilution factor. The parameter, k, is a measure of the number of lines acting on the wind; α, is a measure of the number of optically thick to thin lines, such that if there were only strong lines contributing to the line acceleration then $\alpha = 1$. The parameter, δ, quantifies the ionization in the wind (this number is small). Finally, the parameter t is the dimensionless optical depth parameter (Castor, Abbott & Klein 1975) which is given by:

$$t = \kappa_e v_{th} \rho (dr/dv) \tag{3.14}$$

where κ_e is the electron scattering opacity, and v_{th} is described by the mean thermal velocity. Calculations have shown that the force multiplier also varies with metallicity as, $M(t) = M(t)_{\odot}(Z/Z_{\odot})^{1.0}$ (Lamers & Cassinelli 1999). The CAK formalism for describing the mass-loss rate can be given by

$$\dot{M}_{cak} = \left(\frac{\kappa_e v_{th}}{4\pi}\right)\left(\frac{\kappa_e}{4\pi}\right)^{\frac{1}{\alpha}}\left(\frac{1-\alpha}{\alpha}\right)^{\frac{1-\alpha}{\alpha}}(\alpha K)^{\frac{1}{\alpha}}\left(\frac{L_*}{c}\right)^{\frac{1}{\alpha}}(GM_*(1-\Gamma_e))^{\frac{\alpha-1}{\alpha}} \tag{3.15}$$

where $K = (n_e/W)^{\delta}$, and $M_*(1-\Gamma_e)$ is the effective mass which takes account of the reduction of gravity by the free-electron scattering. Although this analytical solution provides a good estimate of the mass-loss rates for hot stars, there are a number of assumptions which are made before reaching this equation. For example, the effects of line blanketing are not considered and line interactions only occur once within the wind. Equation 3.15 is also only valid when the force multiplier parameters, K and α are constant.

3.2.3 Mass-loss Predictions

Considering a simple, optically thick line we can estimate the mass-loss rate for a star, assuming that the wind is driven by the radiation pressure for this single line. This is often referred to as the *'point source approximation'* and can be expressed to describe the rate at which photons transfer momentum to the wind, resulting in a steady state flow acceleration (which is independent of velocity) given by

$$v\frac{dv}{dr} \approx \frac{L}{\dot{M}c^2}v\frac{dv}{dr} \tag{3.16}$$

We can now simply cancel the acceleration term from each side which implies that, $\dot{M} \approx$ L/c^2. However, in reality the winds of hot, massive stars are driven not just by one line but many optically thick lines. Considering this we can modify Equation 3.16 such that

the mass loss simply increases with the number of optically thick lines,

$$\dot{M} \approx N_{thick} \frac{L}{c^2} \tag{3.17}$$

Observationally, we can now write a definition to describe the star's 'wind efficiency' (i.e. the efficiency of transferring radiative momentum into wind momentum).

$$\eta = \frac{\dot{M} v_\infty}{L_*/c} \simeq N_{thick} v_\infty / c \tag{3.18}$$

For OB stars η is typical ≤ 1, whereas for WR stars, with their strong stellar winds η can be as high as 50. This revelation that a WR star's wind could have a wind efficiency larger than 1 was coined the 'wind momentum problem', and initially there were suggestions implying that the WR winds were not radiatively driven. More recent theoretical work explained the problem that WR winds could not be expressed using the single-scattering formalism, but in fact due to the spherical expansion of the wind, there are no two points at any given depth within the wind with the same velocity component. This means that a photon can be absorbed and re-emitted (scattered) before being absorbed again by another overlapping optical thick line and therefore can be absorbed multiple times. This absorption of photons in different spectral lines is called *multiple scattering.* These assumptions, combined with very efficient momentum transfer, that help explained why WR stars could have such large values of η (Owocki & Gayley 1999).

3.2.4 Metallicity Dependence

As already discussed the driving mechanism of the winds of massive stars is radiation pressure from optically thick lines (Castor, Abbott & Klein 1975; Abbott 1982). The contribution from spectral lines of hydrogen and helium is limited, as there are very few spectral lines in the relevant spectral range for which massive stars emit the bulk of their energy. Most of the line driving is therefore from metal lines and this implies that the metal content of a massive star should control the strength of the emitted stellar wind.

The first observational evidence indicating a possible metallicity dependence for stellar wind parameters were observed in the difference between the terminal wind velocities for Galactic and Magellanic Cloud O stars (Garmany & Conti 1985; Prinja 1987). Both sets of authors found the terminal velocities for the stars in the Magellanic Clouds are consistently lower than their Galactic counterparts. Subsequent studies also indicated a mass-loss – metallicity relationship for O stars (Puls *et al.* 1996), which theoretical work also supports

(e.g. Vink, de Koter & Lamers 2001; Kudritzki & Puls 2000). The idea of a metallicity dependence was initially hypothesised by Castor, Abbott & Klein (1975), (Abbott 1982) and Kudritzki, Pauldrach & Puls (1987). They all agreed that the mass-loss should scale as a power-law,

$$\dot{M} \propto Z^m \tag{3.19}$$

where initial predictions for the power-law index, m, varied from 0.5 (Kudritzki, Pauldrach & Puls 1987) to 0.94 (Abbott 1982). More recently, comprehensive studies by Vink, de Koter & Lamers (2001) have concluded that m is closer to 0.85, a finding very close to that also previously determined by Leitherer, Robert & Drissen (1992) who found $m \simeq 0.8$.

Unfortunately the situation for WR stars, both WN and WC classes, is less clear. This is in part due to the fact that fully self consistent models of their stellar winds have yet to be presented. It is believed that the winds of WN stars are predominately driven by iron-group elements, like their O star progenitors, and therefore should have the same dependence as O stars. The case for WC stars is still debatable, since their winds contain an over-abundance of carbon and oxygen. Crowther *et al.* (2002) investigated the importance of line driving from carbon and oxygen in WC stars and concluded that the contribution of ions (~250 eV) at the base of the wind was vital in initiating an outflow. Their test calculations found that the ionization potential for both carbon and oxygen do not lie in the necessary range, but instead ions from Ne, Ar and other Fe-group elements are crucial in commencing the outflow from WCE stars.

Even though a metallicity dependence has been recognised for WR stars for some time, it was not until the work by Nugis (1989) that a mass-loss scaling was devised. He found that $\dot{M}$ scaled as $Y^{2.5}Z^{1.0}$, where Y and Z are the mass fractions of helium and heavier elements respectively. This mass-loss – metallicity scaling was later revised by Nugis & Lamers (2000) who re-evaluated a large number of WR stars, using mass-loss rates determined from their radio emission power, as well as the mass-loss versus emission line equivalent width relation derived by Nugis, Crowther & Willis (1998). The work by Nugis & Lamers (2000) concluded that for WR stars (i.e. both WN and WC stars), $\dot{M} \propto Z^{0.5}$. This scaling is currently employed in the rotating, evolutionary models (Meynet & Maeder 2003).

More recently, Crowther *et al.* (2002) calculated the stellar parameters for six LMC

WC stars and compared them with Galactic WC stars. They found the LMC stars possess higher luminosities and weaker winds, suggesting a scaling similar (i.e. $m \simeq 0.5$) to that discovered by Nugis & Lamers (2000).

3.3 Geometries of Stellar Atmospheres

We now discuss the various geometries employed in computational models of stellar atmospheres, identifying the approximations and simplifications used in these models to describe the atmosphere of a hot star. These assumptions aim to simplify a multi-dimensional problem to a single dimensional. Below are brief descriptions of the common approximations that are made for calculating hot star atmospheres.

3.3.1 Plane Parallel codes

This is the classical method for modelling a one-dimensional atmosphere. In these cases the curvature of the atmosphere is negligible as the radius of the star is far greater than the stellar atmosphere. Not only is the atmosphere considered plane parallel but it is commonly assumed to be horizontally homogeneous. This approximation is applicable for (most) O and B stars as their atmospheres do not extend to large radii, which means that these codes are used to study photospheric lines.

3.3.2 Spherical Geometry codes

This approach is necessary when the radial extent of a star's atmosphere is comparable with the star's radius, i.e. for supergiants, LBVs and WR stars. When considering stars with such extended atmospheres, it is not satisfactory to just simply assume a plane-parallel geometry. Instead we must adopt a more realistic approach by assuming a spherically symmetric, stationary and homogeneous atmosphere. Fortunately, the problem of solving the statistical equilibrium and radiation transfer equations are still one-dimensional. These codes calculate the radiative transfer equations in the co-moving frame (Mihalas, Kunasz & Hummer 1975), or by assuming a static wind geometry and the Sobolev approximation (Castor 1970). The radiative transfer equation (Eqn. 3.3) in

the co-moving frame (CMF), is given by

$$\begin{aligned} \mu\frac{\partial I(r,\mu,v)}{\partial r} &+ \frac{(1-\mu^2)}{r}\frac{\partial I(r,\mu,v)}{\partial \mu} \\ &- \left[\frac{vu(r)}{rc}\right]\left[(1-\mu^2)+\mu^2\frac{dlnv}{dlnr}\right]\frac{\partial I(r,\mu,v)}{\partial v} \\ &= \eta(r,v)-\chi(r,v)I(r,\mu,v) \end{aligned} \tag{3.20}$$

where I is the intensity and μ is the angle cosine. This equation neglects the effects from aberration and advection are ignored. This assumption is valid when solving the transfer and statistical equilibrium equations when the wind's velocity is not too large v/c $\leq$ 0.01 (Mihalas *et al.* 1976); these errors become significant for high velocities such as supernovae (Hauschildt & Wehrse 1991).

3.3.3 Monte Carlo codes

The single biggest advantage of using a Monte Carlo code is that it allows the inclusion of millions of lines that can be computed to produce the emergent spectrum. The first defining stellar atmosphere code that was written using the Monte Carlo technique was that of Abbott & Lucy (1985). Monte Carlo codes are also being used to perform two and three-dimensional geometric calculations although this field is still in its infancy. The biggest problem with these extra dimensions is the computer power and memory capabilities required to achieve realistic results. This is the advantage of using a Monte Carlo code as only certain (random) regions within the atmosphere are calculated at any instance; a process that is repeated until the stellar wind is sampled for an atmosphere which can be constructed.

3.4 Microscopic State of the Atmosphere

3.4.1 LTE Model Atmospheres

Local thermodynamic equilibrium (LTE) simply assumes that the state of the gas (distribution of atomic, ionic and molecular level populations) is specified by the thermodynamic parameters; the absolute temperature, and the total particle density. This can be described by a Maxwellian-like Saha-Boltzmann distribution, which is essentially defined by the local temperature. By combining both the Saha and the Boltzmann distributions it is possible to solve the the LTE population ratio between a particular level i and the

ion state c. Under these LTE conditions the energy balance is held such that $\chi I = \eta$, and the specific intensity equates to the Planck function ($B = \eta/\chi$). This relation is known as *Kirchoff's Law*. LTE model atmospheres are valid when collisions dominate and/or the mean-free path for a given photon is small and hence can be considered to be localised. These conditions predominately occur in B, A, F and G-type stars.

3.4.2 Non-LTE Model Atmospheres

Non-local thermodynamic equilibrium (non-LTE) is simply the break down of the assumptions made under LTE. In other words, LTE holds if all the atomic processes are in detailed balance such that A $\rightleftharpoons$ B, where A and B are particle states for which there has been a transition that has no net difference. This condition is met where the electron densities are high. However, in a stellar wind (i.e. low densities with a strong radiation field), the radiative rates dominate over collisional rates, otherwise we would not observe photons escaping the star's gravity. In these environments the radiation is not in equilibrium and as a result the radiation cannot be described by the Planck function. This departure from LTE is compounded when the level populations diverge from the Saha-Boltzmann distributions, causing an under- or over-population of atomic levels. Such effects are observed in hot star atmospheres and have to be accounted for in modern computational codes. In non-LTE, the populations are permitted to differ from the local Saha-Boltzmann equilibrium values and so it is necessary to calculate these level populations directly by constructing model ions and calculating individual line transitions. The amount by which a population deviates is expressed in terms of the departure coefficient.

3.5 Contemporary Stellar Atmosphere Codes

Non-LTE, computational models have been around for 30 years now, and during that time their progress towards understanding the atmospheres of stellar winds has been astounding. The first stellar models designed to reproduce the observations of the expanding atmospheres of WR stars were developed independently by Hillier (1987*a*) and Hillier (1987*b*) and the Kiel/Potsdam group (Hamann & Schmutz 1987). These early versions only calculated pure helium atmospheres, although later efforts included more complex atoms, such as C, N and O (Hillier 1989; Koesterke & Hamann 1995). However, iron group elements were neglected until more recently due to their extreme complexities and

the enormous number of spectral lines, although their inclusion proves to be extremely important. We provide a brief outline on a number of modern stellar atmosphere codes now available to the astronomical community, highlighting successes/failures for each.

3.5.1 CMFGEN

CMFGEN, (Hillier & Miller 1998) iteratively solves the transfer equation in the co-moving frame subject to statistical and radiative equilibrium. It assumes an extended, expanding atmosphere which is spherically symmetric and in a steady-state. This model can account for many atomic species (including all Fe-group elements). The most recent version now accounts for clumping in the wind, via a filling factor, f. It parameterises the filling factor such that at small velocities it approaches unity, because radiation instabilities close to the base of the wind are not thought to be important. This was the first major non-LTE code to include line blanketing in an extended stellar atmosphere.

3.5.2 ISA-WIND

ISA-WIND by de Koter *et al.* (1997) is another non-LTE code and uses the the *Improved Sobolev Approximation* (ISA). It computes the statistical equilibrium and radiative transfer equations using an approximate lambda iteration method. This method does not depend on the core-halo approximation, but instead treats the photosphere and wind in a unified manner. The line transfer is treated using an improved Sobolev approximation (ISA), in which the diffuse radiation field is correctly taken into account (Puls & Hummer 1988).

3.5.3 WM-Basic

WM-Basic was written and is fully reviewed by Pauldrach *et al.* (2001), the name is an abbreviation of **W**ind **M**omentum – (visual) basic. This radiation driven wind model makes a number of assumptions to dimensionalise the problem; essentially it uses a homogeneous, stationary and spherically symmetrical wind. Unlike the majority of non-LTE codes WM-Basic calculates a non-expanding atmosphere. Its wind is driven through scattering and the absorption of Doppler shifted spectral lines. Another unique aspect of this code is that it was designed to run on a off-the-shelf PC in just a few hours.

3.5.4 TLUSTY

TLUSTY is a non-LTE, plane parallel atmosphere code. It makes the standard 'plane parallel' assumptions that the atmosphere is horizontally homogeneous and is in radiative and hydrostatic equilibrium. The program also allows for fully consistent line blanketing. Full details are given in Hubeny *et al.* (1994). Recent revisions have been improved to include line blanketing (Lanz & Hubeny 2003).

3.5.5 FASTWIND

FASTWIND, the original version of which is described by Santolaya-Rey, Puls & Herrero (1997); calculates stellar atmospheres assuming a consistent photospheric stratification. It also includes an approximate treatment of metal line blocking and blanketing. The code can calculate the line transfer in the co-moving frame (Mihalas, Kunasz & Hummer 1975) or by using a Sobolev approximation with continuum (Puls & Hummer 1988). The biggest difference between this code and the other non-LTE atmosphere codes is that is uses a fast solution algorithm for calculating line profiles that allows for a consistent treatment of incoherent electron scattering.

3.5.6 Potsdam/Kiel Code

This is another more recent non-LTE, line blanketed code which was designed for the use of modelling the atmospheres of WR stars (Gräfener *et al.* 2002). It is an extension from previous work (Hamann & Koesterke 1998) where non-LTE calculations are computed for an expanding atmosphere, which is assumed to be spherically symmetric, stationary and homogeneous. However, the important difference of this code is the inclusion of iron-group elements in their calculations and that they also account for line blanketing. Solutions to the detailed statistical equations for model atoms is simplified via the use of super-levels, which was also successfully implemented into CMFGEN (see Section 3.6.2).

3.5.7 Comparisons

With all the stellar atmosphere codes available we will briefly compare them with a view of modelling the complex structures of a WR star's atmosphere. The first discriminator that immediately helps the process of suitability for WR stars is the disregard for stationary, plane-parallel codes. The assumptions made by these codes (especially a homogeneous

structure throughout the atmosphere) are too basic and unrealistic. This only leaves us with three other non-LTE atmosphere codes; FASTWIND, CMFGEN and the Potsdam/Kiel code. Strictly speaking we should not include the Potsdam code as this is a very recent code that was not available at the start of this study – this is also partly true for FASTWIND. Regardless of availability, CMFGEN includes the full treatment for a large number of highly ionized metal lines which are needed for a detailed analysis of a highly evolved WR stars, especially WC subtypes. Below we discuss some of the finer points regarding the use of CMFGEN and the assumptions made in our calculations.

3.6 Modelling Stellar Atmospheres with CMFGEN

There are a number of non-LTE radiative transfer codes that have been released to the astronomical community. Although none are as widely used as CMFGEN, (Hillier & Miller 1998), for the reasons described below. This atmospheric code has been developed and improved over a number of years and includes many important features that are vital when attempting to spectroscopically analysis massive stars and will be discussed in detail in this chapter. The original version of the code by Hillier (1987*a*) calculated a WN star whose atmosphere entirely comprised of pure helium, it was geometrically spherical and assumed a modified Sobolev approximation, allowing for a continuous radiation field. Latter efforts included carbon into their atmospheric calculations (Hillier 1989) such that the new revised model could attempt to model the (complex) atmospheres of WC stars. The current version is by far more accurate and computes almost all iron-group elements, and also allows a degree of 'clumping' in the wind. Specific details of these extensive modifications are discussed below.

3.6.1 Modelling Technique

For this work we use the non-LTE code of Hillier & Miller (1998) CMFGEN, which iteratively solves the transfer equation in the co-moving frame subject to statistical and radiative equilibrium in the expanding, spherically symmetric and steady-state atmosphere. This work is part of a larger project to study WR stars in a variety of environments and so the modelling techniques applied to the WR stars in our sample are the same as those described by Crowther *et al.* (2002). Specific details of the (extremely complex) He, C, O, Ne, Si, P, S, Ar, Fe model atoms used in our analysis are described in more depth

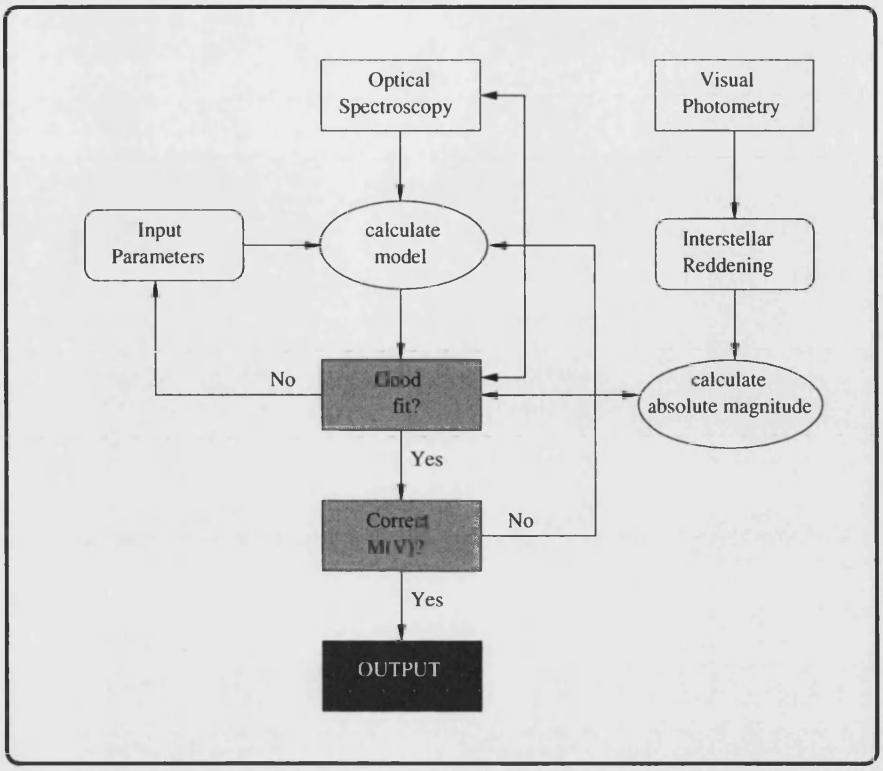

Figure 3.2: Flowchart showing the methodology used to model our sample of single WR stars using both spectroscopic and photometric observations.

in Section 3.6.2. These models account for clumping in the wind, via a filling factor, f, which we set to approximately 0.1 (see Section 3.6.4). Since radiation instabilities are not thought to be important close to the base of the wind we parameterise the filling factor so that at smaller velocities it approaches unity.

Our approach to modelling the data is to calculate a series of models adjusting the stellar parameters until we can match the observed ionization balance, line strengths, widths (and for our un-calibrated datasets, the absolute V-band magnitudes). Because of the effect each parameter can have on the emergent model spectrum this was an iterative process. Initially, matching the line strengths and widths of the modelled spectrum compared with the observations and then altering the luminosity to match either the absolute magnitudes calculated or the absolute (calibrated) flux levels.

Figure 3.2 shows a simple flowchart outlining the iterative stages required to model a WR star which is not flux calibrated, in which an independent determination of the star's absolute magnitude is required. This method is similar for flux calibrated observations, the only difference is that the reddening is determined by de-reddening the observations to

match the (un-reddened) model. This also provides an independent method for obtaining the absolute magnitude.

3.6.2 Treatment of Super Levels

The idea of "super-levels" was first introduced by Anderson (1989) to reduce the number of statistical equilibrium equations that have to be calculated for a stellar atmosphere. This technique is used by CMFGEN where it simplifies the model atoms that are calculated by grouping a number of levels that have similar energies and properties and treating them as one single 'super-level'. This then means that only the populations of the super-levels are used in the rate equations. The only assumption that has to be made is that an individual atomic level has the same departure coefficient as its corresponding super-level. This method has been used in other non-LTE atmosphere codes with success (e.g. Hubeny & Lanz 1995; Dessart *et al.* 2000). There are obvious benefits when considering the (extremely complex) iron-group elements into a stellar atmosphere calculation, as it allows a single model to be calculated by seriously reducing the computational constraints. Model calculations for WC stars in this work, via the use of super-levels, assume a total of 2526 levels (reduced to 788 super-levels), 26,239 spectral lines of He, C, O, Ne, Si, S, P, Ar and Fe are considered. For our largest calculations modelling WN stars we assume a total of 1233 levels (combined to 372 super-levels) for 43,596 spectral lines of H, He, C, N, O, Ne, Si, S, and Fe. For both sets of calculations we used 40 depth points. Table 3.1 summarises the model atomic calculations assumed for both WN and WC stars. Full details for the oscillator strengths, collision and photoionization cross-sections are given in Dessart *et al.* (2000). Almost all the atomic data for this work uses results published by the OPACITY (Seaton 1987; Seaton 1995) and IRON (Hummer *et al.* 1993) projects.

3.6.3 Line Blanketing

The spectra of WR stars are quite often extremely crowded, containing a huge number of emission lines, particularly in the UV, where we see a whole "forest" of (weak) iron lines, shortward of $\approx$ 1800Å (e.g. Herald *et al.* 2001). It was soon recognised in the early theoretical studies that the inclusion of individual lines had a significant impact on the emergent atmosphere (Anderson 1985). Adequately accounting for these lines results in an increase in opacity and hence alters the temperature structure within the wind. Line blanketing causes two main effects within the star's atmosphere, "back-warming"

and "flux blocking". The effect of back-warming is to produce higher temperatures in the inner regions and cooling in the outer regions. It also has an effect on the star's ionization structure, producing a higher ionization close to the star, whilst reducing the wind ionization further out in the wind, the latter effect termed flux blocking.

CMFGEN includes a full treatment of line blanketing although it was not successfully implemented until the working version published by Hillier & Miller (1998). To further emphasise the importance of line blanketing in WR atmospheres, for a typical WC star, approximately 40% of the flux between 1000Å and 10,000Å is in the lines, making it almost impossible to accurately locate the star's continuum over this region (Hillier & Miller 1998). Not only does the inclusion of iron significantly modify the emergent spectrum in the UV region but it also affects individual emission lines in the optical. For instance, in WC stars, iron-blanketed models can increase the strength of C III λ5696 by a factor of 5. This is due to an increased UV continua which through the pumping mechanism of the C III emission lines $\lambda\lambda\lambda$386,574,977 in the UV affect the optical emission line of C III λ5696 (Hillier 1989). Other C III lines (e.g. C III $\lambda\lambda$1909,2296) are also dramatically affected, as well as C IV $\lambda\lambda$5801-12 (Hillier & Miller 1998).

3.6.4 Clumping

Clumping in WR winds has been a topic of debate amongst astronomers for a number of years. There is mounting evidence in favour of a heavily clumped wind in the atmospheres of O stars, LBVs and WR stars. There has been observational evidence for clumping from line profile variability studies in O stars (e.g Robert 1994) and WR (e.g Moffat 1999) stars. Evidence from other groups studying WR stars and LBVs through polarization also concluded that their winds were clumped (e.g. HD 96548 Schulte-Ladbeck (1995) and P Cygni Taylor *et al.* (1991)). Theoretical evidence also indicates that radiation driven winds are unstable and can lead to large amounts of clumping (Owocki, Castor & Rybicki 1988).

Hillier (1991) originally introduced a clumping factor to account for the over-estimation that the models predicted in the electron-scattering wings of certain lines. The addition of this *filling factor* reduced the strength of the electron-scattered wings which in turn meant that the emission line strength could be reproduced with slightly lower mass-loss

Table 3.1: Overview of the model atoms calculations used for both WC and WN model atmospheres. N_f, is the number of full levels, N_s, is the number of assumed super levels and N_t is the corresponding number of transitions.

	I			II			III			IV			V			VI			VII			VIII		
Ion	N_f	N_s	N_t	N_f	N_s	N_t	N_f	N_s	N_t	N_f	N_s	N_t	N_f	N_s	N_t	N_f	N_s	N_t	N_f	N_s	N_t	N_f	N_s	N_t
WC Stars																								
He	39	27	315	30	13	435																		
C				16	9	36	243	100	5513	64	49	1446												
O				29	13	120	154	60	1454	72	30	835	78	41	524	23	17	109						
Ne				48	14	290	101	39	675	68	23	432	117	27	837	34	15	135						
Si										33	23	183												
P										28	16	57	28	18	138									
S										77	29	506	26	14	58	11	7	24						
Ar							36	10	67	105	23	834	61	24	276	81	21	606	37	18	133	12	7	26
Fe										280	21	4223	182	19	2163	190	29	2028	153	14	1216	70	18	183
WN Stars																								
H	14	8	435																					
He	51	29	579	30	13	435																		
C										18	13	1446												
N							48	33	400	60	34	1065	55	43	1554									
O							13	13	658	72	30	835	46	21	2325	39	33	1475						
Ne							19	10	2294	13	7	9725												
Si										20	12	1090												
S										20	10	3597	20	12	449									
Fe										280	21	8669	182	19	3800	80	10	867	153	14	1898			

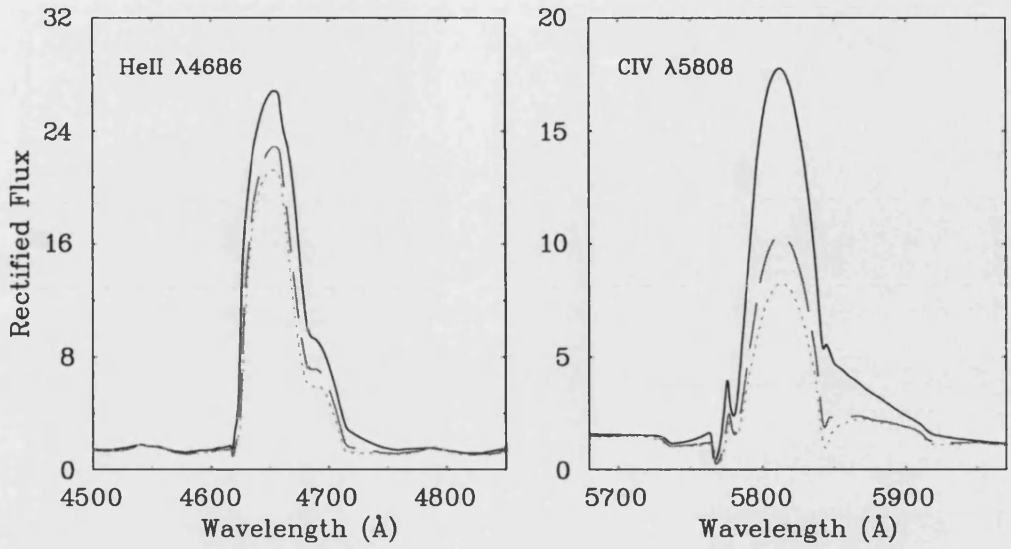

Figure 3.3: Synthetic line profiles for C III-IV/He II λ4650 and C IV λλ5801-12 showing a varied degree of clumping in the wind. An unclumped model is shown in solid ($f = 1$ with $\dot{M} = 6.3$ x $10^{-5}\,M_{\odot}yr^{-1}$), a moderately clumped model is shown as a dashed line ($f = 0.1$ with $\dot{M} = 2.0$ x $10^{-5}\,M_{\odot}yr^{-1}$) and a highly clumped model is shown as a dotted line ($f = 0.01$ with $\dot{M} = 6.3$ x $10^{-6}\,M_{\odot}yr^{-1}$).

rates. This filling factor can be parameterised by:

$$f(r) = a + (1 - a)exp^{[\frac{-v(r)}{b}]} \tag{3.21}$$

where the parameter a equates to the density contrast in the wind at the location b where clumping becomes important. This simply means that radiation instabilities become more important further out in the wind such that this filling factor is parameterised to reach unity as the velocity goes to zero. This parameterisation approximates current theoretical instability models (Runacres & Owocki 2003).

Our models derive $\dot{M}/\sqrt{f}$ rather than mass loss and clumping individually. Figure 3.3 shows the synthetic line profiles for the two strong (optical) WR emission features, C III-IV/He II λ4650 and C IV λλ5801-12. The stellar parameters are typical for a WCE star and are kept constant except we have varied the degree of clumping in the wind such that the filling factors are $f = 1.0, 0.1, 0.01$. The corresponding mass loss was also adjusted. The line strength and red electron scattering wing for C IV λλ5801-12 are extremely sensitive to

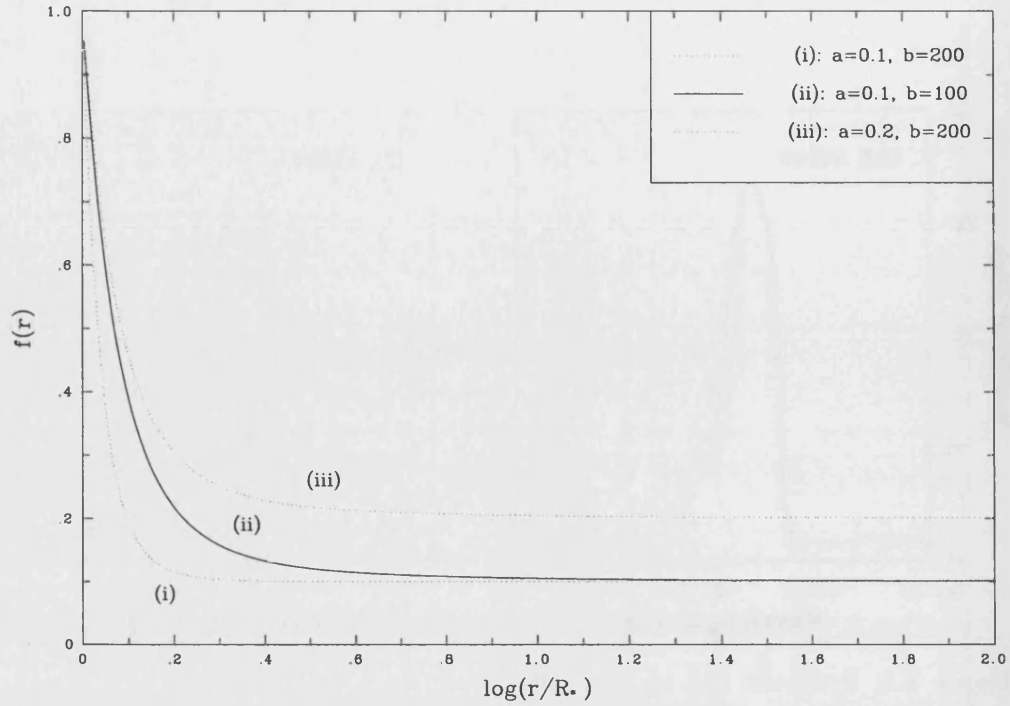

Figure 3.4: The clumped structure in the wind of a WR star with a standard (β = 1) velocity law and an exponent of $\beta = 20$. The terminal wind velocity is set to v_∞=1400kms^{-1}. Typical clumping values assumed in our models are shown; a = 0.1, b = 100 (solid line), with variations of both parameters also shown (dotted lines) to highlight their effects.

the filling factor. The line strength for the blended λ4650 emission feature is also weakly affected by clumping.

Even though our technique for determining the clumping within the wind is not accurate we can confidently rule out the extreme cases (i.e. where $f = 0.01$ or 1.0). Instead we settle for the intermediate case for all our model calculations, where the filling factor is, $f = 0.1$. This is in reasonable agreement with previous, observationally determined values (e.g. $f = 0.0625$; Hamann & Koesterke 1998). This intermediate value for the filling factor also reproduces the line strength and electron scattering wing observed in WC stars (see Chapter 6 for examples). Recently, theoretical calculations are attempting to reproduce line profile variabilities due to inhomogeneities in the wind which will help in the understanding of the physical properties of stellar atmospheres (e.g. Dessart & Owocki 2002).

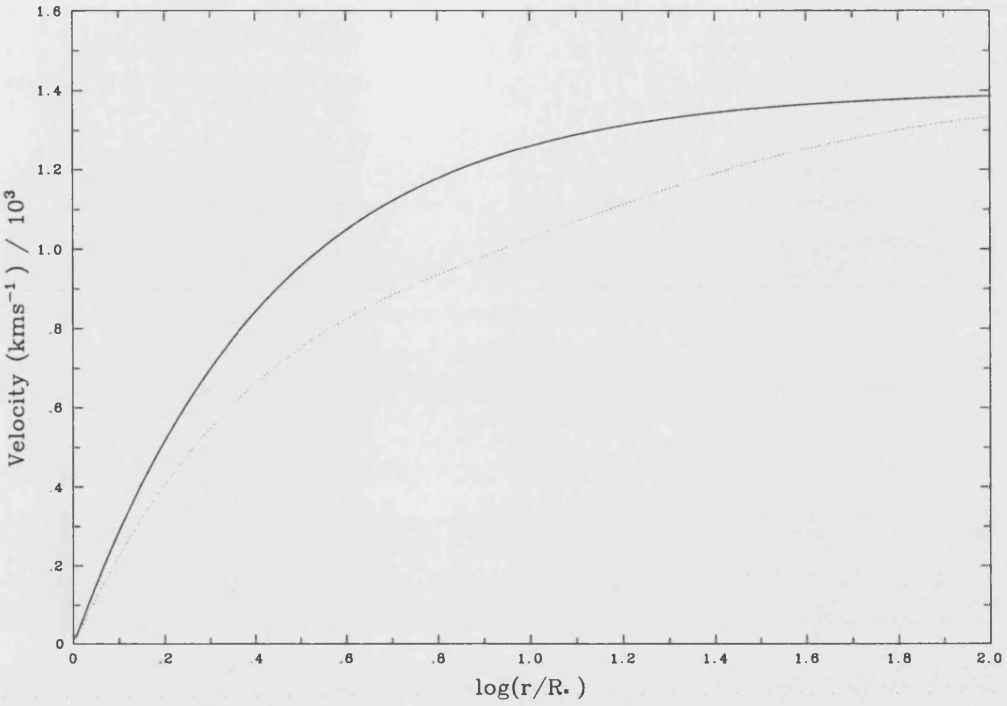

Figure 3.5: The wind velocity structure for a WR star showing both a standard β=1 law (solid line) and a second velocity law with β=1 and an exponent of β=20 (dotted line). The parameters used for these structures are, v_0=0, v_{core}=1.0kms^{-1}, v_{ext}=300kms^{-1}, v_∞=1400kms^{-1}, h_{eff}=0.01R$_*$ and R$_*$=1.0R$_\odot$.

3.6.5 Velocity Law

Traditionally WR atmospheres were modelled adopting a standard $\beta = 1$ velocity law, as is the case for O stars, although this becomes more complex when considering WR atmospheres due to their extremely broad emission lines. In more recent years there has been conflicting evidence to suggest, both observationally and theoretically, a more slowly accelerating outflow. In the standard $\beta = 1$ velocity law, the velocity at any depth in the wind is dependent on the exponent β - with the largest accelerations occurring close to the star and very little acceleration at large distances. This idea was questioned when Koenigsberger (1990) observed some WN binary systems and found that the wind appeared to be accelerating out to distances of 14R$_\odot$. Later work, again studying WR binaries supported this theory (Auer & Koenigsberger 1994). Theoretical work also concluded that there

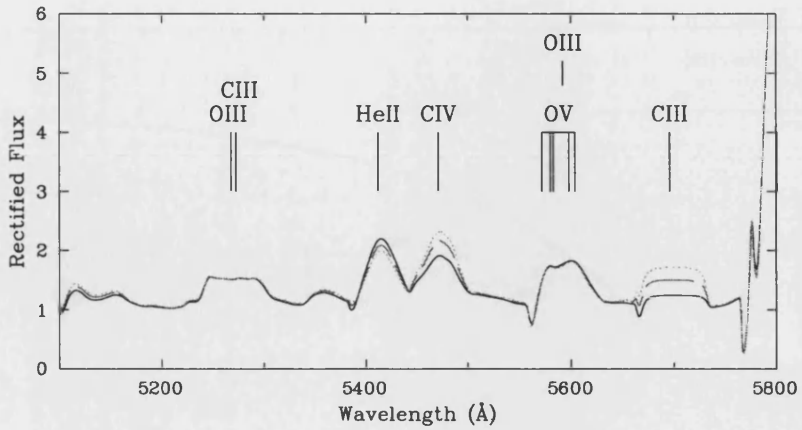

Figure 3.6: Comparison of synthetic models showing the sensitivity λ5471 of the He II λ5411 and C IV λ5471 emission lines for a variety of carbon abundances - 0.15 by number (solid), 0.3 by number (dashed) and 0.5 by number (dotted).

was still a significant acceleration within the wind at large radii (e.g Gayley, Owocki & Cranmer 1995; Schmutz 1997). This means that the standard $\beta = 1$ law cannot be used for WR stars.

These results are taken into account by CMFGEN which adopts a two-component velocity law within a stellar atmosphere in such a way as to match observational datasets. It does this by adjusting the normal $\beta = 1$ law, but with the addition of a secondary β component. This velocity law is in the form

$$v(r) = \frac{V_0 + (V_\infty - V_{ext} - V_0)(1 - R_*/r)^{\beta_1} + V_{ext}(1 - R_*/r)^{\beta_2}}{1 + (V_0/V_{core})exp[(R_* - r)/h_{eff}]} \tag{3.22}$$

where V_{ext} and V_∞ are the intermediate and terminal velocities respectively (typically $v_{ext} \sim v_\infty$ - 300 kms^{-1}), β_1 and β_2 are the exponents used in the adopted form of velocity law (for our WC models we use $\beta_2 = 20$).

3.6.6 Carbon Abundances

Chemical abundances are one of the many fundamental parameters computed using CMFGEN; calculating abundances of H, He, N are important for WN stars, while elements of He, C and O are important to constrain WC stars. Unfortunately, observations of extragalactic WR stars only permit optical spectroscopic studies – this hinders their analysis

because of the limited number of emission lines available to constrain their parameters (see Chapter 6 for more concise description of methods employed). Here we discuss and identify the emission lines used to constrain the chemical abundances for WR stars solely from their optical spectra.

To determine the C/He abundance for WC stars we use the (relatively) unblended diagnostic lines of He II λ5411 and C IV λ5471. These prove excellent indicators of variations in the C/He abundance. Figure 3.6 shows the region around the carbon diagnostic lines, He II λ5411 and C IV λ5471, for a series of models calculated with C/He of 0.15 by number, 0.3 by number and 0.5 by number. The relative strength of these lines are used to derive the C/He abundance in our sample of WC stars. C III λ5696 also varies between these models although this emission line is also sensitive to other parameters such as ionization and temperature in the wind. For the few cases where we detect C IV λ5808 emission in WN stars we use this line to estimate the C/He abundance.

3.6.7 Oxygen Abundances

Unfortunately we are more restricted when it comes to good diagnostic lines for the O/He abundance. This is due to a lack of unblended recombination lines available, also oxygen produces a more complex ionization structure compared with He and C. The only available optical emission line which is sensitive to O/He variations is the blended emission line, O III-V λ5590. However, previous observational studies by Crowther *et al.* (2002), using spectra covering far-UV – NIR, were able to determine the oxygen abundance for six WC stars in the LMC by comparing a number of UV lines (e.g. O V λ1815,O III λ2983, O IV λ3072 and O IV $\lambda\lambda$3560-3). Unfortunately on detailed inspection the oxygen abundances required to match the line strengths for these lines indicated (relatively) minor discrepancies. Crowther *et al.* (2002) also found that, in some cases, if the line strength for O III-V λ5590 was matched then it slightly over-estimated the O/He abundance compared with the UV diagnostics. This means that our calculated oxygen abundances, and hence our O/C determinations should be taken with caution, and suggest an internal accuracy of $\sim$50% in our derived mass fractions.

Figure 3.7 shows three synthetic spectra with various oxygen abundances – 5%, 10% and 20% by mass – covering the near-UV to the optical. It highlights that there are a number of near-UV oxygen emission lines which are sensitive to variations in the abundance of oxygen (e.g. O IV λ3072), and very few oxygen lines which vary in the optical regime.

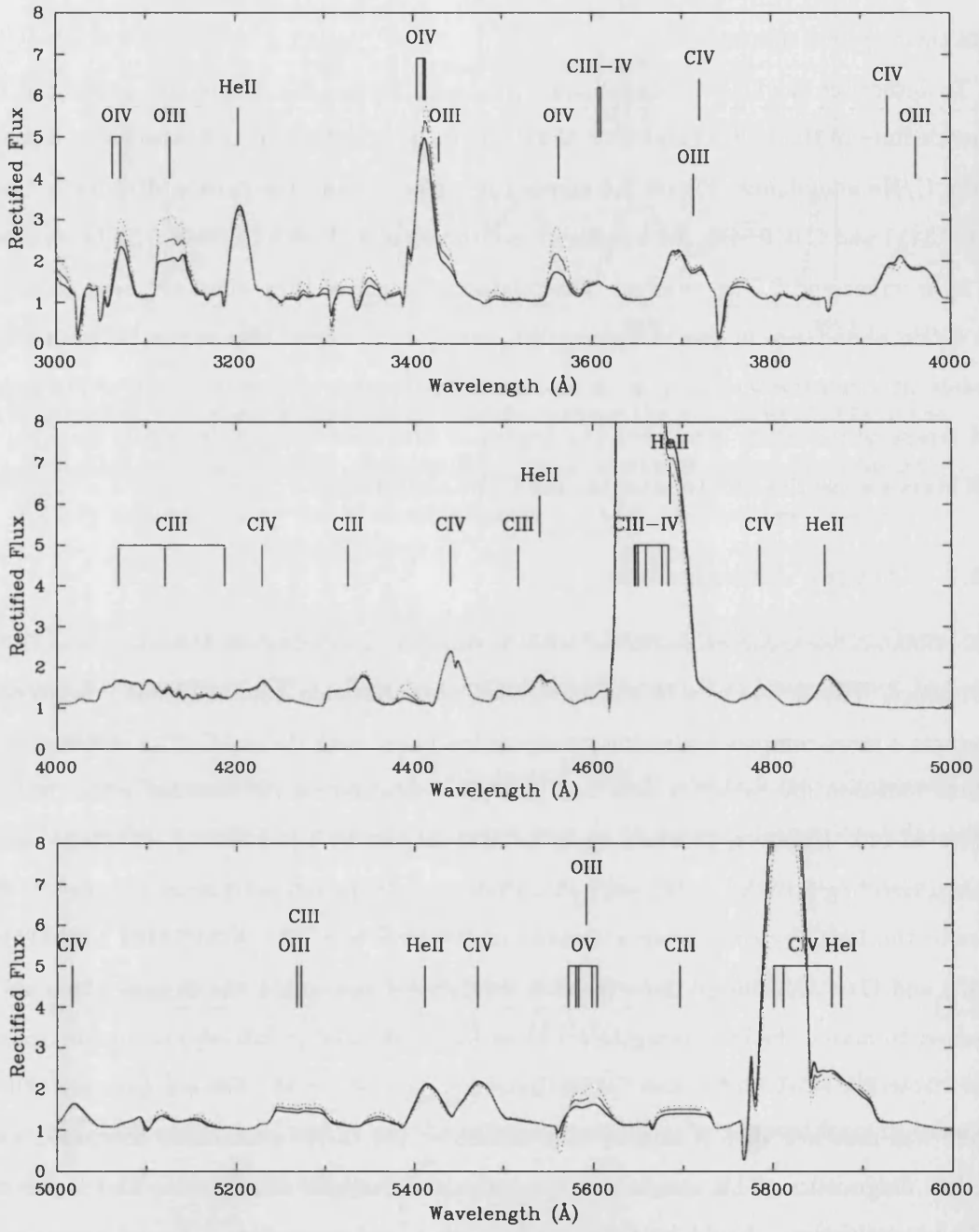

Figure 3.7: Comparison between rectified near-UV/optical synthetic spectra showing a variety of oxygen abundances – 5% (solid), 10% (dashed) and 20% by mass (dotted).

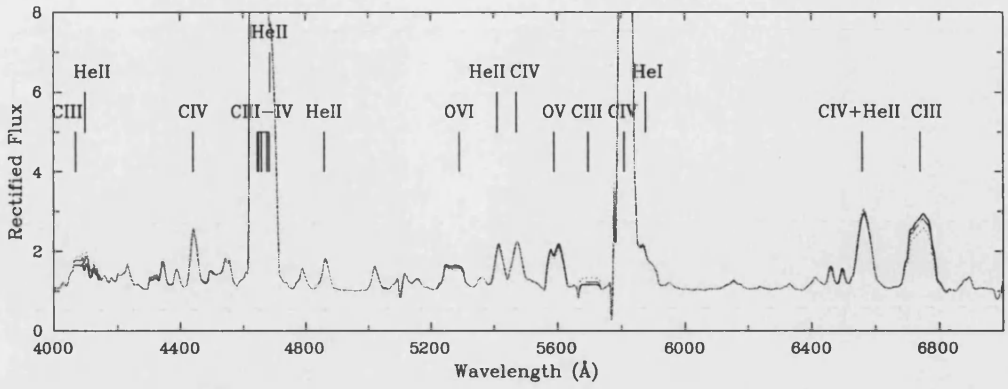

Figure 3.8: Comparison between rectified near-UV/optical synthetic spectra showing a variety of iron abundances – $0.5\,Z_\odot$ (solid), $Z_\odot$ (dashed) and $1.5\,Z_\odot$ (dotted). The theoretical optical spectrum is almost unchanged over this range of iron abundances.

Unfortunately due to the large extinction of dust, extra-galactic studies of WR stars are often unable to achieve high enough signal-to-noise blueward of $\sim$ 4000Å. As previously discussed, this only leaves the blended optical emission line O III-V λ5590 as a diagnostic indicator.

3.6.8 Iron Abundances

Another limitation with using optical spectra is that only tentative conclusions can be reached about the metallicity of the WR environment, as the iron-group elements predominately effect lines in the UV. We highlight this by running three separate models with identical parameters except for the iron-group elements. As well as the usual calculations to include He, C, N, O, we also compute a more complete model to include ions of Si, Ne, S, P, Ar and Fe. We alter these iron-group elements for $0.5\,Z_\odot$, $Z_\odot$ and $1.5\,Z_\odot$. The difference between the emergent optical spectra is very small and does not effect the diagnostic emission lines. These results are shown in Figure 3.8 for an early-type WC star.

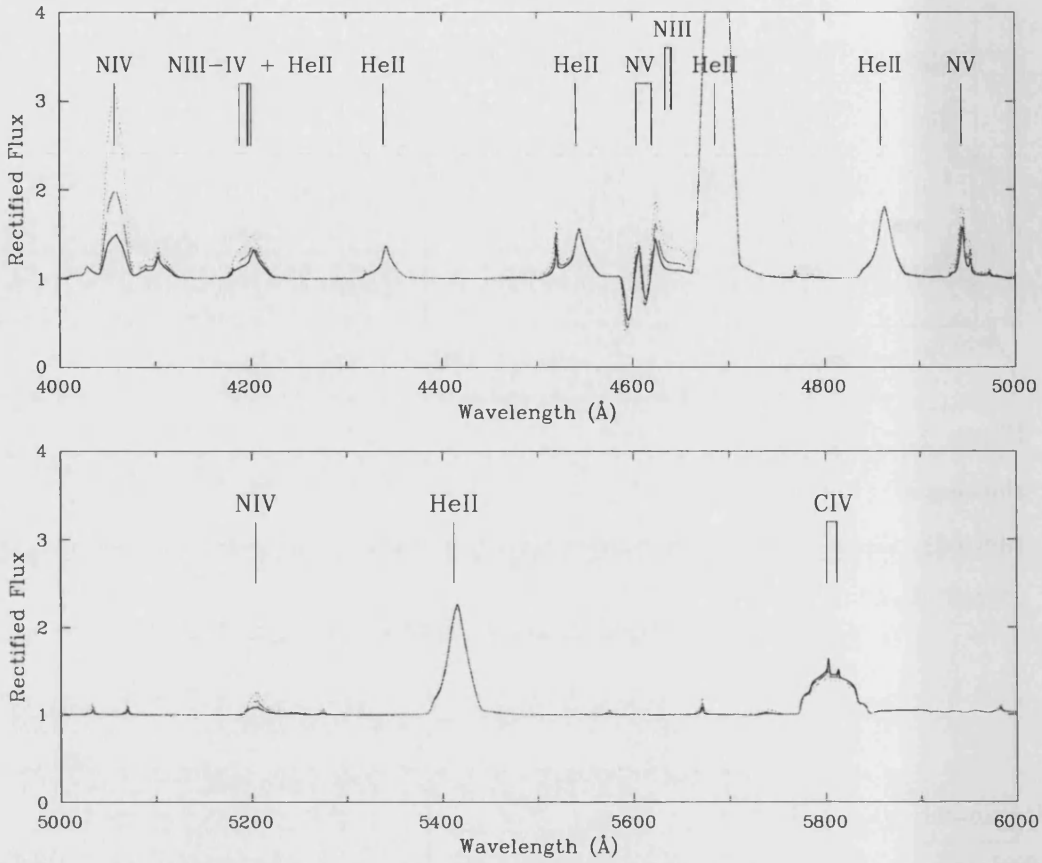

Figure 3.9: Comparison of synthetic models showing the sensitivity of the nitrogen lines (e.g. N IV λ4057, N V λ4604 and N III λ4640) abundances – 0.15 (solid), 0.3 (dashed) and 0.5 by number (dotted).

3.6.9 Nitrogen Abundances

Fortunately deriving the chemical abundances for WN stars is somewhat easier than WC stars, as we have a number of diagnostic lines available. After we are confident that the temperature and ionization balance are well matched, we can adjust the abundance of nitrogen using N IV λ4057, N V λ4604 and N III λ4640 as diagnostics.

3.6.10 Hydrogen Abundances

The hydrogen abundances we determine are less certain, especially for WN stars with weak hydrogen emission. However, where possible we use the blended H I-Balmer/He II-

Pickering decrement present in the optical, predominately relying on Hα-He II $\lambda\lambda$6560,6563, to derive hydrogen abundances. Unfortunately due to this emission line being blended and quite often contaminated with nebular emission (if detectable) we also use blended Hβ λ4861 and Hγ λ4341 emission lines. The classification scheme devised by Smith, Shara & Moffat (1996), states that hydrogen is detected if the (H+He) lines, λ4340 and/or λ4861, clearly exceed the height of a line drawn between the peaks of the pure He II lines, $\lambda\lambda\lambda$4200,4541,5411 – simple visual inspection can be used as a quick tool to estimate the presence of hydrogen.

CHAPTER 4

Analysis of Extragalactic Wolf-Rayet Stars

We postpone until Chapters 6–5 the detailed spectroscopic analysis of extragalactic WC and WN stars with the model atmosphere code of Hillier & Miller (1998), comparing the inferred stellar parameters with environmental metallicity. However, we wish in the present chapter to perform a series of simple analyses on the spectroscopic observations discussed in Chapter 2. We investigate the possibility for a simple correlation between spectroscopic morphology and environmental metallicity, as well as the prospect that early WC stars have a uniform line flux (Smith, Shara & Moffat 1990). We also re-evaluated the metallicity gradient for a number of spiral galaxies in our sample using recent H II calibrations.

4.1 Metallicity Gradients

Early observations of H II regions identified that there was a clear radial oxygen abundance gradient in the disks of spiral galaxies (Searle 1971; Smith 1975). These studies showed that the oxygen abundance was higher towards the centre, gradually declining further from the galactic centre. This ignited a flurry of observational studies which further identified oxygen abundance gradients for a large sample of galaxies (e.g. Vila-Costas & Edmunds 1992; van Zee *et al.* 1998).

Studying the oxygen content of galaxies proves useful not just in the understanding of the chemical properties of galaxies (and their evolution), but also because it can be

used to trace the metal content of galaxies. Oxygen is commonly used as it is both easily observed and is reliably established - in contrast to other elements such as nitrogen or carbon.

Observational investigations predominately use the optical emission lines from H II regions to accurately determine abundances. Early methods used the temperature sensitive [O III] λ4363 line which is weak in metal-rich environments (abundances are derived from accurate measurements of the line ratio; [O III] $\lambda\lambda$4959,5007/λ4363), and so Pagel *et al.* (1979) devised an empirical calibration to derive the oxygen abundance from observations of H II regions, using the ratio between a series of (strong) [O II] to [O III] emission lines, where the weaker [O III] λ4363 was absent. This technique is known as the R_{23} method. The exact ratio employed to determine the R_{23} is given as:

$$R_{23} = ([\mathrm{O\,II}]\lambda\lambda 3726, 3729 + [\mathrm{O\,III}]\lambda\lambda 4959, 5007)/H\beta \tag{4.1}$$

The R_{23} method soon became widely accepted and is still used by a number of authors today, although there were other groups who utilised the optical emission seen from supernova remnants (SNRs) to also derive oxygen, nitrogen and sulphur abundances (e.g. Blair *et al.* 1982*a*; Dopita *et al.* 1984). Unfortunately these techniques heavily rely on detailed, (sophisticated) shock models before abundances can be calculated, as a result published results tended to vary somewhat.

As previously discussed, the weak, temperature sensitive [O III] λ4363 line can be used to accurately calculate oxygen abundances in H II regions. Unfortunately confident detections of this weak emission line in H II regions in nearby galaxies have proven difficult. As a result there have been a number of semi-empirical calibrations using the R_{23} index to determine oxygen abundances in extragalactic H II regions, as this technique only requires line fluxes for the stronger emission lines (see Equation 4.1). In recent years there have been a number of observationally based R_{23} calibrations (e.g. Edmunds & Pagel 1984; McCall, Rybski & Shields 1985). The latest calibration by Zaritsky, Kennicutt & Huchra (1994) converts the R_{23} index into an oxygen abundance by providing a polynomial fit to three averaged semi-empirical calibrations (Edmunds & Pagel 1984; Dopita & Evans 1986; McCall, Rybski & Shields 1985), all derived observationally, and is well approximated by

$$12 + \log(O/H)_Z = 9.265 - 0.33x - 0.202x^2 - 0.207x^3 - 0.333x^4 \tag{4.2}$$

where $x \equiv \log R_{23}$. The R_{23} index is double-valued due to the nature of nebular lines in metal-rich and metal-poor H II regions (see Kobulnicky, Kennicutt & Pizagno (1999) for

an excellent review on measuring nebular abundances in distance galaxies), so in order to decide which regime is best suited to the dataset the [NII] λ6583/[OIII] $\lambda\lambda$4959,5007 line ratio can be used as an indicator for the galaxy's metallicity. The mean relation by Zaritsky, Kennicutt & Huchra (1994) is good only for the upper, metal-rich regime. There have been other calibrations, most notably the extensive calibration based on photoionization models by McGaugh (1991), whose models take into account the effects of varying the ionization parameter in both metal-rich and metal-poor regimes.

The problem with the existing R_{23} calibrations are that they were calibrated against out-dated, temperature derived abundances available at the time. Since then there have been a much larger sample of metal-rich H II regions observed. Pilyugin (2000) used this larger sample of accurately determined oxygen abundances to re-calibrate abundances derived using the R_{23} method. He found that this larger sample of revised observations can be approximated by

$$12 + \log (O/H)_{R_{23}} = 9.50 - 1.40x_{2,3} \tag{4.3}$$

where $x = log\, R_{23}$. This relationship is only valid for H II regions with 12+log(O/H) > 8.15. Pilyugin (2003) has also recently reported another technique simply using the strong oxygen lines of [OII] $\lambda\lambda$3726,3729 and [OIII] $\lambda\lambda$4959,5007 (relative to Hβ), to obtain oxygen abundances in H II regions. According to Pilyugin (2003), O/H abundances in H II regions determined from the traditional R_{23} method can be overestimated in regions with a low excitation parameter, P, which is defined as the contribution of the radiation in the [OIII] lines to the 'total' oxygen radiation. The method by Pilyugin (2003) can be mathematically described as:

$$12 + \log (O/H)_P = \frac{R_{23} + 54.5 + 59.45P + 7.31P^2}{6.07 + 6.71P + 0.37P^2 + 0.243R_{23}} \tag{4.4}$$

He argues that oxygen abundances determined using the R_{23} method involve a systematic error depending on the excitation parameter (Pilyugin 2000), and that the traditional R_{23} method is valid in high excitation regions, but fails to provide realistic abundances in low excitation regions. Such that the R_{23} methods can over estimate abundances by $\sim$0.3dex or more in low excitation regions.

The empirical (R_{23}) methods commonly used (Edmunds & Pagel 1984; McCall, Rybski & Shields 1985; Dopita & Evans 1986; McGaugh 1991) are based on a limited number of oxygen abundances derived using the temperature sensitive lines and out-dated H II region

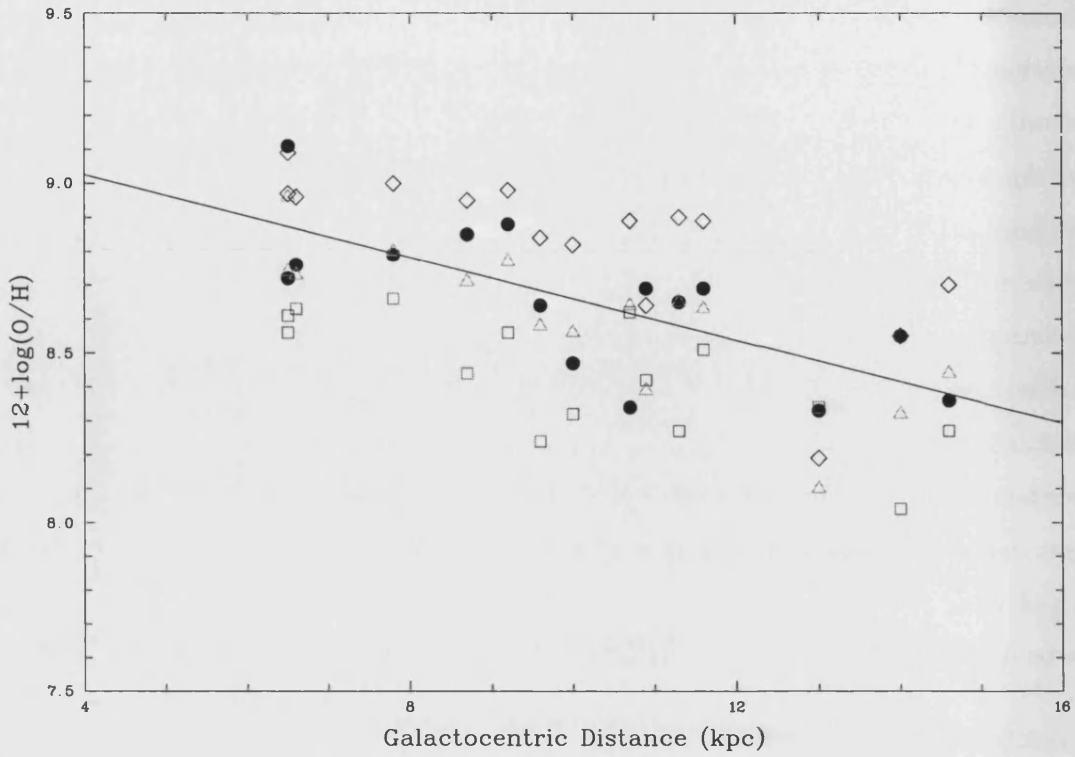

Figure 4.1: Oxygen abundance gradient in Galactic H II regions taken from Shaver *et al.* (1983) (filled circles). These results are compared with, re-calibrated H II regions data using the empirical R_{23} calibration by Zaritsky, Kennicutt & Huchra (1994) (open diamonds), revised R_{23} calibration by Pilyugin (2000) (open triangles), and the P-method by Pilyugin (2003) (open squares).

models, available at the time. These R_{23} calibrations do not reproduce the latest available data (Pilyugin 2000). These differences can be explained by the fact that the R_{23} method ignores the physical conditions in the H II region (Pilyugin 2000).

If we are to observationally infer a mass-loss – metallicity connection for WR stars (see Chapters 6 – 5), then it is important to determine an accurate metallicity gradient in the regions we observe WR stars. This section will focus on modern abundance calibrations, in which we re-analyse observations of extragalactic H II regions enabling us to determine metallicity gradients across spiral galaxies in the Local Group.

Table 4.1: Oxygen abundances in galactic H II regions from Shaver *et al.* (1983). Also listed are the abundances derived from three different calibrations.

H II Region	R_G (kpc)	12+log(O/H) Shaver et al. (1983)	Pilyugin (2003)	Pilyugin (2000)	Zaritsky et al. (1994)
NGC 6604-1	6.5	9.11	8.61	8.96	9.09
NGC 6604-2	6.5	8.72	8.56	8.74	8.97
M 16	6.6	8.76	8.63	8.73	8.96
1 Cen-2	7.8	8.79	8.66	8.80	9.00
RCW 40	8.7	8.85	8.44	8.71	8.95
RCW 34	9.2	8.88	8.56	8.77	8.98
RCW 19	9.6	8.64	8.24	8.58	8.84
Rosette-1	10.0	8.47	8.32	8.56	8.82
S 252-1	10.7	8.34	8.62	8.64	8.89
RCW 16-1	10.9	8.69	8.42	8.39	8.64
RCW 8	11.3	8.65	8.27	8.65	8.90
RCW 6	11.6	8.69	8.51	8.63	8.89
RCW 5-1	13.0	8.33	8.34	8.10	8.19
G 201.6+1.6	14.0	8.55	8.04	8.32	8.55
S 284	14.6	8.36	8.27	8.44	8.70

4.1.1 Comparisons

Before we re-calibrate the abundance gradients for a number of spiral galaxies in the Local Group, we further examine the methods available to derive oxygen abundances where detections of [O III] λ4363 are limited. To do this we analyse the galactic metallicity gradient, extending the method used by Pilyugin, Ferrini & Shkvarun (2003) and compare a number of calibration techniques against accurate abundances calculated from observations which include temperature sensitive lines. There is a good reason to assume that the current Galactic H II region abundance gradient is correct (mainly due to the good agreement between young stars and gas), and is safe to use as a calibration tool. There have been a number of observational studies using early B-type main-sequence objects to determine abundance estimates, these results are in excellent agreement with those found from the

study of H II regions (e.g. Smartt & Rolleston 1997; Rolleston *et al.* 2000; Gummersbach *et al.* 1998).

We use a selection of 15 galactic H II regions observed by Shaver *et al.* (1983), who combined both radio and optical spectroscopy to determine electron temperatures. Only using observations from where reliable measurements for both [O II] $\lambda\lambda$3726,3729 and [O III] $\lambda\lambda$4959,5007 were obtained (see Table 4.1). We compare the oxygen abundances originally determined by Shaver *et al.* (1983) with our re-calibrated abundances using the empirical calibrations by Zaritsky, Kennicutt & Huchra (1994), Pilyugin (2000) and Pilyugin (2003), all of which are discussed in the text above. These results are shown in Figure 4.1, a least squared fit to the data by Shaver *et al.* (1983) is also shown and is described by, $12+\log(O/H)_{SH} = 9.27 - 0.061R_G$. The galactocentric distances for the H II regions are taken from Deharveng *et al.* (2000).

Using the previously determined metallicity gradient by Shaver *et al.* (1983) as a guide, we find that the three empirical calibrations varied somewhat. The typical R_{23} calibration by Zaritsky, Kennicutt & Huchra (1994) tends to over-estimate the oxygen abundance compared with the abundances found by Shaver *et al.* (1983). Whereas the recent (P-method) calibration by Pilyugin (2003) consistently predicts lower oxygen abundances than found by Shaver *et al.* (1983), although both these calibrations reproduce a very similar gradient. Finally, we also construct a galactic metallicity gradient using the re-calibrated R_{23} method by Pilyugin (2000). We find that these results agree best with the metallicity gradient by Shaver *et al.* (1983), closely matching both the oxygen abundances and the metallicity gradient. Considering these results, we chose to adopt this method, using previously published H II region line fluxes, to revise the metallicity gradients for a number of Local Group galaxies.

4.1.2 Metallicity Gradient in M 33

M 33 is an ideal laboratory for studying the metallicity effects in WR stars. With its low orientation, low reddening, and radial abundance gradient seen across the disk of the galaxy, it provides us with a number of WR stars located in a variety of metallicities.

The metallicity gradient across M 33 has been well studied using a number of different techniques. Work by Dopita, D'Odorico & Benvenuti (1980) used observations of supernova remnants in M 33 to obtain oxygen, nitrogen and sulphur abundances. Similar work was carried out by Blair & Kirshner (1985) and Smith, Kirshner & Blair (1993)

who all calculated abundances of oxygen to infer an abundance gradient. Although as discussed above there were large discrepancies between these results, primarily due to the dependence on shock models required before accurate abundances can be derived.

Alternative metallicity gradients may be obtained from H II regions. These too rely on models, although they are well-tested and (mostly) observationally based. For M 33 H II regions were observed by Smith (1975), Kwitter & Aller (1981), Vilchez *et al.* (1988), and Garnett, Odewahn & Skillman (1992). Since then these datasets have been re-analyzed by Henry & Howard (1995), Zaritsky, Kennicutt & Huchra (1994) and Garnett, Odewahn & Skillman (1992), using calibrations calculated from observations of H II regions (e.g. Edmunds & Pagel 1984). Notably, the paper by Zaritsky, Kennicutt & Huchra (1994) used previously published work (including data collected by McCall, Rybski & Shields 1985) to recalibrate the data and derive new abundances.

After considering the results discussed in Section 4.1.1 we follow the method of Pilyugin (2000) who re-calibrated previous datasets derived using temperature sensitive emission lines to calculate nebular oxygen abundances. We have used the observational data of H II regions taken by Smith (1975), Kwitter & Aller (1981) and Vilchez *et al.* (1988) to calculate the metallicity gradient for M 33, using oxygen as a metallicity tracer. For completeness we also compare the oxygen abundances derived from B supergiants by Monteverde *et al.* (1997). In the few cases where multiple observations of the same H II region were available, CCD data from Vilchez *et al.* (1988) were favoured.

We feel for the majority of our observations the re-calibrated R_{23} relation by Pilyugin (2000) (see Equation 4.3) appears robust. Recall, this relationship is valid for metallicities above 12+log(O/H) > 8.15. As a further internal check their [NII]/[OIII] line ratios seem to represent a metal-rich sample, above the cut-off value (Kobulnicky, Kennicutt & Pizagno 1999). Figure 4.2 shows the re-calibrated oxygen abundances across M 33, there is evidence that there is a steep gradient ranging from above solar in the nucleus to more SMC-like far out in the disk. For completeness a range of metallicities from solar to the SMC are shown in Figure 4.2 (and subsequent metallcity gradients). We take these values from recent publications, assuming the revised solar metallicity to be 12+log(O/H) = 8.66 (Asplund 2003). Whereas we use recent observational determinations for the LMC and SMC metallicities. Assuming oxygen abundances of 12+log(O/H) $\simeq$ 8.4 (Korn *et al.* 2002) and 12+log(O/H) $\simeq$ 8.2 (Rolleston *et al.* 2003) for the LMC and SMC respectively. These results were derived from the chemical analysis of main sequence B stars and are in good

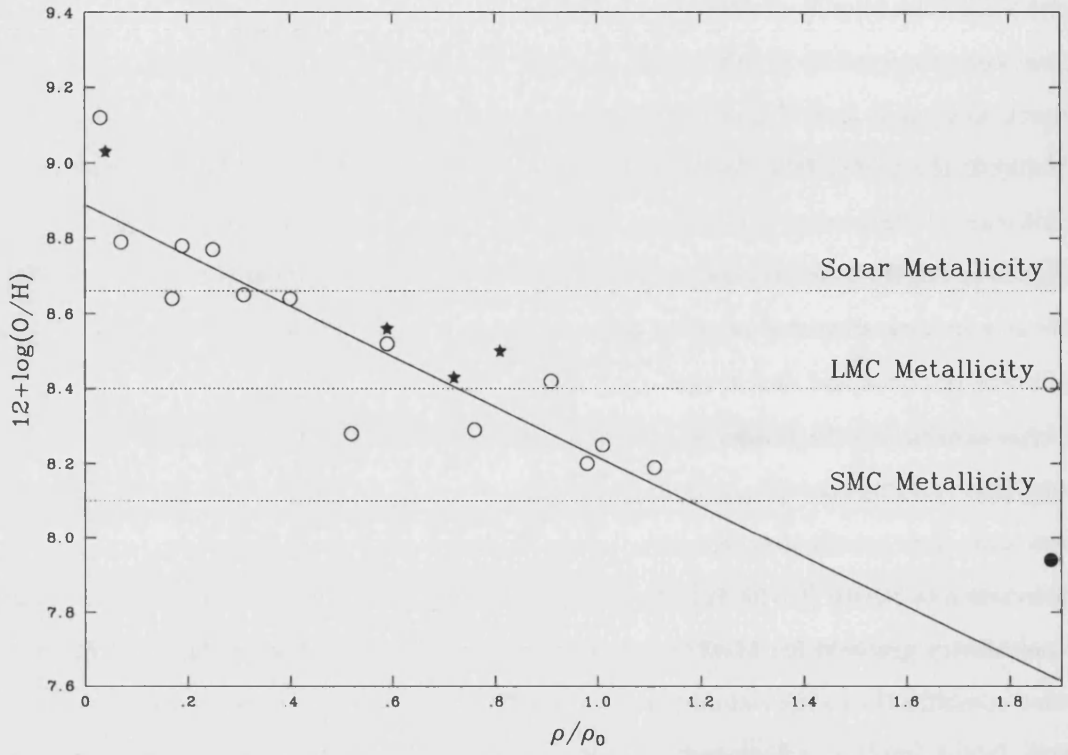

Figure 4.2: Oxygen abundance gradient for M 33 using observed H II regions using the re-calibrated R_{23} method by Pilyugin (2000). The observational data shown are taken from Smith (1975), Kwitter & Aller (1981), Vilchez *et al.* (1988) and Garnett *et al.* (1992) (open circles). For comparison, oxygen abundances derived from B supergiants are taken from Monteverde *et al.* (1997). Two values for the H II region MA1, which is located far out in the disk, are shown. As well as using the calibration by Pilyugin (2000), the oxygen abundance is also determined using the metal-poor calibration by McGaugh (1991) (filled circle). The least squares fit to this data is also shown.

agreement with previous determinations from H II regions.

A least-squares fit to the data taken for H II regions (excluding MA1, see below for discussion) reveals a gradient of -0.671 dex/ρ_0, compared with -0.740 dex/ρ_0 calculated by Zaritsky, Kennicutt & Huchra (1994), this revised metallicity gradient for M 33 can be expressed as:

$$12 + log(O/H)_{M33} = 8.889 - 0.671\rho/\rho_0 \tag{4.5}$$

Performing a simple statistical test we find that the data appear well correlated with the correlation coefficient, R $\simeq$ -0.90 – it is negative because the data are strictly anti-correlated. Further analysis reveals that the probability that the two parameters display a linear correlation is P $\simeq$ 49%.

The data taken by Garnett, Odewahn & Skillman (1992) for the H II region, MA1 (Mayall & Aller 1942), has also been included in Figure 4.2 as its the only H II region to be observed at a large galactocentric distance. If the pre-determined abundance gradient is correct, then we should expect this object to be more suited to a metal-poor regime. Indeed the observed [NII]/[OIII] line ratio confirms this. Unfortunately, as with most modern calibrations, the Pilyugin (2000) relationship is only valid for the upper, metal-rich regime. There have been other calibrations which attempt to calculate low metallicity environments, most notably the extensive calibration based on photoionization models by McGaugh (1991), whose models take into account the effects of varying the ionization parameter in both metal-rich and metal-poor regimes. Although this method still relies on theoretical R_{23} values. For accuracy we also re-calibrated MA1 using the metal-poor calibration by McGaugh (1991) and included it in Figure 4.2. If our inferred metallicity gradients are correct then it is clear that MA1 is situated in a very metal deficient region, and in fact our revised R_{23} value supports this.

Comparing the different calibration methods discussion in Section 4.1.1, the conflict of results highlights the uncertainties in determining accurate abundance gradients. This is clearly seen when considering that the predicted metallicity in the central region of M 33 varies by $\sim$0.5 dex between the calibration by Zaritsky, Kennicutt & Huchra (1994) and the more recent calibration by Pilyugin (2003). Even though we expect the metallicity to reduce with increasing distance from the centre of M 33, exactly by how much is still debatable. Unfortunately the field of determining oxygen abundances from extragalactic stellar sources is still in its infancy and with so few observations for M 33 we are unable to

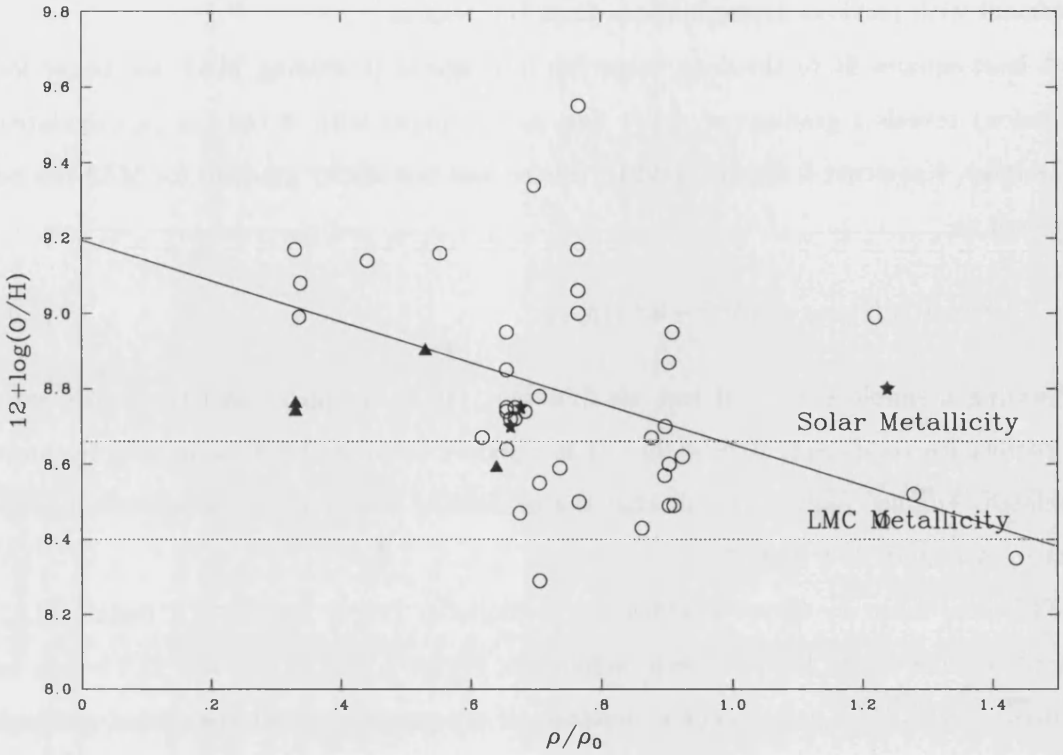

Figure 4.3: Oxygen abundance gradient for M 31 calculated from re-calibrated observations of H II regions. The observational data shown are taken from Dennefeld & Kunth (1981), Blair *et al.* (1982*b*) and Galarza *et al.* (1999) (open circles), using the calibrations of Pilyugin (2000). For completeness stellar oxygen abundances taken from Venn *et al.* (2000) (filled stars), and the averaged OB association abundances by Trundle *et al.* (2002) (filled triangles). A least squares fit to the nebular data only is also shown.

independently determine a metallicity gradient based on OB supergiants. For the four B supergiants measurements available it would tend to agree well with the Pilyugin (2000) calibration inferred in this work.

4.1.3 Metallicity Gradient in M 31

The nuclear regions of M 31 have long been suspected of being metal-rich dropping off to lower metallicities further in the disk. The question of exactly how metal-rich and how steep a metallicity gradient has varied between authors. Thankfully there have been a number of observational studies which can help us to explore the metallicity gradient

across M 31. We again consistently re-derive the abundance gradient across M 31 using the well determined R_{23} method, in conjunction with observations of H II regions.

The first observational program to examine H II regions in this galaxy were reported by Dennefeld & Kunth (1981), then shortly afterwards a number of H II regions were studied by Blair *et al.* (1982*b*). More recently a much larger sample of nebulae were observed by Galarza *et al.* (1999), all of these datasets were included in our analysis. We only include data from Galarza *et al.* (1999) that had been identified as 'centre-bright' H II regions, and that had concise measurements of line fluxes and not just upper/lower limits.

We have re-calibrated these fluxes to give us an oxygen abundance using the calibration described by Pilyugin (2000), which is observationally based. More details regarding this calibration is given in Section 4.1. Even though there is a scatter of points, especially at galactocentric distances 0.6 – 0.9 ρ/ρ_0, our revised metallicity gradient for M 31 predicts a steep, metal-rich metallicity gradient. These results are shown in Figure 4.3. Although the metallicity gradient is shown to extrapolate all the way back to the nuclues, in reality this is not the case. At galactocentric distances of $\sim$0.2ρ the inner galactic disk will truncate and the bulge will dominate. Within the bulge there are no H II regions and very few young stars. Those relatively rare young stars that are location within the bulge are not physically linked to their counterparts in the disk (Smartt *et al.* 2001*b*).

For completeness, stellar oxygen abundances are shown, using A-F type supergiants taken from Venn *et al.* (2000) and averaged OB type supergiants by Trundle *et al.* (2002). The stellar abundances observed by Venn *et al.* (2000) are clustered amongst our intermediately located H II regions, whilst the averaged OB supergiant abundances by Trundle *et al.* (2002) appear to agree reasonable well except for those centrally located; indicating a somewhat lower oxygen abundance. A least-squares fit to the data shown in Figure 4.3, only using re-calibrated data from the H II regions in our sample, reveals a metallicity gradient of -0.543 dex/ρ_0, and can be fully described by

$$12 + log(O/H)_{M31} = 9.195 - 0.543\rho/\rho_0 \tag{4.6}$$

We find that due to the range of observed abundances at $\sim$0.8ρ statistically the data appears less correlated than determined for the metallicity gradient in M 33. We calculate a correlation coefficient, R $\simeq$ -0.45 and find that the probability that the two parameters are linearly correlated is P $\simeq$ 24%.

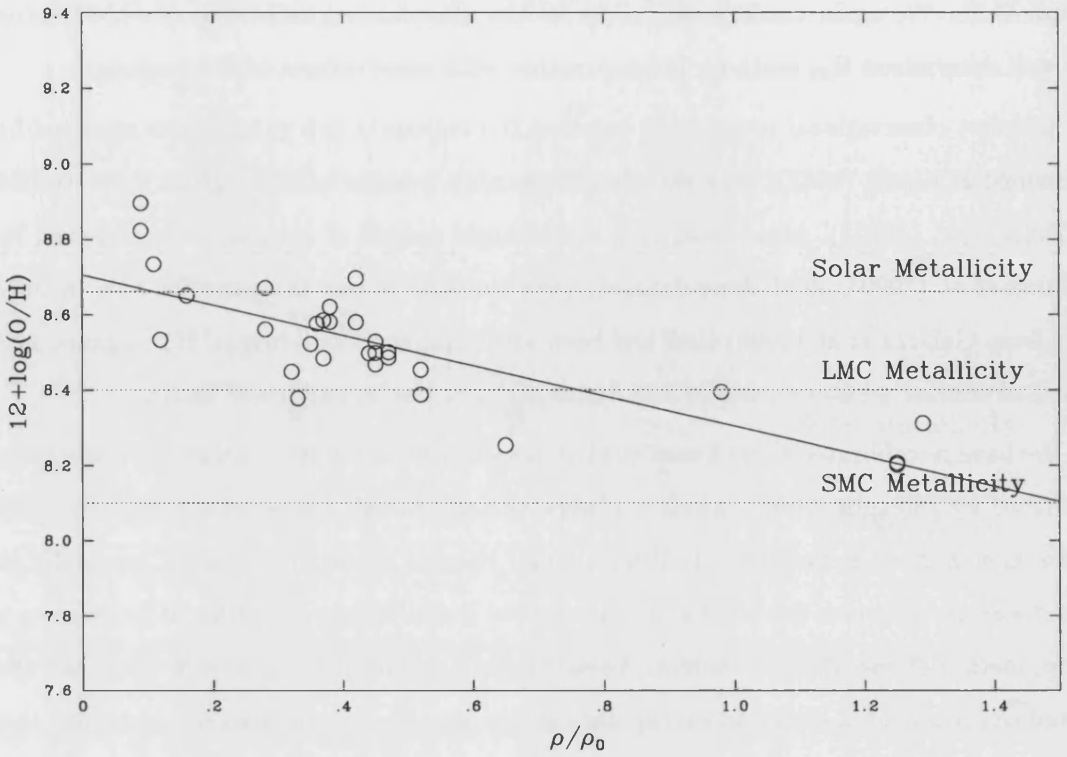

Figure 4.4: Oxygen abundance gradient for NGC 300 using observed H II regions using the re-calibrated R_{23} method by Pilyugin (2000). The observational data shown are taken from Pagel *et al.* (1979), Webster & Smith (1983) and Christensen, Petersen & Gammelgaard (1997) (open circles). The least squares fit to this data is also shown.

4.1.4 Metallicity Gradient in NGC 300

The Sculptor Group galaxy NGC 300 is another spiral galaxy for which there have been no recent observations to study its H II regions. We continue to re-analyse previous (reddening-corrected) line intensities measured from H II regions to establish a revised metallicity gradient for NGC 300.

We use observations of oxygen line intensities from Pagel *et al.* (1979), Webster & Smith (1983) and Christensen, Petersen & Gammelgaard (1997), where multiple observations occur we use those from Christensen, Petersen & Gammelgaard (1997) in preference as they are superior. Again using the re-calibrated R_{23} method by Pilyugin (2000) we have determined the metallicity gradient for NGC 300. Our results can be seen in Figure 4.4. We find a steep metallicity gradient across the disk of the galaxy and a least-squares fit

to these data can be represented by

$$12 + log(O/H)_{NGC300} = 8.705 - 0.401\rho/\rho_0 \quad (4.7)$$

Statistically the metallicity gradient for NGC 300 is significantly correlated with a correlation coefficient, R $\simeq$ -0.80 with a ~29% probabilitiy of a linear correlation.

Comparing our results with previously determined metallicity gradients for NGC 300, we again find a systemically lower and shallower metallicity gradient, due to the revised calibration employed. For example, Deharveng *et al.* (1988) also re-analyzed the same datasets as described above and concluded to have found a somewhat steeper metallicity gradient which was also ~0.2dex more metal-rich than we claim to have found. They used the calibration by Dopita & Evans (1986), which was calibrated against a limited sample of temperature derived oxygen abundances. More recently, Zaritsky, Kennicutt & Huchra (1994) also re-calibrated the metallicity gradient for NGC 300 and found a similar result as Deharveng *et al.* (1988).

This again highlights the need for an extensive observational study of a large sample of H II regions in the Local Group galaxies and beyond. Which with todays ground-based facilities available would be easily viable. Considering the importance placed on both massive-star evolution as well as the significance of metallicity dependences on their stellar parameters, it is vital that we constrain the metallicity for a large sample of Local Group galaxies. This would then enable us to confidently infer the local metallicity for any given extragalactic WR star. It might also be worth investigating the need for producing 'metallicity maps' rather than simple metallicity gradients so that you are using the most accurate metallicity in any given region of these spiral galaxies. Indeed, it is possible that individual H II regions span a range of metallicities at each galactocentric radius.

4.2 WR Emission Line Analysis

In this section we investigate the properties of our large sample of extragalactic WR stars. We probe the claim by Schild, Smith & Willis (1990) who found a linear relationship between the WC line width and galactocentric distance, we also extend this to our (smaller) sample of WN stars. From our sample, where we have calibrated observations, we investigate the possibility that WCE stars have a uniform line flux, after normalizing them to 1kpc initially suggested by Smith, Shara & Moffat (1990).

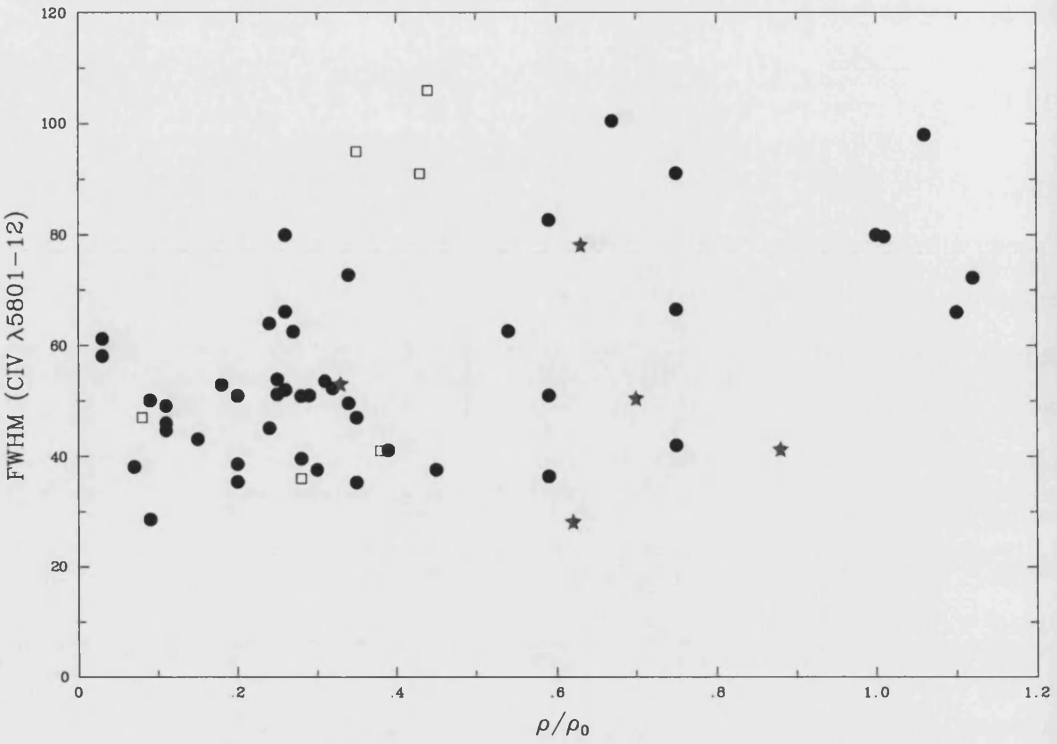

Figure 4.5: The FWHM(C IV $\lambda\lambda$5801-12), in Angstroms versus the galactocentric distance for WCE stars in the spiral galaxies M 33 (filled circles), M 31 (filled stars), and NGC 300 (opened squares).

4.2.1 WC Line Width

Schild, Smith & Willis (1990) claimed a potentially important correlation between the line width of C IV λ5808 with increasing galactocentric distance in M 33, this was later supported by Willis, Schild & Smith (1992). They showed that the FWHM (C IV $\lambda\lambda$5801-12) for WCE stars was narrower for stars close to the nucleus, (located in higher metallicity environments), than those at larger galactocentric distance (located in lower metallicity). However, this relationship was rather tenuous owing to their small sample.

We have measured the FWHM (C IV $\lambda\lambda$5801-12) from our sample of WC stars in M 33, M 31, IC 10 and NGC 300. Table 4.2 lists the FWHM and equivalent widths for both the blended emission feature C III-IV/He II λ 4650 and C IV λ5808. We compared the FWHM (C IV $\lambda\lambda$5801-12) from our dataset of spiral galaxies (i.e. M 31, M 33 and NGC 300) with the values obtained by Willis, Schild & Smith (1992), Dessart (1999) as well as the measurements for OB10-WR1 in M 31, observed and reported by Smartt *et al.* (2001*a*). These results are shown in Fig. 4.5. Where there were multiple measurements in

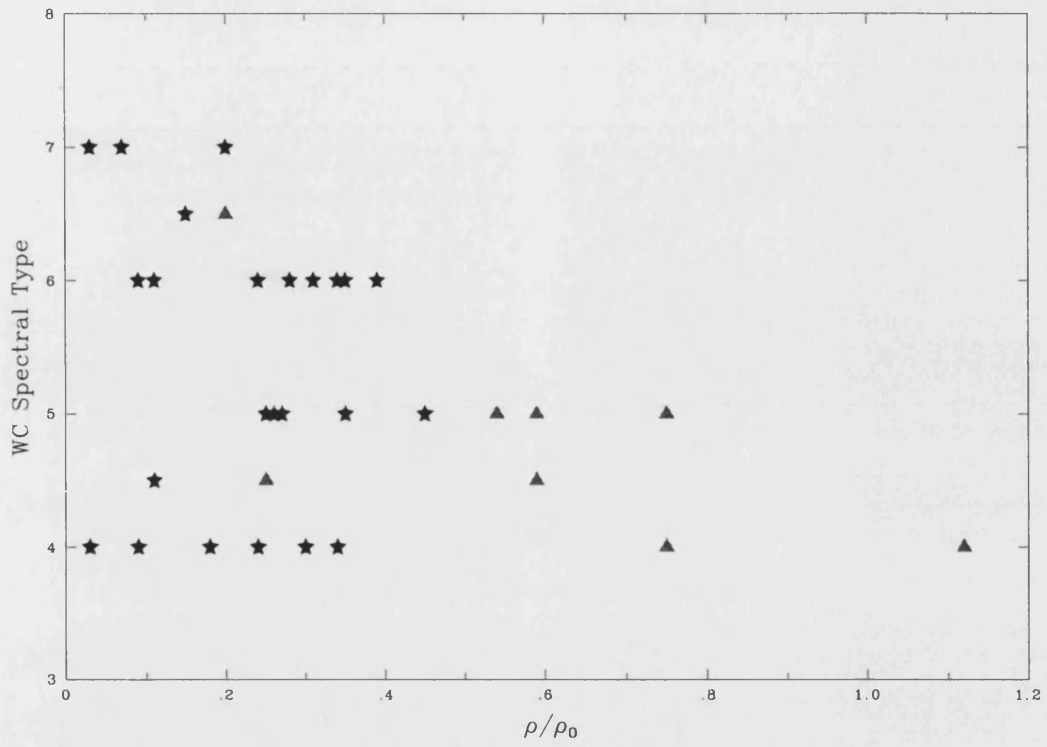

Figure 4.6: WC spectral type plotted as a function of galactocentric distance. We observe a decline in later WC-type further in the disk. Data were taken from Dessart (1999) (filled triangles) and the current sample (filled stars) using stars with confidently determined spectral types.

the M 33 dataset, the values obtained by Dessart (1999), or the current sample were used in preference since these datasets were superior compared with previously published data.

Our much larger sample of WC stars does not favour the correlation by Willis, Schild & Smith (1992), namely FWHM(C IV)= $42(\pm12)\times\rho+41(\pm7)$. Instead, we find a very large spread in FWHM between $0.4 \leq \rho \leq 0.6$. Performing a simple statistically analysis on these data we find a linear correlation coefficient, R = 0.43, and the probability of a linear correlation of 20%.

Nevertheless, there does genuinely seem to be a lack of broad line WC stars towards the central regions of these galaxies, and a lack of narrow line WC stars at larger galactocentric distances. This correlation is still unexplained. Note that if WR stars are assumed to follow the same stellar wind properties as OB stars, their terminal wind velocities would be expected to decrease with decreasing metallicity (Leitherer, Robert & Drissen 1992), in contrast with the (weak) opposite effect observed.

Table 4.2: Emission line measurements of C III λ4650/He II λ4686 and C IV λ5801-12 for the WC stars observed with CFHT-MOS in M 33, VLT-FORS2 in IC 10 and NGC 300, WHT-ISIS in M 31. Star identifications are: M 33, AM = Armandroff & Massey (1985); MC =Massey & Conti (1983); MJ = Massey & Johnson (1998); M 31, Moffat & Shara (1983); OB = Massey, Armandroff & Conti (1986); IC 10, M = Massey, Armandroff & Conti (1992); R = Royer *et al.* (2001); NGC 300, S = Schild *et al.* (2003).

	C III λ4650/He II λ4686		C IV λ5801-12	
Star	log (-EW)	FWHM	log (-EW)	FWHM
		M 33		
MC26	3.10	46.8	3.03	41.1
AM5	2.47	53.0	2.19	52.7
MC33	2.59	58.9:	2.58	37.6
MC35	2.32	38.5:	2.10	35.3
MC39	2.62	59.4	2.48	51.2
MC42	2.34	76.0	2.39	72.7
MC40	2.10	64.6:	2.26	52.9
MC43	2.73	37.8:	2.51	35.4
MC44	1.80	61.1:	1.83	62.5
MJ-C4	1.36	46.8	1.32	44.7
MC45	1.54	52.6	1.60	50.1
MC47	2.98	53.4	2.78	49.1
MC49	2.52	49.1	2.29	46.0
MC52	2.16	56.0:	1.88	58.1
MC53	2.06	53.6:	1.85	28.6
MC54	1.36	35.3	1.30	38.1
MC55	2.76	44.6:	2.52	39.6
MC56	1.84	69.0:	1.89	61.2
MC57	2.32	71.4:	2.43	65.1
AM14	2.89	52.6	2.89	45.1
AM16	3.42	57.1	3.30	47.0
AM17	3.39	60.7:	3.31	52.0
MC65	2.84	59.5:	2.91	49.6
MJ-X19 ...	1.63	43.0	1.59	43.1
MJ-X9	1.79	81.2:	1.85	65.2
MC68	2.36	56.1	2.45	50.9
MC70	2.90	46.4:	2.69	37.6

Continued on next page .....

	C III λ4650/He II λ4686		C IV λ5801-12	
Star	log (-EW)	FWHM	log (-EW)	FWHM
		M 31		
MS5	2.20	23.5:	1.92	28.1
MS12	3.15	80.7:	3.18	78.1:
MS21	3.09	49.0	3.06	41.2
OB48-WR1	2.88	51.0	2.78	50.4
		IC 10		
M1	1.85	65.0	2.04	50
M2	1.94	74.0	2.30	66
R6	2.25	78.0	2.33	82
R5	2.09	79.0	2.11	80
M4	1.70	64.0	1.60	49
M5	2.62	53.0	3.10	79
M7	1.95	84.0	1.91	82
M10	3.06	68.0	3.29	85
M12	1.86	58.0	1.84	49
M13	2.07	58.0	2.04	47
M14	2.67	79.0	2.47	78
M20	2.95	62.0	2.86	52
		NGC 300		
S29	3.21	62.0:	3.16	47.0
S48	3.15	92.0:	3.29	91.0:
S40	2.52	46.0:	2.47	36.0
S24	2.27	52.0:	2.35	41.0
S01	2.56	105.0:	2.77	106.0:
S22	2.20	72.0:	2.77	95.0:

A possible answer which would (partly) explain why we see a lack of broad line WC stars towards the central regions of these spiral galaxies and a lack of narrow line WC stars in the outer disk, could be connected to the distribution of spectral types. We test this theory using M 33 as it is believed that the WR population is reasonably complete. Even though the exact metallicity across M 33 is still a little uncertain there does appear to be a strong metallicity gradient which implies a somewhat lower metallicity in the outer disk compared with the central regions. Assuming current stellar evolution theories are correct, this difference in metallicities would permit later WC stars to form in the inner regions and bias earlier spectral types to form at larger galactocentric distances.

In Figure 4.6 we have plotted the spectral type versus galactocentric distance for the

WC stars in M 33 and there does appear to be a trend towards earlier spectral types at larger galactocentric distances. A similar spectral type distribution was previously discovered for M 33 by Smith & Maeder (1991), who also conclude that this segregation effect was connected to the local initial metallicity. Unfortunately, this hypothesis does not explain why the few WCE stars that are observed in the inner regions of M 33 are surprisingly narrow-lined.

This spectral type – metallicity segregation effect is not unique to M 33. It is also observed in low metallicity regions, such as the LMC, where the *entire* WC content are WCE stars (Breysacher, Azzopardi & Testor 1999) and in metal-rich regions, such as the central regions in M 31, where there appears to be an abundance of WCL stars. Furthermore, a WR subtype distribution has also been noted in the Solar Neighbourhood by van der Hucht (2001). For the known Galactic WC population late-type WC stars are strictly located to within the solar circle (i.e. at close galactocentric distances), with earlier spectral types located at intermediate and large galactocentric distances.

This weak trend between the observed line widths and the distance at which the star is located could simply be a selection effect where narrow-lined, late-type WC stars are only permitted in the central (metal-rich) regions and broad-lined, early-type WC stars are the only WC stars to possibly form in the outer (metal-poor) regions. There are of course factors which could cloud this distribution, such as the effects of forming a WR star through binary systems and the scatter of metal abundances observed in spiral galaxies. Potential selection effects at some level should also be accounted for, for instance, it is easier to identify and measure WR stars in intermediate regions of spiral galaxies where; (i) reddening effects are reduced, (ii) due to clustering of WR stars, observational studies are focused.

4.2.2 WN Line Width

We have applied this method to our WN sample, combining our measurements with previously published data from Massey, Conti & Armandroff (1987*a*), Massey & Conti (1983), Armandroff & Massey (1991) and Massey & Johnson (1998). Where there were multiple measurements data were preferentially taken from the current sample (see Table 4.7) and Armandroff & Massey (1991). These results are shown in Figure 4.7. Even with a large sample of data, as for the WC stars, we again find very little evidence for a correlation of FWHM (He II λ4686) with increasing galactocentric distance. A statistical analysis in

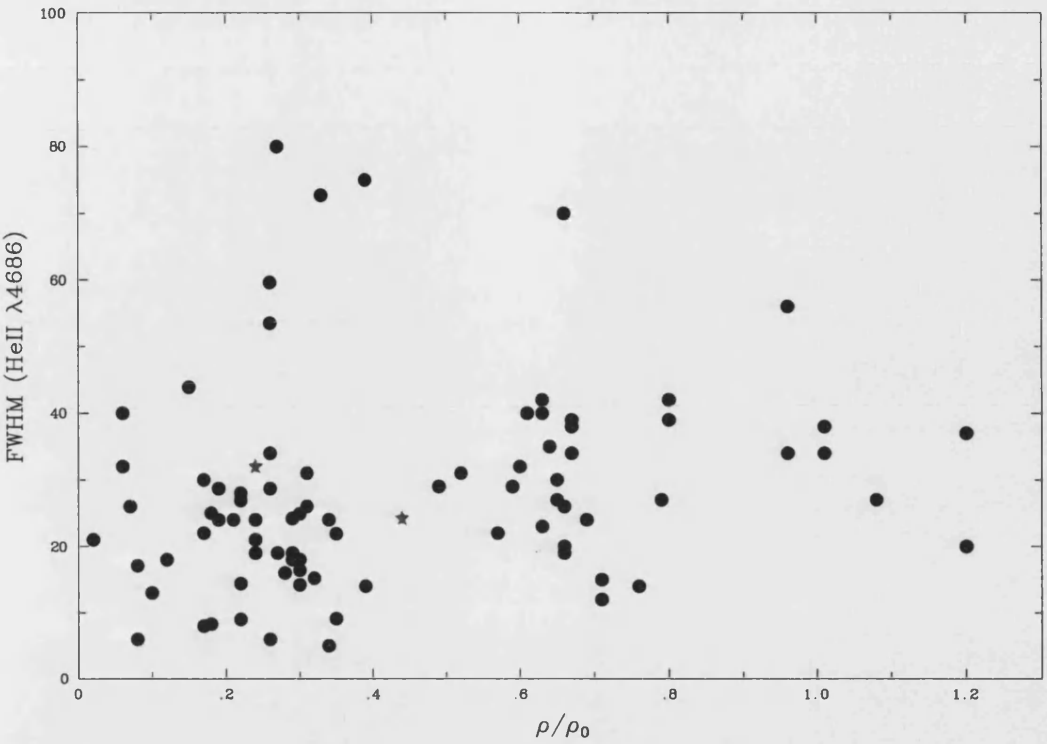

Figure 4.7: The FWHM(He II λ4686), in Angstroms versus the galactocentric distance for WN stars in M 33 (filled circles), using data taken from Massey, Conti & Armandroff (1987*a*), remeasured Massey & Conti (1983), Armandroff & Massey (1991), Massey & Johnson (1998) as well as data from this work. Where possible data were preferentially taken from the current sample and Armandroff & Massey (1991). We also show the measurements made for the two WN stars observed in NGC 300 (filled stars).

these data find a linear correlation coefficient, R = 0.22, with a 15% probability of a linear correlation.

Even though the correlation is weaker for WN stars, to some extent, the same argument could hold for WN stars as for WC stars. In the outer regions (lower metallicity) there is a bias to form early-type WN stars, whereas in the inner regions (higher metallicity) late-type WN stars can evolve. Although the initial mass required to form a WN star is somewhat lower compared with WC stars and so this could explain why the observed trend is even weaker in WN stars.

Table 4.3: Emission line measurements of He II λ4686 for the WN stars observed with CFHT-MOS in M 33 and VLT-FORS2 in NGC 300. Star identifications are: M 33, AM = Armandroff & Massey (1985); MC =Massey & Conti (1983); MJ = Massey & Johnson (1998); M 31, Moffat & Shara (1983); OB = Massey, Armandroff & Conti (1986); NGC 300, S = Schild *et al.* (2003).

	He II λ4686	
Star	log (-EW)	FWHM
M 33		
AM3	1.73	15.2
AM6	1.41	14.2
NGC595-WR9...	1.28	16.4
MJ-G13	1.43	24.2
MCA5	2.16	26.9
MC36	1.91	28.7
MC37	2.13	72.7
MJ-G3	0.97	21.9
MCA8	2.22	24.9
MCA9	1.36	17.1
MC46	2.33	43.9
MC48	2.53	59.6:
MJ-G8	1.49	28.7
MJ-G9	2.45	53.5
MJ-X15	0.99	10.7
OB6-5	0.67	9.1
UIT289	0.38	14.4
NGC 300		
S9	1.76	32.0
S30	2.25	24.2

4.2.3 C IV Line Flux

Smith, Shara & Moffat (1990) observed a large number of LMC WCE stars, and found that their C IV λλ5801-12 line fluxes, when adjusted to a distance of 1kpc, were uniform to log F_λ = -7.6±0.15 ergs^{-1}cm^{-2}. We decided to compare the (de-reddened) C IV λ5808 line fluxes from our M 31 and IC 10[1] WC stars with those observed in the LMC. Using the reddenings derived from comparison with synthetic models (see Section 2.3.4), and

[1]Recently supported by Crowther *et al.* (2003).

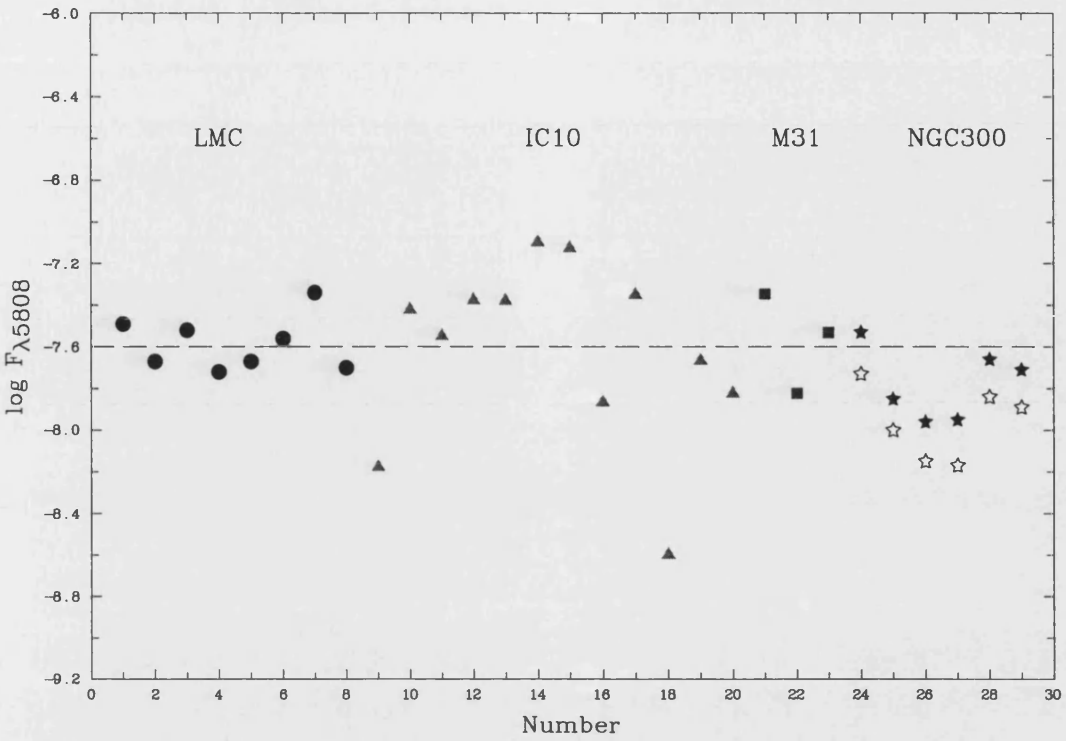

Figure 4.8: The measured C IV λ5808 line fluxes for WCE stars, observed in a number of Local Group galaxies. Results for the LMC (filled circles) are taken from Smith, Shara & Moffat (1990), IC 10 (filled triangles); M 31 (filled squares), and NGC 300 (stars). The dashed line shows the average line flux for the data points measured for the LMC, IC 10 and M 31, due to the uncertainties in the reddening towards NGC 300.

assuming a distance to M 31 of 752kpc, the C IV $\lambda\lambda$5801-12 line fluxes were calculated. Excluding the line flux from M31-MS5, as this is a WCL star, the averaged line flux from our sample of early type WC stars in M 31 is log F_λ = -7.6$\pm^{+0.2}_{-0.3}$ ergs^{-1}cm^{-2}.

We also repeated this process to include the WCE stars in IC 10, de-reddening the spectra using the colour excesses listed in Table 2.9. We found that the WC stars in IC 10 also displayed a similar averaged line flux when normalized to 1kpc, and although our calculated reddenings are not accurate (due to the assumptions made for the intrinsic colours), we still find that the average line flux is; log F_λ = -7.5$^{+0.2}_{-0.6}$ ergs^{-1}cm^{-2}. This spread in results can be partly explained by our imprecise reddenings. Given our relatively small number statistics and the errors associated on both our averaged values it appears that these results support the original theory by Smith, Shara & Moffat (1990); that WCE

stars do seem to have a universal line flux.

Finally, we perform a self-consistent comparison of datasets and so include the averaged WC line flux for the carbon-sequence WR stars in NGC 300. These results along with all those described above are shown in Figure 4.8. For NGC 300 we show two datasets, one using the reddenings described by Schild *et al.* (2003) for the two WCE stars modelled, for the remaining four stars in our sample we use a representative value of $E_{B-V} = 0.15$. The second set of measurements were taken after de-reddening the spectra by $E_{B-V} = 0.28$, which was derived from the averaged H II region line measurements published by Deharveng *et al.* (1988), assuming that $E_{B-V} = C(H\beta)/1.46$ (Pottasch 1984).

These two methods give averaged line fluxes for WCE stars in NGC 300 of log F_λ = -8.0±0.2 ergs^{-1}cm^{-2} and log F_λ = -7.8±0.2 ergs^{-1}cm^{-2} using reddenings of $E_{B-V} = 0.15$ and 0.28 respectively, and a distance of 2.0Mpc. The normalized line fluxes calculated with higher reddenings agree better with those calculated for the other (flux calibrated) WCE stars in our sample. However, there is still a ~0.2 dex discrepancy between these results and those calculated for the other Local Group galaxies.

These larger averaged line fluxes can be explained by the uncertainty in our estimated reddenings (see Section 2.5.3) used and/or any error which is associated with our assumed distance. We need more conclusive independent reddenings before we can confidently disregard the original findings by Smith, Shara & Moffat (1990), purely because one set of results do not support the majority of our observations.

One might argue that previous measurements made by Smith, Shara & Moffat (1990) contained low number statistics and that this sample was only taken from WC stars in a very similar environment. Now the situation is very different, we now have a number of independently observed datasets taken in regions containing very different metallicities (i.e. LMC, M 31, IC 10 and NGC 300) and yet we still find a uniform C IV λ5801-12 emission line flux of, $F_\lambda = -7.6^{+0.4}_{-0.7}$ ergs^{-1}cm^{-2} for early type WC stars - excluding the results from NGC 300.

4.2.4 Identifying Single WC stars

The effects of multiplicity makes the interpretation of stellar spectroscopy much more difficult, both for the analysis and when comparing results with stellar evolutionary models. Binary evolutionary calculations are much more complicated than single star models (Vanbeveren, de Loore & van Rensbergen 1998). Since a great deal less is known about

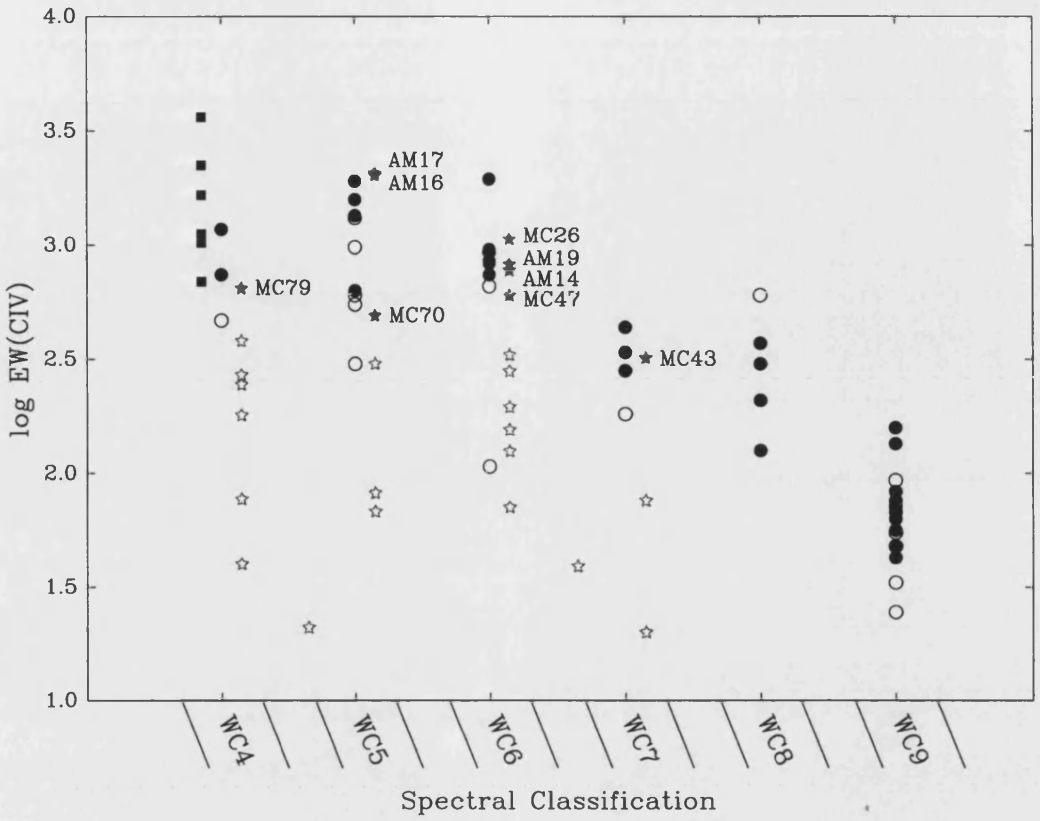

Figure 4.9: Comparisons between the log[EW(C IV)] versus WC spectral type, for Galactic (circles), LMC (squares) and M 33 (stars) stars. This was used as an indicator of potential multiplicity. The data for the Galactic and LMC stars were taken from Torres, Conti & Massey (1986). The open symbols indicate that the stars are in known binaries, apart from the M 33 sample, where we cannot be certain.

binary physics due to the complexities involved in evolutionary calculations (e.g. RLOF, common envelope phases, properties of mass transfer, angular momentum, mixing).

Single stars are preferred because their observed light is not contaminated by that of a companion, making the spectroscopic analysis more reliable. They are also more desirable because their properties can be compared to stellar evolutionary predictions which suffer from fewer speculations. There have been successful, well tested methods to resolve both the WR and O star components for binary systems (e.g. De Marco & Schmutz 1999; De Marco *et al.* 2000). These methods rely on well resolved optical absorption lines being observed for the companion star, something which is not easily achievable for extragalactic

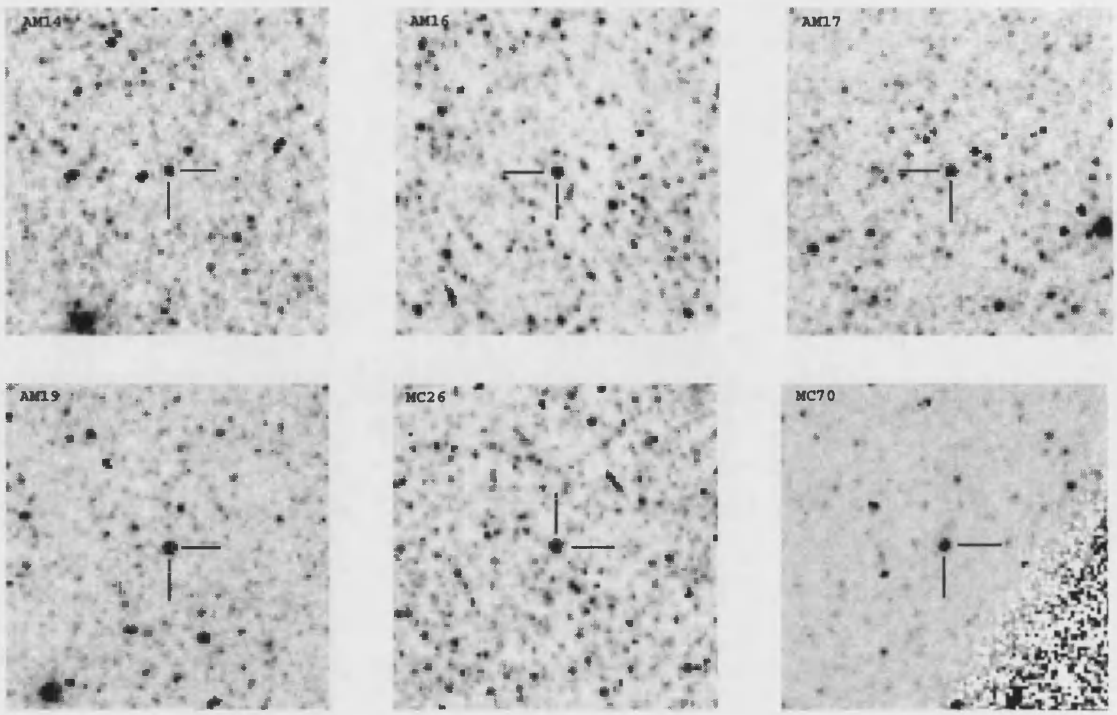

Figure 4.10: HST WFPC2 images taken with the F555W filter. These images identify six WC stars in M 33 that we have assumed to be single from EW measurements. These images are supporting evidence that these stars are single due to their relative isolation plus they are well resolved. The star identifications are shown in the top left-hand corner, and each image has a 10″ x 10″ field of view, orientations are north is up and east is to the left. Note: MC70 lies close to the edge of one of the CCDs which is why there is noise in the bottom right-hand corner of the image.

WR stars. However, there are other techniques although these methods generally rely on orbital solutions, or radial velocity variations (e.g. Foellmi, Moffat & Guerrero 2003*a*) or interpretation of optical O star absorption lines, which represents a formidable challenge for massive stars beyond the Magellanic Clouds.

Our primary focus for this work was to study single WC stars in Local Group galaxies, since they prove to be the most sensitive indicators of massive-star evolution. We used observational data for known Galactic and LMC WR stars taken from Torres, Conti & Massey (1986), and plotted their equivalent widths (EWs) of C IV ($\lambda\lambda$5801-12) against their spectral types. These served as templates to guide us to apparently single stars, in the sense that low EWs are indicative of dilution from a companion star or a chance line-

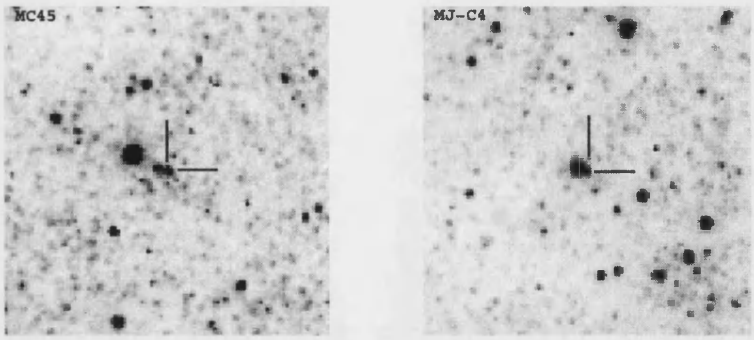

Figure 4.11: HST WFPC2 images taken with the F555W filter. These two WC stars in M 33 showed weak C IV from our EW measurements indicating that their spectra were contaminated. This is supported from the HST images where it is clear that the WR star is either has a companion or is located near a another chance line-of-sight star. These plots follow the same orientation and field of view as the other WR stars shown.

of-sight. Figure 4.9 shows all the program WC stars in M 33 plotted against the Galactic and LMC data, shown as a function of spectral type. The gradual decline in EW(C IV) towards later sub-type is merely due to the general weakening of C IV relative to C III λ5696. Filled symbols indicate probable single M 33 WC stars, which are discussed in Section 6.1.

From a comparison of our equivalent width measurements we have identified nine potentially single WC stars (see Figure 4.9), their broad-band (Johnson) m_V and m_B magnitudes are shown in Table 2.4 (apart from MC79). In an attempt to test this assumption we have identified a number of these stars from archival HST/WFPC2 images (see Chandar, Bianchi & Ford (1999) for discussion of data), observed with the F555W filter. Figure 4.10 shows six stars that we have inferred as single. We have used these detailed images to see whether each star appears well resolved and isolated, supporting the claim they are potentially single, albeit at a spatial resolution of 0.1″ per pixel. This is the case from all six stars where data were available.

As a self-consistency check, using our equivalent width measurements (Fig. 4.9) we have also looked to see whether some of the WC stars with *weak* C IV emission appear to be contaminated and unresolved. Figure 4.11 shows MJ-C4 (M33-WR73) and MC45 (M33-WR76), again from archival HST/WFPC2 images taken with the F555W filter. Both appeared to be non-spherical and have multiple components which are unresolved at

the resolution of the images. This suggests that we are observing either a nearby bright star or a chance line-of-sight object. This gives us more confidence that our technique is successful; at least at identifying obvious single candidates.

Unfortunately, these HST images alone are not evidence for single stars. The angular separation of WR147 and its companion star in the Galaxy was found to be 0.6″ at 1.9kpc (Moran *et al.* 1989). Projecting WR147 to M 33 would imply a separation of 1.4mas. Consequently, we do not claim that HST imaging provides hard evidence that these stars are single, merely that there are no obvious sources of contamination close to the star. HST images, in conjunction with the large EW measurements, provide a possible method for identifying potentially single stars at large distances merely from individual spectra.

The binary frequency of WR stars can have strong implications on the evolution of a massive star (Foellmi, Moffat & Guerrero 2003*a*). Analysis of single stars is achievable with CMFGEN and so its extremely useful to identify single stars before an attempt to model them is made. There are a number of different techniques that can be employed to determine the binary nature of an observed WR star. For our sample of WR stars in M 33, where we were unable to reliably flux calibrate these data, we compared their measured EW(C IV) and compared them with known single and binary WR Galactic stars. We now discuss another approach to potentially identify single extragalactic WR stars, where we are confident of their absolute flux levels, as in the case for our sample of M 31 and IC 10 WR stars.

In Figure 4.12 we have plotted the line strength of C IV $\lambda\lambda$5801-12 against our estimated absolute visual magnitudes, using our measured spectrophotometry for M 31 (see Table 2.7 and Table 2.9 for M 31 and IC 10 respectively). This method allows us to estimate the level (if any) of contamination by OB chance line-of-sight stars or from a binary companion. We also compare our measurements with single and binary stars in the LMC taken from Smith, Shara & Moffat (1990).

This figure suggests that MS21 and MS12, in M 31, are potentially single, whereas MS5 and OB48-WR1 are in fact binary stars or that their spectra are contaminated. An attempt at modelling all four of these stars are made (see Chapter 6), in the cases where we suspect they are binary, a contaminating Kurucz (1979) O star model is added to the synthetic spectra before comparing it with the observations. We also determine from this comparison that it is highly likely that from our sample of IC 10 WC stars; [MAC92] 10 and [MAC92] 20 are single.

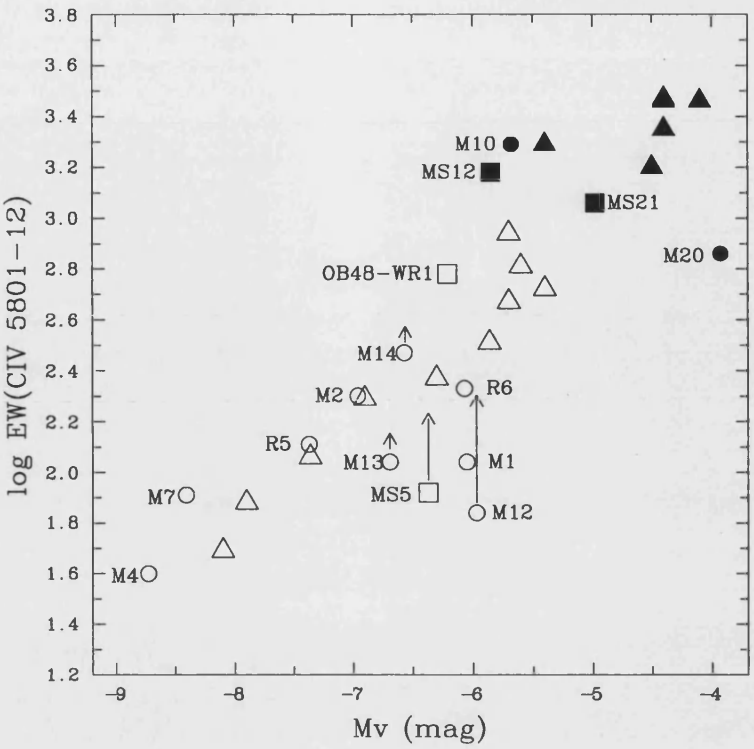

Figure 4.12: Measured line strength C IV $\lambda\lambda$5801-12 versus absolute visual magnitude for WC stars in IC 10 (circles), M 31 (squares), and the LMC (triangles). The opened symbols signify (inferred) binary stars and filled symbols signify single stars. These data were taken from Smith, Shara & Moffat (1990) and Crowther *et al.* (2003) for the LMC and IC 10 data respectively.

Of course other WC stars in our two samples could also be single but we are unable to resolve these individual stars with our current resolution. This effect is shown for [MAC92] 12, [MAC92] 13 and [MAC92] 14 where corrections in their emission line strength have been made for a line-of-sight companion located nearby based on WFPC2 images (these HST WFPC2 images are shown in Appendix C). An attempt to model these single WC stars and derive their their stellar parameters are discussed in Chapter 6.

4.2.5 Identifying Single WN stars

As with our M 33 WC sample, we used observational data for known single Galactic and LMC WN stars by Torres, Conti & Massey (1986), and compared their equivalent widths of He II (λ4686) against their spectral types, using the results listed in Table 4.3. This

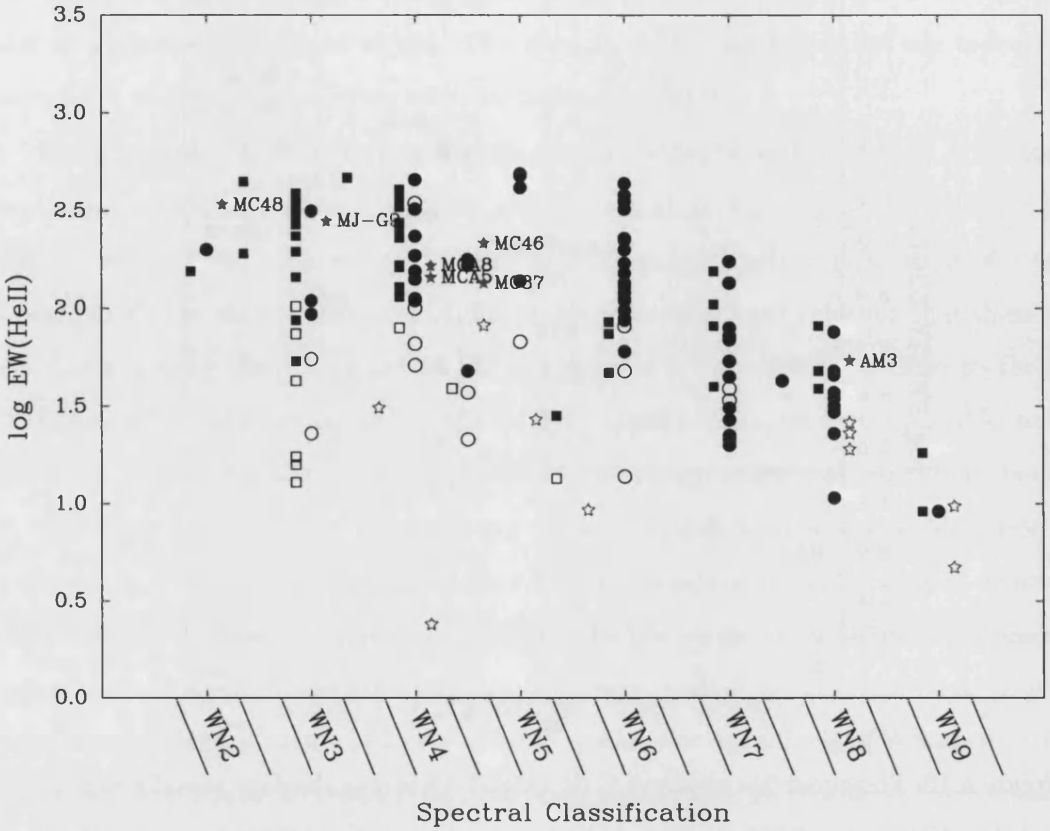

Figure 4.13: Comparisons between the log[EW(He II)] versus WN spectral type, for Galactic (circles), LMC (squares) and M 33 (stars) stars. This was used as an indicator of potential multiplicity. The data for the Galactic and LMC stars were taken from Torres, Conti & Massey (1986). The open symbols indicate that the stars are in known binaries, apart from the M 33 sample, where we cannot be certain.

then enabled us to decide which of our WN stars were apparently single, and which were suffering from dilution due to a companion star or a chance line-of-sight. Figure 4.13 shows all our program WN stars observed in our sample compared with their Galactic and LMC counterparts as a function of spectral type. Filled symbols indicate probable single WN stars, of which we have identified six potentially single after comparing their EW(He II). As discussed in Section 4.2.4, without obvious absorption features or a series of quality exposures in the search for radial variations then it is very difficult to accurately determine the multiple nature from our sample.

Our equivalent width comparison we identified seven potentially single WN stars from

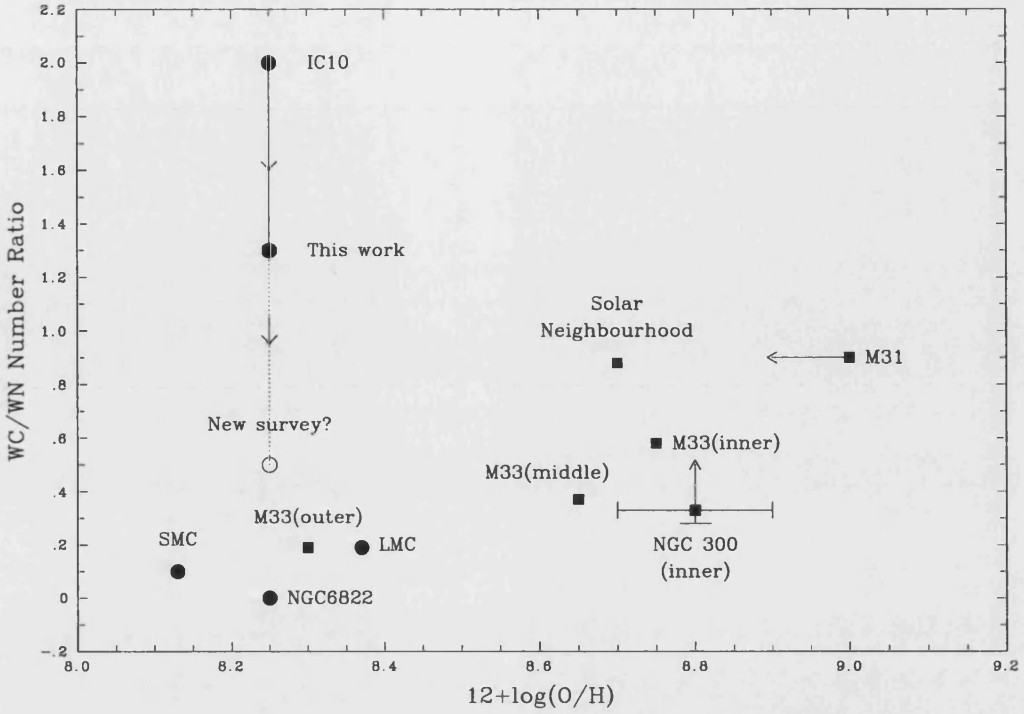

Figure 4.14: WC/WN ratio versus oxygen abundance for Local Group galaxies reproduced from Crowther *et al.* (2003), showing the revised WC/WN ratio for IC 10. Also shown is the revised WC/WN ratio for the Sculptor Group galaxy NGC 300.

our sample, although on closer inspection we decided to exclude MC37 (Massey & Conti 1983). Even though MC37 (M33-WR59) has a large EW(He II), overall its emission line strengths are weak, but appear very broad (FWHM(He II) $\sim$ 70Å) and would explain why the EW(He II) may be confused with a single WNE. For the remaining six possibly single WN stars their broad-band (Johnson) V and B magnitudes have been measured from archival CFHT-12K (see Section 2.2.5) and are shown in Table 2.5. These WN stars are analysed in more detail later in this work (see Chapter 5).

4.3 Revised WC/WN Ratio

After considering our results, as well as previous spectroscopy, we revise the WC/WN ratio to include the Local Group galaxy IC 10 as well as the Sculptor Group galaxy NGC 300.

With our improved spectral types for a significant number of WR stars in IC 10 we

suggest that the WC/WN ratio should change such that; WC/WN = 14/11 $\sim$ 1.3 (we do not include the intermediate WN/CE star, [MAC92]5 in this ratio). As discussed in Section 1.4.1, observations of the WR population in the Local Group have found a linear correlation between the WC/WN ratio and the metallicity in which they are located. Comparing our revised ratio for IC 10 with other Local Group galaxies (see Fig. 4.14), we now find that this reduced ratio is closer to matching the observed correlation. We would expect a WC/WN ratio $\sim$ 0.15, if IC 10 was in keeping with the correlation found for other the other members of the Local Group. For this ratio to match the observed relationship $\sim$80 WN stars would be required - something discounted by Royer *et al.* (2001). Recent narrow-band imaging by Massey & Holmes (2002) claimed to have discovered a further $\sim$75 WN candidates, which still await spectroscopic confirmation.

Of course it is difficult to identify bona-fide WN stars simply from the detection of a He II λ4686 excess, so a certain amount of caution is required. Examining Fig. 3 in Massey & Holmes (2002), there are $\sim$15 stars with WN excesses greater than 0.5 mag, most of these are most likely genuine WN stars, from comparison with their control field and that there are spectroscopically confirmed WN stars of similar excesses. Assuming these stars were unaccounted WN stars then this would change the WC/WN ratio to $\sim$ 0.5 (as indicated in Figure 4.14). However, Massey & Holmes (2002) boldly claimed that all stars with excess between 0.3–0.5 mag were legitimate WN stars, drastically altering the WC/WN ratio to $\sim$ 0.3. Their argument was based around the spectroscopic *detection* of a WN star, WR24, which has an excess of $\sim$ 0.3 mag. As discussed the nature of WR24 (Massey & Holmes 2002) was debated by Crowther *et al.* (2003), who pointed out that stars with an equivalent width of He II λ4686 $\simeq$ 4Å was not consistent with a genuine WR star. We await spectroscopic confirmation for the other WN candidates identified by Massey & Holmes (2002) before the WC/WN ratio for IC 10 can be agreed. Of course the ratio of WC to WN stars could be unusually large for this galaxy, relative to the Local Group, which would support the theory that IC 10 has recently under-gone a short, co-eval burst of star formation.

Due to the limited nature of previous surveys the observed WC/WN ratio for NGC 300, prior to this work, was very high ($\sim$ 2). Using our results, both from our spectroscopy, and narrow-band imaging we re-address the WC/WN ratio for this spiral galaxy in the Sculptor Group and compare these results with previously studied galaxies in the Local Group.

With the absence of narrow-band filters centred around C IV λ5808, plus a nearby continuum, to discriminate between WN and WC stars (e.g. Royer *et al.* 2001), we use Figure 2.9 to identify potential WR subtypes. As discussed, Figure 2.9 plots the continuum magnitudes versus the WR excess (m_{4781} - m_{4684}) for both spectroscopically confirmed WR stars as well as candidate WR stars. By including the spectral type for the known WR stars we find that stars with the largest WR excesses are predominately WC type, with WNE and WNL stars having less WR excess. Considering this, we infer at least 13 WR stars in NGC 300 are WC-type, 12 of which are spectroscopically confirmed, plus #5. We suggest that another 3 are possibly WC binaries, hence their weaker WR excesses (these are, #12,#31 and #33), with the remainder allocated WN status. This subsequently changes the WC/WN ratio for the inner regions of NGC 300 to; $\geq$ 12/46 = 0.3, or more likely, $\geq$ 15/43 = 0.35. Figure 4.14 shows that our revised WC/WN ratio for the central regions of NGC 300 compares well with a comparative region of M 33 (Massey 2003). We also find that it appears to follow the observed trend as the Local Group galaxies.

CHAPTER 5

Properties of WN stars

In this chapter we use the non-LTE, stellar atmospheres code of Hillier & Miller (1998), CMFGEN, which iteratively solves the transfer equation in the co-moving frame subject to statistical and radiative equilibrium in the expanding, spherically symmetric and steady-state atmosphere (see Chapter 3). Although we have a limited observational sample of extragalactic WN stars, we chose to perform detailed analysis for a number of Galactic and Magellanic Cloud WR stars in order to compare their stellar parameters. We can then assess whether the properties of WN stars show any possible scaling with the local metallicity.

As with our WC spectra, our approach to modelling the data is to calculate a series of models adjusting the stellar parameters until we can match the observed ionization balance, line strengths/widths (and for some datasets, the absolute magnitudes). Because of the effect each parameter can have on the emergent model spectra this was an iterative process. Initially, the line strengths and widths of the modelled spectrum were matched and then the luminosity was altered to match the absolute (scaled) flux levels.

5.1 Detailed Analysis for individual WN Stars

Modelling the spectra of WN stars is a little more straight forward than their WC counterparts, due to the relatively well resolved emission lines available. When simply considering the optical regime for WN stars there are also more emission lines of adjacent ionization species available than for WC stars. This means that the ionization and temperature can be better constrained.

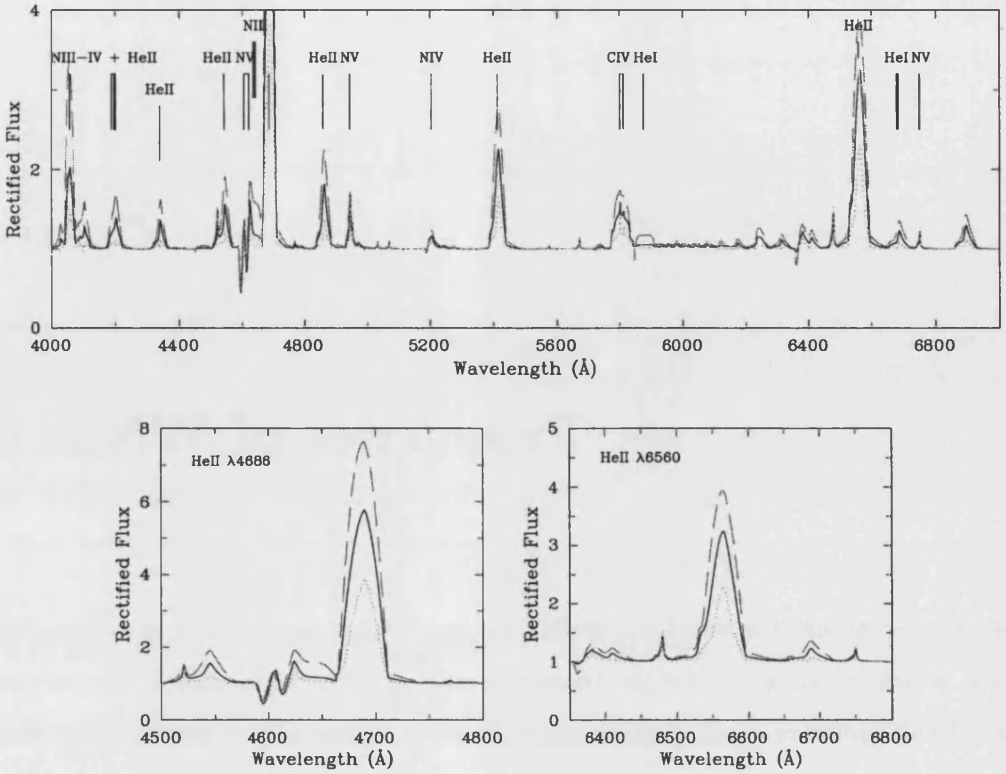

Figure 5.1: Comparison between rectified optical synthetic spectra showing a variety of mass-loss rates; 2.5×10^{-6} $M_{\odot}yr^{-1}$ (dotted), 5×10^{-6} $M_{\odot}yr^{-1}$ (solid) and 1×10^{-5} $M_{\odot}yr^{-1}$ (dashed). The theoretical optical spectrum is moderately unchanged over this range except for the strong WR emission features, He II λ4686 and He II λ6560.

We only have normalized, optical spectra for our sample of WN stars in M 33 (our largest sample of extragalactic WN stars), plus our datasets for a selection of Galactic and Magellanic Cloud WN stars also contain a number of uncalibrated spectra. We therefore decided to consistently analyse the datasets using the rectified spectra. Fortunately unlike many extragalactic studies this is combined with well determined reddenings providing an accurate determination of each star's absolute magnitude, which is later matched by our theoretical model.

We use a number of nitrogen lines to determine the temperature and ionization balance. For WNL stars we predominately use the N III λ4640 and N IV λ4057 emission lines, this is also used in conjunction with N V λ4604 for WNE stars. For very early WN-type stars such as WN3 the temperature is less accurate as we have no signature of N IV λ4057 to

help us determine the upper-limit of the star's effective temperature. These lines also give us a handle on the nitrogen abundance as they are also sensitive to changes in N/He ratios (see Section 3.6.9).

The mass-loss rates can be constrained primarily using the He II λ4686 and He I λ5876 emission lines and to some extent the nitrogen emission lines described above. Again this can be more accurate at lower temperatures where we see strong He I emission. Other weaker helium lines are also considered such as He II $\lambda\lambda$5411,6560 and He I λ6678.

As already mentioned the nitrogen abundance is estimated by the strength of a series of nitrogen lines, the hydrogen abundance however is calculated using the presence of (blended) Balmer/Pickering emission lines, although we mainly use the strong He II-Hα $\lambda\lambda$6560,6563 emission line. For the few cases where we see significant C IV λ5808 emission, we use this line alone to estimate the C/He number. Using all of this information we are able to confidently model the optical observations of WN stars and determine their fundamental parameters.

To illustrate the potential error in estimating the mass-loss rates of WN stars we have computed a series of synthetic models using 'typical' WNE parameters and varying the mass-loss rates by a factor of two. These results are shown in Figure 5.1. This figure highlights the effect that an increased mass-loss has on the ionization balance within the wind and is predominately seen through the varying line strengths of the He I-He II emission lines. It also gives us confidence that our estimated mass-loss rates are not wildly erroneous, given the large variations seen in only a moderate change in mass-loss. Theoretical modelling of single WR stars is clearly a multi-dimensional problem. However, with observable constraints on such parameters as the luminosity the situation is somewhat improved, allowing us to iteratively adjust the remanding properties until we match the pre-determined diagnostic emission features achieving a *global* comprise.

5.2 Analysis of WN stars in the Galaxy

Unlike our sample of extragalactic WC stars, there have been very few previous detailed studies of single WN stars for us to be able to directly compare our results with. Therefore, before we analyse our sample of single M 33 WN stars, it is necessary for us start by re-analysing a select sample of Galactic WN stars with well determined distances. Previous detailed studies of Galactic WN stars (e.g. Hamann, Koesterke & Wessolowski 1995)

Table 5.1: Observational parameters for our sample of single Galactic WN stars. All parameters are taken from van der Hucht (2001) and references therein.

Star	Spectral	Position (2000)		m_v	E_{b-v}	D	M_v
	Type	α	δ	(mag)	(mag)	(kpc)	(mag)
WR1	WN4	00 43 28.40	+64 45 35.4	10.51	0.66	1.82	-3.50
WR10	WN5ha	07 59 13.05	-28 44 03.1	11.08	0.49	4.61	-4.25
WR24	WN6ha	10 43 52.27	-60 07 04.0	6.49	0.15	2.63	-6.22
WR66	WN8(h)	15 14 57.72	-59 50 30.2	11.66	0.97	3.27	-4.89
WR78	WN7h	16 52 19.25	-41 51 16.2	6.61	0.41	1.99	-6.57
WR115	WN6	18 25 30.01	-14 38 40.9	12.32	1.30	2.00	-4.52
WR136	WN6(h)	20 12 06.55	+38 21 17.8	7.65	0.47	1.26	-4.78

derived stellar parameters but these models neglected important factors such as line-blanketing and clumping.

For the majority of our Galactic sample we use spectroscopic observations taken from Torres-Dodgen & Massey (1988), although modern observations would be superior, they are still sufficient such that detailed analysis can be under-taken. Table 5.1 lists the basic observational parameters for the Galactic WN stars studied. Their co-ordinates (columns 3 and 4) and narrow-band v magnitudes (column 5) are listed using the filter system devised by Smith (1968). Also shown for each star are the narrow-band reddening (column 6), distance (column 7) and absolute magnitude (column 8), all taken from van der Hucht (2001) and references therein. We chose to use a a revised distance of 2.63kpc for WR24 (P. Crowther; private communication). In general, we shall refer to individual stars by their Wolf-Rayet catalogue number, listed in column 1 (van der Hucht 2001).

Stellar parameters for each of the seven Galactic WN stars are derived and listed in Table 5.2. We compare the calculated theoretical models against our observations in Figure 5.2. Below we discuss successes and failures for each object.

5.2.1 WR1 (HD4004, WN4)

WR1 is the earliest Galactic WN star in our sample and consequently has broad emission lines. This star also displays trace elements of carbon, with clear emission of C IV λ5808

being detected and reproduced by our synthetic model. Our model does fractionally underestimate the N V $\lambda\lambda$4604,4620 emission lines, it also fails to match the line strength of the emission line, He II λ4100, although there are also the known Si IV $\lambda\lambda$4089,4116 emission lines which our model could be insufficiently accounting for. Our results yield a somewhat cooler temperature ($T_* \simeq$ 84kK) than obtained by Hamann & Koesterke (1998) ($T_* \simeq$ 100kK), we also determined a lower mass-loss rate but this is due to the fact that our models account for clumping in the wind.

Recent work by Ignace *et al.* (2003) obtained X-ray observations of WR1 using XMM-Newton and found significant emission "bumps" which are coincident with emission lines, such as Mg XI, Si XIII, and S XV. They also reported very little emission above 4 keV which they suggest is evidence that WR1 is very likely a single star.

5.2.2 WR10 (HD65865, WN5ha)

This weak-lined WN star is excellently reproduced by our synthetic model, including the majority of weaker lines. The blended He II-Hα $\lambda\lambda$6560,6563 emission line is slightly underestimated by our model. Comparing our inferred parameters with those derived by Hamann & Koesterke (1998), we find that the only major difference is that we determined a much cooler temperature $T_* \simeq$ 48kK, whereas Hamann & Koesterke (1998) predicted $T_* \simeq$ 63kK.

5.2.3 WR24 (HD93131, WN6ha)

WR24, a WN6ha star, is another weak, narrow-lined star in which we are successful in calculating a theoretical model that reproduces extremely well the observed optical spectrum. Our results are consistent with those derived by Hamann & Koesterke (1998), except that we have determined a faster terminal wind velocity by $\sim$350kms^{-1}. Measurements of (saturated) P–Cygni profiles in the UV suggest an even faster terminal velocity of v_∞ = 2155kms^{-1} for WR24 (Prinja, Barlow & Howarth 1990). Our models also indicate an extremely hydrogen-rich atmosphere, $\beta_H \simeq$ 46% (by mass) – in good agreement with previous results by Hamann & Koesterke (1998) – this amount of hydrogen is typically observed in WN9–11 or Of stars (e.g. Crowther & Smith 1997; Crowther & Bohannan 1997).

5.2.4 WR66 (HD134877, WN8(h))

WR66 is a late-type WN star for which we have excellent agreement between our observations and theoretical model for almost all important emission lines, including He II λ4686 and He I λ5876. Although our results failed to predict the correct line strength for He I λ6678, the only other discrepancies were for a series of very weak emission lines around $\sim$4500Å. Hamann & Koesterke (1998) derived a cooler temperature ($T_* \simeq$ 32kK), larger luminosity ($logL \simeq$ 5.8), and significantly higher mass-loss rate ($log\dot{M} \simeq$ -3.6). These discrepancies arise due to the difference in our initial assumption in the absolute magnitudes (Hamann & Koesterke (1998) adopt a distance to WR66 of $\simeq$ 7.9kpc). If we adjust their derived luminosity to match our determined absolute magnitude than we find a much better agreement ($logL \simeq$ 5.0).

5.2.5 WR78 (HD151932, WN7h)

We were again successful in reproducing an excellent synthetic optical spectrum for WR78. Our emergent theoretical model did fractionally over-estimate the line strength for N III λ4640, He II λ4686 and He I λ5876. Our stellar parameters are in reasonable agreement with those previously determined by Hamann & Koesterke (1998).

At this point we call into question the WN7h classification given to WR78 by Smith, Shara & Moffat (1996). Recalling the classification scheme devised by Smith, Shara & Moffat (1996), stating hydrogen is detected if the (H+He) lines, λ4340 and/or λ4861, clearly exceed the height of a line drawn between the peaks of the pure He II lines, $\lambda\lambda\lambda$4200,4541,5411 – visual inspection for WR78 shows this is not the case. When we measure the H^+/He^{++} ratios for WR78 we find both discriminators elude to a marginal, '(h)' classification.

Based in this evidence we suggest a simple re-classification for WR78 to WN7(h). This highlights the difficulty in predicting accurate hydrogen abundances in WN stars. This re-classification is supported by our theoretical results where our derived stellar parameters predicts a conservative estimate for the hydrogen abundance, by number, H/He $\approx$ 0.21 (i.e. $\beta_H \approx 5\%$). Compare this to the predicted H abundance for WR78 with two stars designated with 'ha' status, for which our theoretical models estimate H/He $\approx$ 0.72 and 3.54 (by number) for WR10 and WR24 respectively.

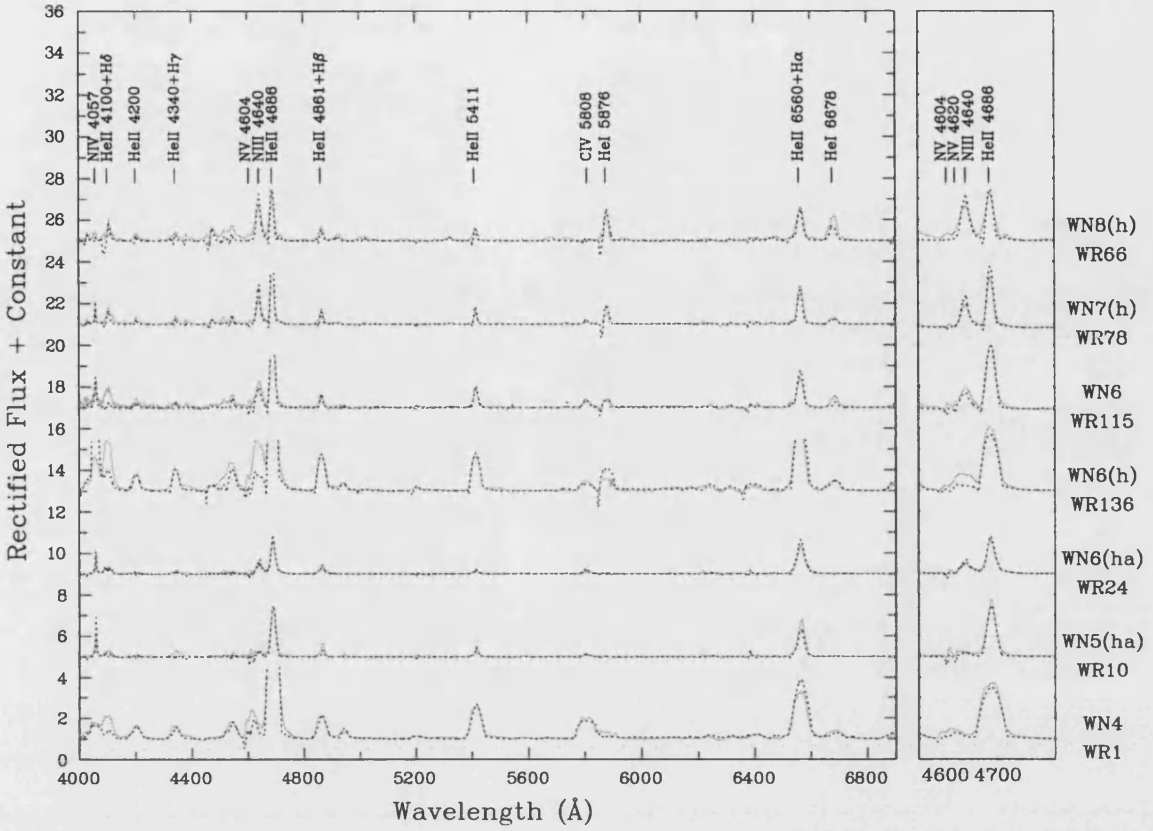

Figure 5.2: Comparison between observations of Galactic WN stars (solid) and our synthetic model (dotted). The panel on the right shows the blended λ4650 feature.

5.2.6 WR115 (IC14-19, WN6)

All the important diagnostic lines are well matched by our theoretical model for WR115 apart from the emission feature at λ4100. But as with WR1 this could be due, in part, to a number of other emission lines which have been insufficiently accounted for, including components from lines such as Si IV λ4089. The inferred parameters for WR115 from our studies indicate a hotter temperature, by $\sim$10kK, and less luminous star, by $\sim 0.3 L_{\odot}$, compared with Hamann & Koesterke (1998).

5.2.7 WR136 (HD192163, WN6(h))

WR136, is also thought to be the central star powering the ring nebula NGC 6888. This WN6(h) star proved the most difficult Galactic WN star to model, with large discrepancies in simultaneously reproducing N IV λ4057 and N III λ4640. To fit the majority of diagnostic lines we finally comprised with a synthetic model that still significantly over-estimated the N IV λ4057 emission line and partly reproduced N III λ4640. It also fractionally under-estimated He II λ4686 and slightly over estimated He I λ5876. Interestingly Hamann & Koesterke (1998) were only able to produce a poor fit quality between their observations and theoretical model. With their parameters suggesting a much more luminous and cooler star. Considering the poor fit of our model to the observations we will give less emphasis to the derived parameters when comparing our result (see Section 5.8).

5.3 Analysis of WN stars in the LMC

We now re-examine a representative selection of single WN stars located in the Large Magellanic Cloud (LMC). Observational studies of individual WR stars in the LMC are more appealing than those in our Galaxy as they have a well determined distance and low interstellar reddening. The LMC also proves an excellent laboratory for massive star studies, with 134 WR stars known (Breysacher, Azzopardi & Testor 1999), it also provides a homogeneous population all located in a metal-poor environment ($Z \simeq 0.4Z_{\odot}$; Russell & Dopita 1990).

There have been a number of recent detailed studies examining the WN population in the LMC, in which their stellar parameters were determined (e.g. Crowther & Smith 1997; Crowther, Hillier & Smith 1995; Hamann & Koesterke 2000). Unfortunately the methods used to determine these parameters differ from the techniques employed in this work. There are also subtle differences in factors such as the non-LTE codes used between previous studies and this work (see Section 3.6 for more details).

We have selected a sample of eight single WN stars located in the LMC for which we have optical spectroscopy (P. Crowther; private communication). A large number of the spectra used were observed and published by Torres-Dodgen & Massey (1988). Before we proceed into specific details regarding the modelling of these WN stars, we must first confidently either independently calculate absolute visual magnitudes for each star or alternatively use another reliable source. For this work we use the narrow-band v

Table 5.2: List of derived stellar parameters for the single WN stars in the Galaxy taken from our sample. The absolute magnitudes calculated from the models are also shown. The current stellar masses were calculated using the relationship derived from Schaerer & Maeder (1992).

Star	Alias	Spectral Type	T_* kK	R_* $R_\odot$	$logL$ $L_\odot$	$log\dot{M}$ $M_\odot yr^{-1}$	v_∞ km s^{-1}	H/He	N/He	β_H %	β_{He} %	β_N %	m_v (mag)	E_{b-v} (mag)	M_v (mag)	$\frac{\dot{M}v_\infty}{(L/c)}$	M_* $M_\odot$
WR1	HD4004	WN4	84	2.31	5.33	-5.08	2000	0.008	0.005	0	98	2	10.51	0.66	-3.50	3.81	10.9
WR10	HD65865	WN5ha	48	5.96	5.23	-5.60	1540	0.72	0.006	15	83	2	11.08	0.49	-4.25	1.11	—
WR24	HD93131	WN6ha	41	16.86	5.86	-4.57	1560	3.54	0.009	46	52	2	6.49	0.15	-6.22	2.84	—
WR66	HD134877	WN8(h)	39	8.48	5.18	-4.98	1300	0.27	0.005	6	92	2	11.66	0.97	-4.90	4.40	—
WR78	HD151932	WN7h	40	19.18	5.93	-4.65	1100	0.21	0.004	5	93	1	6.61	0.41	-6.56	1.42	—
WR115	IC14-19	WN6	49	9.24	5.29	-5.21	1400	0.001	0.005	0	98	2	12.32	1.30	-4.54	2.17	10.3
WR136	HD192163	WN6(h)	78	2.81	5.42	-4.63	1540	0.46	0.009	10	87	3	7.65	0.47	-4.79	6.70	—

Table 5.3: Observational parameters for our sample of single WN stars in the LMC. All parameters are taken from Breysacher *et al.* (1999) and references therein. The absolute magnitudes were calculated using a distance of 50.0kpc (Kennicutt *et al.* 1998).

Star	Spectral	Position (2000)		m_v	E_{b-v}	M_v
	Type	α	δ	(mag)	(mag)	(mag)
Brey1	WN3b	04 45 32.07	-70 15 11.3	15.93	0.08	-2.89
Brey2	WN2b	04 49 36.22	-69 20 54.2	16.22	0.12	-2.77
Brey6	WN4b	04 55 31.29	-67 30 01.7	14.10	0.07	-4.68
Brey13	WN8h	05 03 08.84	-66 40 57.3	12.73	0.08	-6.09
Brey20	WN4b	05 16 38.91	-69 16 40.4	14.71	0.07	-4.07
Brey26	WN6(h)	05 22 22.54	-71 35 57.8	12.72	0.08	-6.10
Brey45	WN4b	05 27 52.61	-68 59 07.3	14.92	0.07	-3.86
Brey90	WN6(h)	05 38 57.14	-69 06 05.2	12.16	0.16	-6.99

magnitudes and E_{b-v} values published by Breysacher (1986). The absolute magnitudes are calculated assuming a distance modulus of (m - M)$_0$ = 18.50 (corresponding to 50.0kpc; Kennicutt, Stetson, Saha, Kelson, Rawson, Sakai, Madore, Mould, Freedman, Bresolin, Ferrarese, Ford, Gibson, Graham, Han, Harding, Hoessel, Huchra, Hughes, Illingworth, Macri, Phelps, Silbermann, Turner & Wood 1998), these values are listed in Table 5.3 (column 7) along with their coordinates (columns 3 and 4) and spectral types (column 2).

Our final stellar parameters are shown in Table 5.4 and a comparison between the models and rectified observations are shown in Figure 5.3. Below we review all eight WN stars and discuss our results for the individual stars.

5.3.1 Brey1 (FD1, WN3b)

The signal-to-noise for this WN3b star is not ideal, especially redward of approximately 6000Å, but we were still able to use the observations to identify important emission lines that are used in determining the stellar parameters. Our artificial model spectrum overestimates the N V $\lambda\lambda$4604-4620 blend a little, and predicts no N IV λ4057, which is not seen in the observations. It is worth noting at this point that for very early WN stars, such as

Brey1 (Breysacher 1981), the temperature determinations are not as accurate with only a limited number of temperature sensitive emission lines available in the optical regime.

The optical spectrum of Brey1 was analysed by Koesterke *et al.* (1991), they derived two sets of parameters due to the uncertain detection of He I λ5876. Our stellar parameters (see Table 5.4) tend to agree closer to their second, and hotter, set of results. Foellmi, Moffat & Guerrero (2003*b*) recently included Brey1 in their survey of WR stars in the LMC and concluded that it did not produce any significant radial velocity variations and as such was ruled out as a possible spectroscopic binary.

5.3.2 Brey2 (AB14, WN2b)

Brey2 (Breysacher 1981) is an extreme WN2b star and is an interesting object for many reasons, not only because of its rare spectral type, but also because of the associated nebula (DEM L6; Davies, Elliott & Meaburn 1976). Pakull (1991) first detected nebular He II emission around Brey2, which was later observed to have a moderate chemical enrichment Garnett & Chu (1994). The small wind blown bubble surrounding the central star was observed to be expanding at $\sim$16kms^{-1} (Chu, Weis & Garnett 1999). More recently, Nazé *et al.* (2003) observed the (faint) He II emission and claimed that it extended over an area of 22 $\times$ 17pc^2 , they also discovered an even fainter region of He II emission associated with the interstellar bubble blown by the progenitor of Brey2.

Producing a synthetic model for Brey2 also provided some extreme results (see Table 5.4 for stellar parameters). Again, as with Brey1, our derived temperature should be taken with caution as N IV λ4057 was absent, and detection of N V λ4604 was very weak – which highlights the extreme ionizing radiation required for such low quantities of N^{+3} or N^{+4}. Although our temperature determinations are not precise, an unusually high temperature was required to unsure that N IV λ4057 was absent (i.e. fully ionized) and N V λ4604 was weak. Our derived hydrogen abundances are also only approximate as our spectral coverage was limited to $\lambda\lambda$4000–6000 and excludes Hα λ6563. Overall our synthetic model predicts the optical spectrum for Brey2, although it does slightly overestimate the (weak) N V $\lambda\lambda$4604,4620 emission feature. A recent detailed observational survey by Foellmi, Moffat & Guerrero (2003*b*) concluded that Brey2 was single.

5.3.3 Brey6 (HD32109,WN4b)

The emission lines for Brey6 (Breysacher 1981) are surprisingly broad (FWHM(He II) $\sim$ 70Å), in fact Breysacher (1981) classified this star as *peculiar* due to its unusually broad emission line spectrum. It was studied in detail by Koesterke *et al.* (1991), who also commented on the abnormally strong He II λ5411 emission line, their inferred stellar parameters are very close to those determined by this work, except for the mass-loss rate which they claimed was $\sim$0.8dex larger. We successfully reproduce all the emission line strengths for the observed optical spectrum of Brey6, although our model failed to predict the rounded line profiles for the majority of emission lines. Brey6 was observationally confirmed to be single by Foellmi, Moffat & Guerrero (2003*b*).

5.3.4 Brey13 (HD33133, WN8h)

Brey13 (Breysacher 1981), spectral classification WN8h, has the latest spectral-type in our sample of LMC WN stars. Garnett & Chu (1994) identified an ejecta ring nebula associated with Brey13 which was chemically enriched (He/H and H/H both a factor of two higher than LMC H II region values), Dopita *et al.* (1994) later reported this nebula to extend $30'' \times 40''$ in diameter with a morphology similar to NGC6888. Crowther & Smith (1997) likened Brey13 to the Galactic WN8 star, WR40, both in terms of its spectral appearance and its ring nebula.

Stellar parameters for this object were derived by Crowther & Smith (1997) and except for a slightly higher mass-loss rate and cooler temperature, ours do not greatly differ. A similar conclusion can be found when comparing our results with those determined by Koesterke *et al.* (1991). Our theoretical model closely matches our observations; only slightly under-estimating the line strength of the He II λ4686 and the blended emission line He II-Hβ $\lambda\lambda$4859,4861.

5.3.5 Brey20 (WS14, WN4b)

Dopita *et al.* (1994) observed a small ring nebula around Brey20 (Breysacher 1981) measuring $12'' \times 19''$ in diameter, this nebula is believed to be associated with the star. Compared with the other two WN4 stars in our sample (Brey6 and Brey45), the derived temperature for this single WNE star (Foellmi, Moffat & Guerrero 2003*b*) is somewhat cooler. Brey20 is generally well matched, N V $\lambda\lambda$4604,4620 is slightly under-estimated

although at the resolution of the data its difficult to resolve the two separate emission lines.

5.3.6 Brey26 (HD36063, WN6(h))

This is yet another WN star in the LMC that has an associated nebula surrounding it. Dopita *et al.* (1994) reported that this ring nebula has a 16″ diameter which when observed in Hα has a bright knot to the east of the star. Moffat (1989) claimed that Brey26 (Breysacher 1981) is a binary with a fast period, $P \simeq 1.9$ days, implying either a close binary system or large intrinsic variations. There are no photospheric absorption lines observed in the optical spectrum for this star. Unfortunately this star was not included in the recent survey by Foellmi, Moffat & Guerrero (2003*b*) and so without any further quantitative information regarding a possible companion we have assumed that Brey26 is single.

The stellar parameters for Brey26 were investigated by Koesterke *et al.* (1991), Crowther & Smith (1997) and Hamann & Koesterke (2000). The inferred temperatures from these three studies range from, $T_* \simeq 33 - 40$kK, our calculated parameters point towards a slightly higher temperature ($T_* \sim 42$kK). All three studies also agree at a mass-loss rate of $log\dot{M} \sim$ -4.2 $M_\odot yr^{-1}$, whereas we predict a lower mass-loss rate $log\dot{M} \sim$ -4.7 $M_\odot yr^{-1}$. We are successful in reproducing all the (optical) emission lines observed for Brey26, including weak emission lines such as He I λ5876

5.3.7 Brey45 (WS33, WN4b)

There is very little specific details regarding this strong-lined, single (Foellmi, Moffat & Guerrero 2003*b*), WN4b star in the literature. Dopita *et al.* (1994) commented there was no nebulosity around Brey45 (Breysacher 1981). Its spectroscopic appearance is very similar to Brey20, except that its emission lines are somewhat broader. This is seen in our derived stellar parameters, where apart from the small difference in inferred temperatures, they are very similar. For this WN4b star the observational spectrum is well reproduced by our model, except that He II λ4686 and the He II-Hα $\lambda\lambda$6560,6563 blend are slightly over-estimated, although the data quality redward of ~6200Å is significantly reduced.

5.3.8 Brey90 (HDE269928, WN6(h))

Brey90 (Breysacher 1981) is a weak-lined WN6(h) star, which is located in the core region of the 30 Doradus nebula. Within this dense region Brey90 has produced a wind blown bubble (Dopita *et al.* 1994). Stellar parameters were previously derived by Crowther & Smith (1997), they deviate somewhat from those inferred from this work, with the main discrepancies arising in temperatures, mass-loss rates and hydrogen abundances. Our observations for Brey90 are well reproduced by our model including He II λ4686 and the weaker nitrogen lines (e.g. N IV λ4057).

Early work by Moffat (1989) tentatively claimed that Brey90 was a binary star with a long spectroscopic period, $P \simeq 25.2$ days. There has yet to be any studies to confirm or disprove these early findings. For this work we have assumed that Brey90 is single; should the binary nature for this star change, revisions to our determined parameters would be required.

5.4 Analysis of WN stars in the SMC

As described throughout this work, metallicity plays a vital role in the evolution of a massive star altering the efficiency of mass loss during a star's life. Exactly how sensitive these effects are during the WR phases (i.e. WN, WC and WO) are yet to be confirmed. We extend our study of single WN stars, this time to the metal poor ($Z \simeq 0.2Z_{\odot}$; Russell & Dopita 1990) galaxy, the Small Magellanic Cloud (SMC).

The WR population in the SMC, of which ~90% are WN-type, have been well studied. Most recently Foellmi, Moffat & Guerrero (2003*a*) carried out an intensive spectroscopic survey searching for WR binaries. They revise the current catalogue of known WR stars in the SMC, including the two newly confirmed WN stars discovered by Massey & Duffy (2001); we chose to use the nomenclature from this catalogue throughout this work.

Until recently it was commonly believed that almost all WR stars in the SMC were binary systems; this was due to their very weak emission-lined spectra. Also stellar evolution theory suggests that for WR stars to form in such a metal deficient region then it would be favourable that they should form from a Roche-lobe overflow in a binary system where the progenitor WR star was initially formed below the minimum initial mass required to form such an object. This was recently called into question, when Foellmi, Moffat & Guerrero (2003*a*) spectroscopically observed the radial velocities of all the known WN stars in the

Table 5.4: List of derived stellar parameters for the single WN stars in the LMC taken from our sample. The absolute magnitudes calculated from the models are also shown. The current stellar masses were calculated using the relationship derived from Schaerer & Maeder (1992).

Star	Alias	Spectral Type	T_* kK	R_* $R_\odot$	$logL$ $L_\odot$	$log\dot{M}$ $M_\odot yr^{-1}$	v_∞ km s^{-1}	H/He	N/He	β_H %	β_{He} %	β_N %	m_v (mag)	E_{b-v} (mag)	M_v (mag)	$\dot{M}v_\infty/(L/c)$	M_* $M_\odot$
Brey1	FD1	WN3b	90:	1.78	5.27	-5.41	1700	0.001	0.002	0	99	1	15.93	0.08	-2.90	1.74	10.1
Brey2	AB14	WN2	160:	0.36	4.88	-5.09	1720	0.001:	0.002	0	99	1	16.22	0.12	-2.78	9.02	6.2
Brey6	HD32109	WN4b	90	3.63	5.89	-4.56	3000	0.001	0.001	0	99	1	14.10	0.07	-4.20	5.21	24.6
Brey13	HD33133	WN8h	41	14.69	5.74	-4.75	840	1.40	0.003	26	73	1	12.73	0.08	-6.10	1.33	—
Brey20	WS14	WN4b	78	3.71	5.64	-5.21	1500	0.001	0.005	0	98	2	14.71	0.07	-4.04	1.04	19.5
Brey26	HD36063	WN6(h)	42	14.57	5.78	-4.69	1300	0.88	0.002	18	81	1	12.72	0.08	-5.69	2.16	—
Brey45	WS33	WN4b	90:	2.48	5.56	-5.05	1700	0.001	0.005	0	98	2	14.92	0.07	-3.85	2.04	14.9
Brey90	HDE269928	WN6(h)	40	23.26	6.10	-4.53	1350	1.40	0.003	26	73	1	12.16	0.16	-7.03	1.55	—

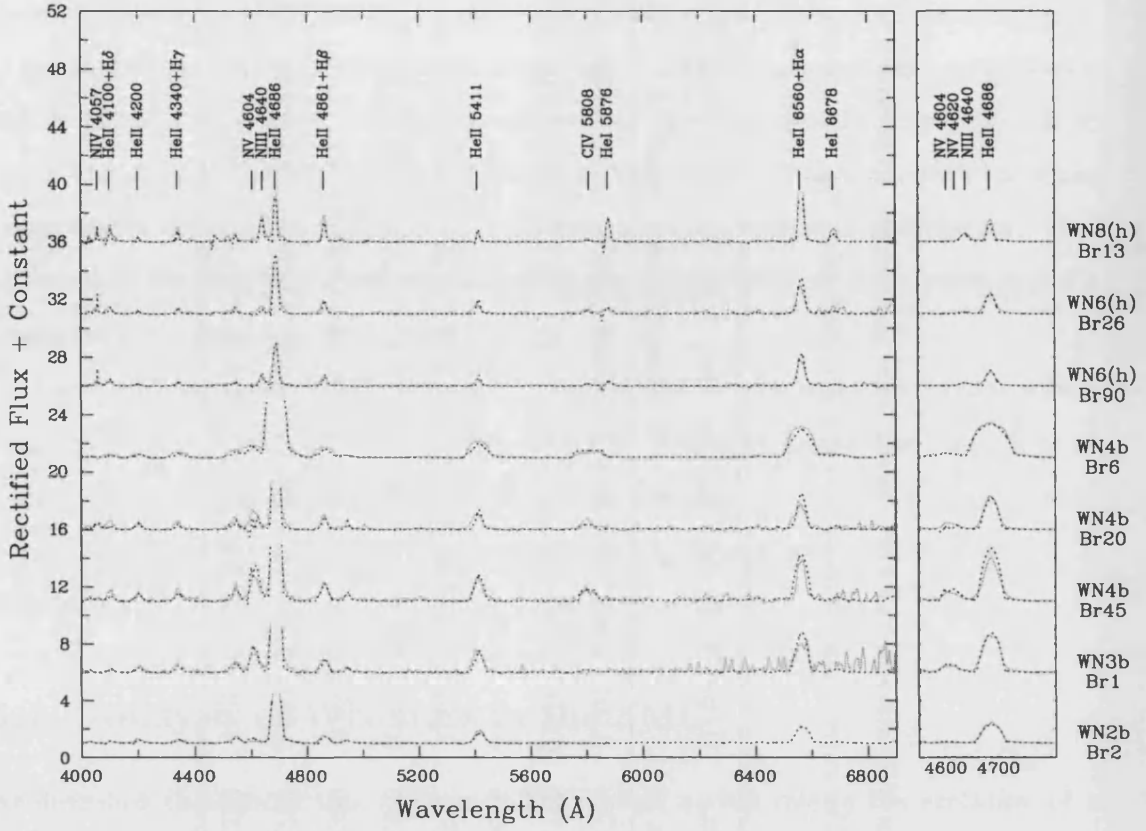

Figure 5.3: Comparison between observations of WN stars in the LMC (solid) and our synthetic models (dotted). The panel on the right shows the blended λ4650 feature.

SMC as well as the WNE stars in the LMC. They surprisingly found that instead of the expected 100% binary frequency of WR stars in the SMC it was more like 40%.

The total number of known WR stars in the SMC[1] is 11, observational surveys have searched sufficiently deep (e.g. $m_V \simeq 17$mag; Massey & Duffy 2001) such that no more WN stars are expected. From these 11 WR stars, Foellmi, Moffat & Guerrero (2003*a*) found that 6 showed no signs of periodic variability and hence at the detection level it was assumed they are bona-fide single stars. We were provided with high-resolution spectra[2]

[1]Recent spectroscopic observations by Massey, Olsen & Parker (2003) reported the discovery of a previously unknown WN3–4 star, although its He II excess identified it as a WR candidate in an earlier imaging survey the wrong star was observed.

[2]Kindly provided by C. Foellmi (Univ. Montreal)

Table 5.5: Observational parameters for our sample of single WN stars in the SMC. All parameters are taken from Foellmi, Moffat & Guerrero (2003*a*) and references therein, apart from the apparent visual magnitudes and reddenings which are taken from Zaritsky *et al.* (2002). The absolute magnitudes were calculated using a distance of 60.0kpc (van den Bergh 2000).

SMC-#	Spectral	Position (2000)		m_V	E_{B-V}	M_V
	Type	α	δ	(mag)	(mag)	(mag)
WR1	WN3ha	00 43 42.23	-73 28 54.9	15.24	0.28	-4.52
WR4	WN6h	00 50 43.06	-73 27 07.8	13.43	0.20	-6.08
WR9	WN3ha	00 54 29.30	-72 44 34.1	15.43	0.15	-3.93
WR10	WN3ha	00 45 28.78	-73 04 45.2	15.55	0.58	-5.14
WR11	WN4h:a	00 52 07.36	-72 35 37.4	15.85	0.08	-3.29

(see Foellmi, Moffat & Guerrero 2003*a*) for 5 recently confirmed single stars in the SMC, we analyse them in exactly the same manner as other WN stars described in this chapter.

As we are using the absolute magnitude to constrain the luminosity it is vital that use reliable photometry, reddenings and distances in calculating the absolute magnitudes. There have been a number of photometric studies of the stellar population in the SMC, all of which have measured their UBV magnitudes, including all the the WR objects. Unfortunately for the two newly confirmed WR stars (SMC-WR10 and SMC-WR11), discovered by Massey & Duffy (2001), there are conflicting photometric observations published. We decided to use the photometric observations published by Zaritsky *et al.* (2002) who surveyed an 18 deg^2 area of the SMC, for which apart from SMC-WR10 and SMC-WR11 their photometry agreed to within 0.1 mag.

The reddenings and hence the absolute magnitudes were calculated assuming an intrinsic colour excess of $(B\text{-}V)_0 = -0.32$, which was also adopted by Massey & Duffy (2001) when calculating their absolute magnitudes. We tested the validity of this by determining the reddening independently (using a Galactic foreground reddening of $E_{B-V} = 0.03$ and an internal SMC reddening of $E_{B-V} = 0.23$, as parameterized by Calzetti 2001), for SMC-WR1 using flux calibrated UV and optical data in conjunction with our synthetic model. We used SMC-WR1 to test this assumption as it was the only object where IUE

data were available, which meant that we could accurately constrain the reddening. We were then able to determine the intrinsic (B-V) colour excess. We found that our initial assumption was consistent with the intrinsic colour excess calculated from our observations and synthetic model and so used this value in determining the absolute magnitudes for all 5 objects.

For the distance to the SMC we use a distance modulus of $(m - M)_0 = 18.9$ (van den Bergh 2000), which equates to 60kpc, throughout this work. Table 5.5 lists the coordinates (columns 3 and 4), apparent visual magnitudes (column 5), reddenings (column 6) and the final calculated absolute magnitudes (column 7) used for all the single WN stars analysed. SMC-WR# (column 1) and recently revised spectral types (column 2) are taken from Foellmi, Moffat & Guerrero (2003*a*).

We compare our theoretical models with our observations in Figure 5.4, and the derived stellar parameters are given in Table 5.6. Below we discuss previous findings as well as our results specific to each individual star.

5.4.1 SMC-WR1 (AV2a, WN3ha)

This early-type WN star was observed by Moffat (1988) and Massey & Duffy (2001). Both noted that the emission lines of He II λ4686 and N V $\lambda\lambda$4603,4620 are strong.

Our synthetic model reproduces the observations excellently, including all intrinsic absorption line profiles. The only slight criticism is that He II-Hα $\lambda\lambda$6560,6563 is fractionally underestimated.

5.4.2 SMC-WR4 (Sk 41, WN6h)

This is the only WNL star in the SMC with clear detection of N IV λ4057 and (weak) N III $\lambda\lambda$4634,4640. There are also no signs of absorption in its optical spectrum and it was fittingly classified WN6h by Foellmi, Moffat & Guerrero (2003*a*). SMC-WR4 was confirmed as single by Foellmi, Moffat & Guerrero (2003*a*), however, they did detect signs of photometric variability with a periodic signal, $P \simeq 6.6$ days. They reason that this variability can be explained by large-scale rotating structures.

SMC-WR4 is the only WN star from our sample which was previously assumed single and modelled accordingly by Crowther (2000). Our synthetic model is in very good agreement with the observed optical data. Comparing our results in Table 5.6 with those published by Crowther (2000), who interestingly also compared his model to IR data,

overall the agreement is good. We find that our derived luminosity is somewhat higher and as a result we predict a fractionally higher larger mass-loss rate. We also used a slightly cooler temperature and a reduced wind velocity. The majority of these effects can be explained due to line blanketing and the fact that we assumed a brighter absolute magnitude.

5.4.3 SMC-WR9 (MG9, WN3ha)

Extensive observational studies of the WR content in the SMC by Foellmi, Moffat & Guerrero (2003*a*) revealed that SMC-WR9 met the primary requirement for a binary status (i.e. spectroscopic binary), indicating a long period, $P \simeq 37.6$ days. Although they concluded that as all other indicators implied a single star status (e.g. photometric variability) it was likely that SMC-WR9 was single but further investigation was needed to confirm the binary nature of this star. For this work we assume that the observed spectrum is solely from a WR star.

We again achieve another excellent agreement between model and observations, the difference here was that we have increased the the rotational broadening of the model to $v \sin i = 150 \mathrm{kms}^{-1}$ to match the observed line strengths and widths especially for the weaker nitrogen lines.

5.4.4 SMC-WR10 (WN3ha)

The optical spectrum of SMC-WR10 appears extremely similar to SMC-WR1, where apart from slight differences in terminal wind velocities, this is reflected in the final parameters derived for both stars (see Table 5.6).

This WN3 star was also well reproduced by our models, only slightly under-estimating the line strength of Hα. Again to imitate the observed line profiles we have to broaden the model to $v \sin i = 150 \mathrm{kms}^{-1}$. This star was very similar to SMC-WR1 in both appearance and stellar parameters, the only major difference being that SMC-WR10 is a little brighter. It was also found to have a somewhat faster terminal wind velocity.

5.4.5 SMC-WR11 (WN4h:a)

SMC-WR11 has the weakest line strengths of any of the five WN stars modelled. To match the observed line widths we applied a broadening to our synthetic model, $v \sin i =$

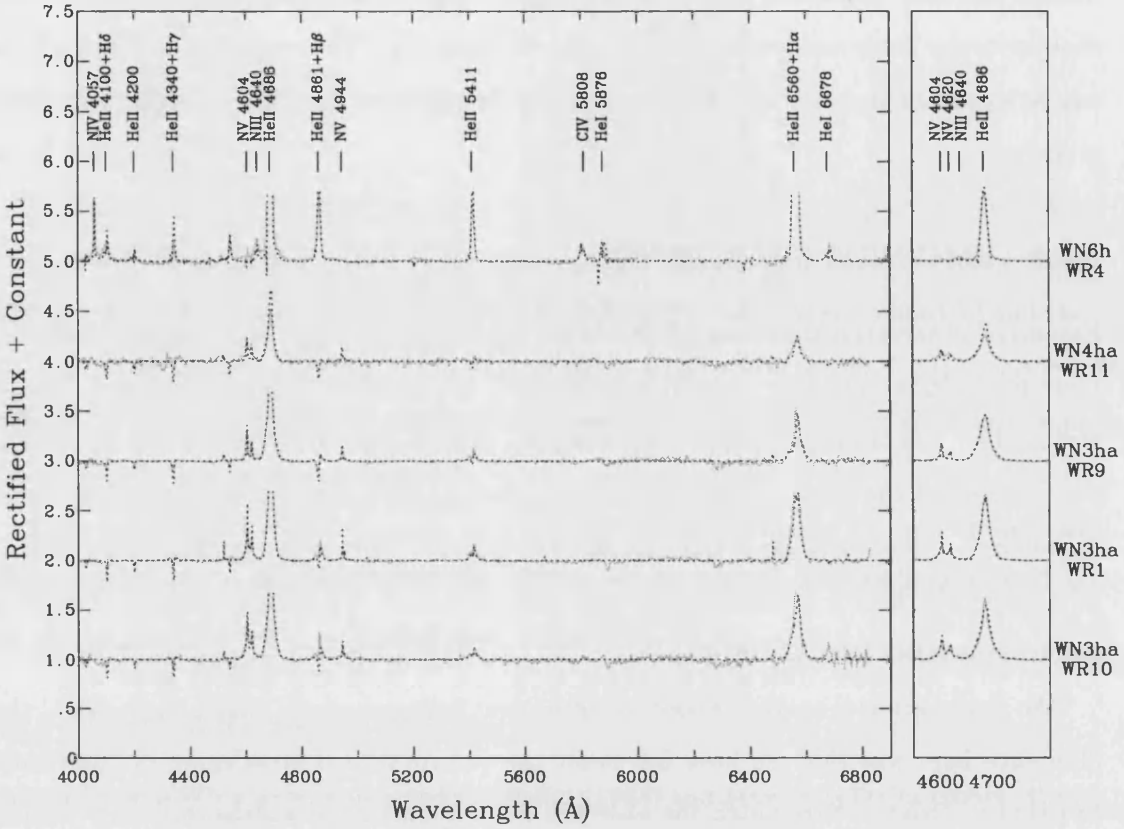

Figure 5.4: Comparison between observations of WN stars in the SMC (solid) and our synthetic models (dotted). The panel on the right shows our fit to He II λ4686.

200kms^{-1}. Apart from He II λ4686 being a fraction over-estimated, our synthetic model matched other features in both emission and absorption very well.

Foellmi, Moffat & Guerrero (2003*a*) discussed the 'probable' nature of intrinsic hydrogen observed in SMC-WR11. Our model fit predicts H/He $\approx$ 1.00 (i.e. $\beta_H \approx 20\%$), although this parameter cannot be constrained very accurately owing to the lack of hydrogen abundance sensitive lines. We cannot use the hydrogen criteria devised by Smith, Shara & Moffat (1996) due to lines such as He II λ4541 being observed in absorption. The emergent model spectrum for this star predicts that in the He II-Hα $\lambda\lambda$6560,6563 blend, Hα contributes $\approx$ 40% of the line strength. Combining this with the fact that our theoretical model reproduces almost all lines for this star, we claim that hydrogen is abundant

in the atmosphere of SMC-WR11. Our estimated hydrogen abundance for SMC-WR11 compares with other WN stars which have been classified 'h' (e.g. WR10).

5.5 Analysis of WN stars in NGC 6822

The WR population in the dwarf irregular galaxy NGC 6822 was first explored by Westerlund *et al.* (1983) where they reported a newly discovered WR star using a grism. They obtained subsequent spectroscopy which confirmed the WR nature of the star and which they described as showing characteristics of a WN3 star. Later surveys of this nearby galaxy by Armandroff & Massey (1985) using interference filters found 12 WR candidates including the previously discovered WN star by Westerlund *et al.* (1983). This number was later reduced to four when spectroscopy of all candidate WR stars were taken by Massey, Conti & Armandroff (1987*a*). Interestingly all four of these WR stars were classified as WN-type.

Metallicity studies of NGC 6822, as with many galaxies within the Local Group, have been limited. To date there have only been a few studies which measured oxygen abundances by observations of H II regions. Early work by Pagel, Edmunds & Smith (1980) found an abundance of 12+log(O/H) = 8.25 ± 0.07, which means its metallicity is intermediate between both Magellanic Clouds. This was confirmed later by Skillman, Terlevich & Melnick (1989). Since then with the introduction of large 8-metre ground-based facilities, studies of individual stars within Local Group galaxies have been made possible. Venn *et al.* (2001) analysed two A-type supergiants in NGC 6822 using high-resolution spectroscopy and concluded that the oxygen abundance, 12+log(O/H) = 8.36 ± 0.19, is in good agreement with the nebular oxygen results. They did however suggest that the oxygen abundance may vary across the galaxy but stressed that additional observations are required before the radial chemical properties of the galaxy are confidently constrained.

We have obtained high-resolution, flux calibrated, optical spectroscopy of NGC6822-WR12, using the notation as catalogued by Massey & Johnson (1998), (P. Crowther; private communication) using the VLT-FORS2. To perform a consistent analysis we compare our model results with rectified observations. Our observations achieve a resolution and signal-to-noise such that detailed analysis can be undertaken in order to determine the star's fundamental parameters.

Table 5.7 outlines the basic observational parameters for NGC6822-WR12, including

Table 5.6: List of derived stellar parameters for the single WN stars in the SMC taken from our sample. The absolute magnitudes calculated from the models are also shown. The current stellar masses were calculated using the relationship derived from Schaerer & Maeder (1992).

SMC-#	Alias	Spectral Type	T_* kK	R_* $R_\odot$	$logL$ $L_\odot$	$log\dot{M}$ $M_\odot yr^{-1}$	v_∞ km s^{-1}	H/He	N/He	β_H %	β_{He} %	β_N %	m_V (mag)	E_{B-V} (mag)	M_V (mag)	$\frac{\dot{M}v_\infty}{(L/c)}$
WR1	AV2a	WN3ha	85	5.27	6.12	-5.51	1750	2.00	0.002	33	66	1	15.24	0.28	-4.52	0.20
WR4	Sk 41	WN6h	40	16.61	5.80	-4.97	910	2.25	0.001	36	64	0	13.43	0.20	-6.08	0.76
WR9	MG9	WN3ha	95	3.72	6.01	-5.51	2500	1.80	0.001	31	69	0	15.43	0.15	-3.93	0.37
WR10	.....	WN3ha	85	7.02	6.37	-5.19	2250	2.00	0.002	33	66	1	15.55	0.58	-5.14	0.30
WR11	.....	WN4h:a	95	2.85	5.78	-5.92	2150	1.00	0.001	20	80	0	15.85	0.08	-3.30	0.21

Table 5.7: Observational parameters of NGC6822-WR12 taken from Massey & Johnson (1998). The apparent visual magnitude was taken using spectrophotometry.

Star	Spectral	Position (2000)		m_V	E_{B-V}	M_V
	Type	α	δ	(mag)	(mag)	(mag)
NGC6822-WR12	WN4	19 45 13.44	-14 45 12.1	18.82	0.18	-5.36

its apparent visual magnitude, which was taken from spectrophotometry. Our apparent visual magnitude is identical to that observed previously by Bianchi *et al.* (2001*a*), who also derive a reddening of $E_{B-V} = 0.35$. This apparent magnitude is somewhat brighter than originally published by Westerlund *et al.* (1983), who claimed $m_V = 19.5$ mag. They also assumed an average reddening of $E_{B-V} = 0.3$ and a distance modulus of $(m - M)_0 = 23.2$ (which approximates to $\simeq$ 440kpc), giving them an absolute magnitude of $M_V =$ -4.6.

Our technique of calculating the absolute magnitude is somewhat refined, in that we use an independently derived reddening by comparing our calibrated observations with our (un-reddened) synthetic model. This method suggested a reddening for NGC6822-WR12 of $E_{B-V} = 0.18$. Of course this value would be better constrained with calibrated UV and/or IR observations. For the distance determination we use the findings from Kennicutt, Stetson, Saha, Kelson, Rawson, Sakai, Madore, Mould, Freedman, Bresolin, Ferrarese, Ford, Gibson, Graham, Han, Harding, Hoessel, Huchra, Hughes, Illingworth, Macri, Phelps, Silbermann, Turner & Wood (1998), in which they use observations of Cepheids. They find a distance modulus to NGC 6822 of $(m - M)_0 = 23.62$ (corresponding to 530kpc). Using this information we calculate that NGC6822-WR12 has an absolute visual magnitude of $M_V =$ -5.36, almost a magnitude brighter than claimed by Westerlund *et al.* (1983). We model the spectra of NGC6822-WR12 using the method described in Section 5.1, adjusting the luminosity until it matches the calculated absolute magnitude. This method has consistently been employed for all our comparisons of WN observations.

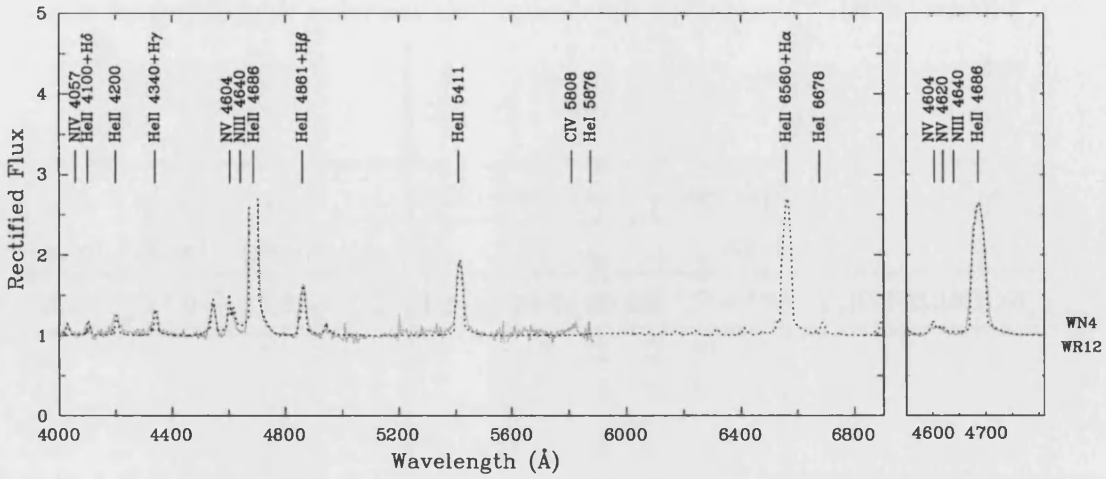

Figure 5.5: Comparison between rectified VLT-FORS2 observations of NGC6822-WR12 (solid) and our synthetic model (dotted). The panel on the right shows how well we have fitted He II λ4686.

5.5.1 NGC6822-WR12 (LB-f2-75, WN4)

This star was originally identified as the first detected WR star in NGC 6822 (Westerlund *et al.* 1983). NGC6822-WR12 was later identified in a large UBV photometric survey of NGC 6822 by Bianchi *et al.* (2001*b*) who subsequently obtained spectroscopic observations. Bianchi *et al.* (2001*b*) calculated effective temperatures (and reddenings) for the large proportion of (bright) stars in NGC 6822 by fitting the observed magnitudes to theoretical magnitudes by convolving the HST WFPC2 filter transmission curves with model O-M star atmospheres by Bessell, Castelli & Plez (1998). These synthetic models were calculated covering the temperature interval 3500–50,000K.

In a later paper by Bianchi *et al.* (2001*a*) they analyse spectroscopic observations of NGC6822-WR12, for which they publish previously determined results; they find an effective temperature of $T_{eff} \simeq$ 39,000kK and $logL \simeq 5.72$ $L_{\odot}$. They also use the WN classification scheme by Smith, Shara & Moffat (1996) and conclude that NGC6822-WR12 is a WN3(–4) with no hydrogen.

Our calculated stellar parameters are listed in Table 5.8. These theoretical models were computed with an SMC-like metal content, although as discussed in Section 3.6 the exact metallicity has very little effect on the emergent optical spectrum. Our model does

an excellent job of reproducing the observations, unfortunately our spectrum does not extend as far as Hα λ6563 and so our hydrogen abundance is very uncertain, although with such an early-type WN we do not expect much, if any, hydrogen. Also using the hydrogen criteria calculated by Smith, Shara & Moffat (1996), measuring the emission line peaks we find the pure helium lines (e.g. He II λ5411) are much stronger than the combined (H+He) lines, indicating very little, if any, hydrogen. We also infer a very low nitrogen abundance by number, N/He $\approx 9\times10^{-4}$ (i.e. $\beta_N \approx 0.3\%$), this is not surprising considering that NGC 6822 is a metal-poor galaxy. These results are also similar to those inferred from our sample of WN stars in the SMC, except that *all* the WN stars in the SMC have lots of hydrogen in their atmospheres. Given the difficulties in obtaining accurate hydrogen abundances and that our observations do not extend as far as Hα λ6563 we cannot confidently claim that NGC6822-WR12 has no hydrogen.

Our stellar parameters derived from tailored analysis to NGC6822-WR12 do not agree with those quoted by Bianchi *et al.* (2001*a*) who used crude, inappropriate (LTE) model calibrations to infer a temperature. We find a significantly (~2.5 times) hotter temperature and a much brighter luminosity.

5.6 Analysis of WN stars in M 33

Now we have consistently analysed a large sample of WN stars located in various environments we can compare our results with our single WN stars in M 33. As discussed in Chapter 2 our primary motivation behind studying the WR population in M 33 was to observe as many WC stars as possible. We did however observe a small sub-sample of WN stars if they were located close to a target WC star and there was sufficient space within the mask. During our observing run we were able to collect data for 17 WN stars, from which our equivalent width measurements of He II λ4686 identified 6 candidate single stars. This technique is discussed in greater detail in Section 4.2.5.

We attempt to derive a number of their stellar parameters and compare them with results of WN stars in other Local Group Galaxies. Below we discuss the successes and failures of our models for each star, the final parameters for each star are listed in Table 5.10. We compare our seven rectified observations with our synthetic models in Figure 5.6.

Table 5.8: Derived stellar parameters for a WN star in NGC6822. The absolute magnitude calculated for the model is also shown.

NGC6822-#	Alias	Spectral Type	T_* kK	R_* $R_\odot$	$logL$ $L_\odot$	$log\dot{M}$ $M_\odot yr^{-1}$	v_∞ km s^{-1}	H/He	N/He	β_H %	β_{He} %	β_N %	m_V (mag)	E_{B_V} (mag)	M_V (mag)	$\dot{M}v_\infty/(L/c)$	M_* $M_\odot$
WR12	LB-f2-75	WN4	100	3.77	6.11	-4.60	1100	0.001	0.001	0	100	0	18.82	0.18	-5.41	1.05	36.0

Table 5.9: Broad-band photometry calculated from archival HST WFPC2 images and/or measured from ground-based, CFHT-12K images. The absolute magnitudes were calculated using $E_{B-V} = 0.15$ and $(m - M)_0 = 24.56$ mag (see Chapter 2.2.5). The metallicities for each star were calculated using the calibrations derived in Section 4.1.2.

M33	Alias	$12+log(O/H)$	m_V		m_B		M_V
WR#			HST	CFHT	HST	CFHT	mag
42	AM3	8.68	—	18.23	—	17.97	-6.76
54	MCA5	8.74	—	21.46	—	20.92	-3.46
74	MCA8	8.69	—	21.18	21.95:	20.75	-3.72
80	MC46	8.78	—	20.57	—	19.84	-4.69
83	MC48	8.71	—	19.40	—	19.60:	-5.62
91	MJ-G9	8.70	22.18	21.64	—	22.80:	-2.84

5.6.1 AM3 (NGC595-WR1, WN8)

This WNL has extremely narrow emission lines which at the resolution of the data makes determinations such as the hydrogen abundance very difficult, as the nebular component is almost impossible to resolve from the stellar emission.

5.6.2 MCA5 (WN5-6)

This model has reproduced the majority of emission lines, except for N IV λ4057 which for this star is unusually strong.

5.6.3 MCA8 (WN6)

This WNE star looks very similar in appearance to MCA5 and not surprisingly has similar stellar parameters. Again the N IV λ4057 line is strong and was difficult to match. Our data for this star starts to suffer from fringing at around 6400Å and so Hα is partially eaten away.

Table 5.10: List of derived stellar parameters for the single WN stars in M 33 taken from our sample. The absolute magnitudes calculated from the models are also shown assuming an $E_{B-V} = 0.15$.

Star	Alias	Spectral	T_*	R_*	$logL$	$log\dot{M}$	v_∞	H/He	N/He	β_H	β_{He}	β_N	m_V	M_V	$\frac{\dot{M}v_\infty}{(L/c)}$	M_*
M33-#		Type	kK	$R_\odot$	$L_\odot$	$M_\odot yr^{-1}$	km s^{-1}			%	%	%	(mag)	(mag)		$M_\odot$
WR42	AM3	WN8	40	20.70	6.00	-4.74	990	0.50	0.005	11	87	1	18.23	-6.75	0.90	—
WR54	MCA5	WN5-6	69	3.06	5.28	-5.43	1600	0.001	0.005	0	98	2	21.46	-3.42	1.52	10.2
WR74	MCA8	WN6	70	3.62	5.45	-5.37	1520	0.001	0.006	0	98	2	21.18	-3.77	1.13	12.8
WR80	MC46	WN5	80	4.24	5.84	-4.76	2250	0.001	0.006	0	98	2	20.57	-4.63	2.80	22.7
WR83	MC48	WN/CE	80	6.16	6.15	-4.08	2900	0.001	0.003	0	98	1	19.40	-6.02	8.45	38.8
WR91	MJ-G9	WN5-6	88:	2.06	5.36	-5.42	2580	0.001	0.002	0	99	1	22.18	-2.85	2.09	11.3

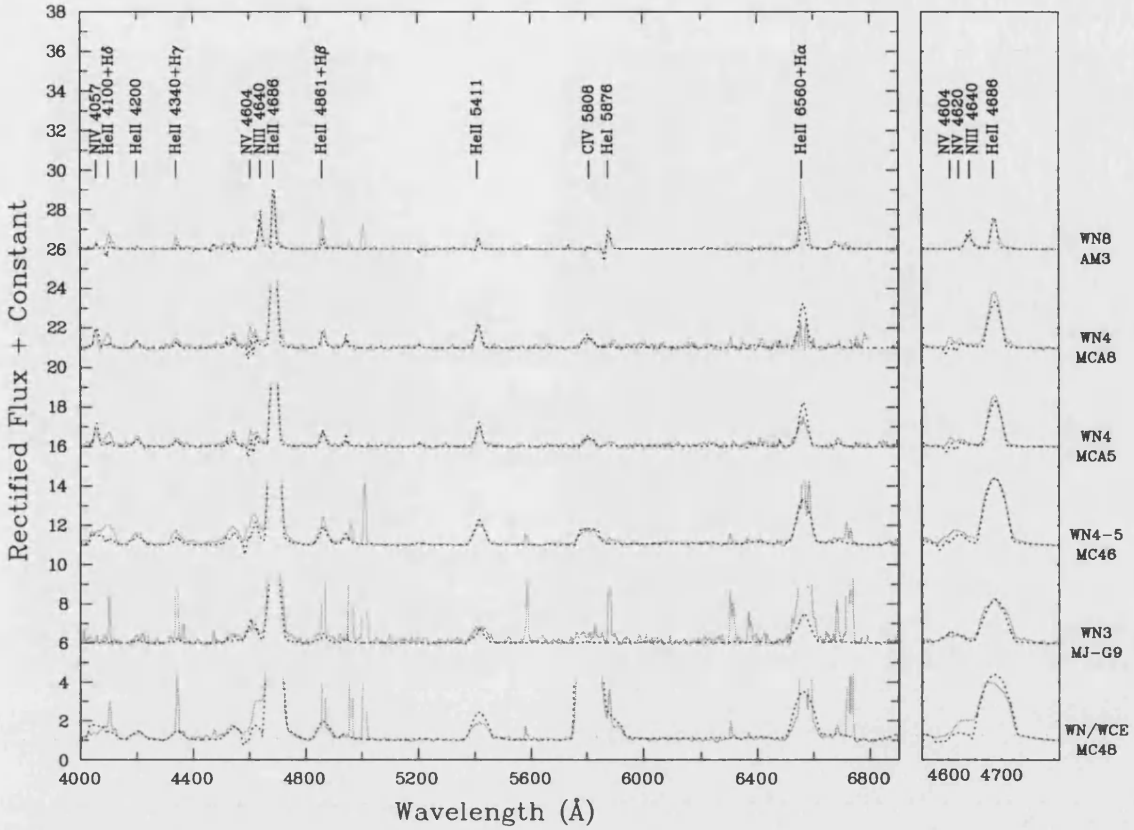

Figure 5.6: Comparison between CFHT-MOS WN stars (solid) and our synthetic model (dotted). The panel on the right shows the fits to He II λ4686.

5.6.4 MC46 (W&C11, WN5)

Both N V emission lines at $\lambda\lambda$4604-20 are strong for this WNE star. The underlying stellar component of the Balmer lines seem well reproduced which gives us confidence in the hydrogen abundance. Overall, our synthetic model does an excellent job at reproducing the stellar spectrum.

5.6.5 MC48 (W&C13, WN/WCE)

This interesting WN/WCE star has proven difficult to model. It appears to have a WNE-type spectrum with a gross over-abundance of carbon. In fact the strength of the C IV λ5808 line is comparable to the strong He II λ4686 line. Interestingly C IV λ5471 also seems to be present although very weak. This spectrum also shows strong nebular emission.

Table 5.11: List of 'typical' stellar parameters for a WNE star, considering three different scenarios. (i) WN star is single (O/WR=0); (ii) star has been diluted from an T_*=30kK, log g=4.0 OB star of equal visual magnitude (O/WR=1); (iii) again, star has been diluted by the same OB star, but with twice the visual magnitude (O/WR=2).

O/WR	T_*	R_*	$logL$	$log\dot{M}$	v_∞	H/He	N/He	β_H	β_{He}	β_N	$M_{V(WR)}$	M_*
	kK	$R_\odot$	$L_\odot$	$M_\odot yr^{-1}$	km s^{-1}			%	%	%	(mag)	$M_\odot$
0	78	3.24	5.54	-5.40	1600	1.0×10^{-3}	4.5×10^{-3}	0	98	2	-3.62	16.4
1	78	2.29	5.24	-5.64	1600	1.0×10^{-3}	4.5×10^{-3}	0	98	2	-2.87	11.3
2	78	1.73	5.00	-5.80	1600	1.0×10^{-3}	4.5×10^{-3}	0	98	2	-2.43	8.6

5.6.6 MJ-G9 (WN5-6)

The emission lines for M33-WR91 were weaker than most of the other single WN stars. This brings into question whether this WN star is single, even if it has a large EW. The spectrum for this star is heavily contaminated by nebular emission.

5.7 Effects of contamination

Accurately determining whether an extragalactic WR star is single or not is difficult, and this issue was discussed in Sections 4.2.4 and 4.2.5. To re-iterate, when spectroscopically observing individual stars at large distances within the Local Group, small slit widths amount to large spatial scales. Combine this with the fact that, visually faint, massive stars are commonly located in crowded regions containing large stellar populations, confidently resolving and obtaining uncontaminated spectra for single WR stars can be difficult. Fortunately with the advent of modern 8-metre class telescopes with multi-object spectrographs, we are able to simultaneously observe multiple stars in nearby galaxies achieving the resolution and signal-to-noise required to perform tailored analysis.

We attempt to reproduce the effect of a contaminating OB star, whether it be a binary star or a chance line-of-sight star. This is achieved through co-adding a model spectrum of an OB star, normalized to the same flux level, to a model WR spectrum to evaluate the effect that an incorrect assumption for the star's luminosity would have on our theoretically derived stellar parameters (see Table 5.11).

We test this idea and for completeness we have calculated three different cases, (i) a single WR star (i.e. O/WR = 0); (ii) a WR star with contamination from a nearby OB

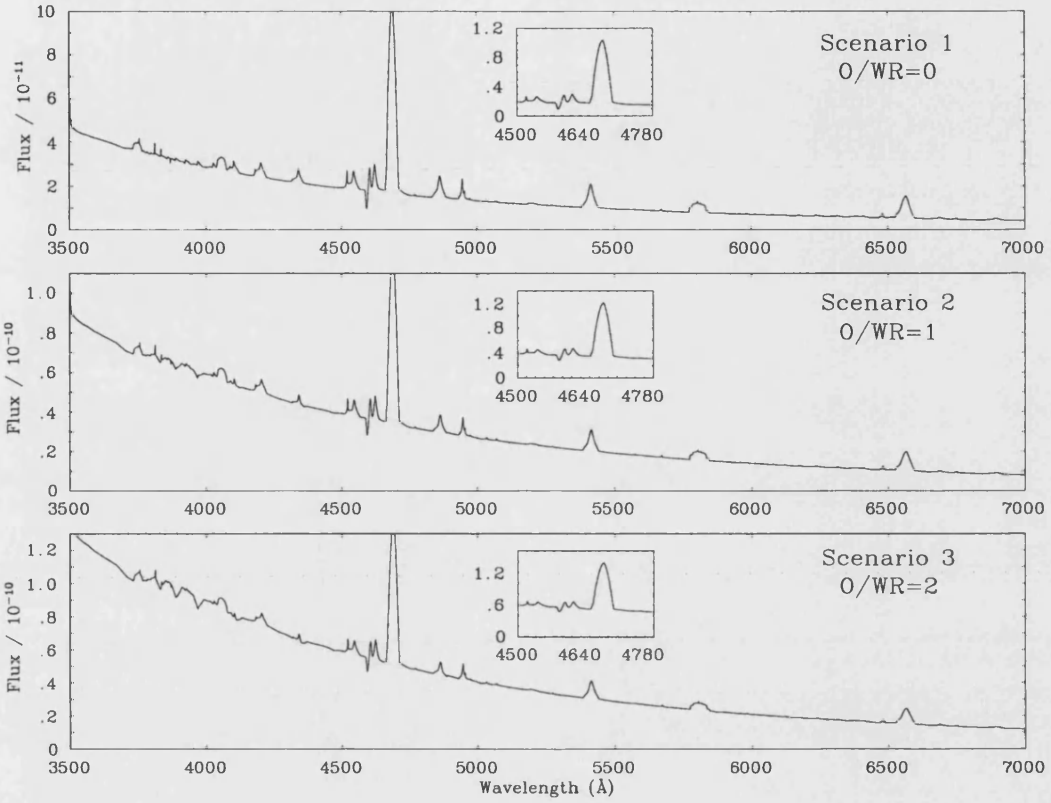

Figure 5.7: Simulated effect of multiplicity, by co-adding a scaled model spectrum of an OB star to a model WNE spectrum to examine the effects on theoretically derived stellar parameters (see Table 5.11). For completeness we have calculated three different cases, (i) a single WR star (i.e. O/WR = 0); (ii) a WR star with contamination from an a OB star of equal continuum brightness (O/WR = 1); (iii) a WR star with contamination from a nearby OB star with a continuum twice as bright (O/WR = 2). For the companion we used a generic OB star model of $T_* = 30$kK, $\log g = 4.0$ taken from the Kurucz (1979) grid within DIPSO.

star of equal continuum brightness (O/WR = 1); (iii) a WR star with contamination from a nearby OB star with a continuum twice as bright (O/WR = 2). For the contaminating source we use a generic OB star model of T_*=30kK, $\log g$=4.0 taken from the Kurucz (1979) grid within DIPSO. Figure 5.7 shows these results. This technique is valid at optical wavelengths where the underlying shape of both stars' continua can be approximated but its use at UV wavelengths is not very reliable because the continua become very different.

Measuring the resulting merged spectra, we find that the line strengths for the synthetic model were diluted such that the EW(He II) was reduced by a factor of approximately two when O/WR = 1 and a factor of three for O/WR = 2. This can be argued as evidence for using the EW(He II), versus spectral type, as an indicator of potential multiplicity, even if its only effective as an indicator in the most obvious cases where the contaminating source has approximately equal visual continuum brightness.

These contaminating effects are highlighted further in Figures 5.15 and 5.18. In the following sections we indicate the effect that an contamination from an OB star of equal continuum brightness would have on our derived stellar parameters. An incorrect assumption of the star's apparent magnitude would mean that our models grossly over-estimate the stellar luminosity of the WR star.

5.8 Comparisons

This section now collates the results discussed above and compares a number of stellar parameters, including both basic observables, as well as theoretically inferred parameters such as surface chemistries and mass-loss rates. We have consistently analysed WN stars located in a variety of Local Group galaxies spanning a metallicity range of approximately a factor of six. We begin by comparing our calculated theoretical models inferred from optical spectra with previously obtained ultraviolet IUE observations.

5.8.1 UV Spectroscopic Observations

Throughout this chapter we have used a series of optical emission lines as diagnostics to determine stellar parameters. As we have been evaluating well studied Galactic and LMC WN stars, we are fortunate enough that a number of these objects have previously been observed with space-based, ultraviolet instruments; namely the International Ultraviolet Explorer (IUE). Hence, we can use these observations to test how accurately our models,

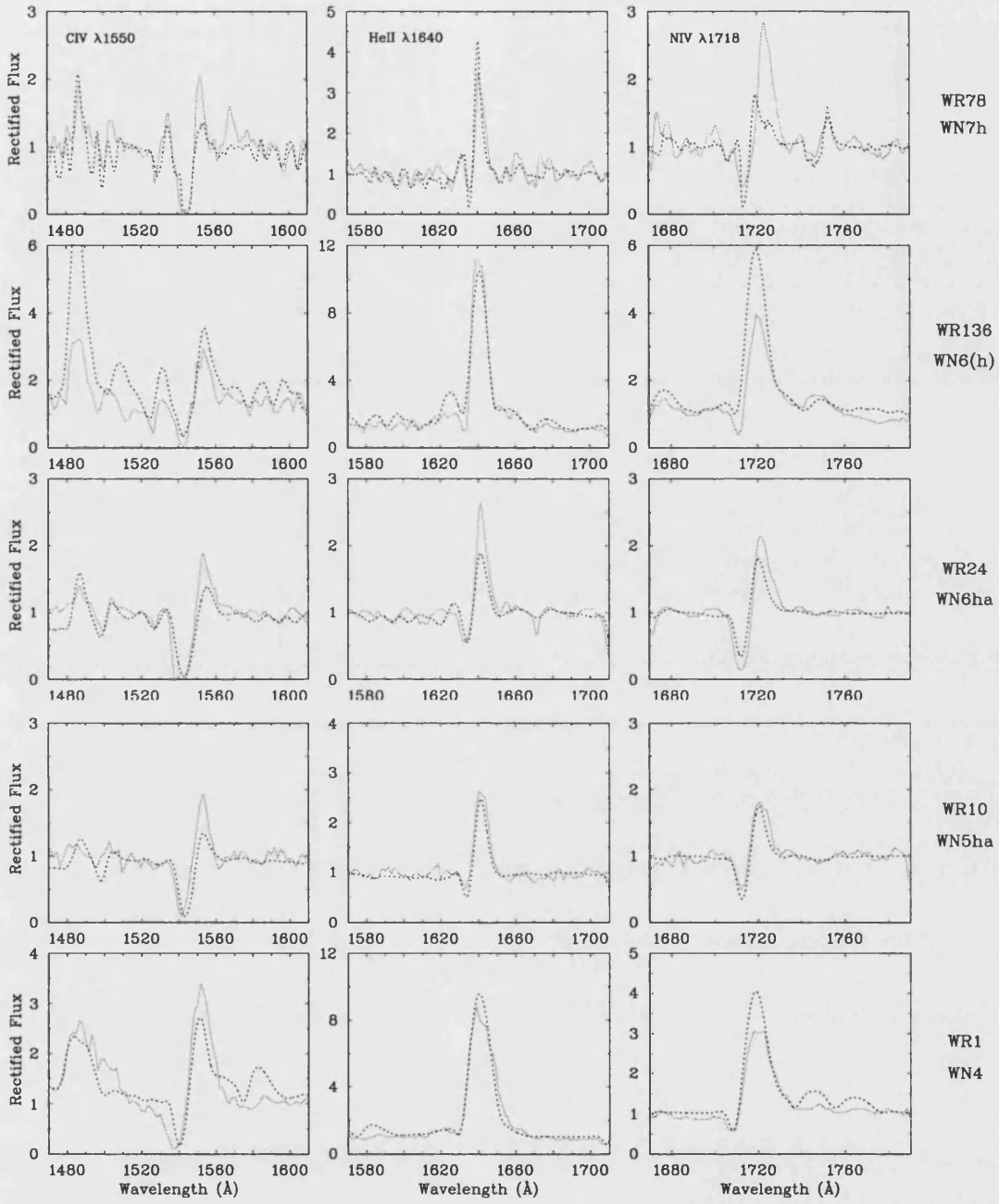

Figure 5.8: A comparison between rectified archival IUE data (solid) for the Galactic WN stars in our sample – where available – and our theoretical models (dotted). These models were derived using their optical emission line spectra. Line profiles are shown for C IV λ1550, He II λ1640 and N IV λ1718.

derived using only optical spectra, reproduce these stars at UV wavelengths.

In Figure 5.8 we compare rectified IUE observations of a number of the Galactic WN stars studied in this work with our optically inferred synthetic models. We only show the line profiles for the strongest emission lines observed at UV wavelengths; C IV λ1550, He II λ1640 and N IV λ1718. We do not discuss the emission components from Si IV $\lambda\lambda$1722,1727 even though we recognise that they appear strong in WN7–8 stars, although we do note that even though our models include Si IV they are generally under-estimated in our sample (for a review on UV emission lines in WR stars see Willis 1998).

Overall, our Galactic WN models well reproduce the UV spectra, simulating the correct line widths/strengths. There are a few objects where we find significant discrepancies. For WR78 we find that although we match C IV λ1550 and He II λ1640, N IV λ1718 is under-estimated; this is surprising considering that we confidently reproduce almost all the nitrogen emission lines in the optical regime. WR136, which proved rather difficult to reproduce at optical wavelengths, was well matched in the UV apart from C IV λ1550 and N IV λ1718 which we over-estimate – this is one Galactic WN star which could benefit further investigation. The only other major discrepancy from our sample of Galactic stars was for WR1. Our synthetic model over-predicts the line strength of N IV λ1718.

The same three emission line profiles (C IV λ1550, He II λ1640 and N IV λ1718) are shown for our complete sample of LMC WN stars in Figures 5.9 and 5.10. Again our theoretical models sufficiently reproduce the observations. There were a few cases where significant discrepancies occurred. Brey6, for which our optical comparisons looked so promising, failed to predict sufficient N IV λ1718 emission, for which we clearly detect emission in the observations, although both C IV λ1550 and He II λ1640 are matched extremely well. This inadequacy in predicting the line strength for N IV λ1718 can be explained partly due to an over-estimated temperature, as there was no N IV λ4057, only a blend of N V $\lambda\lambda$4604,4620, for us to accurately constrain the temperature.

There were also inconsistencies between observations and theoretical models for Brey45 and Brey2. Our synthetic model for Brey45 over-predicts both He II λ1640 and N IV λ1718. Recalling the difficulties with our model when reviewing the optical regime we find that He II λ4686 is also fractionally over-estimated. As with Brey6, Brey45 is an early-type WN star and is absent of N IV λ4057 emission for us to confidently estimate the temperature, hence the discrepancies seen in the UV regime could possibly be explained by a marginal error in our predicted temperature and mass-loss rate. The other early-type WN star

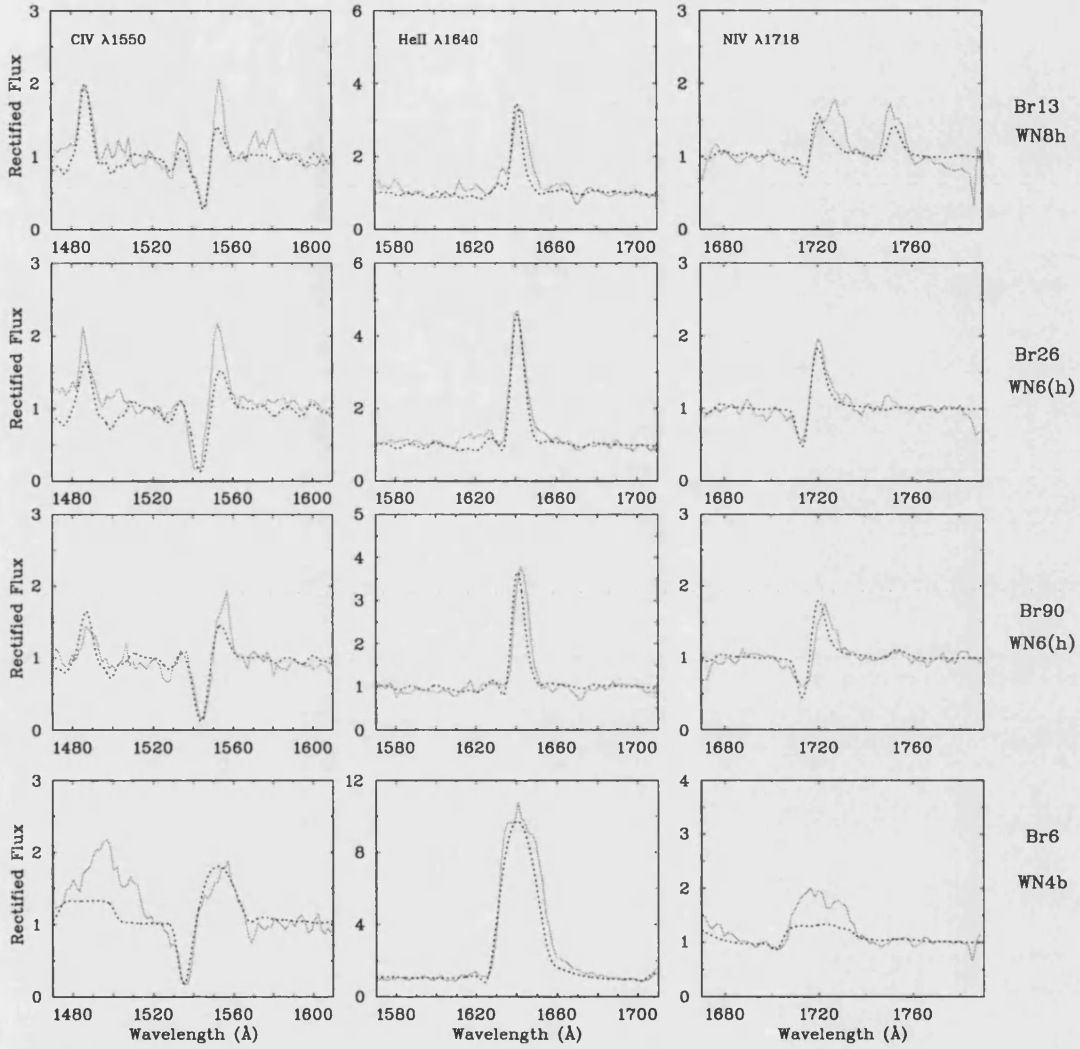

Figure 5.9: A comparison between rectified archival IUE data (solid) for the LMC WN stars in our sample and our theoretical models (dotted). These models were derived using their optical emission line spectra. Line profiles are shown for C IV λ1550, He II λ1640 and N IV λ1718.

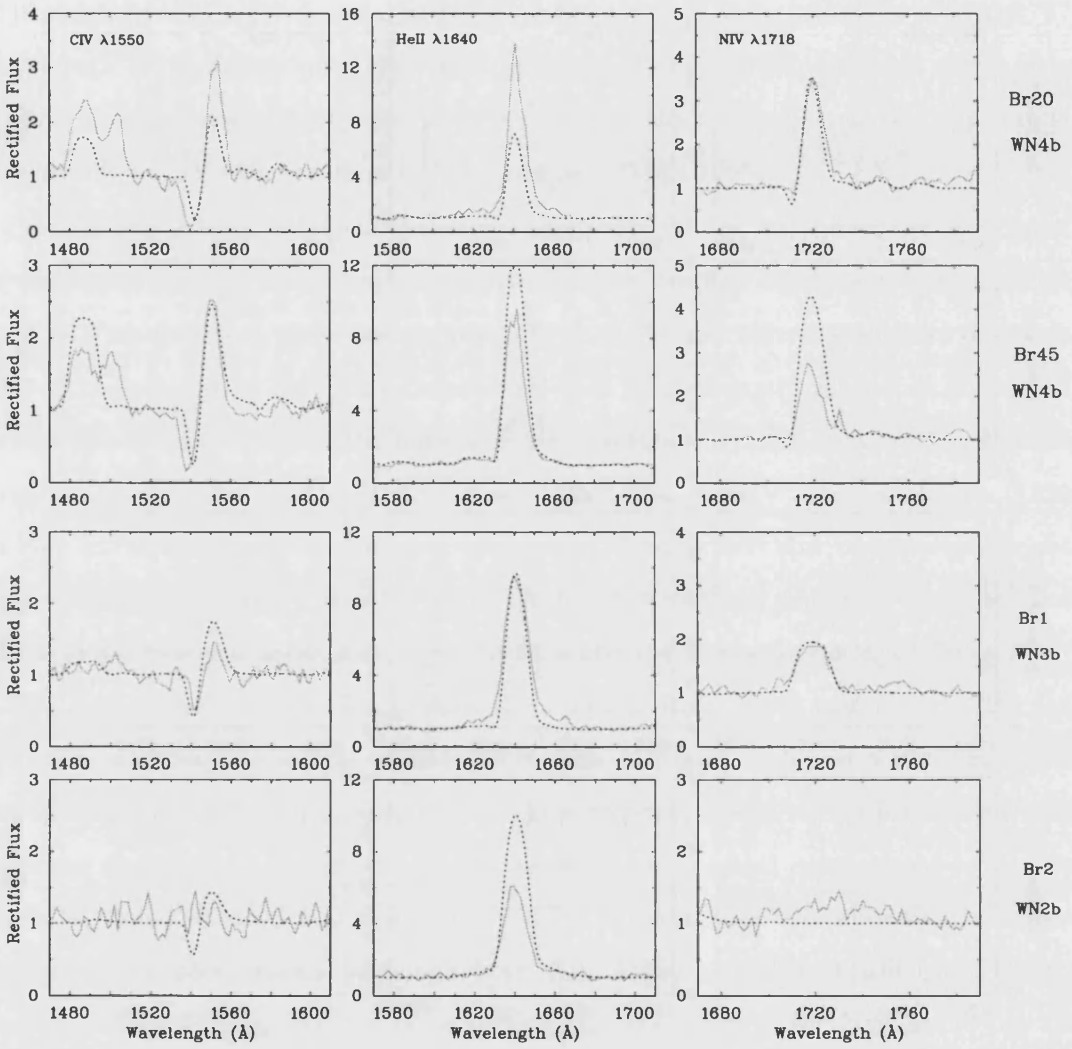

Figure 5.10: A comparison between rectified archival IUE data (solid) for the LMC WN stars in our sample and our theoretical models (dotted). These models were derived using their optical emission line spectra. Line profiles are shown for C IV λ1550, He II λ1640 and N IV λ1718.

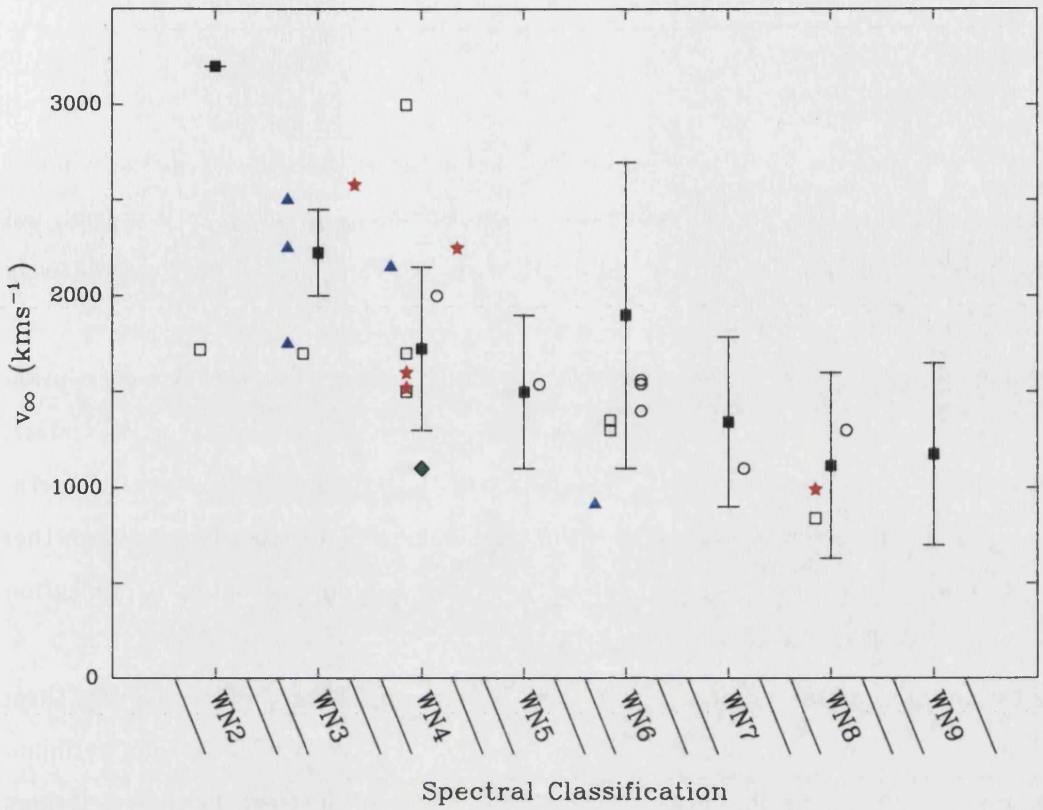

Figure 5.11: A comparison between the terminal wind velocities for Galactic WN stars (open circles), LMC (open squares), SMC (filled triangles) M 33 (filled stars) and NGC 6822 (filled diamonds) versus spectral type. We also show the averaged Galactic terminal velocities taken from van der Hucht (2001) (filled squares) along with the standard deviation from these averaged values.

which is worthy of further discussion is Brey2. For this extreme WN2b star our models predicted an extremely high temperature ($T_* \simeq 160$kK) and very little emission in any nitrogen lines. The same can also be said of its UV spectrum. We curiously do not detect any C IV λ1550, although our model estimates a weak emission, and no discernible emission is seen for N IV λ1718 either. Our results also over-estimate the He II λ1640 emission line. Unfortunately, with such a lack of emission lines we are unable to further test our optically derived parameters.

Overall, our theoretical models provide good agreement with their observed UV spectra. It is reassuring that our stellar parameters derived solely from optical emission lines are not grossly inaccurate and that we are producing realistic estimates for future extra-

galactic WR studies.

5.8.2 Wind Velocity

As described in Section 3.6.5, the terminal wind velocity is the velocity in the wind at a large distance from the star Obtaining accurate terminal wind velocities is crucial, not only because they are required in calculations of mass-loss rate, but also in quantitatively describing the stellar wind from a hot star.

Previous optical spectroscopy by Crowther & Smith (1997) showed that a correlation existed between the terminal velocity and stellar temperature for late-type WN stars, although there was no significant difference between Galactic and LMC stars. Unfortunately, we do not attempt this analysis as the temperatures determinations by Crowther & Smith (1997) were better constrained, as they used a number of adjacent ionization species which are sensitive to temperature variations.

Instead, we compare our derived terminal velocities in Figure 5.11, plotting them as a function of spectral type. Overall, we see a gradual trend of increasing terminal velocity with earlier spectral type, although there is a large scatter. Leitherer, Robert & Drissen (1992) prescribed a metallicity dependence for massive stars which scales the terminal velocity with metallicity to the power of 0.13 ($v_{\infty,Z} \propto Z^{0.13} v_{\infty,\odot}$) – this has yet to be confirmed observationally. The effect metallicity might play on the terminal velocity has important consequences for population synthesis codes (e.g. Smith, Norris & Crowther 2002) as well as computed grids of massive star wind models calculated at various metal abundances (e.g. Vink, de Koter & Lamers 2001). Considering the observed scatter for each spectral type, there does not appear to be a significantly reduced terminal velocity for WN stars in low metal poor environments. We are unable to confirm the (weak) metallicity – terminal velocity scaling proposed by Leitherer, Robert & Drissen (1992).

We compare our derived terminal velocities for the seven Galactic WN stars studied in our sample with previously published velocities. From the results given in Table 5.12 we see there is a large spread between various authors and methods. This highlights the difficulties in obtaining accurate terminal wind velocities for WR stars. Generally, our inferred velocities agree well earlier studies.

Conventional methods to measure the terminal wind velocity use saturated UV P–Cygni line profiles (e.g. Prinja, Barlow & Howarth 1990) of resonance line of ions such

Table 5.12: Comparison of published terminal velocities of Galactic WN stars with those inferred from this work.

Star	v_∞ (kms^{-1})								
	1	2	3	4	5	6	7	Av.	8
WR1	2000	2100	—	—	2135	2000	2400:	2127	2000
WR10	1500	—	—	1475	1460	1500	—	1484	1540
WR24	1200	—	—	2155	1855	1200	—	1603	1560
WR66	—	—	—	—	—	1500	—	1500	1300
WR78	1200	—	1200	1365	1385	1200	—	1270	1100
WR115	—	—	1200	—	—	1280	—	1240	1400
WR136	1600	1760	1660	1605	1705	1600	1490	1631	1540

REFERENCES – (1) Schmutz *et al.* (1989) (2) Howarth & Schmutz (1992) (3) Eenens & Williams (1994) (4) Prinja *et al.* (1990) (5) Rochowicz & Niedzielski (1995) (6) Hamann & Koesterke (1998) (7) Ignace *et al.* (2001) (8) This Work

as C IV or N V or from IR line profiles of He I at 1.083μm and 2.058μm (e.g. Eenens & Williams 1994). More recently, Ignace *et al.* (2001) used the method developed by Barlow, Roche & Aitken (1988) to determine wind velocity estimates using the forbidden IR lines of [Ca IV] at 3.207μm and [Ne III] at 15.56μm.

Unfortunately extragalactic studies of hot, massive stars do not realistically permit such detailed observations, especially at UV wavelengths. As these techniques were not available we use optical spectroscopy, making (calculated) adjustments to the theoretical models until the observational line widths were reproduced. This process is slightly easier for WN stars, compared with WC stars due to the relatively un-blended emission lines observed in their spectra. We investigate whether our determined terminal wind velocities are correlated with the observed FWHM(He II λ4686). We list the measured equivalent widths from our sample of single WN stars in Table 5.13, except for our sample of M33 WN stars which can be found in Table 4.3. Our aim is to provide an independent method for estimating the terminal velocity for WR stars using a strong optical emission line.

Table 5.13: Emission line measurements of He II λ4686 from our sample of Galactic, LMC, SMC and NGC 300 WN stars.

	He II λ4686	
Star	log (-EW)	FWHM
Galactic		
WR1	2.56	40.2
WR10	1.76	19.0
WR24	1.53	17.3
WR66	1.67	17.1
WR78	1.65	13.8
WR115	1.90	18.8
WR136	2.49	29.8
LMC		
Brey1	2.48	35.4
Brey2	2.22	36.6
Brey6	2.68	73.0:
Brey13	1.85	11.8
Brey20	2.35	28.6
Brey26	2.05	22.7
Brey45	2.51	31.6
Brey90	1.85	21.2
SMC		
WR1	1.46	20.3:
WR4	1.72	13.2
WR9	1.36	22.7:
WR10	1.41	13.9:
WR11	1.04	18.7:
NGC 6822		
WR12	2.16	26.8

We see from our results plotted in Figure 5.12 that there is a steep correlation between the terminal velocity with FWHM(He II λ4686) as we move from our sample of WNL to WNE stars. These data are fitted by a simple polynomial which can expressed as

$$v_\infty = 118078\,[-9.67 \times 10^{-3} + 4.12 \times 10^{-3}(FWHM(\mathrm{He\,II}) + 4.196)^{0.5}] \qquad (5.1)$$

The relationship described in Equation 5.1 excludes four of our SMC WNE stars (SMC-WR1, WR9, WR10 and WR11) and the Galactic WNE star, WR24, as their line profiles were very different to the rest of our sample. Typically for our sample of WN stars the He II

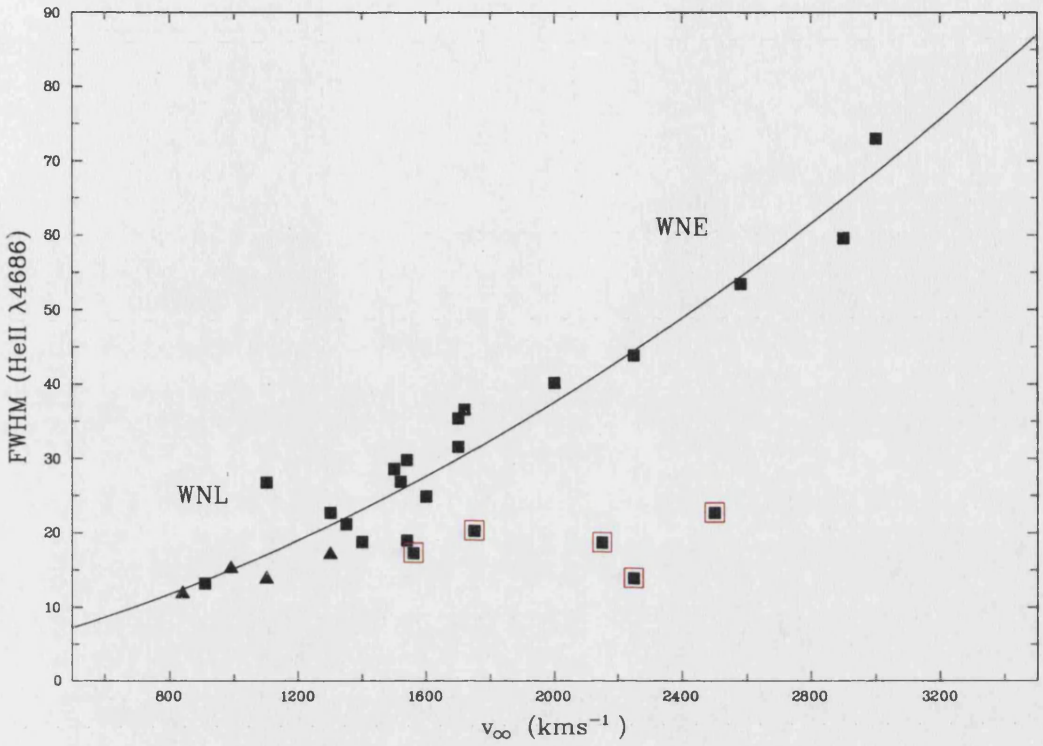

Figure 5.12: Calculated terminal velocities versus measured FWHM(He II λ4686) for WNL stars (triangles) and WNE stars (squares). A polynomial fit to the data is also shown, we exclude four SMC WNE stars and the Galactic WNE star, WR24 (boxed), as they all have skewed line profiles unlike the rest of our dataset.

λ4686 emission line could be well reproduced using a Gaussian line profile to obtain the FWHM, although for four of our SMC stars and one Galactic WN star their line profiles were skewed such that the FWHM were measured visually. We suggest that these skewed line profiles could be an artifact of low wind density. This is supported as all five stars in question have low mass-loss rates, high hydrogen contents and the lowest equivalent widths of all our sample. For these reasons coupled with the fact that they do not appear to follow the observed correlation for the remainder for our sample we do not include their results in our fit.

It is hoped that Equation 5.1 will provide a good first order approximation for future detailed studies of extragalactic WN stars, for which UV and/or IR datasets are not available. Using Equation 5.1, a simple measurement of a strong, optical emission line could translate into an initial estimate for the terminal wind velocity when computing stellar atmosphere models for WN stars. Needless to say, subsequent (minor) adjustments

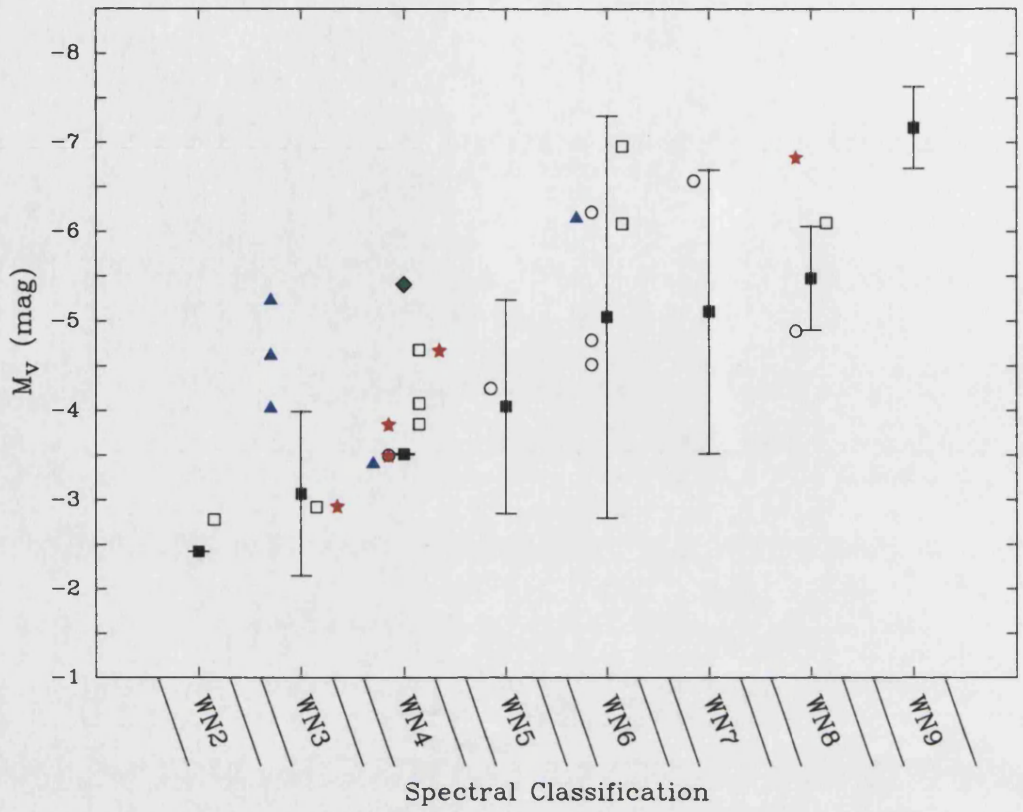

Figure 5.13: A comparison between the absolute visual magnitudes for Galactic WN stars (opened circles), LMC (open squares), SMC (filled triangles), M 33 (filled stars) and WN stars in NGC 6822 (filled diamond), versus spectral type. The averaged Galactic values from van der Hucht (2001) are also shown (filled squares), along with the upper and lower limits.

would possibly be required before accurately reproducing the line widths of the optical spectrum. Future similar studies would increase the number of measurements to constrain this relationship; there maybe even a different correlation for strong- and weak-lined WN stars.

5.8.3 Absolute Magnitude

In Figure 5.13 we present the absolute visual magnitudes for all single WN stars in our sample as a function of spectral type. Even though we have previously tabulated broad-band, V apparent and absolute magnitudes for a large number of our observed sample, for comparison, we plot narrow-band, v (Smith 1968), absolute magnitudes derived from

our theoretical models. To gauge how our values compare with previously published absolute magnitudes we include those listed in the latest catalogue of Galactic WR stars (van der Hucht 2001). Our results show that there does appear to be a decrease in absolute magnitude from WNL to WNE stars, although with a large scatter. This result was earlier reported by Hamann & Koesterke (1998) who suggested a linear correlation between Galactic WN stars of subtypes WN2–6, with a somewhat constant magnitude $M_v \simeq$ -6.8 mag later than WN7. We would also tentatively suggest that stars located in metal-poor environments (i.e. SMC and NGC 6822) appear intrinsically brighter than those WN stars located in more metal-rich environments.

There are many potential pitfalls in calculating absolute visual magnitudes. Even though modern observations are able to calibrate apparent visual magnitudes to within $\pm$0.1 mag, their are still possible errors in achieving accurate distance determinations and realistic reddenings towards an individual source. Many of these factors are approximated or assumed in the van der Hucht (2001) WR catalogue, which would explain the huge spread of absolute magnitudes and as such caution should be taken with individual results.

5.8.4 Wind Efficiency

In this section, we investigate how wind efficiency number, η, derived from our theoretical models varies with a variety of parameters. The wind efficiency or 'wind performance number' describes how efficiently the momentum from the radiation is transferred to the wind. Values equal to one indicate the 'single scattering limit', in which all photons are only scattered *once* in the wind. Values in excess of one indicate multiple scatterings, (i.e. very efficient momentum transfer).

We compare the wind efficiency for our sample of WN stars with spectral type, temperature, terminal velocity and atmospheric content of helium, all of which are shown in Figure 5.14. We find that apart from the atmospheric content of helium, which appears to increase as the star evolves (i.e. abundance of helium increases with decreasing hydrogen), none of the other parameters show any correlation. There is no clear difference between the separate datasets, except for the four WN3–4 stars in the SMC which again differ from the rest of our sample. Their values of η are considerably lower than the rest of the dataset, with typical $\eta \simeq 0.27$, well below the single scattering limit. These values are comparable with Galactic O supergiants (e.g. HD151804 (O8Iaf) has an observed wind efficiency $\eta = 1.24$; Crowther & Bohannan 1997). Even for the the rest of the data, the

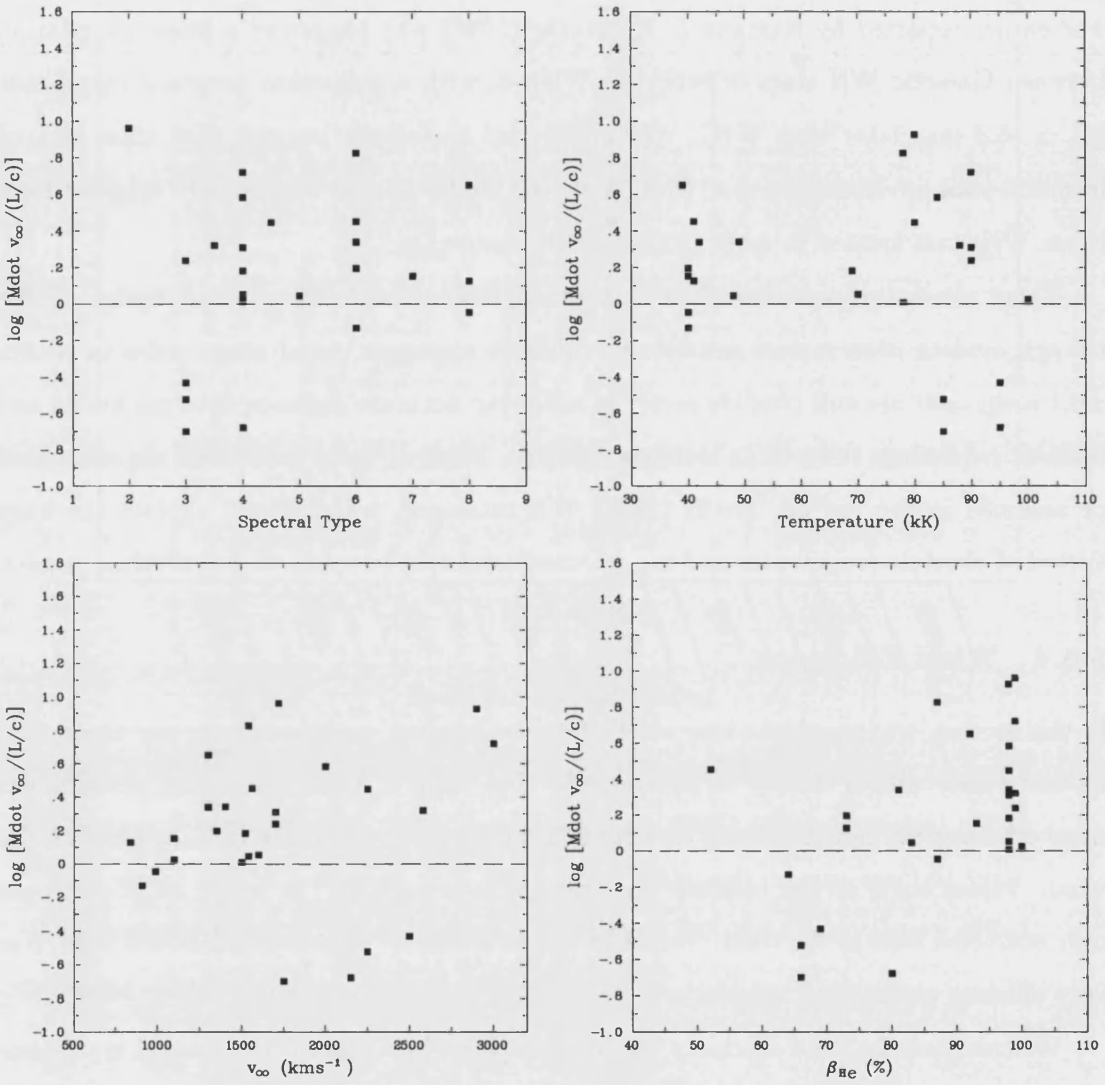

Figure 5.14: Wind efficiency shown as a function of spectral type (upper left panel), temperature (upper right panel), terminal velocity (lower left panel) and abundance of helium (lower right panel). The dashed line shows the single-scattering limit.

derived wind efficiencies can be explained by radiatively driven winds, with a moderate degree of multiple scattering. Our determined wind efficiencies are generally lower than previously published values. For example, all seven of our Galactic WN stars were studied by Hamann & Koesterke (1998), with their wind efficiencies typically a factor of a few larger. This can be explained by clumping and hence our consistently lower wind densities.

5.8.5 Mass-Loss Rates

Throughout this work we have mentioned mass-loss rates and stressed their importance in solving many issues surrounding massive stars. WR stars possess the strongest winds of all hot, luminous stars, with typical observed mass-loss rates $\sim 10^{-5} M_{\odot} yr^{-1}$. If we are able to understand how mass-loss and their surrounding environment influences their stellar parameters, then we will gain a much better insight into the driving force behind these strong outflows. The origin of the additional momentum transferred to the wind, required to explain these stellar winds through radiation driving, is likely to be an opacity problem (Abbott & Lucy 1985; Gayley & Owocki 1995; Springmann 1994) whose theoretical origin is yet to be explained quantitatively. Owocki & Gayley (1999) suggested that current theoretical difficulties in accounting for such strong radiative forces deep in the wind could be explained by a "two-stage" driving process. WR winds could be initiated through strong stellar pulsations, allowing radiative forces to continue to accelerate the stellar winds to large terminal velocities.

We plot the derived mass-loss rates and luminosities in Figure 5.15. Our sample of Galactic, LMC and M 33 WN stars are clustered such that luminosity increases with mass-loss rates. The majority (i.e. 4 out of 5) of the single SMC WNE stars are more luminous and have significantly lower mass-loss rates. In fact the *mean* luminosity of the WN stars in the SMC, $\log(L/L_{\odot}) \simeq 6.1$, is a factor of 2.5 times higher than the other WN stars, $\log(L/L_{\odot}) \simeq 5.7$, studied in our sample. Considering the low metallicity environment within the SMC we would expect that these single stars were formed from extremely high mass stars at the upper end of the IMF. This is consistent with stellar evolutionary theory which in the non-rotating case predicts that the minimum initial mass required to form a WR star in the SMC would be $60 M_{\odot}$ (Meynet *et al.* 1994). This initial mass might reduce a little with the inclusion of rotation but it still very much at the upper end of the initial stellar populations.

Our results also show that the SMC WN stars have substantially weaker winds, by $\sim$1.0

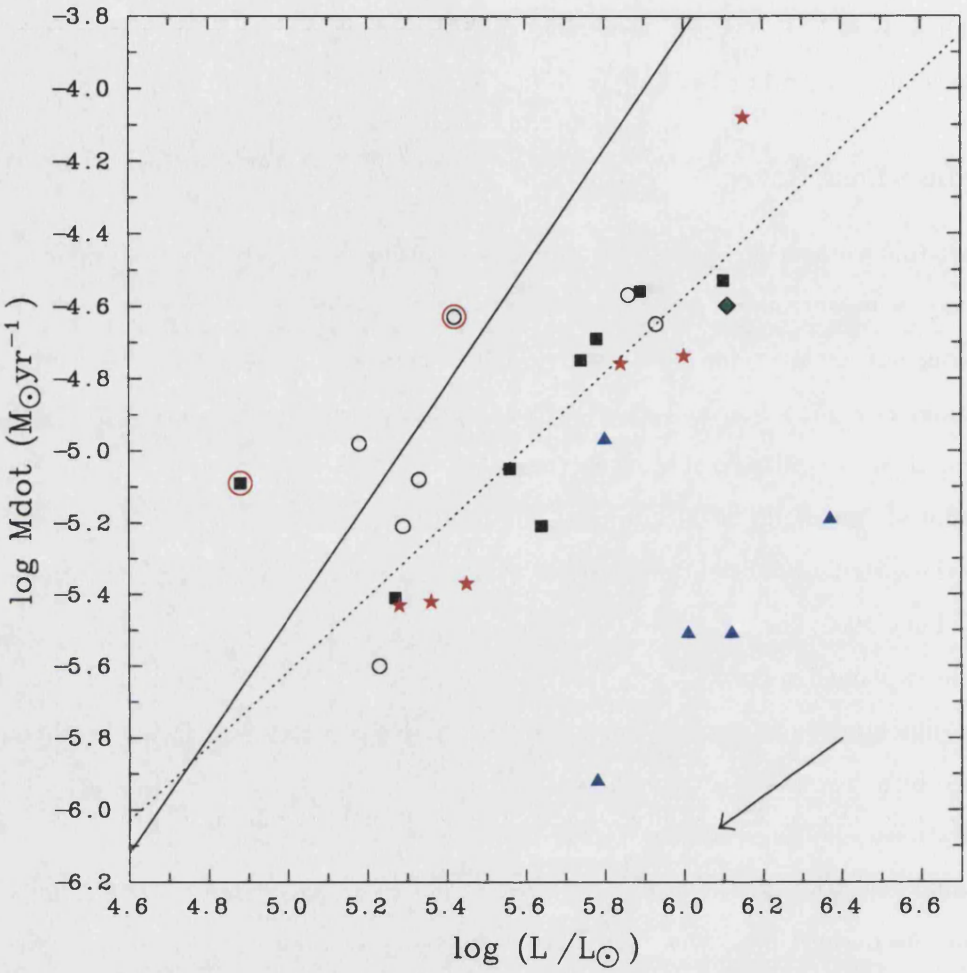

Figure 5.15: Comparison between the mass-loss rates and the luminosities for our sample of single WN stars in M 33 (filled stars), SMC (filled triangles), LMC (filled squares) Galactic (open circles) and NGC 6822 (filled diamond). The solid line correspond to the calibrations of Nugis & Lamers (2000) derived from Galactic WN stars (assuming Z = 0.02), while the dotted line represents a least-squares fit to our data (excluding the SMC WN stars, as well as Brey2 and WR136). The linear vector shows the effect a contaminating OB star of equal visual continuum luminosity would have on our inferred stellar parameters (see Sect. 5.7).

dex, when compared with Galactic/LMC WN stars of similar luminosities. It is unlikely that our derived luminosities are significantly erroneous, given the well known distance and reddening to the SMC. It is clear, even from visual inspection of the optical spectra, that the SMC stars have weaker winds, unless we have incorrectly accounted for some other factor – such as a significant difference in clumping. We speculate as to whether these weaker stellar winds are as the result of a lower natal metallicity. Unfortunately are unable to significantly quantify by what factor the mass-loss rates are affected by metallicity.

We perform a least-squares fit to the data, excluding the SMC sample as well as Brey2 in the LMC and WR136 in the Milky Way. Brey2 is an extreme, early-type WN star with an abnormally high temperature and ionization, and our theoretical model for WR136 failed to successfully reproduce the majority of important diagnostic lines – for these reasons we exclude them from our linear fit. For the remaining sample of stars our data reveals a mass-loss – luminosity relationship of

$$log\dot{M} = -10.80 + 1.04log(L/L_{\odot}) \tag{5.2}$$

This relationship predicts a somewhat shallower gradient than previously suggested by Nugis & Lamers (2000) and steeper than predicted by Hamann & Koesterke (2000) for LMC and Galatic WN stars respectively (see Equations. 5.3 and 5.4)..Although the mass-loss rates of Hamann & Koesterke (2000) were calculated using non-LTE models assuming a clumped atmosphere they neglected other important factors, namely line-blanketing. Hamann & Koesterke (2000) concluded that their stellar parameters derived for their sample of LMC WN stars were not systematically different from the Galactic WN stars studied using the same techniques even though there was a large scatter. They derived an unusually low dependance given by

$$log\dot{M} = -5.69 + 0.20log(L/L_{\odot}) \tag{5.3}$$

The dependance on luminosity increased somewhat when they solely examined the strong-lined WNE stars. However, not only do the mass-loss rates from Nugis & Lamers (2000) include clumping in their calculations, they also included a term to describe the mass-loss dependence on the atmospheric abundance of helium, Y. This discrepancy is discussed later. Their relationship is described by

$$log\dot{M} = -13.60 + 1.63(\pm 0.21)log(L/L_{\odot}) + 2.22(\pm 0.63)logY \tag{5.4}$$

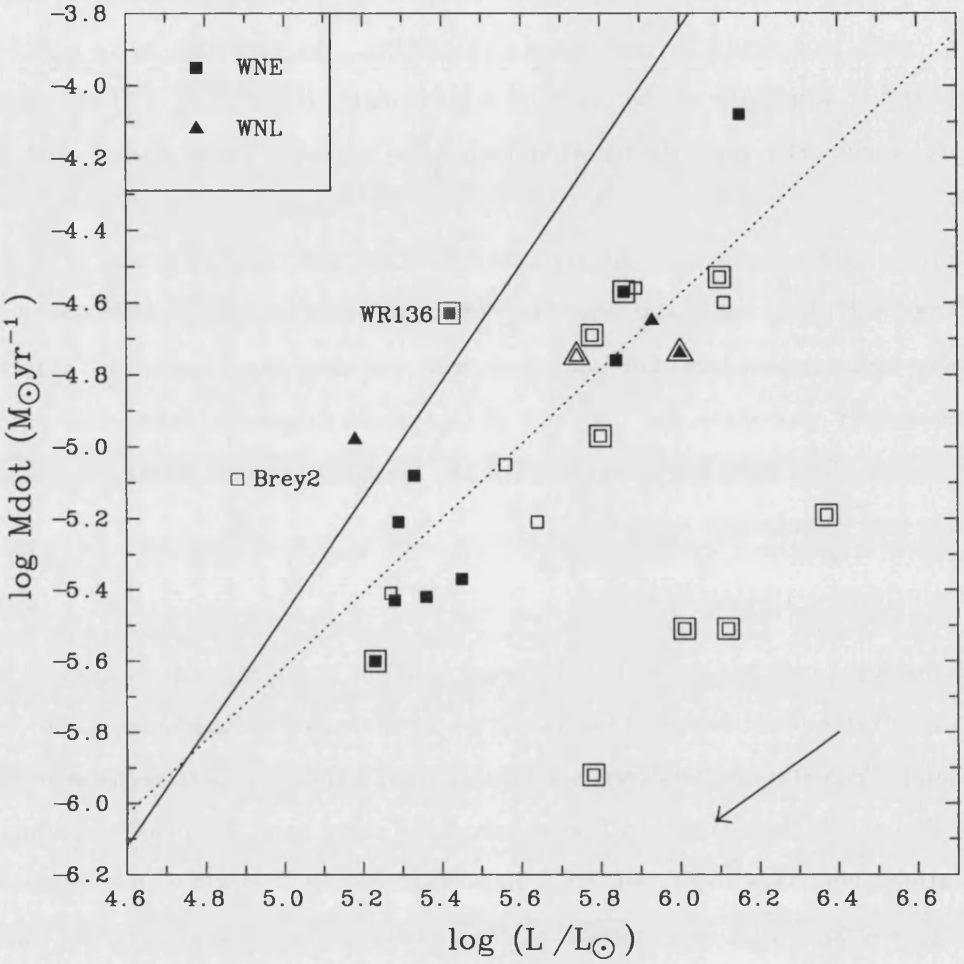

Figure 5.16: Comparison between the mass-loss rates and the luminosities for our sample of WNE stars (squares) and WNL stars (triangles). We indicate stars located in regions with metallicities sub- or super-solar, with open and filled symbols respectively, where $12+\log(O/H)_\odot = 8.66$ (Asplund 2003) and those that have atmospheric abundances of hydrogen, $\beta_H \geq 10\%$ (boxed). The solid and dotted lines as well as the vector are the same as in the previous figure. Brey2 and WR136 are highlighted as they are excluded from the linear fit.

Figure 5.16 plots the same data as in the previous figure but simply separates the data into spectral types (i.e. WNE and WNL stars) as well as indicating the suspected metallicity in which the star is located. We also highlight stars that we have found to have atmospheric abundances of hydrogen, $\beta_H \geq 10\%$, to help compare the H-rich SMC WN stars with the remainding sample of WN stars. The only conclusions that can be drawn from Figure 5.16 is that generally, the stars in regions where, $Z < Z_{\odot}$, appear to be more luminous than stars in more metal-rich regions. Figure 5.14 indicates that hydrogen rich WN stars have weaker winds which could explain the difference between the (H-rich) SMC stars and the (H-poor) Galactic, LMC and M 33 WN stars. Very little can be determined regarding differences in spectral type owing to the very few late-type WN stars analysed in this work.

In Figure 5.17 we compare our derived mass-loss rates for our Galactic WN stars with the clumping-corrected mass-loss rates from published by Nugis, Crowther & Willis (1998). These mass-loss rates were calculated from IR-radio emission, accounting for ionization structure and clumping in the wind, using an empirical formula to obtain final mass-loss rates. Nugis & Lamers (2000) later used these results to determine the dependence of mass-loss rates with luminosity and chemical composition, deriving relationships for both WN (see Eqn. 5.4) and WC stars as well as a generic WR dependence.

We find that the mass-loss rates determined by Nugis, Crowther & Willis (1998) are consistently higher, by a factor of ~0.3 dex, than derived from this work, apart from WR24 which is in excellent agreement. Comparing the determined luminosities between datasets we find that they do not deviate significantly, although the luminosities from Nugis, Crowther & Willis (1998) tend to be fractionally higher.

5.8.6 Atmospheric Abundances

As discussed at the beginning of this chapter we use the blended H I-Balmer/He II-Pickering decrement to derive hydrogen abundances. In Figure 5.18 we plot our inferred atmospheric hydrogen abundances against their derived luminosities. The five WNE stars in the SMC all have moderate hydrogen mass fractions in the range between 20% – 36% and exhibit large luminosities ($log(L/L_{\odot}) \geq 5.8$). In contrast, all the WN stars in M 33, except for AM3, show hydrogen free atmospheres. In fact 14 WN(E) stars (or 52%) in our sample are hydrogen free.

We compare these results with the latest evolutionary predictions, including rotation by

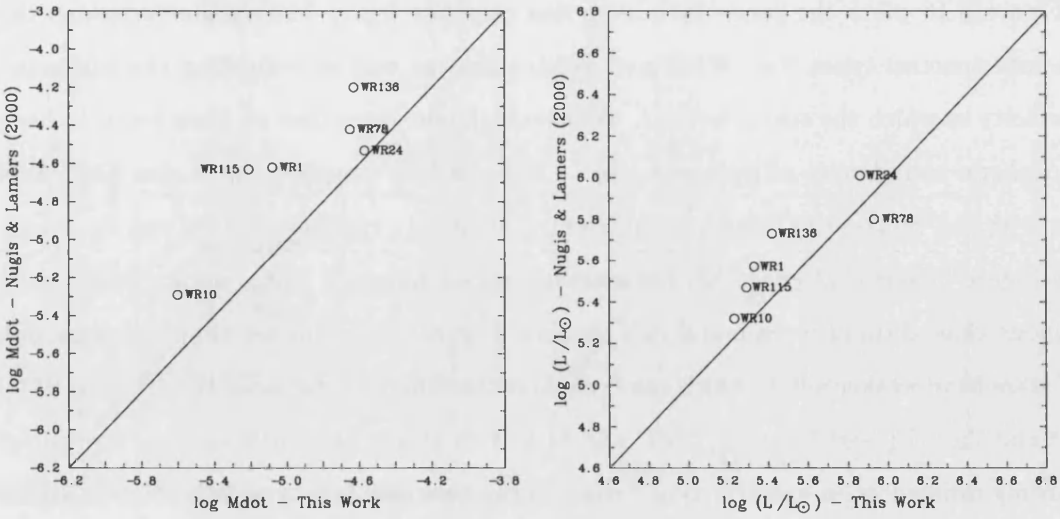

Figure 5.17: Comparison between the mass-loss rates (left panel) and the luminosities (right panel) derived from our sample of single Galactic WN stars and those determined by Nugis, Crowther & Willis (1998).

Meynet & Maeder (2003), for WR stars at solar metallicity. The rotational models shown were calculated with an initial velocity, $v_{\rm init} = 300 {\rm kms}^{-1}$ and span a range of initial masses from $25 M_{\odot}$– $120 M_{\odot}$ all of which are predicted to enter the WC phase at some point during their life. Considering that the evolutionary tracks evolve downwards in this diagram, we see an initial increase in luminosity which is due to main sequence evolution. After this, for stars with masses greater or equal to $25 M_{\odot}$, the luminosity changes – indicating that this figure is sensitive to mass-loss and mixing (Meynet & Maeder 2003). We find that our results are in good agreement with the predicted evolutionary tracks and would suggest that it is likely that the SMC WN stars are descendants of stars with large initial masses ($\sim 80 M_{\odot}$).

Figure 5.19 reproduces the dataset shown in Figure 5.18 but separates the data into early- and late-type WN stars. We also indicate those stars that are deemed to lie within regions with either sub- or super-solar metallicities (for those WN stars in M 33 we use the metallicity gradient described in Section 4.1.2 to determine their local metal content). Generally, our results indicate that WN stars in low metallicity environments display significant quantities of hydrogen in their atmospheres compared with stars in more metal-rich galaxies. Our data also suggest that these stars with high/intermediate atmospheric abundances of hydrogen also have large luminosities – as predicted by the (rotating)

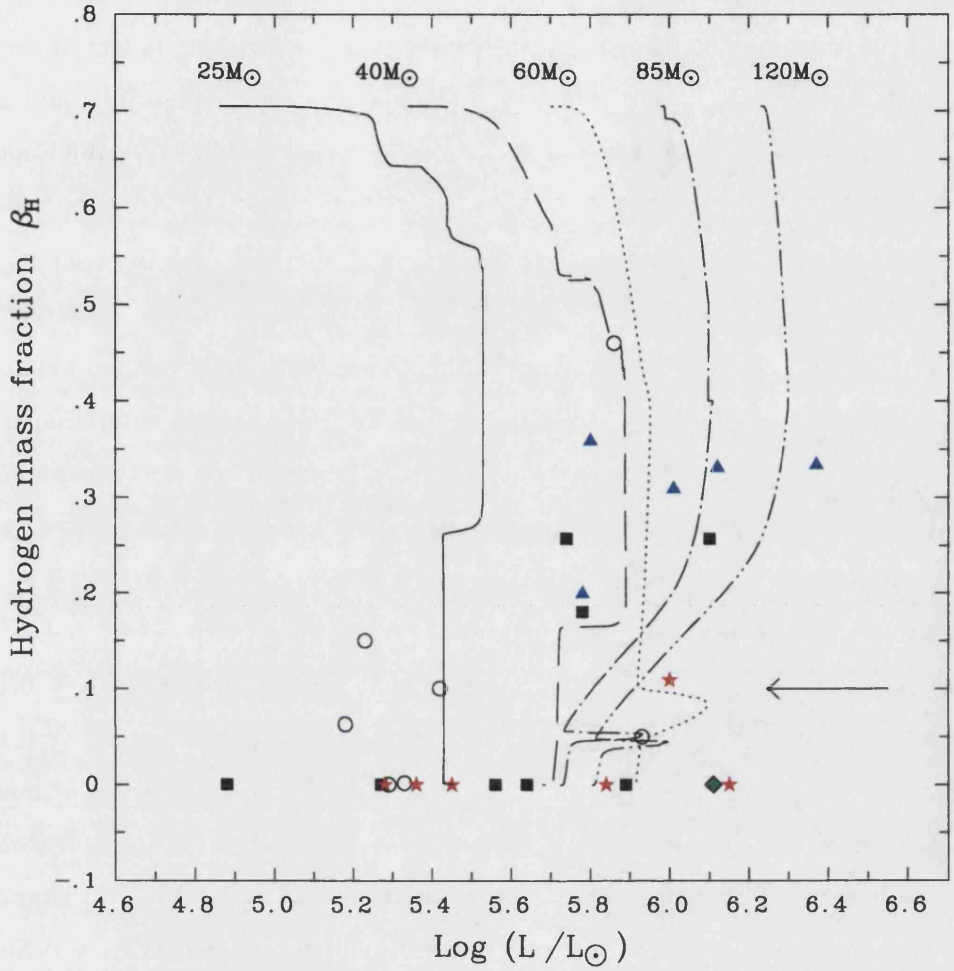

Figure 5.18: Atmospheric hydrogen abundances for our sample of single WN stars in M 33 (filled stars), SMC (filled triangles), LMC (filled squares), Galactic (open circles) NGC 6822 (filled diamond) versus luminosities. Evolutionary predictions shown are for stars with an initial rotational velocity, $v_{ini} = 300 \mathrm{kms}^{-1}$ (Meynet & Maeder 2003) all calculated at solar metallicity. These evolutionary models are shown at five initial stellar masses, $25M_\odot$ (solid), $40M_\odot$ (dashed), $60M_\odot$ (dotted), $85M_\odot$ (dot-dashed) and $120M_\odot$ (dot-dot-dashed). The linear vector shows the effect of a contaminating OB star of equal visual continuum brightness would have on our calculated parameters (see Sect. 5.7).

evolutionary models. The only notable difference between our sample of early- and late-type WN stars is that all the WNL stars studied appear to contain at least a moderate amount of hydrogen in their atmosphere which is supported through evolutionary ideas that late-type WN stars are the precursors of their early-type descendants. In fact Meynet & Maeder (2003) suggest that a plot of hydrogen abundance versus luminosity could be used to study various evolutionary stages of WR stars (i.e "slash stars", LBV, WNE and WNL).

Finally, we (tentatively) suggest an alternative means of discriminating between stars with significant quantities of hydrogen, classified 'h', and those with only a marginal abundance of hydrogen, labelled '(h)'. Rather than replacing the original method devised by Smith, Shara & Moffat (1996), it could be used as an extra tool to determine the amounts of hydrogen in a star's atmosphere. With the increased use and acceptance of modern atmosphere models in which the hydrogen abundance can be computed, we propose that the derived theoretically predicted mass fraction of hydrogen be used as a discriminator to distinguish between the two groups.

For example, we could assign a dividing line such that stars with $0.05 \leq \beta_H \leq 0.15$ are assigned the '(h)' classification, and stars with atmospheric abundances $\beta_H \geq 0.15$ classified with the extension, 'h'. If we chose this criteria to classify WN stars with/without significant quantities of hydrogen then we would need to revise the spectral types for three WN stars within our sample. WR78 would be revised from WN7h to WN7(h); Brey26 would be altered from WN6(h) to WN6h and Brey90 would be reclassified as a WN6h when previously classified as a WN6(h). We would also revise AM3 in M33 to include a '(h)' suffix. Of course this point may be minor but perhaps with future work we could find a relationship between a series of observables and the mass fraction of hydrogen in a star's atmosphere and this could prove a useful tool in helping clarify or refining evolutionary ideas of massive stars.

5.8.7 Current Stellar Masses

A mass – luminosity relationship for WR stars has been previously well documented (e.g. Maeder 1983; Maeder & Meynet 1987; Langer 1989), although it has been noted that late-type WN stars fail to obey these relations and are excluded from mathematical calibrations. These models assume a simple stellar structure of what is essentially a helium star. Heger & Langer (1996) discuss the effect of "wind darkening", in which

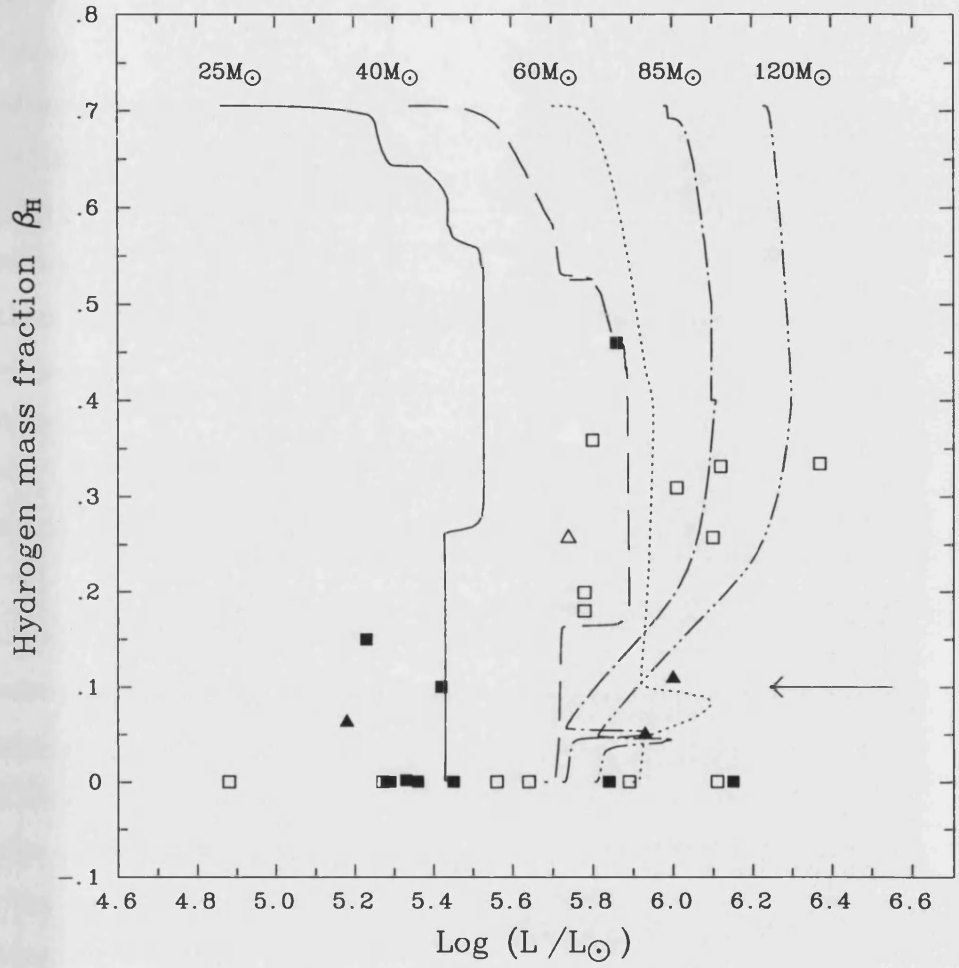

Figure 5.19: Comparison between the atmospheric hydrogen abundances (by mass fraction) and the luminosities for our sample of single WNE stars (squares) and WNL stars (triangles). There are a number of WN stars showing no hydrogen which are clustered at the zero level. We indicate stars located in regions with metallicities sub- or super-solar with open and filled symbols respectively, where $12+\log(O/H)_\odot = 8.66$ (Asplund 2003). The same rotating evolutionary tracks are shown as in the previous figure.

the luminosities generated deep within in a WR star, L_{nuc}, are higher than the observed luminosities, L_*, ultimately resulting in a slightly higher predicted mass.

Using the mass – luminosity relationship determined by Schaerer & Maeder (1992) for hydrogen-free WN stars (i.e. WNE) as well as WC and WO stars, we calculate that our sample of Galactic stars (without hydrogen) have current stellar masses which lie in the range 10–11$M_\odot$. This range is somewhat larger for the LMC stars studied revealing a range 6–25$M_\odot$. Unfortunately the Schaerer & Maeder (1992) calibration is not valid for any of our WN stars in the SMC due to the presence of hydrogen, although if this relationship is assumed then owing to the high luminosities derived the predicted current stellar masses are much larger, with an upper limit of ~60$M_\odot$. We estimate that for the WNE star, NGC6822-WR12 it has a large stellar mass of 36$M_\odot$. Finally, for our sample of WN stars in M 33 we estimate a range of current masses similar to those predicted for the LMC WN stars, with a range 10–39$M_\odot$.

5.9 Conclusions

We have used medium/high resolution spectroscopic observations previously obtained for a number of single Galactic, LMC, SMC and NGC 6822 WN stars, from a variety of sources. We have produced a series of iterative models which reproduce the optical spectra for our targets stars; with the prerequisite of matching a number of diagnostic lines, which combined with accurate photometry and reddening determinations provide us with stellar parameters. This unique set of consistently derived stellar parameters has then enabled us to extend our techniques to determine parameters for our recently obtained observations of WN stars in M 33, providing us with a unique insight into the WN population across the Local Group of galaxies.

To check the validity of our approach, solely using optical spectra, we compare our theoretical spectra with archival IUE observations of Galactic and LMC WN stars. Overall, the comparison is reassuring, with the majority of our models reproducing both the line strengths and widths of the predominant emission lines in the UV (i.e. C IV λ1550, He II λ1640 and N IV λ1718). This check provides us with confidence that our results are not unrealistic. Of course they could be refined if UV – IR data were available but unfortunately this is not often the case for extragalactic studies of WR stars.

Comparing our determined terminal wind velocities from our sample we found a steady

increase in velocity from late to early spectral type, although we still observed a scatter. There appears to be no significant difference in terminal velocities between our datasets and hence we are unable to observationally confirm whether there is a metallicity dependence on terminal velocity as has been theoretically suggested (e.g. Leitherer, Robert & Drissen 1992). The observed scatter can be partly explained due to the difficulty in obtaining precise terminal velocities from optical spectra. This is highlighted in Table 5.12 for which we compare previously published terminal velocities for the single Galactic WN stars studied in this work with the terminal velocities inferred from our synthetic models. We see a range of quoted velocities, a number of which were measured using UV observations, some of which are consistent with our determined values. Using these terminal velocities we have mathematically described a simple equation from an initial estimate for a terminal wind velocity using the measured FWHM(He II λ4686). This may serve as a useful tool in future extragalactic studies of WR stars where a similar analysis would be desirable.

We also found that there is a weak relationship between our derived absolute visual magnitudes and spectral types. Furthermore, it appears that the WN stars in low metallicity environments are somewhat brighter than their counterparts that lie in more metal-rich surroundings. This difference can be explained in terms of luminosity, where we find that the SMC and NGC6822 WN stars are generally towards the upper end of our observed limit.

Our study has also allowed determinations of the stellar wind efficiency, which has been the subject of debate over recent years as to whether or not these high wind efficiencies can be explained through line driving. We find that accounting for clumping and line-blanketing as well as considering the contribution from multiple scattering we find that our results indicate lower wind efficiencies than had been previously suggested. Consequently, we are able to explain the principal driving force in the wind via the widely accepted theory of radiation driven wind models. The majority of our results estimate the typical wind efficiency to be $\sim$3, while our sample of SMC WN stars are predicted to have much lower wind efficiencies which are less than the single-scattering limit.

One of the main aims of this work was to identify any stellar parameters which indicate a sensitivity to metallicity variations, and mostly importantly mass-loss rates. Our results indicate that there is very little difference in mass-loss between the Galactic WN stars and their counterparts in the LMC. A noticeable difference is not seen until our sample

of SMC WN stars are also considered. It is clear, even through visual inspection of their optical spectra that their stellar winds are weaker and our results clearly support this idea. Not only are their winds weaker but they are significantly brighter, indicating that they descended from stars with extremely large initial masses. This idea is suggested by stellar evolution theory, in which the initial mass required to form a WR star increases with decreasing metallicity, which is directly connected to the mass-loss rates necessary to denote a star WR status. We tentatively propose a mass-loss – metallicity dependence for WN stars which, if confirmed, would be slightly stronger than predicted for O stars ($\dot{M} \propto Z^{0.5-0.8}$). We require further spectroscopic observations of WN stars again at extreme metallicities before a possible dependence can be quantified.

Given the uncertainties surrounding our derived hydrogen/nitrogen abundances it is difficult to lay strong claims for any noticeable trends regarding atmospheric abundances. Although our derived abundances are good approximations, our results do agree well with current evolutionary models. We see that the majority of the WN stars in both the Magellanic Clouds contain traceable quantities of hydrogen in their atmospheres. We support the idea suggested by Meynet & Maeder (2003) that a plot of mass fraction of hydrogen versus (log) luminosity could be a used as a tool to investigate the evolutionary sequence of massive stars. We also propose that this plot could be used as another method to discriminate between stars with marginal or significant mass fractions of hydrogen in their atmosphere.

To conclude, we find that the single WN stars in the LMC are not that dissimilar to their Galactic counterparts. When we extend this analysis technique to study the few single WN stars in the SMC there is a noticeable difference in both spectral appearance and derived stellar parameters. We speculate that the lower mass-loss rates inferred from our work support theoretical ideas that WR stars, of the nitrogen sequence, are sensitive to metallicity variations and can be explained in terms of radiation driving (even if they are not responsible for initiating the wind). Almost all of the SMC WN stars appear to have substantially larger luminosities, indicating they formed from the most massive stars within an initial stellar population. We need to further investigate and analysis more WR stars located in regions of largely differing environments as the observed scatter of stellar parameters clouds any possible effects that metallicity may play on their parameters. Perhaps these effects are observed strongest in low metallicity environments where there are a number of unsaturated lines which drive the outflows.

CHAPTER 6

Properties of WC stars

This chapter continues to use the non-LTE, stellar atmospheres code of Hillier & Miller (1998), CMFGEN, which iteratively solves the transfer equation in the co-moving frame subject to statistical and radiative equilibrium in the expanding, spherically symmetric and steady-state atmosphere (see Chapter 3). By comparing recent, ground-based spectroscopic observations of single, extragalactic WR stars with our theoretical, synthetic spectra we are able to derive a number of important stellar parameters. These parameters can then be compared to determine any possible scaling of WR properties, with the local metallicity.

Our approach to modelling the data is to calculate a series of models adjusting the stellar parameters until we can match the observed ionization balance, line strengths/widths, (and for some datasets, the absolute magnitudes). Because of the effect each parameter can have on the emergent model spectra this was an iterative process. Initially, the line strengths and widths of the modelled spectrum are matched and then the luminosity is altered to match the absolute (scaled) flux levels.

6.1 Detailed Analysis for individual WC Stars

We provide a brief over-view of the methods/diagnostics used to model WC stars using only their optical spectra. To check that we are achieving a correct wind ionization balance we would ideally use un-blended emission lines from adjacent ionization stages. In practice this is not possible because of blending and there are not always a selection of adjacent

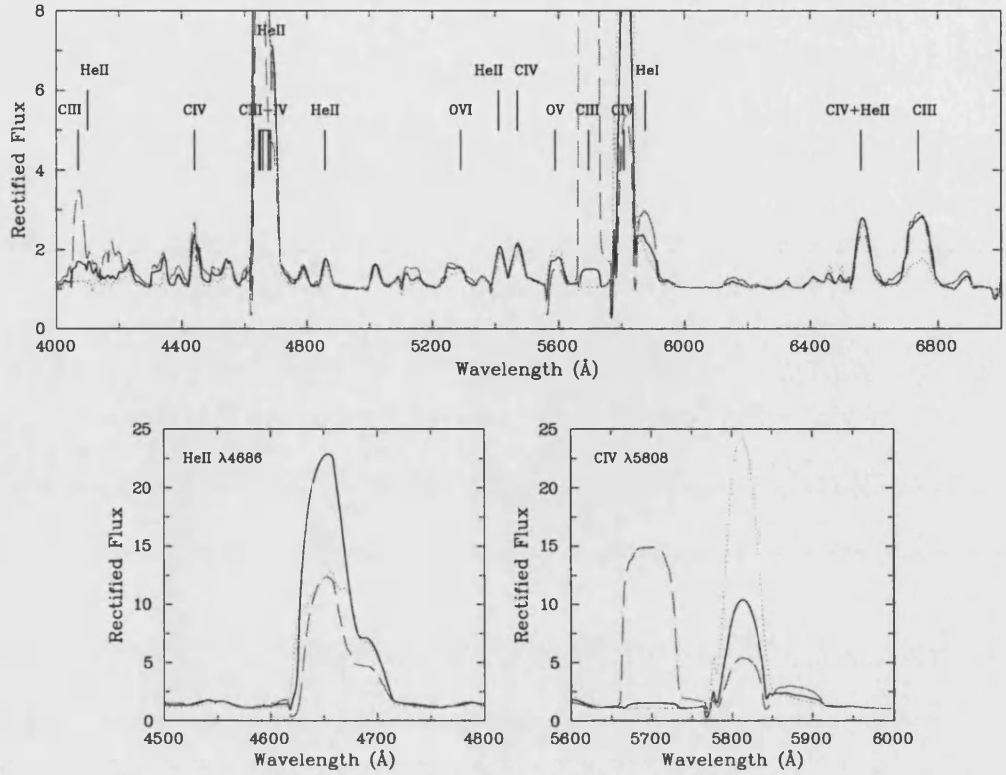

Figure 6.1: Comparison between rectified optical synthetic spectra showing a variety of mass-loss rates; 1×10^{-5} $M_{\odot}yr^{-1}$ (dotted), 2×10^{-5} $M_{\odot}yr^{-1}$ (solid) and 4×10^{-5} $M_{\odot}yr^{-1}$ (dashed). The theoretical optical spectrum is almost unchanged over this range except for the strong WR emission features (C IV λ5808 and He II λ4686), as well as the wind denisty sensistive C III λ5696 emission line.

ionization stages for each species (e.g. He I λ5876 cannot be resolved, especially in low density winds). As a result the derived temperatures should be treated as approximate.

With only a limited spectral coverage in the optical regime, we were constrained to a number of useful lines that we could reliably use to determine the star's parameters. The approach that we used was to select a number of emission lines that are known to be affected by changes in wind density, ionization, temperature and abundances. For the C/He abundance we use the (relatively) unblended diagnostic lines of He II λ5411 and C IV λ5471. Unfortunately we are more restricted when it comes to good diagnostic lines for the O/He abundance. The only available line is O III-V λ5590, but previous studies show that this emission line alone cannot be reliable (Crowther *et al.* 2002), and if anything, when its line strength is to be matched then the oxygen abundance tends to be somewhat

overestimated. This means that the calculated oxygen abundances, and hence our O/C determinations should be taken with caution.

Other diagnostic lines used were C III λ6740, which along with the strong C IV λλ5801-12 emission line can be used to determine the ionization balance (and temperature) in the wind. The strong, blended feature at λλ4650-4686, comprising of C III-IV-He II is notoriously difficult to match, as is C III λ5696, such that less importance was placed on reproducing these features. Our primary aim was to match C IV λ5808, C III λ6740, the abundance diagnostic lines (He II λ5411, C IV λ5471 and O III-V λ5590) with less of an emphasis on the other strong features as they are consistently under/over-estimated. This task is made even more difficult with only optical data, and so few emission lines to constrain our parameters. Apart from He, C, and O all the other metals were set to solar metallicities for our calculations - this assumption is not important as slight variations in the heavy metals content do not effect the emergent optical spectra (Section 6.8.5).

Considering the diagnostic emission lines adopted in our analysis we perform a simple comparison to highlight the effect that mass-loss alone has on the derived spectrum. Figure 6.1 shows the theoretical, optical spectrum for a 'typical' WCE star, over-plotted with the emergent synthetic spectra after varying the mass-loss rate by a factor of two in both directions. The effect drastically alters the line strengths of both dominate WR emission features (C III-IV-He II λλ4650-4686, and C IV λ5808 emission). The different wind densities also impact on the C III λλ5696,6740 emission lines, the latter of which is used as an important diagnostic emission line. This figure highlights the difficulty in accurately reproducing the observed optical spectrum in WC stars. It also underlines why our method identifies a number of pre-determined diagnostic emission features and attempts to produce a satisfactory *global* solution.

6.2 Analysis of WC stars in M 33

Our equivalent width measurements identified nine potentially single WC stars in M 33. The spectra for MC79 (Massey & Conti 1983) are not of high enough quality for detailed analysis and so this star is not discussed further in our sample. This is unfortunate as MC79 is the only potentially single star that lies beyond ~50% of the Holmberg radius. If the assumed H II region abundance gradient is correct then the remaining eight single WC stars ought to lie in regions of approximately solar metallicities (see Table 6.1).

Table 6.1: Broad-band photometry calculated from archival HST WFPC2 images and/or, measured from ground-based, CFHT-12K images. The absolute magnitudes were calculated using $E_{B-V} = 0.15$ and $(m - M)_0 = 24.56$ mag (see Chapter 2.2.5). The metallicities for each star were calculated using the calibrations derived in Section 4.1.2.

M33	Alias	12+*log*(*O*/*H*)	m_V		m_B		M_V
WR#			HST	CFHT	HST	CFHT	mag
38	MC26	8.63	20.90	21.03	20.68	—	-4.12
69	MC43	8.75	—	20.49	—	20.60	-4.32:
82	MC47	8.82	—	20.46	—	20.40	-4.48:
105	AM14	8.73	21.26	21.56	21.71	—	-3.76
110	AM16	8.65	20.28	20.79	20.88	—	-4.74
111	AM17	8.71	20.58	20.73	20.36	—	-4.44
116	AM19	8.66	19.66	19.61	19.41	—	-5.36
129	MC70	8.59	19.98	19.87	19.77	—	-5.04

Table 6.2 shows the model parameters for the eight selected WC stars that produced the best match to rectified observed spectra. Figure 6.2 shows the observations for our eight selected stars, along with our synthetic models. The general failures and successes are common in most cases, for instance C III λ5696 is repeatedly under-predicted in all cases. This line has been noted to be insensitive to changes in certain stellar parameters (Crowther *et al.* 2002) and so was not used as an indication of the ionization balance and temperature for the selected stars. Below we discuss any finer details that are relevant for each star.

6.2.1 MC26 (AM1, WC6)

MC26 was originally identified as a WC star by Massey & Conti (1983). For this WC6 star the observational spectrum is well reproduced by our model, except that the carbon-helium blend at λ4650 is slightly over predicted. The oxygen abundance indicator, O III-V λ5590 is well reproduced.

6.2.2 MC43 (AM13, WC7)

This WC7 star, also discovered by Massey & Conti (1983), is well reproduced by our model apart from the strong emission line at λ4650 and C IV λ5808.

6.2.3 MC47 (WC5)

MC47 (Massey & Conti 1983) is generally well matched, the two strong WC features at λ4650 and λ5808 are over-estimated. The oxygen feature at λ5590 is also well matched for this star, although this line alone cannot be used as an accurate indicator for the oxygen abundance.

6.2.4 MC60 (AM14, WC5)

Of all the single WC stars, AM14 (Armandroff & Massey 1985), alias MC60 (Massey & Conti 1983) is the faintest and as a result has the lowest signal-to-noise, although almost all the weaker emission lines have been well reproduced in our model. Both the strong WR features, the carbon-helium blend at λ4650 and C IV λ5808 are over-estimated.

6.2.5 MC61 (AM16, WC6)

The line strength of C IV λ5808 for AM16 (Armandroff & Massey 1985), alias MC61 (Massey & Conti 1983) was significantly stronger than the other WCE stars from our sample and so careful consideration to the ionization balance in the wind was required before we could match the observations. The only line not well re-produced was the blended carbon-helium feature at λ4650 which was under predicted.

6.2.6 MC62 (AM17, WC6)

AM17 (Armandroff & Massey 1985), alias MC62 (Massey & Conti 1983), also gave us the same difficulties as AM16 where the majority of lines seemed to be consistently under-estimated. The final model calculated is in reasonable agreement, matching the important abundance indicators, which interestingly determined a large oxygen abundance for this star. The model did however fail to accurately reproduce the strong C IV λ5808 emission line.

6.2.7 MC65 (AM19, WC6)

AM19 (Armandroff & Massey 1985), alias MC65 (Massey & Conti 1983), has well resolved lines and was well reproduced by our model. The line strength of C III-He II λ4650 is slightly over-estimated which generally proves less sensitive compared to other strong lines.

6.2.8 MC70 (WC5)

MC70 (Massey & Conti 1983) differs from the other single stars in that its wind velocity is faster and carbon and oxygen abundances are significantly lower. It also has the lowest temperature of the present sample. Our synthetic model does an excellent job at matching both the strong and weak features. The only discrepancy was seen in C IV λ5808 where we failed to match the relatively weak emission line.

6.3 Other Interesting WC Stars in M 33

Among our sample of WR stars in M 33 we discuss two WC stars, that although were not identify as single, we feel are different and should be investigated further in future work. The observations of these two WC stars appear to have unusual optical spectra – predominately due to their low carbon abundances. Unfortunately these observations appear to be contaminated (see Section 4.2.4) such that the WR features are diluted.

6.3.1 MC33 (AM8, WC4)

We have identified MC33 (Massey & Conti 1983) as being worthy of future investigation, mainly due to the relative strengths of the He II λ5411 and C IV λ5471 emission lines. As already discussed these lines are used to derive the C/He abundance. Implying an extremely low enrichment of carbon for MC33. This is accentuated due to He II λ5411 appearing rather strong, plus the blended carbon/helium emission feature at λ4650 seems to be slightly asymmetric on the red wing. The optical spectrum for MC33 is shown in Figure 6.3. We also note that the blended oxygen emission line at λ5590, used to estimate the O/He abundance, also appears rather weak.

As suggested by Smith & Maeder (1991), we hypothesis whether in evolutionary terms the unusually low carbon (and perhaps oxygen) abundance observed in MC33 may indicate that this star has only recently entered the WC phase. This would explain why we do not observe many products of He-burning. We would require further, more detailed

Table 6.2: List of derived stellar parameters for the single WR stars in M 33 from our sample, including the absolute magnitudes calculated from the models. The current stellar masses were calculated using the relationship derived from Schaerer & Maeder (1992).

M 33-#	Alias	Spectral Type	T_* kK	R_* $R_\odot$	$logL$ $L_\odot$	$log\dot{M}$ $M_\odot yr^{-1}$	v_∞ km s^{-1}	C/He	O/He	β_{He} %	β_C %	β_O %	m_V (mag)	M_V (mag)	$\dot{M}v_\infty$ (L/c)	M_* $M_\odot$
WR38	MC26	WC6	85	1.66	5.11	-4.71	2350	0.28	0.065	47	40	12	20.90	-4.12	17.5	10.3
WR69	MC43	WC7	75	2.18	5.13	-5.00	2000	0.28	0.025	51	43	5	20.70	-4.32	7.2	10.1
WR82	MC47	WC6	85	2.07	5.31	-4.68	2600	0.28	0.085	45	38	15	20.54	-4.48	13.2	12.8
WR105	AM14	WC6	75	1.63	4.88	-5.11	2150	0.29	0.075	46	40	14	21.26	-3.71	10.7	7.8
WR110	AM16	WC5	95	2.23	5.56	-4.60	2300	0.29	0.100	44	38	17	20.28	-4.74	7.7	17.3
WR111	AM17	WC5	95	2.06	5.49	-4.63	3000	0.34	0.260	34	35	30	20.58	-4.44	10.8	16.1
WR116	AM19	WC6	85	3.67	5.68	-4.44	2600	0.29	0.085	45	39	15	19.66	-5.37	9.8	20.5
WR129	MC70	WC5	70	4.33	5.61	-4.74	2200	0.16	0.018	64	31	5	19.98	-5.09	4.8	18.3

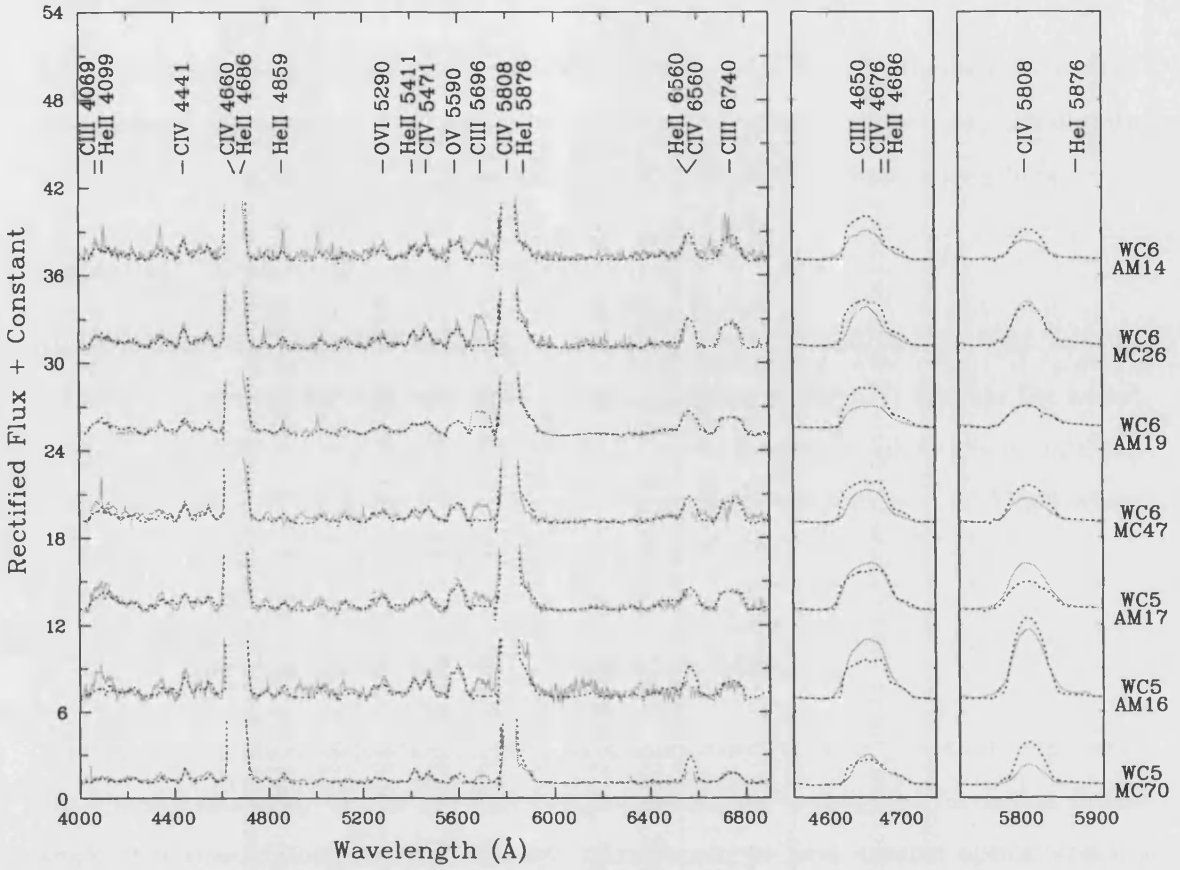

Figure 6.2: Comparison between rectified CFHT-MOS spectroscopy of four WC5-6 stars (solid) and our synthetic model (dotted). Note that the panels on the right showing the carbon-helium blend at λ4650 and C IV λ5808 were reduced by a factor of eight.

analysis of MC33 sufficiently accounting for the contaminating source/binary star before firm conclusions may be drawn.

6.3.2 MC53 (W&C16, WC6)

MC53 (Massey & Conti 1983) is another WCE star with a curious optical spectrum. We have revised the spectral classification for MC53 from WC4–5 (Smith, Shara & Moffat 1990) to WC6, based on the detection of C III λ5696. The optical spectrum for MC53 is shown in Figure 6.3. What makes MC53 different from the other WC6 stars studied in M33 is, (i) its narrow lines, (ii) barely detectable C IV λ5471 emission line and (iii) very weak O III-V λ5590 emission. The measured line width for MC53 appears unusually

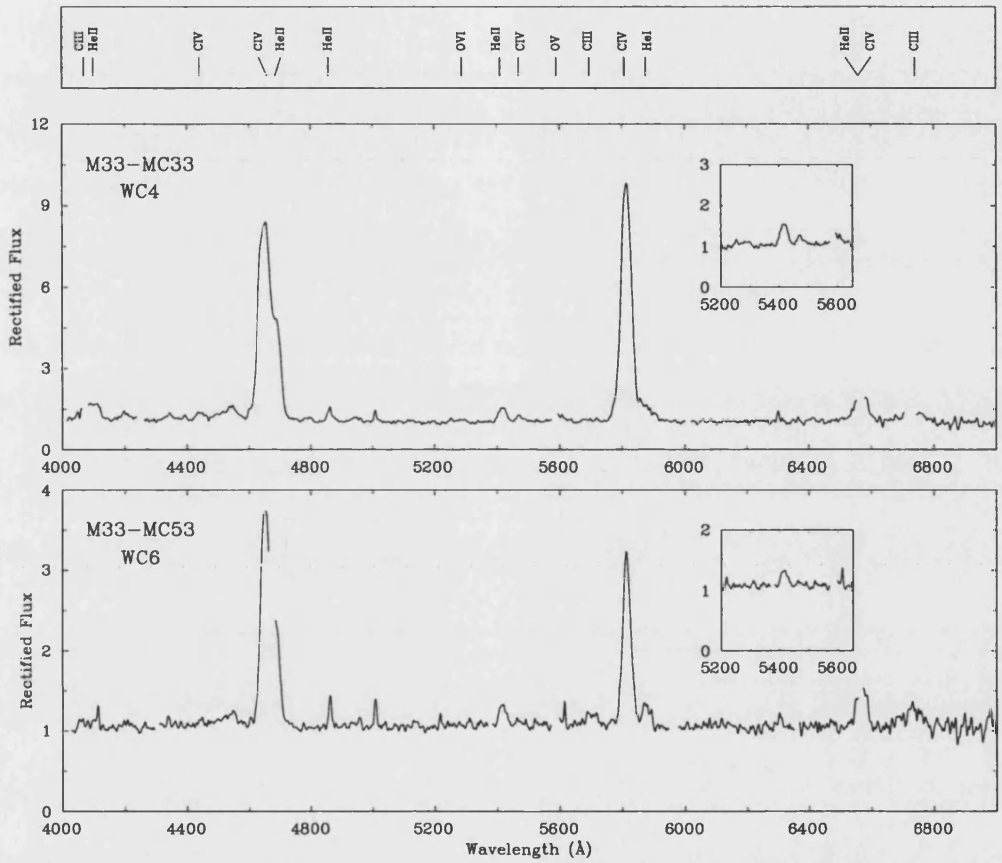

Figure 6.3: Normalized spectra of M33-WR52 (MC33, WC4) and M33-WR92 (MC53, WC6) in M 33. Comparisons of emission line strengths suggest that these stars are contaminated (see Section 4.2.4), this explains their weak emission lines. The small panels show the weak emission lines of He II λ5411 and C IV λ5471, these line are used as abundance diagnostics. Note that C IV λ5471 is unusually weak indicating that these WCE stars have very low carbon abundances.

narrow (i.e. FWHM(C IV λ5808) $\simeq$ 29Å) compared with the other WC6 stars in M 33. For example, of the four single WC6 stars in M 33 modelled in this work, we find their FWHM of C IV λ5808 to be in the range 40–50Å, with an average determined terminal wind velocity of $\sim$2500kms^{-1}.

Through experience, we suggest that, except for the line strength of C III λ5696, the optical spectrum for MC53 could be well reproduced with a theoretical model for a 'typical' late-type WC star. Even though it meets to the spectral classification criteria for an early-type WC star. We estimate that the observed line widths for this star implies a terminal wind velocity of $\sim$1100kms^{-1} (see Section 6.8.5), comparable to a WC7–8 star. We also note that He II λ4686 appears resolvable from the series of (normally) blended C III-IV $\lambda\lambda$4647-4651 emission lines – again typically observed in late-type WC stars. We would once again require further detailed analysis for MC53 and its companion for any real conclusions to be drawn.

We find a similar conclusion for MC53 as for MC33, in that its line widths (and hence terminal wind velocity) and surface chemistries are indicative of a late-type WC star, although its spectral classification denotes an early-type WC star. We suggest that MC53 could have evolved from a narrow-lined WN star straight to a WC phase. So we are observing a star which has recently undergone the transition between the two WR spectral types. This evolutionary sequence is predicted in the (non-rotating and rotating) theoretical models by Meynet *et al.* (1994) and Meynet & Maeder (2003) for a star with an initial mass of 40M$_\odot$ (see Section 1.2.2).

To conclude, we have highlighted two WC stars that appear to have unusual and contrasting emission features. The WCE star MC33 appears a 'normal' WCE star with an anomalous low abundance of enriched elements, which are indicated by the strength of the abundance diagnostic lines (i.e. He II λ5411, C IV λ5471 and O III-V λ5590). MC53 on the other hand is slightly more interesting as it is classified a WCE star but has spectral features of a WCL star. One possible explanation is that it has evolved from its brief life as a WNL star, which are known to have narrow emission lines, directly to the WCE phase. This could explain why we see the abnormally low wind velocities and decreased carbon enrichment. This hypothesis is supported by stellar evolution theory, assuming that its initial mass is $\simeq$ 40M$_\odot$.

6.4 Analysis of WC stars in M 31

Our observations of four known WC stars in M 31 has revealed two potentially single stars, MS12 and MS21 (Moffat & Shara 1983). Although we only observed a small number of WR stars in M 31 this sample is significant as it provides examples of a late-type WC star as well as an early-type WO star. Both these types are rare and so far WCL stars are observed to be confined to M 31 and the Solar neighbourhood.

We model both single WC stars as well as the two contaminated WC stars by merging their observed spectrum with a theoretical OB star spectrum taken from the grid by Kurucz (1979). Model calculations for these four WC stars were less comprehensive, only including spectral lines of He, C, O, Si and Fe. The effect that other elements such as Ne and S have are negligible and predominately alter the line strengths of C IV λ5808 and C III-He II λ4650 by $\sim$10% and do little to affect to final stellar parameters. Details for each star are given below. The inferred stellar parameters are listed in Table 6.3, we also include the published stellar parameters for OB10-WR1 examined by Smartt *et al.* (2001*a*).

6.4.1 MS21 (WC6)

This WC6 star, discovered by Moffat & Shara (1983), is well matched apart from C IV λ5808 line and the carbon-helium blend at λ4650, both of which are slightly underestimated. C III λ6740 is also fractionally too weak. Recent experience suggests that these lines increase when other atomic species are included into the synthetic model calculations. Our abundance diagnostic lines are well reproduced, as are any of the weaker features within the observed spectra. Figure 6.4 shows a comparison between our spectroscopic observations and our synthetic models.

6.4.2 MS12 (WO4)

Using the classification scheme detailed by Crowther *et al.* (1998) we have identified MS12 (Moffat & Shara 1983) not as a WC4 star but as a WO4 star. This classification scheme predominately uses the emission line ratios of O VI λ3818/C IV λ5808 and O VI λ3818/O V λ5590 to distinguish between WC4–WO1 stars, for both central star planetary nebular (CSPN; i.e. low mass stars) and massive WO stars.

This object, as with most WO stars, is extremely difficult to model due to its strong

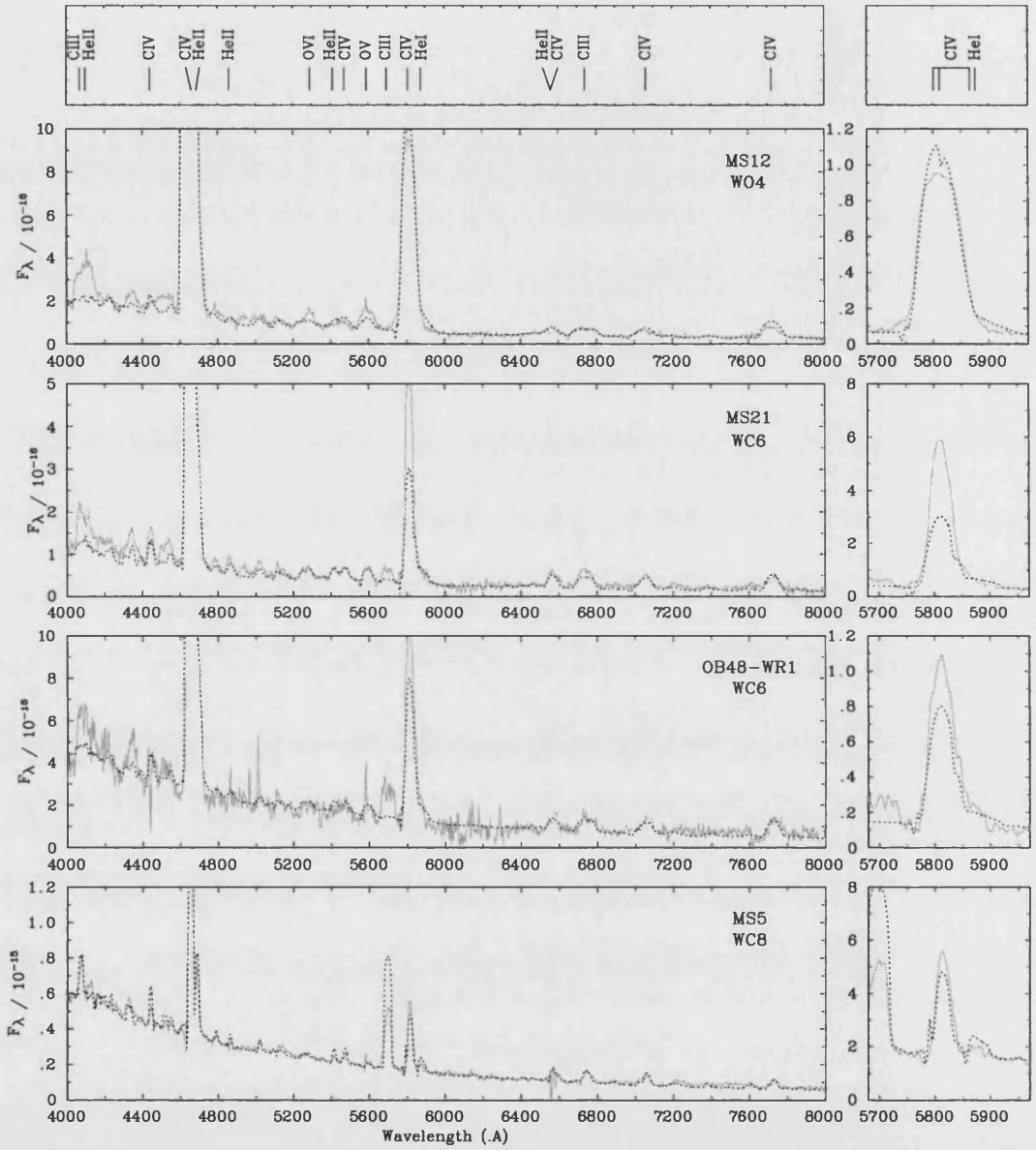

Figure 6.4: Comparison between our flux calibrated WHT-ISIS observation (solid) of WC stars in M 31 and our synthetic model (dotted). The panel on the right shows the blended $\lambda\lambda$5801-12 feature.

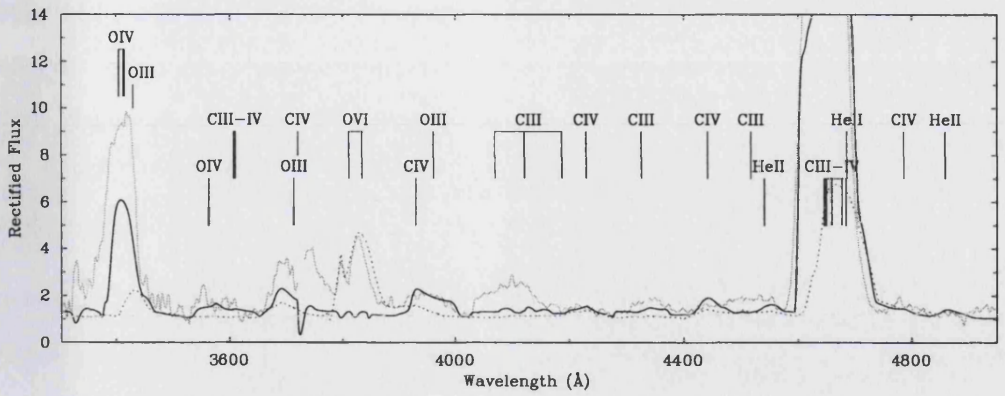

Figure 6.5: Comparison between WHT-ISIS observation of MS12 in M 31 and our two synthetic models; one matches the strong optical WR features (solid), and the second attempts to reproduce the strong O VI $\lambda\lambda$3811,3834 emission line (dotted).

oxygen emission lines which are formed due to high ionization lines such as O VI. The synthetic model shown in Figure 6.4 looks very similar to a spectrum of a typical WC4 star, although it fails to match any of the strong oxygen lines which distinguish it as a WO(4) star.

For this star we calculated two sets of models, the first (which is shown in Figure 6.4) reproduces the line strengths/widths for the main WC emission features as outlined in the beginning of this chapter. The second model was calculated to determine the parameters necessary to match the highly ionized oxygen lines - unfortunately this model fails to reproduce any of the other strong WR features. Both sets of parameters are listed in Table 6.3. Figure 6.5 compares these two models with our observations over a spectral range 3400 – 5000Å showing the success and failures of both models in reproducing the oxygen emission lines.

Comparing the first synthetic model, apart from the strong oxygen lines, we successfully reproduce our observations. The line strength for the strong emission line at λ4650 is a little weaker than our observations, as is the blended emission line at ~4100Å. The second, much hotter synthetic model fails to predict the line strengths for any of the main optical emission lines, consistently under-estimating them all. It does however, match the O VI $\lambda\lambda$3818,3834 emission lines. These lines require a much harder ionizing source to increase their strength and hence match the observed data. These highly ionized features

were only matched only when the stellar temperatures reached temperatures of 140,000K. Unfortunately at these temperatures the ionizing flux is so strong that we see very little recombination of C III and the WR features at λ4650 and λ5808 appear hugely under-estimated. It also under-predicts the other strong oxygen lines, such as O IV λ3412. This highlights the current problems with our atmosphere models in understanding the physics of the wind of WO stars.

6.4.3 MS5 (WC8)

From our equivalent width measurements (Fig. 4.12) we identified that it was unlikely that MS5 (Moffat & Shara 1983) was single, so we cannot simply calculate a model and directly compare this to our observations. Our approach to determine the stellar parameters for MS5 was to first calculated a WR model, essentially assuming that it was single, then co-add this model with an O star model by Kurucz (1979) with parameters; $L_O = 2L_{WR}$ and $T_* = 30{,}000$K log g = 4.0. This 'combined' model spectrum was then compared with the observed spectra and is shown in Figure 6.4. The 'combined' model now matches the observed spectra very well apart from C III λ5696 which is over-estimated, although as discussed in Section 6.1, less emphasis is given to this line when attempting to match the observed data. One way of determining the level of contamination for MS5, assuming our WR model was correct, is by adjusting the level of the contaminating source until we match the observed spectra, making sure that the luminosity of the polluting source is kept realistic. It is worth noting that there could be multiple sources polluting the spectra of MS5.

From our 'combined' synthetic spectra we derived the interstellar reddening towards MS5 to be $E_{B-V} = 0.26$ which assuming a distance to M 31 of 752kpc (Freedman *et al.* 2001) and an observed magnitude of $m_{V(sys)} = 18.82$ gives an absolute magnitude of $M_{V(sys)} = -6.37$. Taking this a stage further, if our previous postulation that $L_O = 2L_{WR}$ and $M_{V(sys)} = -6.37$ are correct then the absolute magnitude for the combined system can be separated giving us an absolute magnitude for the WR star. This gives; $M_{V(O)} = -5.93$ $M_{V(WR)} = -5.18$, which means that MS5, if resolvable would be observed with a visual magnitude of $m_V = 20.01$.

6.4.4 OB48-WR1 (IT 5-01, WC6)

To match the observed spectra of OB48-WR1 (Massey, Armandroff & Conti 1986) we diluted the resultant model with a single O star model taken from Kurucz (1979), using the same method as discussed above for MS5. This time we inferred a somewhat lower dilution factor assuming that $L_O = L_{WR}$. This combined O star – WR model has the same successes and failures as reported for MS21 – i.e. under-estimation for C IV λ5808 and C IVHe II λ4650. The main difference between OB48-WR1 and MS21 is that OB48-WR1 appears to be far more luminous than MS21, which in turn means that we calculate a much larger current mass for this star (see Table 6.3).

Continuing the same logical assumptions as for MS5, combining our derived reddening, $E_{B-V} = 0.34$ with our distance (752kpc) and apparent magnitude, $m_{V(sys)} = 19.23$, we calculate an absolute magnitude of $M_{V(sys)} = -4.98$. If our earlier assumption that $L_O = L_{WR}$ is correct then it would imply a visual magnitude of $m_{V(WR)} = 19.98$, and an absolute magnitude for OB48-WR1 of $M_{V(WR)} = -5.46$. This is reasonable and in fact is almost identical to the absolute magnitude derived for OB10-WR1 (Massey, Armandroff & Conti 1986) by Smartt *et al.* (2001*a*). The parameters for OB48-WR1 listed in Table 6.3 are for the WR component only.

6.5 Analysis of WC stars in IC 10

A comparison of line strength measurements (Figure 4.12) with known single/binary WC stars identified that two WC stars in our observed sample, [MAC92] 10 and [MAC92] 20 (Massey, Armandroff & Conti 1992), display line strengths indicative of single WC stars. We attempt to model these two stars, listing their inferred parameters in Table 6.4. A comparison between our observations and our computed theoretical models is shown in Figure 6.6. We continue using a reduced model calculation for the two WC stars in IC 10, only including spectral lines of He, C, O, Si and Fe (as followed in Section 6.4). Below we discuss the results obtained for both stars.

6.5.1 [MAC92] 10 (WC7)

This late-type WC star is intriguing for a number of reasons; (i) it is the only bona-fide WC7 star in IC 10 (except for [MAC92] 15 which was classified a WC6–7 by Massey, Armandroff & Conti 1992), which is surprising given that the metallicity in IC 10 is $\sim 0.3 Z_\odot$

Table 6.3: List of derived stellar parameters for the WR stars in M 31 from our sample, including the absolute magnitudes that were calculated using the inferred reddenings. The current WR stellar masses were calculated using the relationship derived from Schaerer & Maeder (1992). Note that for MS5 and OB48-WR1 both the observed (system) visual magnitudes and the assumed WR magnitudes are shown. There are two sets of parameters for MS12, the first set are those required to model the generic WR features, and the second set are those needed to match the strong oxygen emission lines. The parameters determined by Smartt *et al.* (2001*a*) for OB10-WR1 are also shown for comparison.

Star	Spectral	T_*	R_*	$logL$	$log\dot{M}$	v_∞	C/He	O/He	β_{He}	β_C	β_O	$m_{V(sys)}$	$m_{V(WR)}$	$M_{V(sys)}$	$M_{V(WR)}$	E_{B-V}	$\underline{\dot{M}v_\infty}$	M_*
	Type	kK	$R_\odot$	$L_\odot$	$M_\odot yr^{-1}$	km s^{-1}			%	%	%	(mag)	(mag)	(mag)	(mag)	(mag)	(L/c)	$M_\odot$
MS5	WC8	70	4.08	5.56	-4.64	1400	0.30	0.010	51	46	2	18.82	20.01	-6.37	-5.18	0.26	4.3	16.9
MS12	WO4	90	3.61	5.89	-4.33	3600	0.50	0.065	36	54	9	19.83	19.83	-5.85	-5.85	0.42	10.7	28.4
—	—	140	1.49	—	-4.55	—	—	—	—	—	—	—	—	—	—	—	6.4	28.1
MS21	WC6	85	2.69	5.53	-4.60	2600	0.28	0.085	46	38	16	20.73	20.73	-4.98	-4.98	0.43	9.3	16.7
OB48-WR1	WC6	80	4.65	5.90	-4.38	2600	0.28	0.065	48	40	12	19.23	19.98	-4.98	-5.46	0.34	3.8	28.1
OB10-WR1	WC6	75	4.10	5.68	-4.30	3000	0.10	0.025	–	–	–	19.32	19.32	-5.40	-5.40	0.18	15.4	21.0

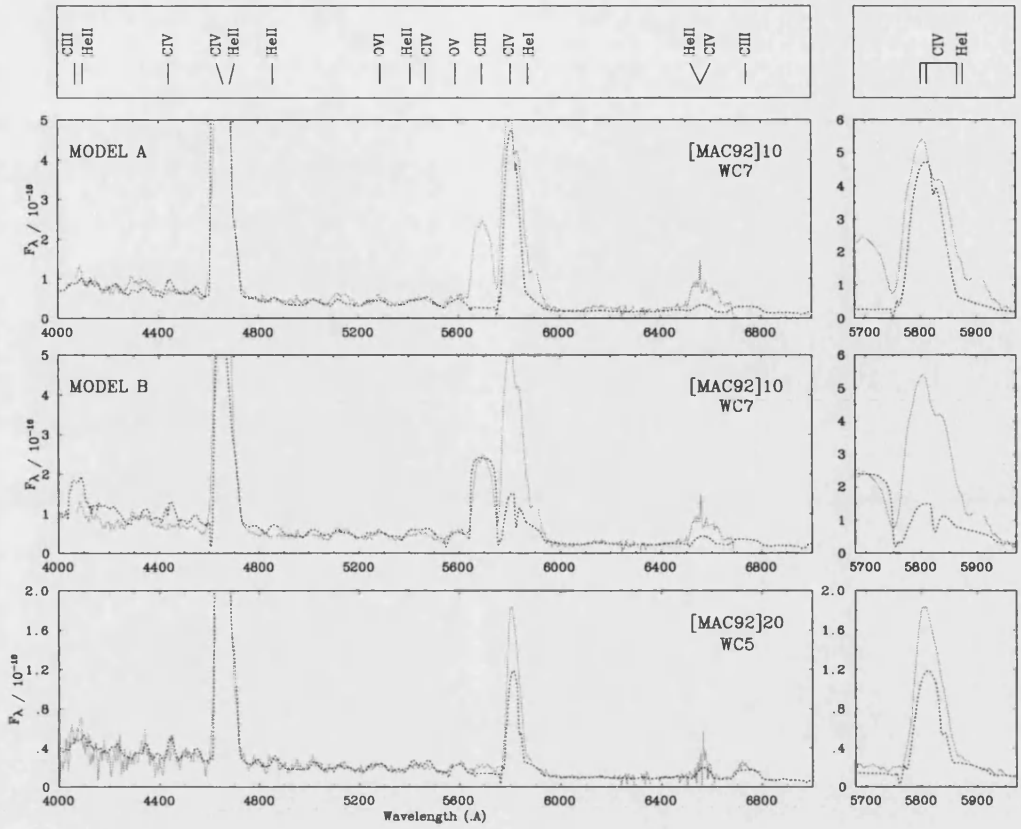

Figure 6.6: Comparison between our flux calibrated Gemini-GMOS observations (solid) of WC stars in IC 10 and our synthetic models (dotted). The panel on the right shows the C IV λ5808 emission line. Two synthetic models are shown for [MAC92] 10, details are discussed in the text.

(Lee *et al.* 2003), (ii) its emission lines appear very broad (i.e. FWHM(C IV $\approx$ 85Å), even broader than WC4 stars in IC 10. For these reasons it was very difficult to calculate a synthetic model which reproduced the observed optical spectrum.

It was challenging to simultaneously match the C III λ5696 and C IV λ5808 emission lines, especially with such large terminal wind velocities required to match the broad line widths. The line strength of C III λ5696 is reduced with both decreasing mass-loss rates (which is required to match C IV λ5808), and with increasing wind velocity (which is required to reproduce the observed line widths).

As we failed to reproduce both C III/C IV we computed two sets of parameters for this WC star, the first (Model 'A'), in keeping with other models, matched the strong WR emission lines and failed to predict any C III λ5696 emission. The second (Model

'B'), disregarded the main WR features but attempted to match the C III λ5696 emission line. Both of these synthetic models are shown in Figure 6.6. To match the C III λ5696 emission line, we needed to more than double the mass-loss rate between Model 'A' and Model 'B'. Unfortunately both models failed to reproduce the blended C IV/He II λ6560 emission line. This interesting star highlights some of the downfalls of the current stellar atmosphere models, and it requires more attention than is given in this work.

We found that for our theoretical model to match our observations of [MAC92] 10, we needed to de-redden our spectrum by $E_{B-V} = 0.65$. This is in contrast to the much larger colour excess determined from our narrow-band photometry $E_{b-v} = 0.98$ (i.e. $E_{B-V} = 1.19$). This inconsistency could be due to a number of possibilities, either our assumption that the intrinsic colour for a WR is $(v - r)_0$= -0.2 mag, or that our inferred reddening from our synthetic models is underestimating the real colour excess due to the spectral range in which we can compare the observations and theoretical models. The latter is less likely responsible for the discrepancy as even over 4000 – 7000Å the reddening can be constrained to ~0.5 mag. For consistency we use our observed broad-band photometry and model derived reddenings to calculate the absolute visual magnitude (see Table 6.4), and not the absolute magnitude derived via our narrow-band photometry.

6.5.2 [MAC92] 20 (WC5)

[MAC92] 20 first reported by Massey, Armandroff & Conti (1992) appears like a typical WC5 star and is well reproduced by our model, except for C IV λ5808 which is under-estimated, and the blended emission line at λ4650 which is slightly over-estimated. Comparing our reddenings derived from narrow-band photometry and our synthetic models we again find an inconsistency of $\Delta E_{B-V} = 0.27$ mag. We choose to use our model derived reddenings in our absolute visual magnitudes.

6.6 Analysis of WC stars in NGC 300

We continue to perform detailed analyses for a number of single WC stars in a variety of environments by extending this to NGC 300. Unfortunately due to the large uncertainties in the reddening towards this galaxy we could not accurately derive independent reddenings for each star from photometry. As a result we were unable to calculate realistic absolute magnitudes which we have used (in part) to determine potentially single WC

Table 6.4: List of derived stellar parameters for the WC stars in IC 10 from our sample, including the absolute magnitudes that were calculated using the inferred reddenings. The current WR stellar masses were calculated using the relationship derived from Schaerer & Maeder (1992). There are two sets of parameters for [MAC92] 10, the first set are those required to model the generic WR features, and the second set are those needed to match the C III λ5696 emission lines.

Star	Spectral Type	T_* kK	R_* $R_\odot$	$logL$ $L_\odot$	$log\dot{M}$ $M_\odot yr^{-1}$	v_∞ km s^{-1}	C/He	O/He	β_{He} %	β_C %	β_O %	m_V (mag)	M_V (mag)	E_{B-V} (mag)	$\underline{\dot{M}v_\infty}$ (L/c)	M_* $M_\odot$
[MAC92] 10	WC7	100	1.25	5.15	-4.92	3100	0.56	0.085	33	56	11	20.9:	-4.97	0.65	12.9	10.7
—	—	100	1.25	—	-4.54	—	—	—	—	—	—	—	—	—	31.3	11.4
[MAC92] 20	WC5	85	1.34	4.93	-5.10	2600	0.26	0.065	49	38	13	22.0	-3.65	0.58	11.9	8.2

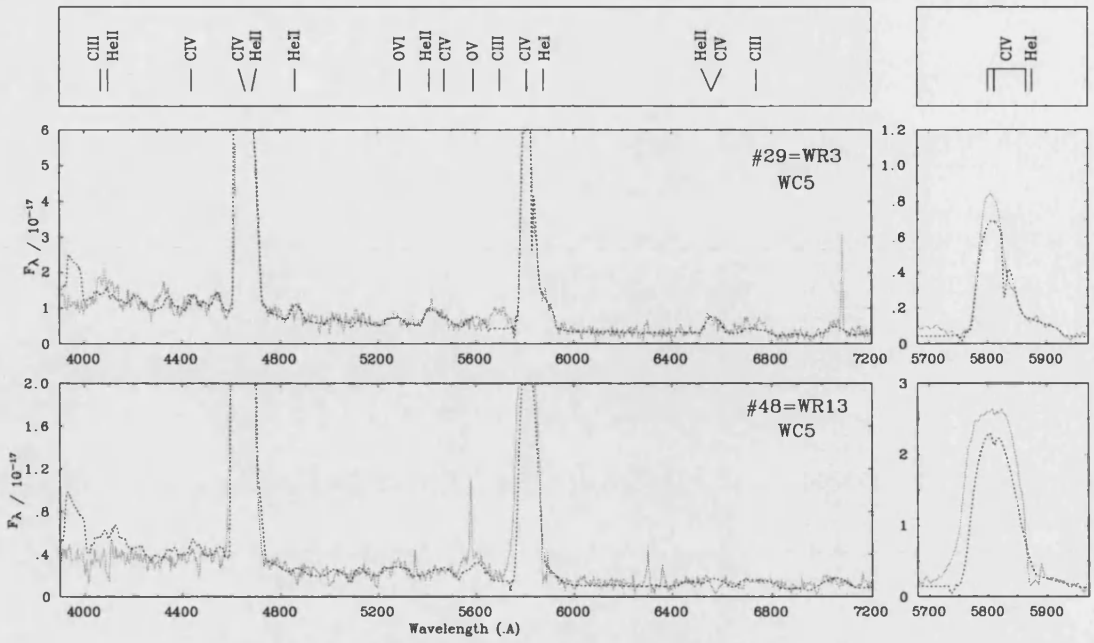

Figure 6.7: Comparison between our de-reddened, flux calibrated VLT-FORS2 observations (solid) of NGC300-#29 (WC5) and NGC300-#48 (WO4) and our synthetic model (dotted). The panel on the right shows the blended λ4650 feature.

stars (see Section 4.2.4). So instead, from visual inspection, combined with the equivalent widths measurements we have inferred two WC stars which are possibly single; NGC300-#29 and NGC300-#48. These stars are studied, using the same techniques, and their stellar parameters are listed in Table 6.5. Figure 6.7 compares our synthetic spectra with our observations.

6.6.1 NGC300-#29 (WR3, WC5)

Overall, our observations are well reproduced by our theoretical model, except that C III λ5696 is not predicted, as is C IV λ5808. The only available oxygen diagnostic, O III-V λ5590, appears weak, suggesting a low oxygen content.

6.6.2 NGC300-#48 (WR13, WO4)

Unlike MS12 in M 31 (Section 6.4.2) we only calculate one model for #48, concentrating on reproducing the majority of the various diagnostic lines. Generally, our synthetic spectrum

Table 6.5: List of derived stellar parameters for the WC stars in NGC 300 from our sample, the absolute magnitudes are also shown using the inferred reddenings and observed apparent visual magnitudes. The current WR stellar masses were calculated using the relationship derived from Schaerer & Maeder (1992).

NGC 300	Alias	Spectral	T_*	R_*	$logL$	$log\dot{M}$	v_∞	C/He	O/He	β_{He}	β_C	β_O	m_V	M_V	E_{B-V}	$\underline{\dot{M}v_\infty}$	M_*
#		Type	kK	$R_\odot$	$L_\odot$	$M_\odot yr^{-1}$	km s^{-1}			%	%	%	(mag)	(mag)	(mag)	(L/c)	$M_\odot$
29	WR3	WC5	100	1.87	5.50	-4.60	2700	0.08	0.050:	69	17	14	21.61	-5.23	0.10	10.5	15.8
48	WR13	WO4	95	1.47	5.20	-4.80	3750	0.50	0.100	34	52	14	21.87	-5.12	0.15	18.4	8.3

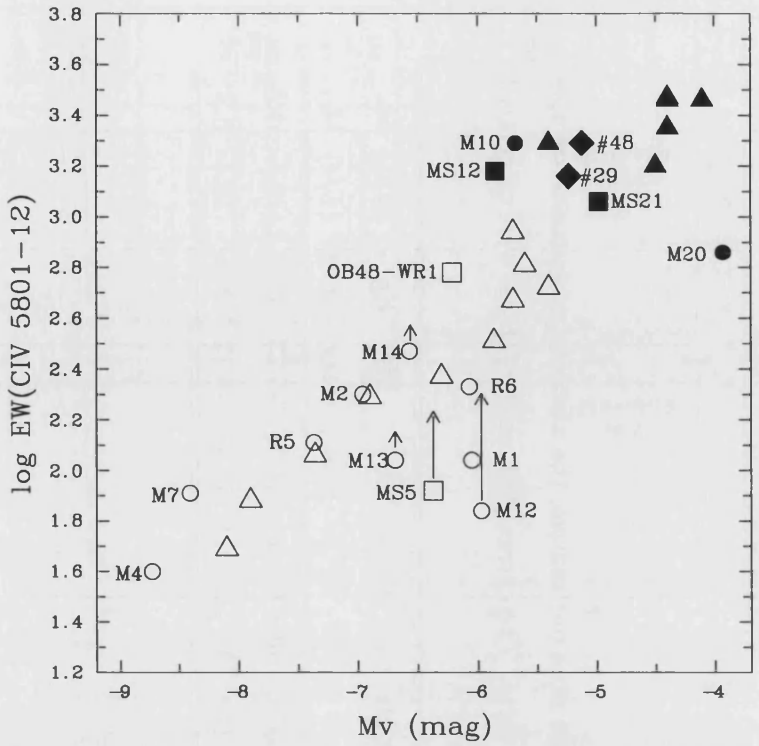

Figure 6.8: Measured line strength C IV $\lambda\lambda$5801-12 versus absolute visual magnitude for WC stars in IC 10 (circles), M 31 (squares), LMC (triangles) and NGC 300 (diamonds). The open symbols signify (inferred) binary stars and filled symbols signify single stars. These data were taken from Smith, Shara & Moffat (1990) and Crowther *et al.* (2003) for the LMC and IC 10 data respectively.

is in reasonable agreement with our FORS2 observations. The extremely broad lines for this WO star hindered detailed comparisons, although the C III-IV/He II λ4650 blend is rather too strong compared with the observations. Unlike its counterpart, NGC300-#29, the O III-V λ5590 emission line suggests a much larger oxygen content (O/He $\geq$ 0.1), in keeping with its spectral classification.

We test our earlier assumption that #29 and #48 were potentially single. By using the reddenings derived from our (un-reddened) theoretical model comparisons with our observations, we calculate absolute visual magnitudes. These magnitudes, combined with their measured EW(C IV) can be compared against previously known/inferred single stars. We find that both #29 and #48 are apparently single (see Figure 6.8).

Table 6.6: List of 'typical' stellar parameters for a WCE star, considering three different scenarios. (i) WC star is single (O/WR=0); (ii) star has been diluted from an T_*=30kK, log g=4.0 OB star of equal visual magnitude (O/WR=1); (iii) again, star has been diluted by the same OB star, but with twice the visual magnitude (O/WR=2).

O/WR	T_*	R_*	$logL$	$log\dot{M}$	v_∞	C/He	O/He	β_{He}	β_C	β_O	$M_{V(WR)}$	M_*
	kK	$R_\odot$	$L_\odot$	$M_\odot yr^{-1}$	km s^{-1}			%	%	%	(mag)	$M_\odot$
0	85	2.26	5.38	-4.70	2600	0.28	0.085	46	38	16	-4.48	13.9
1	85	1.60	5.08	-4.92	2600	0.28	0.085	46	38	16	-3.73	9.8
2	85	1.30	4.90	-5.06	2600	0.28	0.085	46	38	16	-3.29	8.1

6.7 Effects of contamination

The question of contamination becomes an important issue when attempting to resolve single stars within external galaxies. For example, a 1.5″ slit width corresponds to a spatial scale of ∼ 6pc at a distance of 816kpc (equivalent to M 33). Add to this the fact that the majority of WR stars are located in crowded regions containing large stellar populations, the task of obtaining uncontaminated WR spectra is made very difficult.

We have simulated binary effects by co-adding a normalized model spectrum of an OB star to a model WR spectrum to determine the effects that an incorrect assumption for the star's luminosity would have on our theoretically derived stellar parameters (see Table 6.6). For completeness we have calculated three different cases, (i) a single WR star (i.e. O/WR = 0); (ii) a WR star with contamination from a nearby OB star of equal continuum brightness (O/WR = 1); (iii) a WR star with contamination from a nearby OB star with a continuum twice as bright (O/WR = 2). For the companion we used a generic OB star model of T_*=30kK, log g=4.0 taken from the Kurucz (1979) grid within DIPSO. These results are shown in Figure 6.9. We caution the use of this technique at UV wavelengths as the underlying continuum shape becomes very different but is reasonable when only considering optical wavelengths. These levels of contamination simulated represent a plausible scenario. Recently a quadruple WR system was observed by Demers *et al.* (2002), in which they uncovered a (WR+O) + (O+O) stellar system in GP Cephei. Their studies found that for the (WR+O) component, both stars had equal M_v. These effects are considered when we compare stellar parameters.

We find that the line strengths for the synthetic model were diluted such that the

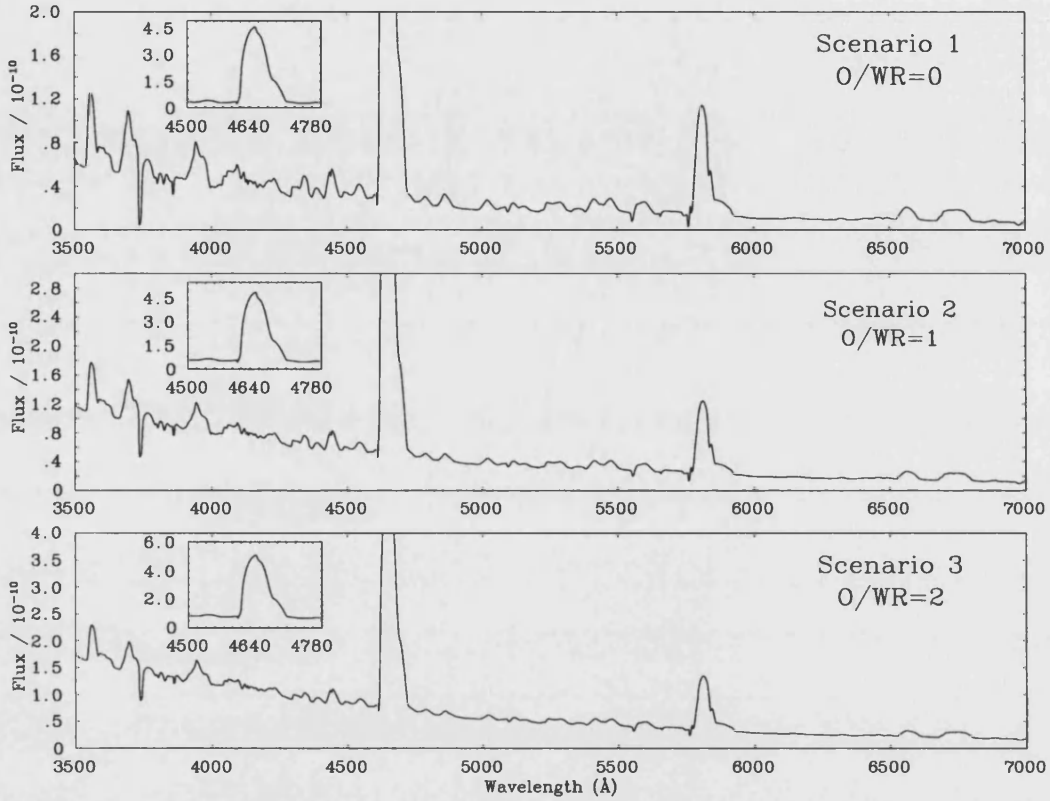

Figure 6.9: Simulated effect of multiplicity, by co-adding a scaled model spectrum of an OB star to a model WCE spectrum to examine the effects on theoretically derived stellar parameters (see Table 6.6). For completeness we have calculated three different cases, (i) a single WR star (i.e. O/WR = 0); (ii) a WR star with contamination from an a OB star of equal continuum brightness (O/WR = 1); (iii) a WR star with contamination from a nearby OB star with a continuum twice as bright (O/WR = 2). For the companion we used a generic OB star model of $T_* = 30$kK, $\log g = 4.0$ taken from the Kurucz (1979) grid within DIPSO.

EW(C IV) was found to be reduced almost by a factor of two for O/WR = 1 and a factor of three for O/WR = 2. This could then be used as evidence, to some extent, that using the EW(C IV) versus spectral type (see Sect. 4.2.4), as our indicator of possible multiplicity is valid in obvious cases where the contaminating source has approximately equal visual continuum brightness. In the more extreme cases in our sample of M 33 WC stars, where $\log \mathrm{EW(C\,IV)} \simeq 1.7$ (see Fig. 4.9), we would need to dilute the spectrum, using the synthetic model described in Table 6.6, heavily to match these weaker values. If our assumption that the contamination was due to a hot OB stars is correct, then it would imply a O/WR ratio of approximately ten to dilute C IV enough to match the weakest of these observations.

Figures 6.14 and 6.16, in the following section, highlight the effects that contamination from another OB star can have on a WR star's stellar parameters. This occurs if the observed absolute magnitude is assumed to be from a single source but is in fact from multiple sources. This would cause a gross over-estimation in stellar luminosity of the WR star. The vector shown indicates the effect that a contaminating source with a visual continuum luminosity equal to that of the WR star would have on our derived parameters.

6.8 Comparisons

We are now in the unique position where we have stellar parameters for ~17 single WC stars, spanning a metallicity range of approximately a factor of 10. We can then directly compare these results to investigate whether their properties are affected by the local metallicity. We start by studying the contrast in the observable WR properties (e.g. v_∞, M_V), and then compare a number of stellar parameters inferred from our theoretical models (e.g. $\dot{M}$, chemical abundances).

6.8.1 Wind Velocity

Determining the physical parameters for our (selected) sample of extragalactic WC stars is helpful in the understanding of WR stars. The terminal wind velocity is one of the many fundamental stellar parameters which are important for a number of reasons; terminal velocities are required to accurately determine mass-loss rates, and are important for studies of wind interactions in the ISM. Theoretical studies also predict a metallicity scaling for the terminal velocity (which is dependent on α, the CAK force multiplier,

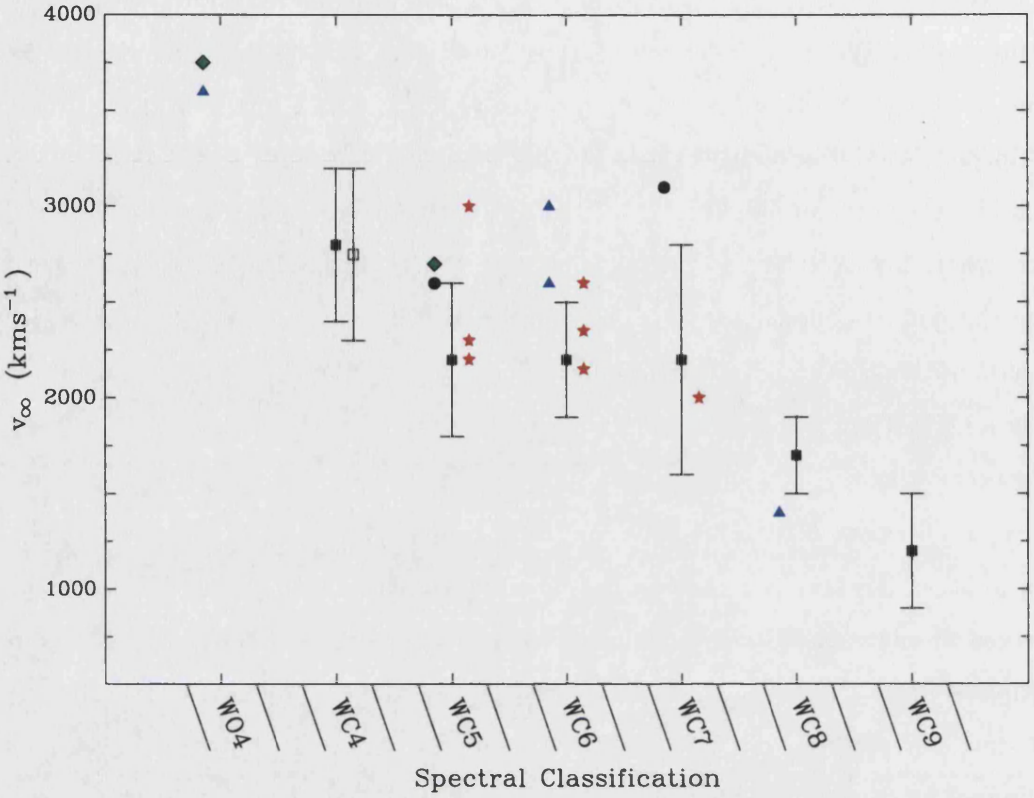

Figure 6.10: A comparison between the terminal wind velocities for Galactic WC stars (filled squares), LMC (open square), M 31 (triangles) M 33 (stars), IC 10 (circles) and NGC 300 (diamonds) versus spectral type. The values plotted for the Galaxy and LMC are the averaged values taken from van der Hucht (2001) and Crowther *et al.* (2002) respectively, and the range of observed limits are also shown.

and the escape velocity). Leitherer, Robert & Drissen (1992) prescribed a metallicity dependence for the terminal velocity which scaled to the power of 0.13 ($v_{\infty,Z} \propto Z^{0.13} v_{\infty,\odot}$), which has yet to be confirmed observationally.

We perform a simple comparison between the terminal wind velocity from our observed WC stars with published velocities for Galactic and LMC WC stars. These are plotted as a function of spectral type (see Fig. 6.10). In this case there was no discriminator needed as to whether the velocities plotted were measured from binary systems or not, as this should not affect the calculated wind velocity. The terminal velocities for the known Galactic WC population taken from van der Hucht (2001) are also shown in Figure 6.10,

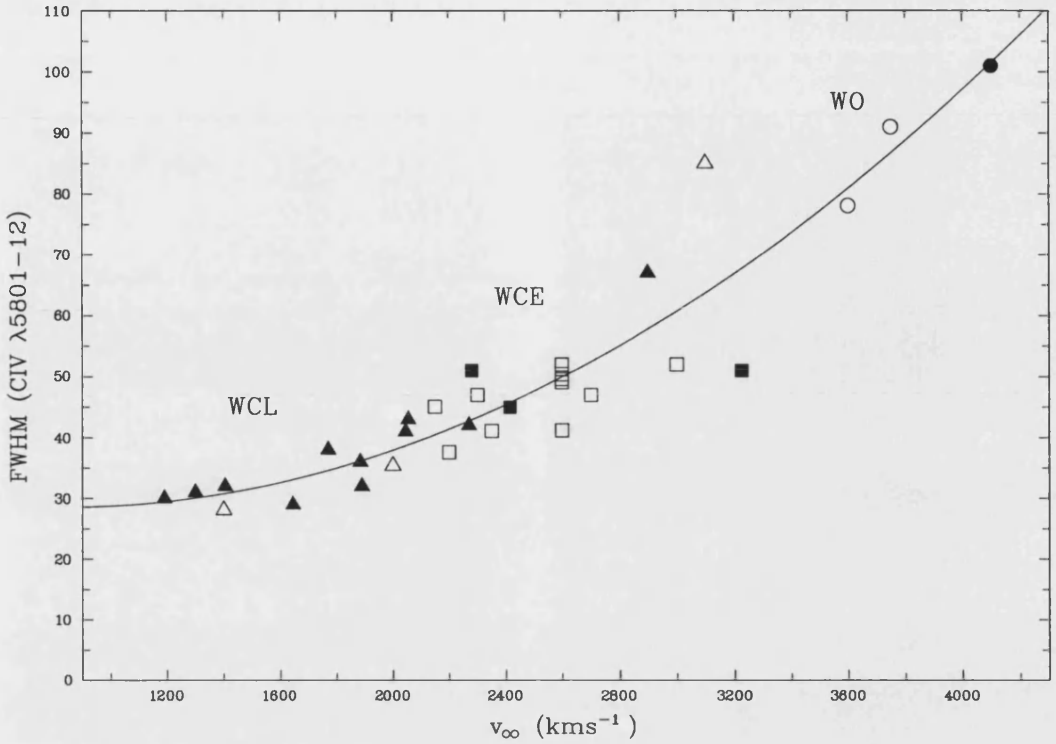

Figure 6.11: Terminal velocities for our sample of extragalactic WC stars determined from our theoretical models (opened symbols) versus measured FWHM(C IV $\lambda\lambda$5801-12) for WCL stars (triangles), WCE (squares) and WO stars (circles). These are compared with the terminal velocities for Galactic WC stars taken from Prinja, Barlow & Howarth (1990) and Sand 2 in the LMC from Crowther *et al.* (2000) (filled symbols), which were measured from UV P–Cygni profiles.

including the range of observed limits. The terminal velocities for six WC4 stars in the LMC are also plotted and were taken from Crowther *et al.* (2002).

Overall, there does appear to be a trend of increasing terminal wind velocity towards earlier WC subtype (with a scatter). There is no discernible segregation between the samples of stars, unlike the theoretical predictions. Not only is the theoretical dependence between terminal velocity and metallicity weak ($v_\infty \propto Z^{0.13}$), but considering the observed scatter any possible variation in the terminal velocity due to the local metal content would be undetectable. For example, assuming the average terminal wind velocity collated by van der Hucht (2001) for WC5 stars ($v_\infty \simeq 2200 \mathrm{kms}^{-1}$) is representative, the proposed difference in terminal velocity between a WC5 star located in a region of solar metallicity

and one located in a region of half-solar metallicity is $\sim$190kms^{-1}. Compare this with the observed scatter of 400kms^{-1} quoted by van der Hucht (2001) for Galactic WC5 stars and it highlights the difficulties with accurately observing a discernible difference between WR stars in various environments. There is however, a large spread in the values for Galactic WC7 stars, ranging from 1500 – 3600kms^{-1}, which dos not follow the gradual trend of increasing terminal velocity. [MAC92]10 in IC 10 is also observed to have an unusually fast wind, perhaps suggesting that there are a distinct sub-class of WC7 stars.

Terminal velocities for hot, massive stars are traditionally measured from observed UV P–Cygni absorption profiles (e.g. Prinja, Barlow & Howarth 1990) or from IR He I line profiles (Howarth & Schmutz 1992). Unfortunately with only optical spectroscopy available these techniques were not available and so (calculated) adjustments to the theoretical models were made until the observational line widths were reproduced. We investigate whether our determined terminal wind velocities are correlated to the observed FWHM(C IV $\lambda\lambda$5801-12). The aim is to provide an independent method for estimating the terminal velocity using a strong optical emission line.

We plot our inferred terminal velocities versus measured FWHM(C IV $\lambda\lambda$5801-12) for the WC and WO stars in our dataset (see Fig. 6.11). We also compare these results with accurately derived terminal velocities for Galactic WC stars, using the measured terminal velocities from Prinja, Barlow & Howarth (1990), and Sand 2, a WO star in the LMC, from Crowther *et al.* (2000) all derived from UV P–Cygni profiles. We use the observed FWHM measurements given by Smith, Shara & Moffat (1990). We find the terminal velocity gradually increases as we move from WCL to WCE, with a sharper (more scattered) increase towards early type WC and WO stars. We fit these data with a simple polynomial that can be described by

$$v_\infty = 73529\,[0.011 + 5.22 \times 10^{-3}(FWHM(\mathrm{C\,IV}) - 28.725)^{0.5}] \qquad (6.1)$$

Equation 6.1 will not provide an exact determination of the terminal velocity but should be effective in inferring a good first order approximation for modelling extragalactic WC stars. It would simply require a FWHM measurement of the strong emission line, C IV $\lambda\lambda$5801-12, before calculating an initial estimate for the terminal velocity of the wind. This would serve as a quick and helpful tool in calculating stellar atmosphere models, of course minor adjustments to the final terminal velocity could possibly be required before accurately reproducing the spectroscopic observations.

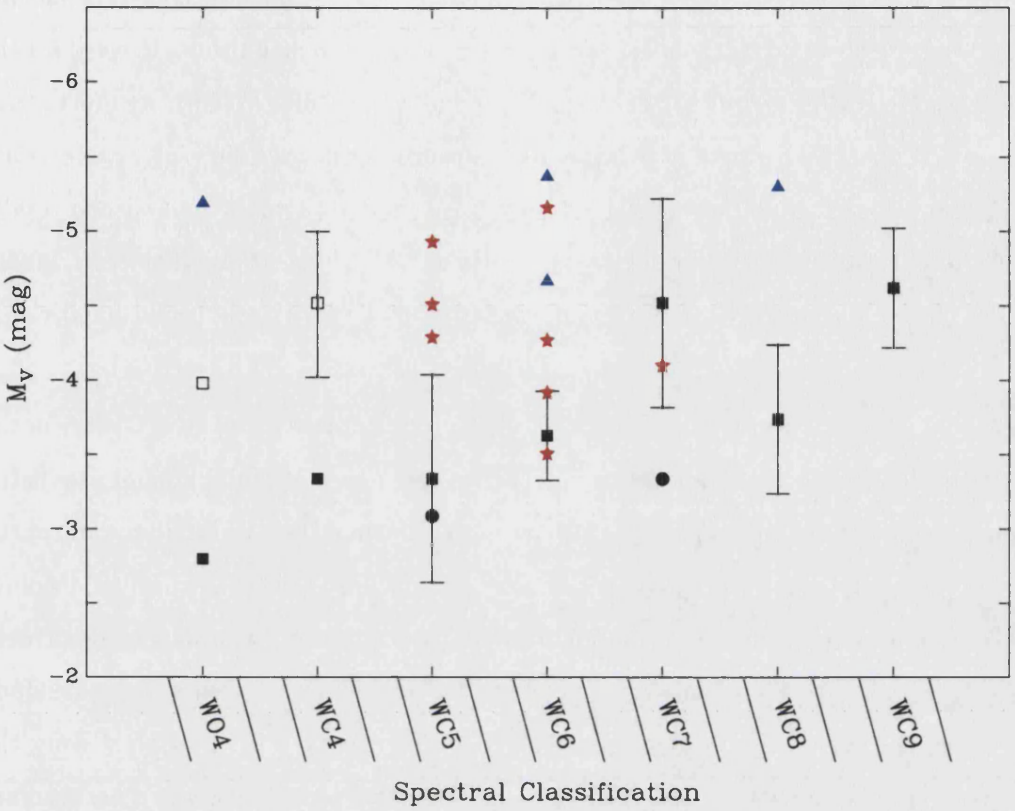

Figure 6.12: A comparison between the absolute visual magnitudes for Galactic WC stars (filled squares), LMC (open square), M 31 (filled triangles), M 33 (filled stars) and the WC stars in IC 10 (filled circles), versus spectral type. The data for the Galactic and LMC WC stars were taken from van der Hucht (2001) and Crowther *et al.* (2002) respectively as well as the LMC WO star, Sand2, taken from Crowther *et al.* (2000).

6.8.2 Absolute Magnitude

Obtaining accurate absolute magnitudes for most WR stars can prove very difficult, this is mainly due to an either unknown, or in most cases, an uncertain distance to the WR star. Combined with this the problem of obtaining an accurate reddening towards the star, the task of calculating precise absolute magnitudes can be very difficult.

Our method for calculating absolute visual magnitudes is to use our observed apparent magnitudes, combined with our model inferred reddenings (except for our sample of M 33 WR stars where we assumed a generic reddening), and assuming the independently derived distances discussed in Chapter 2. Figure 6.12 shows the absolute visual magnitudes,

measured in narrow-band v (Smith 1968), for our sample of extragalactic WC stars inferred from our theoretical single star models. We include the absolute magnitudes derived for the two contaminated WR stars in M 31, MS5 (WC8) and OB48-WR1 (WC6), we must stress that these WR magnitudes are less accurate as they were calculated assuming an uncertain, but realistic, level of contamination. These results are again compared to published results for WC stars in the Galaxy (van der Hucht 2001) and the LMC (Crowther *et al.* 2002), and is the reason why we plot narrow-band, rather than the tabulated, broad-band visual magnitudes.

Figure 6.12 shows that there is a scatter of absolute magnitudes for the WC stars in the Local Group. The majority of our dataset lie below the range of absolute magnitudes listed by van der Hucht (2001) and appear intrinsically brighter than their Galactic counterparts. This is highlighted by the WO star in our sample (M31-MS12), which has an absolute magnitude of M_v = -5.19 mag, compared with M_v = -2.80 mag given by van der Hucht (2001), although this too is a single measurement. To help reduce confusion we also include the observed absolute magnitude for Sand2, a WO4 star located in the LMC, using the observed apparent magnitude and reddening by Crowther *et al.* (2000). The absolute magnitude for Sand2 unfortunately does not agree with either dataset but would suggest that WO4 stars have an absolute magnitude somewhat closer to WC4 stars than our sample would otherwise indicate. These discrepancies highlight the potential difficulties in obtained accurate absolute visual magnitudes for extragalactic WR stars. Even with the large spread of magnitudes for each given spectral type there does not appear to be a distinct separation for WC stars from different galaxies and hence various environments.

The Galactic WC7 stars in Figure 6.12 appear to be much brighter than WC6 stars. We know from modelling these objects that there is very little difference in the structure of their stellar winds. This is not the case when including the WC stars from our larger sample. Unfortunately until many more WC stars are observed and confidently assigned distances then little more can be inferred from this diagram.

It must be noted that we are still comparing small number statistics as both our sample, and those published by van der Hucht (2001) only contain relatively small numbers. Also there are still large uncertainties from the van der Hucht (2001) sample associated with a number of the distances to galactic WR stars (i.e. they are assumed to be members of Clusters/OB associations), allowing for their absolute magnitudes to be under-estimated by one or two magnitudes in M_v.

6.8.3 Wind Efficiency

In this section, we investigate the wind efficiency number calculated from our models, this is sometimes referred to as the 'wind performance number' (see Chapter 3). It describes the fraction of momentum from the radiation that is transferred to the ions in the wind and is given by

$$\eta \equiv \frac{\dot{M} v_\infty}{(L_*/c)} \tag{6.2}$$

Wind efficiency values below 1 indicate that the transfer of wind momentum is achieved through the single scattering of continuum photons, while values in excess of 1 indicate very efficient momentum transfer with multiple scatterings becoming extremely important (Owocki & Gayley 1999) – in the dense, optically thick atmospheres of WR stars, this scenario is valid. Theoretically, it was suggested by Lucy & Abbott (1993) that if the ionization in a WR wind was stratified and multiple scatterings occurred then wind efficiencies of, $\eta \sim 10$ could be explained by line driving.

O-star winds are reasonably well explained by radiation driven wind theory (Puls *et al.* 1996). Unfortunately radiation driven wind theory has problems reproducing the large wind efficiency observed in WR winds. Recent results however, have managed to reduce the wind performance number, through the inclusion of clumping and line blanketing, for WN (Herald, Hillier & Schulte-Ladbeck 2001) and WC stars (De Marco *et al.* 2000), such that the driving mechanism for WR stars can still be explained simply by radiation pressure on (optically thick) lines.

Hillier *et al.* (1998) discussed possible factors which affect a star's wind efficiency and which might help explain why WR stars have such large wind efficiencies. These included a connection to the star's wind ionization, highlighting the importance of Fe in driving the outflow, and another mechanism suggested, which at least influences mass-loss, was rotation. These influences have yet to be confirmed or explained.

We investigate how a number of observable parameters vary with respect to the calculated wind efficiency. Figure 6.13 shows four plots, all comparing the theoretical wind efficiencies as a function of chemical enrichment, temperature, spectral type and terminal velocity. None of these appear to be well correlated and there is a large scatter due to the wide range in parameters which are combined to determine the wind efficiency. Our calculated wind efficiencies agree well with previously published values (e.g. Dessart *et al.* 2000; Nugis & Lamers 2000). They also are of a realistic level ($\eta < 20$) which can

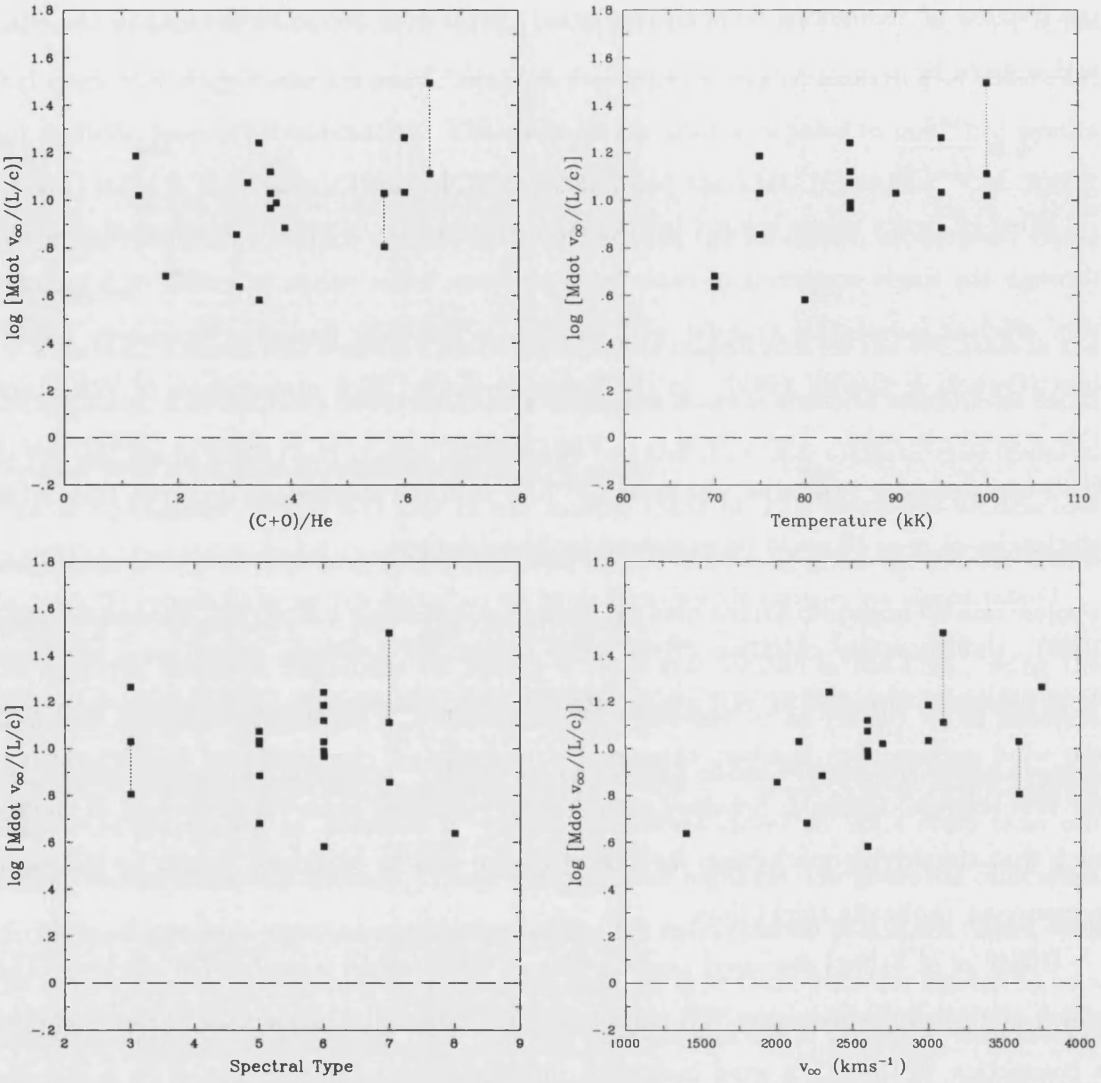

Figure 6.13: Wind efficiency shown as a function of chemical enrichment (i.e. (C+O)/He; upper left panel), temperature (upper right panel), spectral type (lower left panel) and terminal velocity (lower right panel). For the two WR stars where we computed two sets of theoretical models both sets of parameters are shown. The dashed line shows the single-scattering limit.

be attributed to radiation driven winds.

6.8.4 Mass-Loss Rates

As discussed in Chapter 3, theoretical work predicts that massive star winds are driven by radiation pressure from optically thick (and thin) metal lines (Castor, Abbott & Klein 1975). This implies that at a fundamental level the original metal content of the star when it was formed should constrain the outflow from the star. It is well established that the theoretical and observational studies of OB stars have shown that their radiation-driven winds are sensitive to the metallicity from which they were formed (Vink, de Koter & Lamers 2001), providing a metallicity dependence. However, the case for WR stars – their evolved descendants – has remained uncertain, since fully self consistent models of their stellar winds have yet to be presented.

Recent evolutionary models during the WR phase assume; (i) no mass-loss metallicity dependence (Langer 1989); (ii) solely a discrimination between WN and WC stars (Nugis & Lamers 2000); (iii) a full metallicity dependence analogous to O stars (Vanbeveren, de Loore & van Rensbergen 1998). Observationally the importance of establishing a mass-loss dependence is relevant to the ultimate fate of massive stars and gamma-ray bursts (Heger *et al.* 2003). Although it is still believed that radiation-driven winds are responsible for initiating the outflows of WR stars there are still many unanswered questions which could mask the effects of line driving from metal lines, for instance do other enriched elements (e.g. C, N, O) significantly enhance the mass-loss in WR stars?

The question of whether there is a metallicity dependence for mass-loss rates of WR stars was first quantified by Nugis & Lamers (2000). They found that from their sample of 64 Galactic WR stars the mass-loss rates varied with luminosity and metallicity such as:

$$log\dot{M} = -11.00 + 1.29(\pm 0.14)logL + 1.73(\pm 0.42)logY + 0.47(\pm 0.09)logZ \qquad (6.3)$$

with a slightly larger metallicity dependence for WC stars:

$$log\dot{M} = -8.30 + 0.84(\pm 0.17)logL + 2.04(\pm 1.37)logY + 1.04(\pm 1.16)logZ \qquad (6.4)$$

where Y and Z are the chemical composition of helium and metals respectively.

Hamann, Gräfener & Koesterke (2003) recently discussed their results for 15 single Galactic WC4–7 stars, in which they determined approximate stellar parameters using a

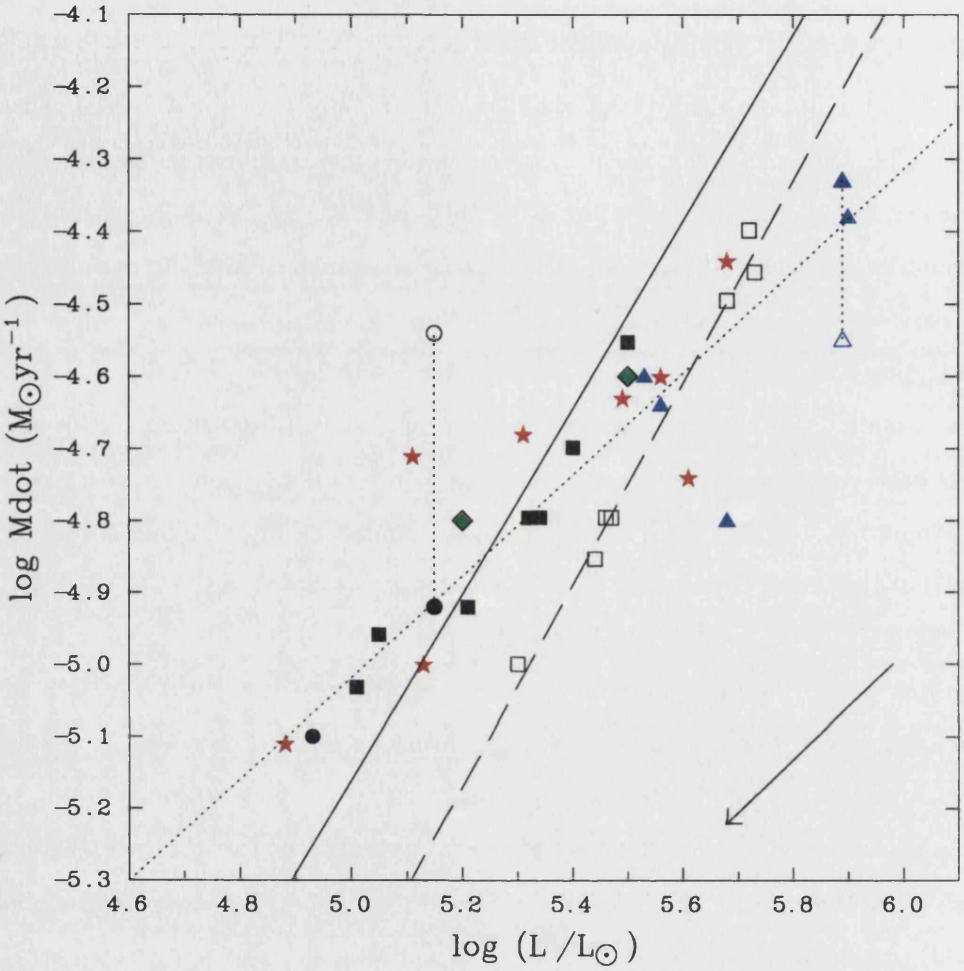

Figure 6.14: Comparison between the mass-loss rates and the luminosities for our sample of single WC stars in M 33 (stars), M 31 (triangles) IC 10 (circles) NGC 300 (diamonds). We also include the sample of Galactic (open squares) and LMC (filled squares) WC stars studied by Crowther *et al.* (2002). The solid line correspond to the calibrations of Nugis & Lamers (2000) for Galactic WR stars, while the dashed line shows the linear fit to the LMC data by Crowther *et al.* (2002). The dotted line represents a least-squares fit to the data. The linear vector shows the effect a contaminating OB star of equal visual continuum luminosity would have on our inferred stellar parameters (see Sect. 6.7).

coarse grid of theoretical models. Comparing their inferred model parameters for their sample they found a small scatter, implying a mass-loss rate – luminosity relationship which is described by

$$log\dot{M} = -8.93 + 1.33log(L/L_{\odot}) \tag{6.5}$$

They note that the spectra of all the WC4–6 stars studied appear extremely similar and that the surface chemistries for their program stars were well approximated by $\beta_{He} = 55\%$ and $\beta_C = 40\%$ (i.e. C/He = 0.24).

A more tailored and comprehensive analysis of WC stars was undertaken by Crowther *et al.* (2002). They performed detailed analysis on a number of LMC WC4 stars and compared these results with Galactic WC stars, analyzed in an identical manner. They found that the Galactic WC stars, compared with their LMC counterparts stars have systematically lower luminosities and higher mass-loss rates. From their results they mathematically describe a mass-loss – metallicity dependence for WC stars with a similar exponent (i.e. $\dot{M} \propto Z^{0.5}$) to that found for O stars (Vink, de Koter & Lamers 2001).

Figure 6.14 compares the observed luminosities and mass-loss rates for our sample of extragalactic WC stars with their LMC and Galactic counterparts. We might expect stars from within a specific galaxy to lie along a particular slope, since all are from the same region. In contrast, individual stars are scattered amongst the Galactic and LMC WC stars, such that no clear metallicity dependence is observed. We perform a least-squares fit to the data and although we do not confirm a metallicity dependence we can measure the relationship between the mass-loss rate and luminosity, which we find to be

$$log\dot{M} = -8.54 + 0.70log(L/L_{\odot}) \tag{6.6}$$

Our derived relationship (shown in Equation 6.6) is similar to the linear relation inferred by (Nugis & Lamers 2000) for WC stars (see Eqn. 6.4), but with a slightly different correlation (i.e. shallower gradient). The opposite can be said when comparing our mass-loss rate – luminosity relationship with that approximated by Hamann, Gräfener & Koesterke (2003). We exclude the (approximate) relation by Hamann, Gräfener & Koesterke (2003) in Figures 6.14 and 6.15 but compare our relation with that inferred by (Nugis & Lamers 2000).

To further test the credence of a mass-loss – metallicity dependence for WC stars we have further divided the dataset into WC stars that lie in regions which we have inferred to

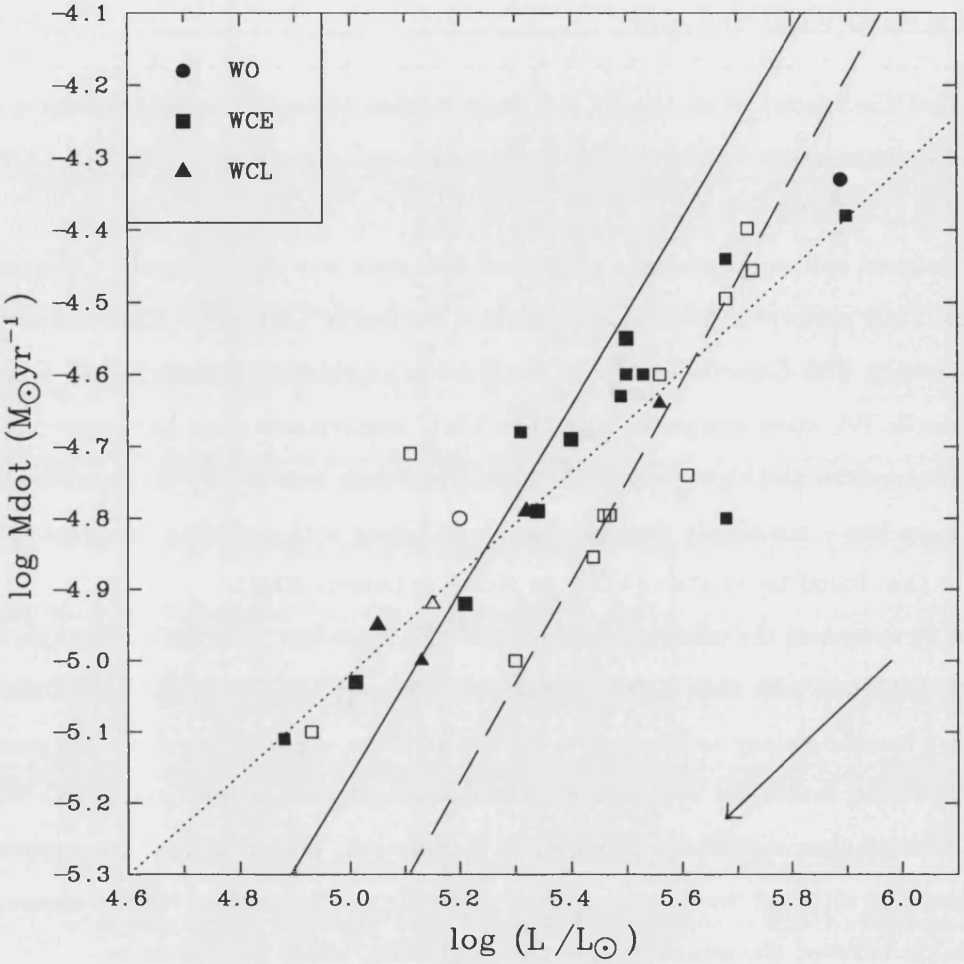

Figure 6.15: Comparison between the mass-loss rates and the luminosities for our sample of single WO stars (circles) WCE stars (squares) and WCL stars (triangles). We again also include the sample of Galactic and LMC WC stars studied by Crowther *et al.* (2002). For stars which are located in regions greater than solar (8.66; Asplund 2003) the symbols appear open whereas WC stars located in sub-solar regions are filled. The solid, dashed and dotted lines as well as the vector are the same as in the previous figure.

have metallicities that are sub- or super-solar. We also segregated the dataset into early- and late-type WC stars. These results are shown in Figure 6.15. We see that there is a spread in mass-loss rates and luminosities. Although they are weakly clustered around the Nugis & Lamers (2000) calibration, their properties conflict with the expected mass-loss – metallicity dependence. For example, we observe stars located in both metal rich and metal poor regions that have similar properties (e.g. MC26 (Massey & Conti 1983) in M 33 and [MAC92] 20 (Massey, Armandroff & Conti 1992) in IC 10). It also calls into question whether mass-loss rates are enhanced with increasing metallicity for WC stars, as proposed by Crowther *et al.* (2002), or whether the carbon and oxygen produced within the star significantly aids line driving, and further accelerates the star's atmosphere. Even though our results do not confirm a metallicity dependence in WC stars, considering the range of environments these stars are located in, the observed scatter is relatively narrow suggesting that the wind densities for WC stars are homogeneous.

6.8.5 Atmospheric Abundances

WR stars provide an important source of chemical enrichment into the surrounding environment via their powerful stellar winds. There are also other sources of chemical enrichment, namely asymptotic giant branch (AGB) stars which are also responsible for producing significant quantities of processed elements. Even though AGB stars have weak winds and produce small quantities of carbon, they are abundant and form in favour of WR stars, as described via the initial mass function. As a result they are still considered important in evolutionary calculations of stellar populations. There are still discrepancies as to which source is more significant at producing CNO elements – WR or AGB stars. Recently, Dray *et al.* (2003) suggested that, at solar metallicities, WR stars produced as much, if not more, carbon enrichment than AGB stars, depending on the stellar models and IMF inferred. Finally, another source of CNO elements comes from type II supernovae (Woosley & Weaver 1995). We assess the amount of chemical enrichment of carbon and oxygen (relative to helium) predicted from our theoretical models.

The majority of the surface carbon and oxygen abundances from our sample all lie within a narrow range. Three WC(E) stars appear to have lower surface abundances compared with the majority of our sample and their Galactic counterparts, MC70 (in M 33), OB10-WR1 (in M 31) and NGC300-#29 (in NGC 300). These three stars have similar surface chemistries to the WCE stars studied in the LMC by Crowther *et al.*

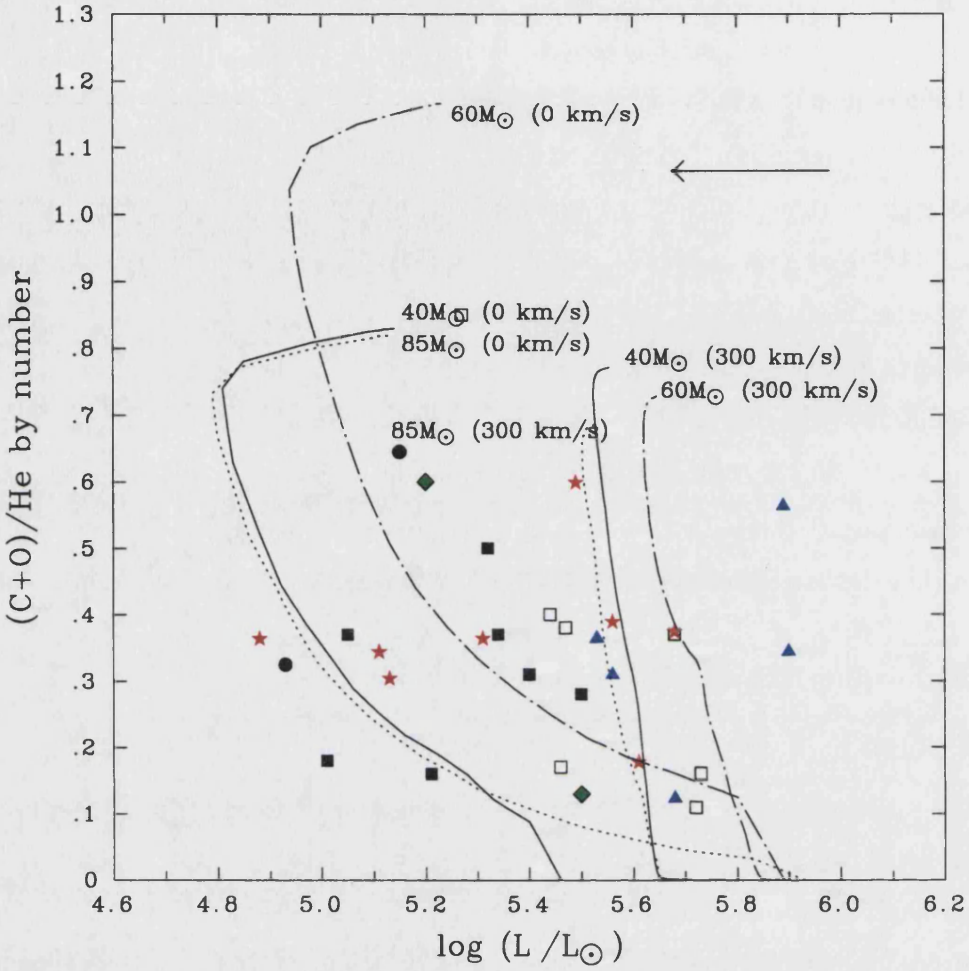

Figure 6.16: Comparison between the (C+O)/He (by number) and the luminosities for our sample of single WC stars in M 33 (stars), M 31 (triangles) IC 10 (circles) NGC 300 (diamonds). We also include the sample of Galactic (opened squares) and LMC (filled squares) WC stars studied by Crowther *et al.* (2002). Evolutionary predictions shown are for non-rotating stars (Meynet *et al.* 1994), and for stars with an initial rotational velocity, v_{ini} = 300kms^{-1} (Meynet & Maeder 2003) all calculated at solar metallicity. Both evolutionary models are shown at three initial stellar masses, 40M$_\odot$ (solid), 60M$_\odot$ (dot-dashed), and 85M$_\odot$ (dotted). The linear vector shows the effect of a contaminating OB star of equal visual continuum brightness would have on our calculated parameters (see Sect. 6.7).

(2002). Similarly we find three WCE/WOE stars with chemically enriched winds, AM17 (in M33) MS12 (in M31) and NGC300-#48 (in NGC300). To match the observed line strengths of our abundance diagnostics, O III-V λ5590, He II λ5411 and C IV λ5471, in these three stars, our models required a larger surface abundance of carbon and especially oxygen compared with the other WC stars in our sample.

Figure 6.16 shows our calculated surface chemistries, (C+O)/He, against their respective luminosity for all the WC stars in our sample. We also show the results published by Crowther *et al.* (2002) and references therein. Individual surface chemistries for our sample of WC stars in M33 and M31 are similar to those predicted for their Galactic and LMC counterparts, with a scatter of abundances amongst late and early spectral types. Recent work by Crowther *et al.* (2002) suggested that the WC spectral type is not governed by a variable surface abundance ratio of processed elements (i.e. carbon and oxygen) as first proposed by Smith & Maeder (1991), but in fact is dominated by mass-loss rates, with secondary effects from temperature variations.

We also show evolutionary predictions for non-rotating (Meynet *et al.* 1994) and more recent, rotating models (Meynet & Maeder 2003), for WR stars at solar metallicity. The rotational models shown were calculated with an initial velocity, $v_{\rm ini} = 300{\rm kms}^{-1}$. As a result of mass-loss and mixing the amount of He-burning products observed at the stellar surface are enhanced, subsequently causing the observed (C+O)/He ratio to increase. Both the lifetimes and the predicted evolutionary tracks are drastically modified with the inclusion of rotation (Meynet & Maeder 2003). The rotational model for a $85{\rm M}_{\odot}$ star is seen to be less luminous than the lower mass models. This is because the track enters the WC phase with a lower mass, which is mainly due to an extended WN phase relative to the non-rotating case.

We again divide the dataset into two groups, those located in regions with metallicity greater than solar, and those which are in regions with metallicities less than solar. These results are shown in Figure 6.17, where we compare the surface chemistries, (C+O)/He (by number), and the luminosities for our sample of WC stars. We find that the abundances of carbon and oxygen are similar for both late- and early-type WC stars and span a range of approximately 0.1–0.5 by number (relative to He). There is however, an enhanced chemistry observed in early-type WO stars and a select number of early-type WC stars which could well be transitional WO stars. Although we do not confirm a WC spectral type – carbon abundance relationship predicted by Smith & Maeder (1991), the carbon-

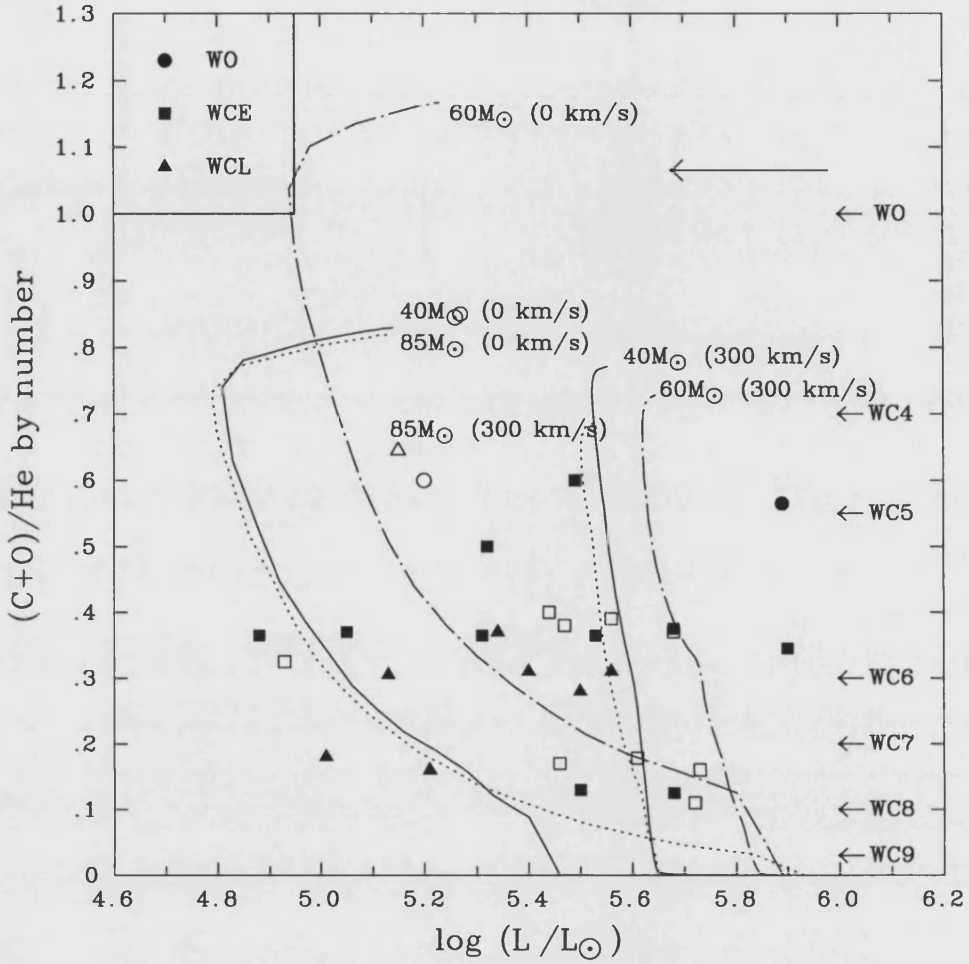

Figure 6.17: Comparison between the (C+O)/He (by number) and the luminosities for our sample of single WO stars (circles) WCE stars (squares) and WCL stars (triangles). We also include the sample of Galactic and LMC WC stars studied by Crowther *et al.* (2002). For stars which are located in regions greater than solar (8.66; Asplund 2003) the symbols appear open whereas WC stars located in sub-solar regions are filled. The same evolutionary tracks are shown as in the previous figure. The estimated (C+O)/He ratios for each WC spectral type by Smith & Maeder (1991) are also shown.

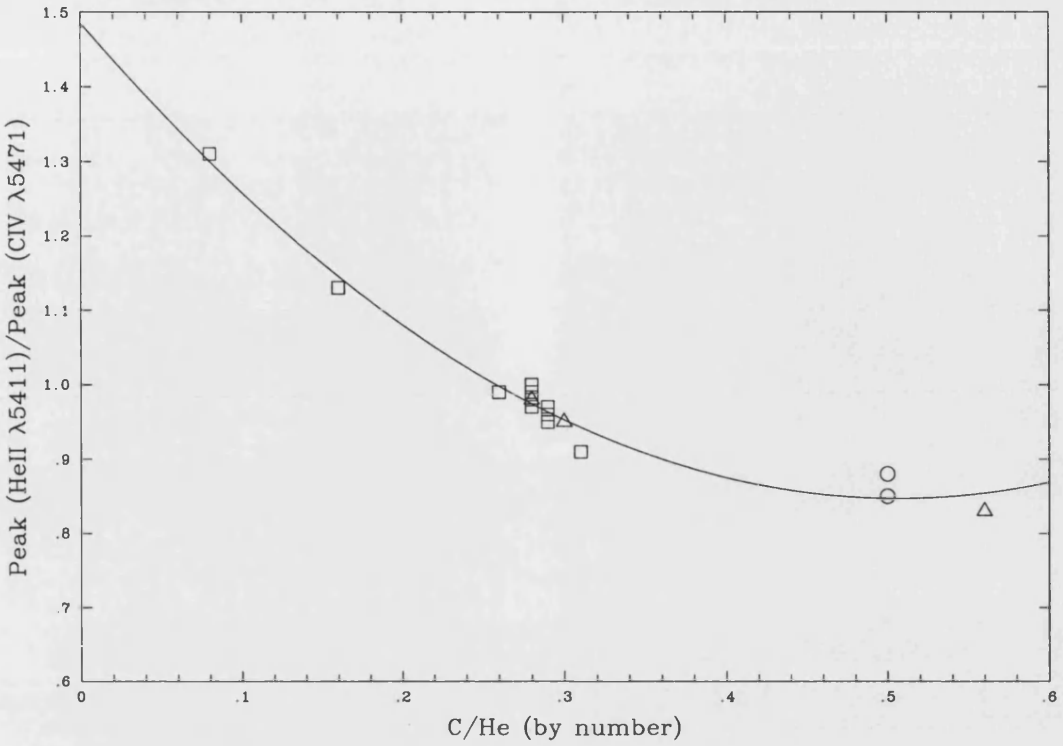

Figure 6.18: Calculated carbon abundance, C/He, by number versus peak flux ratio of He II λ5411 and C IV λ5471 for WCL stars (triangles), WCE (squares) and WO stars (circles). The solid line shows an unweighted, least-squares polynomial fit to the data.

oxygen abundance could be a useful tool in studies of WO stars. Finally by comparing our dataset, spanning a factor of ∼10 in metallicity, we find that the observed abundances in WC stars appear insensitive to metallicity variations.

We use our representative dataset of WC stars to investigate whether our derived parameters will assist future studies of extragalactic WR stars. As described in Section 6.8.1, we were able to determine a simple formula which could then be used to equate an easily observable, in this case the FWHM(C IV λλ5801-12), and yield an approximation for the star's terminal wind velocity. We continue with these sentiments; this time we compare the theoretical peak flux ratio of He II λ5411 and C IV λ5471 against the derived C/He ratio (by number). Figure 6.18 shows our results. At low carbon abundances the ratio of peak flux is a steep gradient, this becomes much shallower at intermediate and larger abundances. In an attempt to use these results so that the observed peak flux ratio can be used as an indicator of carbon abundance, we fit a unweighted, least-squares polynomial

fit to the data which can be described by

$$C/He = 0.201\,[2.524 - 3.158(Peak_{He}/Peak_{C} - 0.847)^{0.5}] \quad (6.7)$$

As long as these weak emission lines can be observed and accurately measured then Equation 6.7 should give a first order approximation for the C/He abundance, which can then be used as a quick tool to obtain an initial estimate for modelling extragalactic WC stars.

Unfortunately with a lack of calculated carbon abundances in the region 0.32 – 0.50 (C/He, by number), the relationship shown in Equation 6.7 is relatively insensitive to abundances when C/He > 0.32. Figure 6.18 does however, support the suggestion that the parameters of WC stars are widely uniform in nature, as discussed in Section 6.8.4, where we find the majority of WC stars have C/He $\simeq$ 0.3 with only a few objects largely deviating from this cluster.

6.8.6 Current Stellar Masses

Finally, we compare the present masses for the WC stars in our dataset using the inferred stellar parameters. We calculate these stellar masses based on their derived luminosities assuming the relationship described by Schaerer & Maeder (1992). This calibration is valid for WR stars located in various environments as the luminosity is insensitive to chemical composition (Schaerer & Maeder 1992). We find that the WC stars in M 33 lie in the range 6–18$M_{\odot}$, whereas our sample of WC stars in M 31 are predicted to be somewhat higher, ranging 14–25$M_{\odot}$. Interestingly, for the two WC stars studied in IC 10, a low metallicity environment, we calculate a low range of present masses, 7–9$M_{\odot}$– contrary to what you might expect – considering the large initial mass predicted by evolutionary models to form a WC star in such a metal deficit galaxy. Suggesting that either our derived luminosities are severely under-estimated, or that both stars have lost a significant amount of material during their lifetime. Given the difficulties reproducing the observed spectrum for [MAC92] 10 and the unusual nature of this star it is difficult to directly compare with the rest of the sample. The predicted stellar masses for the WC stars in NGC 300 lie within the range 9–14$M_{\odot}$, similar to those predicted for the WC stars in M 33. These current masses also agree well with those inferred by Crowther *et al.* (2002) for six WC stars in the LMC, in which they claim lie between 12–18$M_{\odot}$.

6.9 Conclusions

We have obtained high-resolution optical spectroscopy for a large sample of WC stars located in a number of Local Group galaxies, as well as NGC 300 in the Sculptor Group of galaxies. From our sample we used a series of techniques to identify potentially single WR candidates, of which 17 were carbon-sequence WR stars. Using these probable single WC stars we have evaluated their stellar parameters using the non-LTE, line blanketed model atmosphere code, CMFGEN (Hillier & Miller 1998), accounting for the effect of iron-group elements which are vital in studying WC stars. A comparison of these inferred parameters have surprisingly found that the intrinsic properties for a WC star formed in IC 10 ($\sim$0.3$Z_{\odot}$) are very similar to a WC star formed in M 31 ($\sim$1.5$Z_{\odot}$). This is seen through a number of observables; from mass-loss rates to surface abundances.

Our studies of terminal wind velocities have found a natural progression of increasing terminal wind velocity towards earlier spectral type. We use our calculated terminal velocities and compare them with accurately derived terminal velocities measured from UV absorption profiles. These are then plotted against observed FWHM(C IV $\lambda\lambda$5801-12). We find an increasing but shallow correlation with FWHM and terminal velocity for narrow-lined WC stars, with a somewhat sharper correlation for broad-lined WC stars. This relationship was fitted with a second order polynomial (see Eqn. 6.1), and will provide users with a first order approximation when estimating terminal velocities such that they can be modelled.

We have also compared the absolute visual magnitudes calculated from our sample with those listed in van der Hucht (2001). We observe a (weak) trend among WC spectral types with later type WC stars appearing intrinsically brighter than their early type counterparts. Although we find an increase in the absolute magnitude towards earlier spectral types, we still find a relatively large scatter. These discrepancies can be attributed to a number of factors; mainly concerning the uncertainties in the observed reddenings and distances, but there are also potential errors in incorrect measurements of the apparent visual magnitudes and highlights the caution and difficulty required in determining the absolute magnitudes for extragalactic stars.

The wind efficiency was calculated for our sample of WC stars and was found to be in good agreement with previously published wind efficiencies. From our sample we find that the wind efficiency is typically $\sim$15. Compared with early determinations this is

somewhat reduced, and can be explained by the inclusion of line-blanketing and clumping into our theoretical calculations. Thankfully wind efficiencies of a factor ten times above the single scattering limit can be realistically explained by radiation driven winds, rather than requiring an unknown mechanism. We contrast the derived wind efficiency for our sample against a number of other observable parameters (e.g. abundance, T, v_∞, spectral type) and conclude that none of them appear well correlated.

Theoretically, it is unclear whether WR stars, both WN and WC, are sensitive to the metallicity of the material from which they were formed. As discussed there have been a number of previous descriptions to account for any mass-loss metallicity dependence (e.g. Langer 1989; Nugis & Lamers 2000), although none have been conclusive. We have compared the observed luminosities and mass-loss rates for our sample of WC stars and they do not appear sensitive to metallicity, as originally suggested by Crowther *et al.* (2002). Our results show a spread in mass-loss rates and luminosities for WC stars, with similar parameters being found for WC stars in the metal deficient galaxy IC 10 as for those in the much more metal-rich galaxy M 31. Although we find a scatter, these results are still well approximated by the intrinsic WR calibration calculated by Nugis & Lamers (2000). From the fact that there is very little deviation from this calibration, we claim that the wind density for WC stars is intrinsically uniform. There are still many unanswered questions, such as the role enriched elements such as carbon and oxygen play in significantly enhancing line driving. Plus there are complexities which arise from other factors such as the ionization stratification within a star's atmosphere and photon blocking. These added complications could possibly lead to instabilities which could result in a variable mass-loss rate (Owocki & Gayley 1999).

A similar conclusion was drawn when comparing the calculated surface abundances from our sample. We find that generally the surface chemistries from our sample are very similar to Galactic WC5–8 stars (with known distances) observed by Crowther *et al.* (2002). Also it appears that they is very little difference between the carbon and oxygen abundances observed for stars located in different environments and between early- and late-type WC stars. This implies that the surface chemistries of processed elements (i.e. C and O) are unaffected by metallicity variations.

In summary, the fundamental parameters for our sample of WC stars are similar to Galactic and LMC WCE stars studied in the same manner. This evidence would suggest that the structure of a WC(E) stellar wind is inherently the same – a conclusion supported

by Hamann, Gräfener & Koesterke (2003). We conclude that we find no observational evidence for WC stars displaying a metallicity dependence, and call into question whether mass-loss rates are enhanced with increasing metallicity for WC stars. Unfortunately, due to the uncertainties still surrounding extragalactic metallicity gradients this question cannot be confidently answered. Although the majority of our sample show a homogeneous trend in stellar parameters, we have identified some rather interesting candidates, namely [MAC92] 10 (Massey, Armandroff & Conti 1992) in IC 10, which require further investigation beyond the scope of this work. Further observational studies are required for an even larger sample of WC stars, with accurately evaluated metallicities, before conclusive evidence can be found that WC stars show any to metallicity dependency.

CHAPTER 7

Discussion and Future Work

We conclude by reviewing the main points outlined by this work, highlighting the principal conclusions from most sections. This is followed by a brief description of possible developments for future work.

7.1 Summary

7.1.1 Observations of Extra-Galactic WR stars

With recent advances in astronomical instrumentation, massive stars in Local Group galaxies, with metallicity environments widely different from that of the solar neighbourhood, are now easily accessible to ground-based telescopes. Observationally we achieve two targets: to identify new Wolf-Rayet (WR) candidates through deep, narrow-band imaging surveys, and to obtain new, high quality spectroscopic observations for known extra-galactic WR stars such that detailed analysis may be performed. We present high quality VLT-Focal Reduced/Low Dispersion Spectrograph #2 (FORS2) images for two late-type spiral galaxies; NGC 300 and M 83. Both of these galaxies are located beyond the Local Group at distances in excess of a Mpc. Through the use of narrow-band interference filters, utilizing the strong He II λ4686 and/or C III-IV $\lambda\lambda$4650,4660 emission lines, we have identified a large number of previously unknown WR stars revealing a significant increase in the known population of these galaxies, resulting in new WR catalogues.

Our photometric survey of the nearby galaxy NGC 300 (D $\simeq$ 2.0Mpc) detected 58 WR stars in the central regions of which only 16 had been previously spectroscopically

confirmed – there are a further two known WR stars located beyond our surveyed region – totalling the WR population in NGC 300 to 60. We also spectroscopically observed eight WR stars, four previously known and four newly identified from our survey, all of which are indeed bona fide WR stars. We compare the observed excess magnitudes with spectroscopically confirmed WR stars to infer spectral types. This results in WC/WN $\geq$ 15/43 $\simeq$ 0.35, although until all WR candidates have been spectroscopically observed this ratio is still uncertain.

We also observe the large face-on spiral galaxy M 83, located well beyond the Local Group at a distance of $\simeq$ 4.5Mpc. Previous observational studies examining the large H II region populations in M 83 have indicated an unusually metal rich environment. Uncertainties over the exact metallicity gradient still remain although recently it was suggested that the metallicity in the central regions of M 83 are $\sim 2.5 Z_{\odot}$ (Bresolin & Kennicutt 2002). Our narrow-band imaging encompasses the entire galaxy and reveals over 330 WR candidates. Recent follow-up spectroscopic observations have had an extremely high success rate in confirming these candidates as genuine WR stars. Furthermore, a large proportion of these bona-fide WR stars are late-type WC stars, currently confined to the solar neighbourhood and central regions of M 31, suggesting that M 83 proves a unique metal-rich environment to study massive stars.

We present new, medium resolution spectroscopic observations for a representative sample of known extra-galactic WR stars, in M 33, M 31 and IC 10, significantly improving on existing data. These data were collected using both modern multi-object spectrographs and long-slit spectrographs on both intermediate and large ground-based optical facilities. These galaxies are all members of the Local Group and span a metallicity range of approximately a factor of $\sim$10, providing us with a variety of conditions in which to study individual WR stars. Through the use of the modern non-LTE, expanding atmosphere code, CMFGEN, we are able to model these observations to derive fundamental stellar parameters. This has allowed us to investigate the role that metallicity plays in the derived stellar properties for both WN and WC subtypes.

We have obtained spectroscopy of a large sample of WR stars in M 33 with the Multi-Object Spectrograph (MOS) on the 3.6-metre Canada-France-Hawaii Telescope (CFHT), including 26 WC stars, 13 WN stars plus a WN/C star. In general, spectral types are merely refined, although the spectral type of X9 from Massey & Johnson (1998) is revised from WNL?+abs to WC4+abs, whilst their G1 and C21 candidates are not confirmed as

WR stars. OB66-25, identified by Massey *et al.* (1995) is updated from WN8 to Of.

Due to its large angular size and high inclination we were unable to utilize the benefits of observing M 31 with a Multi-Object Spectrograph and instead used ISIS, the double-armed (long-slit) spectrograph on the 4.2-metre William Herschel Telescope (WHT). We observed four WC stars, improving their spectral types. The spectral classification of MS12, original identified by Moffat & Shara (1983), was refined from WC to an early-type WO star, owing to the clear detection of O IV λ3412 and O VI λ3834.

We also chose to study the WR population in the dwarf irregular galaxy, IC 10. Studies of H II regions in this galaxy point towards a metallicity similar to the SMC ($\sim$0.3$Z_{\odot}$), yet studies of massive stars within IC 10 found a surprisingly large number of WR stars (Massey & Johnson 1998) given its metal-poor environment. Furthermore, the assigned metallicity-sensitive WC/WN ratio for IC 10 of $\sim$2 largely disagrees with the observed trend among Local Group galaxies. Other observational programs found evidence to suggest that this galaxy has recently undergone an intense burst of star formation; due to (i) its large population of H II regions (Hodge & Lee 1990), (ii) its observed non-thermal radio continuum (Yang & Skillman 1993), (iii) its large far-IR luminosity (Melisse & Israel 1994) and (iv) more directly from its high surface density of massive stars (Massey & Armandroff 1995). To confuse issues further, a narrow-band survey by Royer *et al.* (2001) detected new WR stars, increasing the WR population, but more importantly they claimed that three of these were of the rare WC9 spectral type.

Observations of WR candidates previously identified by Massey, Armandroff & Conti (1992) and Royer *et al.* (2001) were obtained using the Gemini Multi-Object Spectrograph (GMOS) on the 8-metre Gemini-North telescope and the 3.6-metre CFHT-MOS. In total we spectroscopically confirm 26 WR stars in IC 10. Generally, of the WR stars listed by Massey, Armandroff & Conti (1992) we simply refine spectral classifications, except for [MAC92] 5, which we revise from WN to a rare WN/CE, intermediate type WR star and the two WR candidates [MAC92] 3 and [MAC92] 16, which our survey revealed not to be genuine WR stars. Our dataset also includes spectroscopic observations of the 13 WR candidates identified photometrically by Royer *et al.* (2001). We reveal that 9 of these candidates are bona-fide WR stars, while the three suspected WC9 stars identified (RSMV 1, 3 and 7), plus the WC candidate RSMV 4 were not verified to be genuine WR stars. These revisions to the spectral types alter the WC/WN ratio to a somewhat lower value of 14/11 $\simeq$ 1.3. Recent narrow-band imaging by Massey & Holmes (2002) has suggested that there

are another ~75 WN stars unaccounted for in IC 10 – if spectroscopically confirmed this would alter the WC/WN ratio providing agreement with the other Local Group galaxies.

7.1.2 Extra-Galactic Metallicity Gradients

If we are to compare observationally inferred stellar parameters of WR stars with a view to searching for metallicity effects, it is vital that we use accurate metallicity estimates. Unfortunately, for almost all the Local Group galaxies and beyond, there is a lack of recent observational surveys examining the content of H II regions used to determine the local metallicity. Complications are further increased due to the number of methods, theoretical and observational, available to estimate metallicities from oxygen emission lines. For instance, there is a lack of consensus within the astronomical community as to which method/models best predict metallicities using H II regions.

The most accurate technique to calculate oxygen abundances is to initially constrain the electron temperature using the [O III] λ4363 emission line. Unfortunately, this line is weak in metal-poor regions and in metal-rich environments it is absent. Combining this with attempting to obtain spectroscopic observations with sufficient signal-to-noise to detect [O III] λ4363 from a H II region located in a nearby galaxy makes the task of determining temperature derived abundances extremely difficult. These complications led to an empirical calibration being developed by Pagel *et al.* (1979) which only relied on observing the strong [O II] $\lambda\lambda$3726,3729 and [O III] $\lambda\lambda$4959,5007 emission lines and subsequently is referred to the $R_{2,3}$ method. Numerous variations and re-calibrations of the $R_{2,3}$ method have since been established (e.g. Edmunds & Pagel 1984; Zaritsky, Kennicutt & Huchra 1994; Pilyugin 2000).

We investigate which of the revised calibrations best approximates the abundances determined from temperature calculations. We do this by comparing the Galactic metallicity gradient derived by Shaver *et al.* (1983), who combined both radio and optical spectroscopy to determine electron temperatures, with oxygen abundances determined for the same H II regions using recent calibrations that only required observations of the strong [O II] and [O III] emission lines. Our comparison reveals that the re-calibrated $R_{2,3}$ method described by Pilyugin (2000) best reproduces the temperature derived abundances by Shaver *et al.* (1983). For this reason we employ the calibration by Pilyugin (2000) to re-examine the metallicity gradients for three spiral galaxies in which we have observed WR stars, M 33, M 31 and NGC 300 – the results of which are considered in a later analysis.

7.1.3 Spectroscopic Morphologies

Our large collection of extra-galactic WR spectra has allowed us to perform a series of simple analyses providing us with information on their morphologies and their potential multiplicity. Comparing the measured line widths for WC stars in spiral galaxies we re-examine the correlation between the line width of C IV $\lambda\lambda$5801-12 with increasing galactocentric distance, originally suggested by Schild, Smith & Willis (1990) and later supported by Willis, Schild & Smith (1992). Our results do not indicate a tight correlation as initially suggested by Schild, Smith & Willis (1990) and that at a intermediate galactocentric distances there is a large scatter in line widths. Although there remains a distinct absence of broad line WC stars in the inner regions and narrow-line WC stars in the outer regions. We suggest a possible explanation for this weak trend in terms of a bias in the distribution of spectral types across a galaxy where there exists a metallicity gradient. This would result in narrow-lined, late-type WC stars forming in the central (metal-rich) regions and broad-lined, early-type WC stars forming in the outer (metal-poor) regions. In fact, the WC population across M 33 displays this distribution, with only the latest spectral types being confined to the galactic centre – there is also evidence to suggest that this is also seen in the solar neighbourhood. We also investigate the line width of WN stars and find an even larger scatter.

We further utilize our flux calibrated dataset by investigating the claim by Smith, Shara & Moffat (1990) who found that the early-type WC stars in the LMC appeared to have uniform C IV $\lambda\lambda$5801-12 line fluxes of log F_λ = -7.6$\pm$0.15 ergs^{-1}cm^{-2} once normalized to 1kpc. We repeat this technique using the spectra which have been reliably flux calibrated. For the WC stars in M 31 we find the averaged line flux, excluding the WCL star MS5, is log F_λ = -7.6$\pm^{+0.2}_{-0.3}$ ergs^{-1}cm^{-2}. In reasonable agreement with the LMC line fluxes found by Smith, Shara & Moffat (1990). For our sample of early-type WC stars in IC 10 we calculated an average line flux of log F_λ = -7.5$^{+0.2}_{-0.6}$ ergs^{-1}cm^{-2}, again supporting the initial result by Smith, Shara & Moffat (1990) but with much larger errors. We associate this scatter in fluxes by our imprecise reddenings. Finally, we also compare the C IV $\lambda\lambda$5801-12 line fluxes for our program stars in NGC 300. The average, reddening corrected, normalized fluxes for the WCE stars in NGC 300 were somewhat smaller with, log F_λ = -7.8$\pm$0.2 ergs^{-1}cm^{-2}. We suggest that this larger discrepancy is again connected to our assumed reddening in NGC 300, as we simply applied a generic reddening for each star.

From a comparison of measured reddenings across NGC 300 in Section 2.5.3 we conclude that it appears highly variable. Considering these findings and the range of galaxies and environments in which these stars are located, we confirm that there does appear to be a universal line flux of C IV $\lambda\lambda$5801-12 for early-type WC stars.

We also explore the effects of multiplicity using measured line strengths to identify potentially single WR stars. We employ two different techniques for our un-calibrated and calibrated spectra. For our dataset of M 33 WR stars we compare their observed line strengths of either C IV $\lambda\lambda$5801-12 or He II λ4686 as a function of spectral type with Galactic and LMC WR stars for which the binary nature is well known. The idea is simple; the more a WR spectrum becomes contaminated, the more diluted the observed line strength will appear. Albeit rather simplistic, this is successful at identifying obvious single stars. For the eight WC stars we suggest are single, we perform a further consistency check by locating them in HST WFPC2 images. For the six where detailed images were available, we discover that each star appears well resolved and isolated. We also find that for two stars which have low observed line strengths and hence contaminated, both appeared to be non-gaussian and have multiple components which are unresolved at the resolution of the images. Although we do note that at the observed resolution we would be unable to resolve a close binary system.

Our second, more reliable, method compares the observed line strengths of C IV $\lambda\lambda$5801-12 with the calculated absolute magnitudes. This technique has a two-fold effect, accounting for both diluted line strengths and excessively bright visual continua, such that a WC star with a binary companion would have a weak observed C IV $\lambda\lambda$5801-12 equivalent width and a much brighter absolute magnitude compared with a single WC star.

7.1.4 Detailed Analysis and Comparison of Extra-Galactic WN stars

We have computed a series of iterative theoretical models which reproduce the optical spectra for a number of previously observed single Galactic, LMC, SMC and NGC 6822 WN stars deriving stellar parameters. We use a series of diagnostic lines to determine the properties of each star, namely, temperature, ionization balance, mass-loss, terminal wind velocity and abundances (e.g. H, He, C, N and O). We also extend this analysis to our sample of single WN stars in M 33, providing us with a unique insight into the WN population across the Local Group of galaxies.

Unlike previous detailed studies of individual WR stars our analysis is limited to utilizing only the optical spectra, so to check the validity of our approach we compare our theoretical spectra with archival IUE observations of Galactic and LMC WN stars. Overall, the agreement is good with the majority of our models reproducing both the line strengths and widths of the predominant emission lines in the UV (i.e. C IV λ1550, He II λ1640 and N IV λ1718). This check provides us with confidence that our results are not unrealistic even if they could be refined.

Once we had analysed all 27 separate spectra we then simply collated and compared their inferred parameters. Comparing our determined terminal wind velocities from our sample we find a steady increase in velocity from late to early spectral type. We also found that the absolute visual magnitudes decrease from early to late spectral type – both comparisons displayed a large scatter. The next parameter we investigated was the wind efficiency number, η, which describes how effectively radiation momentum is transfered into the wind. We found that our derived wind efficiencies were consistently lower than had been previously published. These reductions are connected to the fact that our models account for clumping and line-blanketing and hence lower the derived mass-loss rates. These revised wind efficiencies are $\sim$0.5dex above the theoretical single scattering limit such that they may be explained by the theory of radiation driven winds, accounting for a moderate contribution from multiple scattering. We also concluded that the only parameter which appeared sensitive to the wind efficiency was the chemical abundance of hydrogen, such that it increased with decreasing mass fraction of hydrogen.

Further investigation of the derived mass-loss rates indicate that there is very little difference in mass-loss rates between the Galactic WN stars and their counterparts in the LMC. There is however, a noticeable difference when our sample of SMC WN stars are also considered – with our inferred parameters suggesting significantly weaker winds and higher luminosities. It is clear, even through visual inspection of their optical spectra that their stellar winds are weaker. A comparison of mass-loss rates and luminosities prompted a speculative proposal that there is a mass-loss – metallicity dependence for WN stars; if confirmed, it would be somewhat stronger than predicted for O stars ($\dot{M} \propto Z^{0.5-0.8}$). We require further spectroscopic observations of WN stars, ideally located in an extreme variety of metallicities before we can confidently quantify a metallicity dependence for WN stars.

Our derived abundances are good approximations, with a limited number of abundance

sensitive diagnostic lines available. Given these uncertainties our results still agree well with current evolutionary models (Meynet & Maeder 2003). We see that the majority of the WN stars in both the Magellanic Clouds contain significant quantities of hydrogen in their atmospheres, while the majority of the Galactic and M 33 stars appear hydrogen free. We also support the idea suggested by Meynet & Maeder (2003) that the derived mass fractions of hydrogen could be a used as a tool to investigate the evolutionary sequence of massive stars.

7.1.5 Detailed Analysis and Comparison of Extra-Galactic WC stars

Fortunately, there have been a number of previous detailed spectroscopic studies carried out on WC stars in the Galaxy (e.g. De Marco *et al.* 2000; Dessart *et al.* 2000) and in the Magellanic Clouds (e.g. Crowther *et al.* 2002). We utilize these results and compare our derived parameters for 17 single WC stars in M 33, M 31, IC 10 and NGC 300. An identical method of computing synthetic spectra was employed for our program WC stars as for our WN sample, ultimately reproducing the observed optical spectra and hence determining their stellar parameters.

As with our dataset of WN stars we perform a series of simple comparisons. Our derived terminal wind velocities indicate a progression of increasing terminal wind velocity towards earlier spectral type. Our absolute visual magnitudes display an even weaker correlation with spectral subtype; with late-type WC stars appearing intrinsically brighter than their early-type counterparts. These discrepancies in extra-galactic WR stars, particular highlighted among WO stars, can be attributed to a number of factors; mainly concerning the uncertainties in the observed reddenings and distances and emphasise the difficulties in obtaining accurate absolute magnitudes. The wind efficiencies for our sample of WC stars was found to be typically $\sim$15 and are in good agreement with previously determined values. Theory suggests that wind efficiencies of a factor ten times above the single scattering limit can be realistically explained by radiation driven winds. Further examination of our calculated values did not display any correlation with any other derived parameters.

We have compared the observed luminosities and mass-loss rates for our sample of single WC stars and unlike our program WN stars they do not appear sensitive to metallicity, as suggested by Crowther *et al.* (2002). In fact, our results show a range in observed mass-loss rates and luminosities, with similar derived parameters for WC stars in the

metal-poor galaxy IC 10 as for those in the metal-rich galaxy M 31. For example, the majority (8/12 or 67%) of the early-type WC stars studied all had derived temperatures in the range 80–95kK. These results are still well approximated by the intrinsic WR calibration calculated by Nugis & Lamers (2000) and is similar to the least-squares fit calculated from our dataset. Due to the relatively small deviations from our inferred calibration, we claim that the wind density for an early-type WC star, irrespective of the metallicity, is universally the same. There are of course complications and unanswered questions, such as the role enriched elements such as carbon and oxygen play in further enhancing line driving. We find a similar conclusion when comparing the calculated surface abundances from our sample of WC stars. Generally, the surface chemistries from our sample are very similar to Galactic WC5–8 stars observed by Crowther *et al.* (2002). It would appear that there is also very little difference between the carbon and oxygen abundances observed for stars located in different galaxies and early- and late-type WC stars. This implies that the surface chemistries of processed elements (i.e. C and O) too are unaffected by metallicity variations.

These results can be combined with earlier evidence indicating a uniform line flux for WCE stars and the initial results from Hamann, Gräfener & Koesterke (2003) which also suggest that WC stars display an narrow range of observed properties. Considering all these facts and results, we conclude there is strong evidence to suggest that the environmental metallicity does not play an important role in determining the fundamental properties for (at least early-type) WC stars.

7.2 Future Work

With recent instrumental improvements at 4-metre telescopes (e.g. CFHT-MOS) and the increased accessibility to 8-metre telescopes with modern facilities (e.g. Gemini-GMOS), we now face a prosperous age, enabling observational studies of massive stars in Local Group galaxies and beyond. These facilities offer the possibility of simultaneously observing many WR stars, increasing the exposure time by an order of magnitude over standard (single) long-slit spectroscopy, thereby delivering spectra with a signal-to-noise ratio sufficiently high to permit a detailed quantitative spectroscopic analysis.

Currently, the main limitation for observational studies of massive stars in nearby galaxies is achieving sufficient spatial resolution such that individual stars may be resolved,

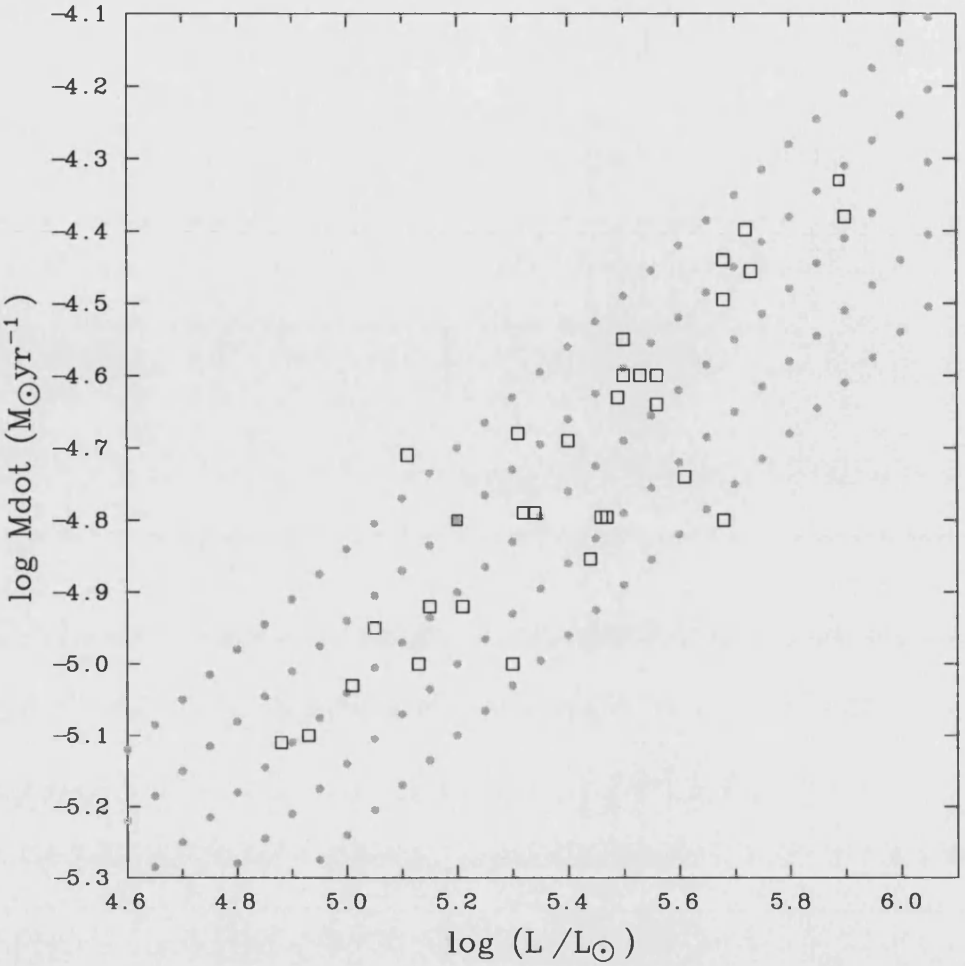

Figure 7.1: Proposed grid of 138 theoretical WC models (filled dots) following the mass-loss luminosity relationship inferred from our results. These models would encompass (almost) all the observed WC stars in our dataset (open squares).

reducing contamination from nearby stars and obtaining reliable photometry. These issues are not important when considering stars in the Magellanic Clouds, but when observational studies are extended to M 33, for example, then the question of multiplicity becomes significant. For instance, observations of stars in the LMC ($D \simeq 50$kpc) at a $1''$ resolution subtends to a 0.25pc spatial scale. To match this resolving power at a distance of M 33 ($D \simeq 816$kpc) you would need to observe the galaxy at a resolution of $0.06''$. This proves challenging, even with the current instruments on the Hubble Space Telescope (HST), where the WFPC2 offers a pixel scale of $0.1''$ and the ACS (with HRC detector) offers an improved pixel scale of $0.025''$. While modern ground-based 8-metre telescopes

with adaptive optics capabilities offer excellent resolution, these facilities are typically optimised for near-infrared wavelengths, suffering serious degradation when used at visible wavelengths. The best of these facilities are VLT/NACO providing a 0.068″/pixel resolution and Gemini-N/Altair with a potentially higher resolution of 0.02″/pixel.

This work has gathered a unique sample of extra-galactic WR stars, in an attempt to answer a number of question proposed by theoreticians. By performing a consistent series of tailored analyses for each star, we have laid the foundations for future observational programs to investigate and possibly confirm, some of our conclusions. For example, the evidence suggesting a mass-loss – metallicity dependence for WN stars requires further observations of individual WN stars situated in extreme metallicities to confirm and possibly quantify any connections. Similarly, further investigations into the properties of WC stars are required to determine whether, as suggested in this work, they do indeed possess intrinsically uniform stellar winds. M 83 is an ideal laboratory to continue with these detailed studies as it contains an unprecedented number of WR candidates, it has an unusually high metallicity, with a recently determined distance, a moderate reddening, is viewed at a low inclination and is observable with modern 8-metre telescopes. This galaxy has the potential to provide us with a large, unparallelled dataset spanning a range of environments unseen within the Local Group.

With this in mind we have already set about producing a number of simple tools to ease and speed the analysis of future spectroscopic observations of extra-galactic WR stars. Increasing the potential number of WR stars for which stellar parameters may be derived and further probing the fundamental properties of massive stars. Already, in this study we have formulated a basic polynomial equation to estimate the terminal wind velocity by simply measuring the FWHM from the strong emission lines of He II λ4686 or C IV λ5808 for WN and WC stars respectively. We have also calculated a relationship which provides a first order approximation between the peak flux ratio of He II λ5411 and C IV λ5471 and the derived C/He ratio, by number. Although currently this relationship is relatively insensitive to abundances with C/He $>$ 0.32, a similar correlation would also be useful for WN stars. We suggest that perhaps an investigation into the relationship between the peak flux ratio of the blended (H+He) lines, $\lambda\lambda$4340,4861 and the peak flux of the pure He II lines, $\lambda\lambda\lambda$4200,4541,5411 could possibly be used to estimate the mass fraction of hydrogen in WN stars.

Considering the relatively narrow range of observed properties for WC stars and the

improved accessibility to modern computers containing fast multi-processors, we propose that a grid of 138 'typical' WC stars models are computed to aid in the analysis of large datasets, shown in Figure 7.1. We choose a number of representative parameters to calculate; $Z = Z_{\odot}$, $v_{\infty} = 2600 kms^{-1}$, C/He = 0.28, C/O = 4.0 and $T_{*} = 90kK$, varying the luminosity and mass-loss accordingly. We estimate that using a standard PC with a Pentium 4 processor it would require ~1100 hours of computing time to produce the full grid of 138 models. This would then provide the user with the chance to, after correcting for the distance, directly compare their flux calibrated WR spectrum with a series of theoretical models. Of course subsequent alterations would still be required but it may speed up the process of analysis. As an aside, if flux calibrated data were not available then the user could use the determined absolute magnitudes as an indicator of luminosity.

Finally, considering the importance of the environmental metallicity in modern studies of massive stars, both theoretically and observationally, it is vital that we use accurate abundances. Undoubtedly, a modern study of a large number of H II regions is urgently required across the Local Group to constrain the local metallicities. Employing an established and accepted semi-empirical calibration (e.g. Pilyugin 2000) when computing the observed oxygen abundances in these H II regions is crucial.

List of Publications

Refereed publications

Wolf-Rayet Stars in M 33. I: Optical Spectroscopy using CFHT-MOS

Abbott, J. B., Crowther, P. A., Drissen, L., Dessart, L., Martin. P., Boivin, G., 2003, in press

Gemini observations of Wolf-Rayet stars in the Local Group starburst galaxy IC 10

Crowther, P. A., Drissen, L., Abbott, J. B., Royer, P., Smartt, S. J., 2003, *A&A* **404** 483

A large Wolf-Rayet population in NGC 300 uncovered by VLT-FORS2

Schild, H., Crowther, P. A., Abbott, J. B., Schmutz, W. 2003, *A&A* **397** 859

Stellar and wind Properties of LMC WC4 stars. A metallicity dependence for Wolf-Rayet mass-loss rates

Crowther, P. A., Dessart, L., Hillier, D. J., Abbott, J. B., Fullerton, A. W., 2002, *A&A* **392** 653

Conference Proceedings

Spectral analysis of WC Stars in M33 using CFHT-MOS

Abbott, J. B., Crowther, P. A., Drissen, L., Dessart, L., Martin, P., 2003, In *Proceedings IAU Symposium No. 212, A Massive Star Odyssey, from Main Sequence to Supernova.* ASP, p.148, (eds. K.A. van der Hucht et al.)

WR stars at 1-2Mpc

Crowther, P. A., Abbott, J. B., Drissen, L., Schild, H., Schmutz, W., Royer, P., Smartt, S. J., 2003, In *Proceedings IAU Symposium No. 212, A Massive Star Odyssey, from Main Sequence to Supernova.* ASP, p.547, (eds. K.A. van der Hucht et al.)

Revised abundances and ionizing fluxes for [WC]-type PN central stars using line blanketed models

Crowther, P. A., Abbott, J. B., Hillier, D. J., De Marco, O., In *Proceedings IAU Symposium 209, Planetary Nebulae*, ASP, in press (eds. M. Dopita et al.)

APPENDIX A

Observations of WR stars in M 33

The rectified optical spectra for WR stars in M 33 taken with the Multi-Object Spectrograph (MOS) on the 3.6-metre Canada-France-Hawaii Telescope (CFHT). The data have been Gaussian-smoothed and rebinned to a spectral resoltuion of 9Å. Emission lines are identified at the top of each page.

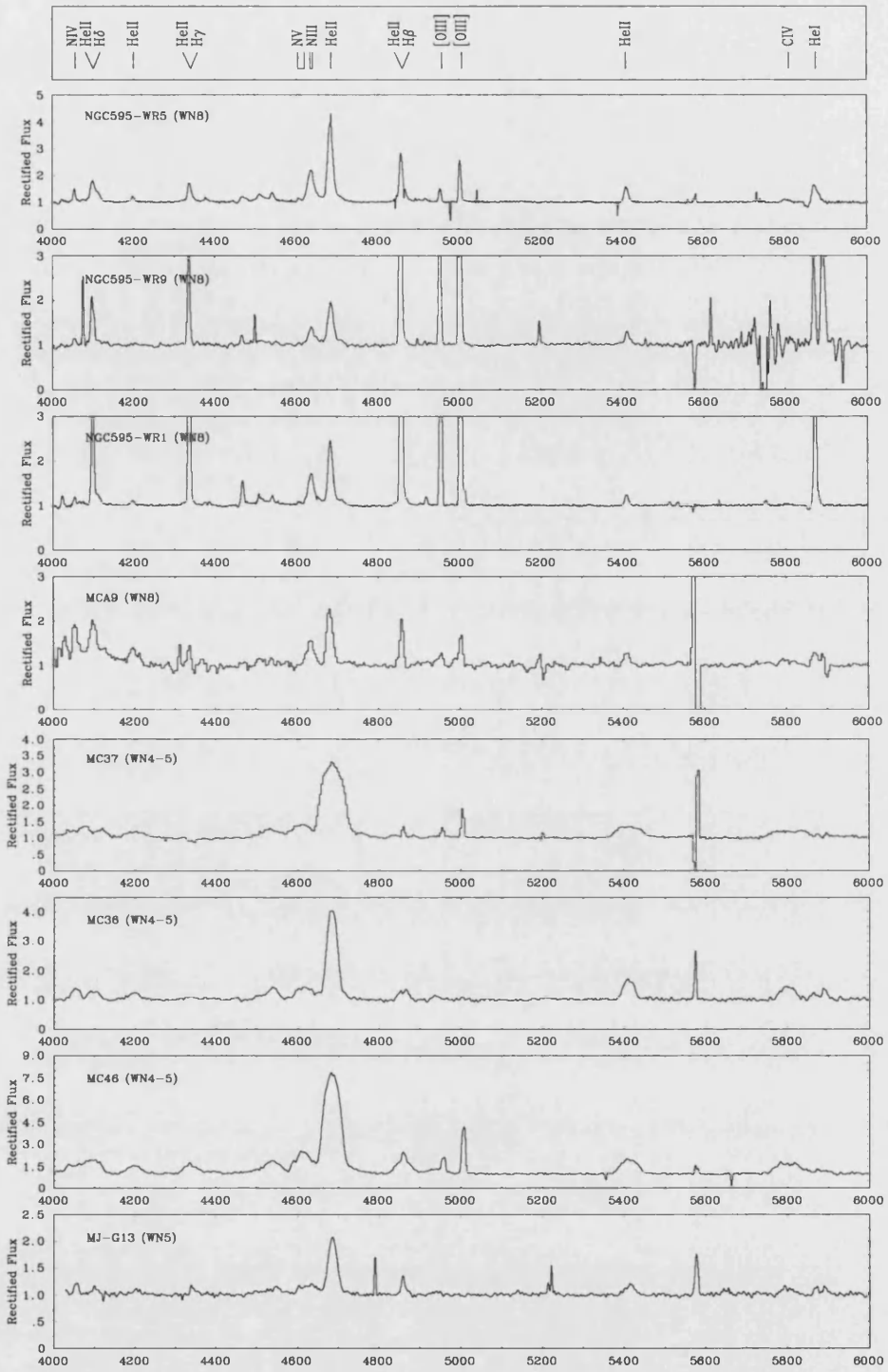

Figure A.1: Plot showing the rectified spectra for the WN stars taken from our sample, covering a spectral range $\lambda\lambda 4000 - 6000$. The spectra have been binned to increase the signal to noise. Note that many of the faint features can be seen and the narrow lines well resolved.

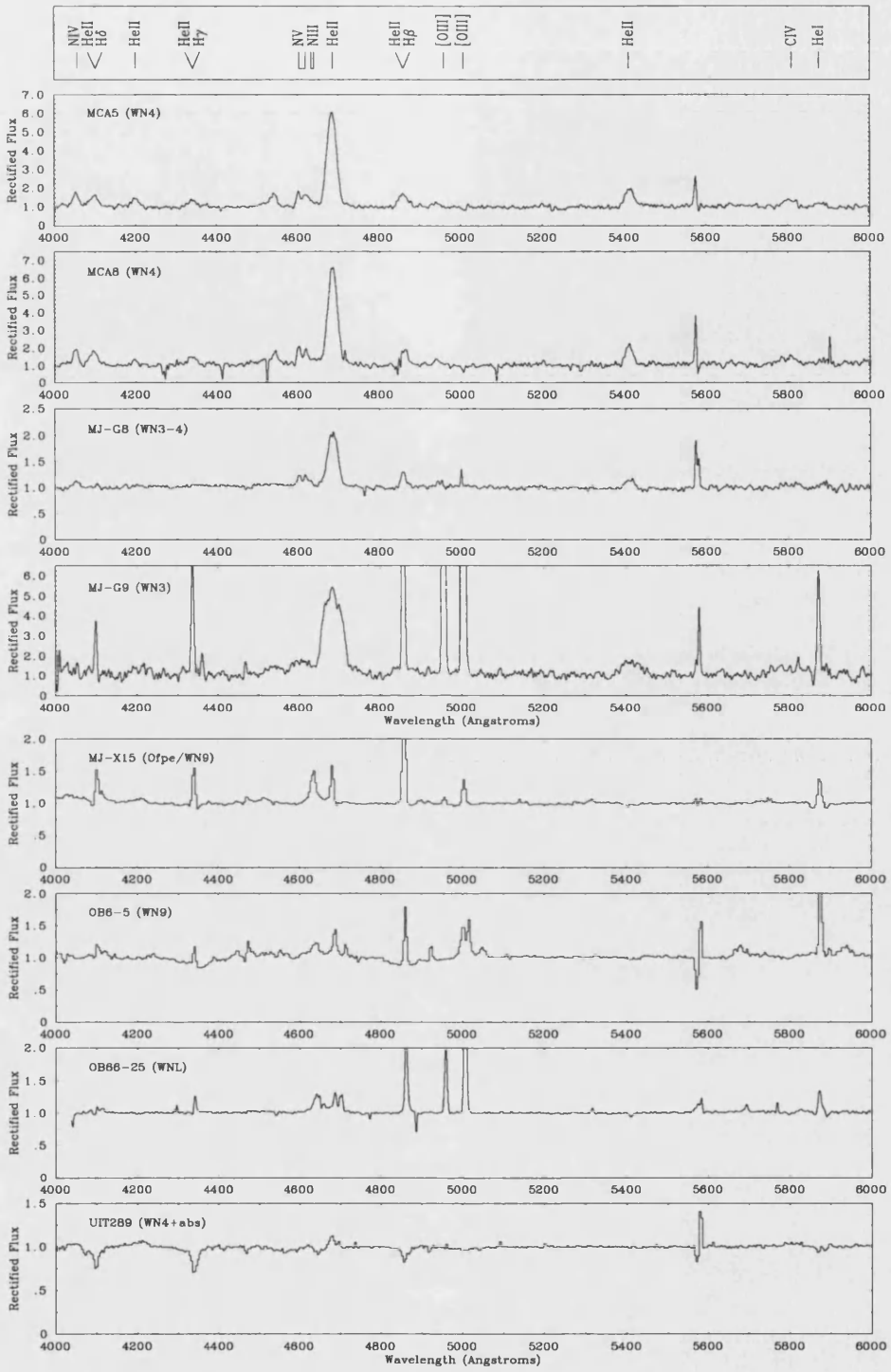

Figure A.2: Plot showing the rectified spectra for the WN stars taken from our sample, covering a spectral range $\lambda\lambda 4000 - 6000$. The spectra have been binned to increase the signal to noise. Note that many of the faint features can be seen and the narrow lines well resolved.

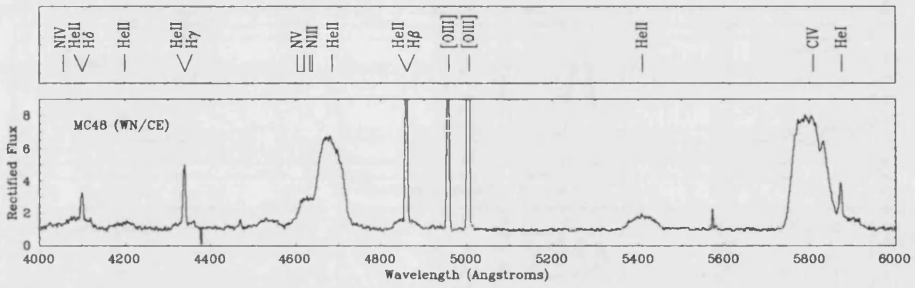

Figure A.3: Plot showing the rectified spectra for the WN/CE star taken from our sample, covering a spectral range $\lambda\lambda 4000 - 6000$. The spectra have been binned to increase the signal to noise. We have also identified a number of principal stellar and nebular lines (top panel).

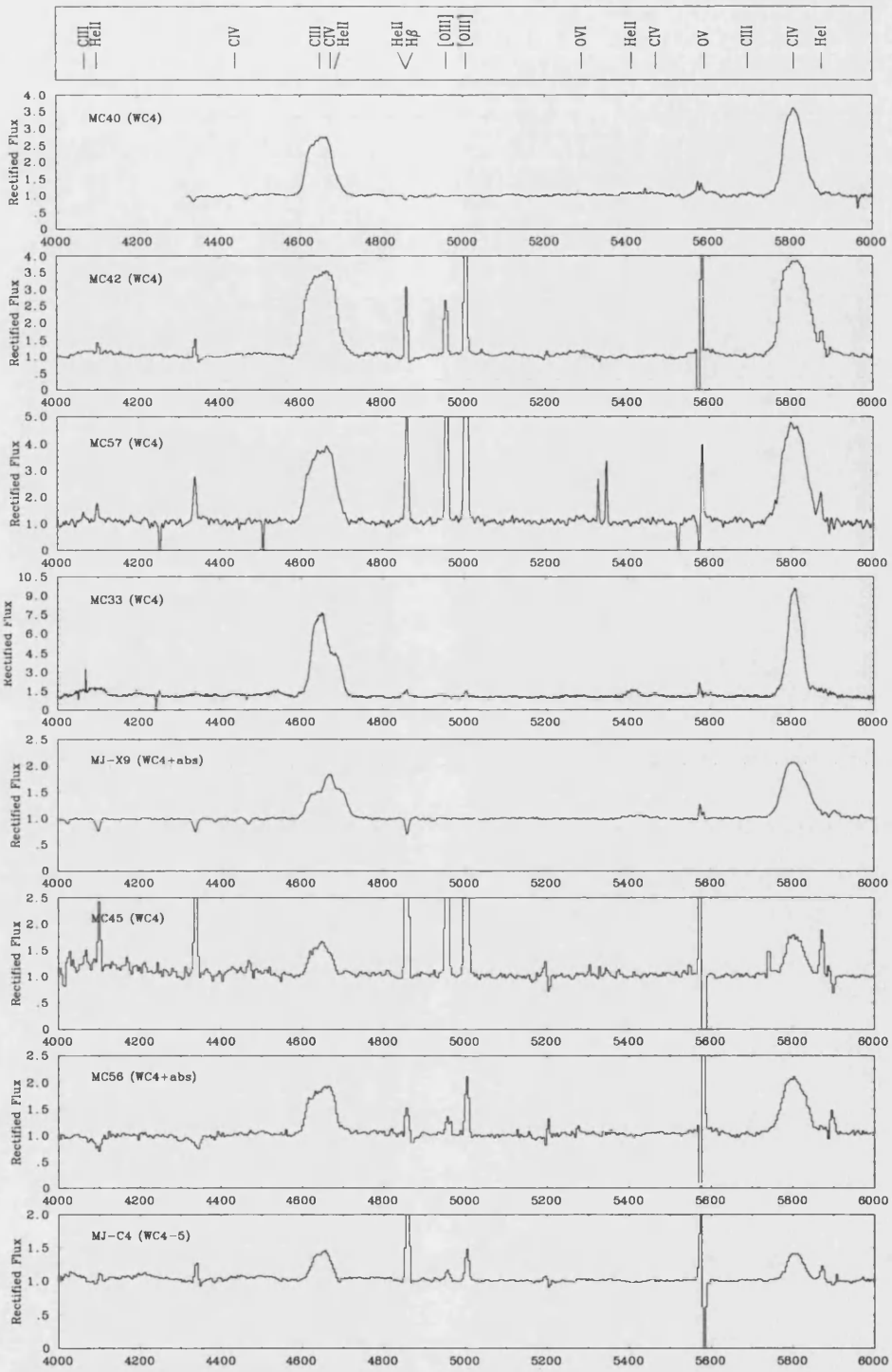

Figure A.4: Plot showing the rectified spectra for the WC stars taken from our sample, covering a spectral range $\lambda\lambda 4000 - 6000$. The spectra have been binned to increase the signal to noise. We have also identified a number of principal stellar and nebular lines (top panel).

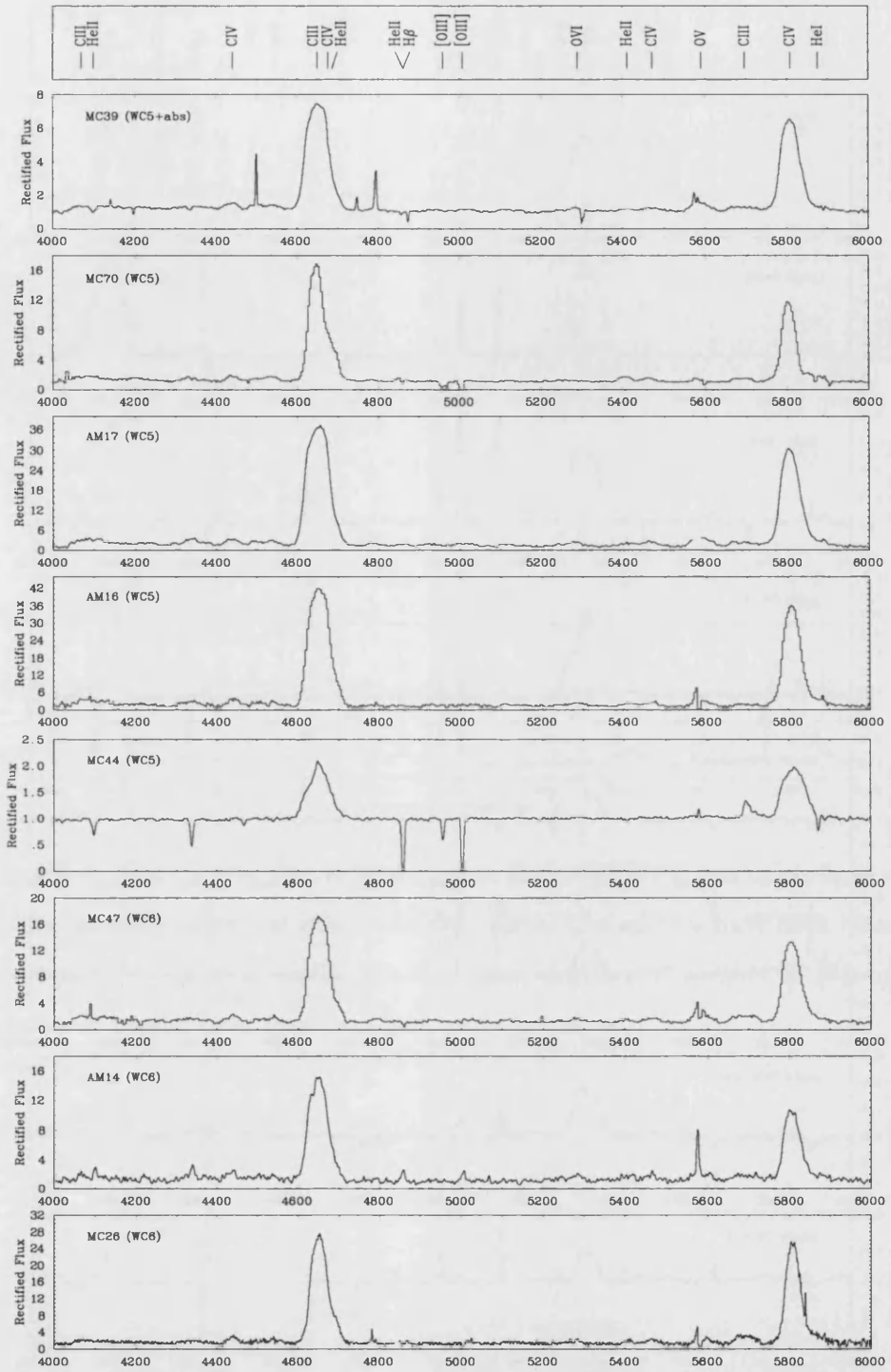

Figure A.5: Plot showing the rectified spectra for the WC stars taken from our sample, covering a spectral range $\lambda\lambda 4000 - 6000$. The spectra have been binned to increase the signal to noise. We have also identified a number of principal stellar and nebular lines (top panel).

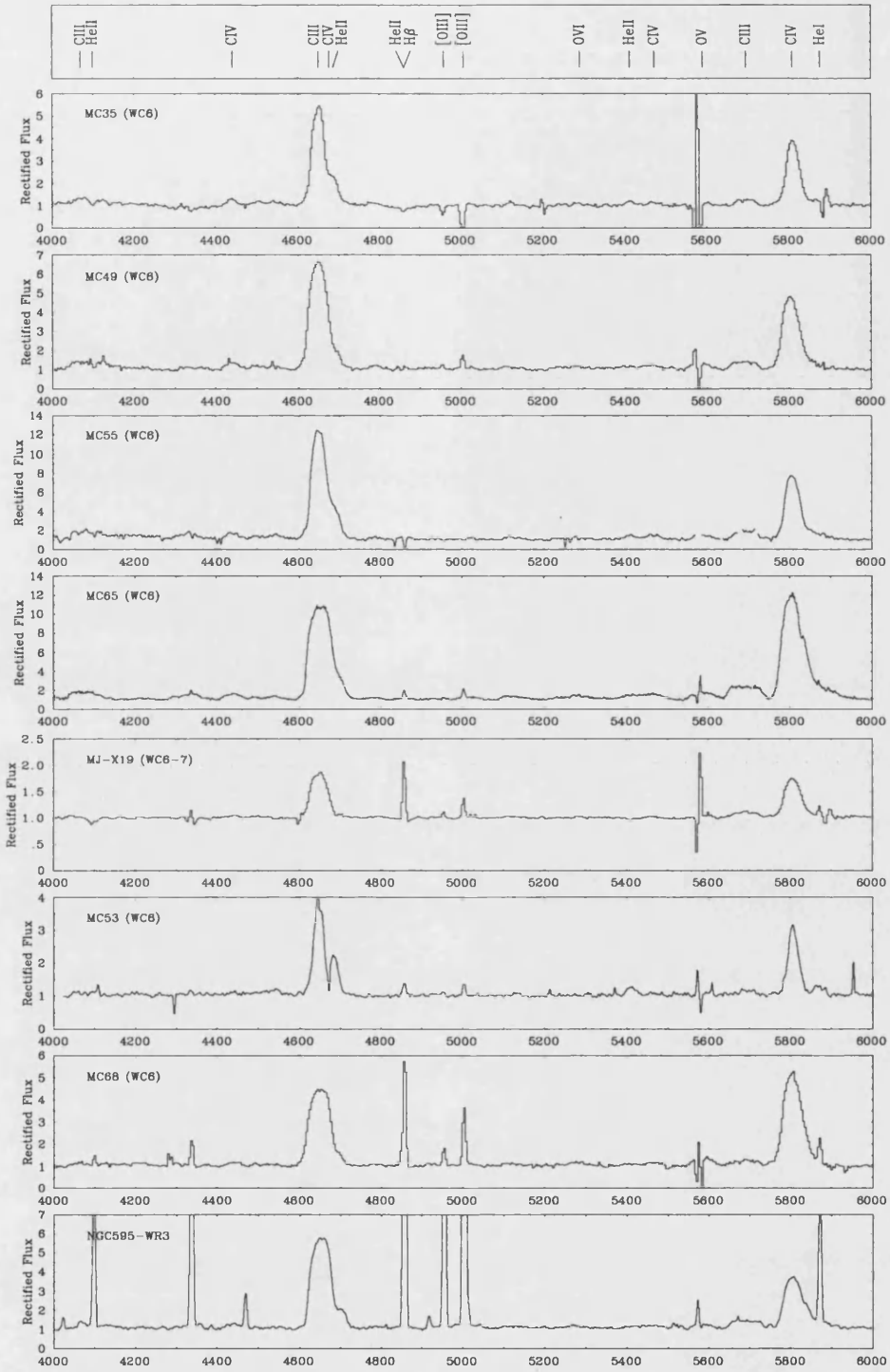

Figure A.6: Plot showing the rectified spectra for the WC stars taken from our sample, covering a spectral range $\lambda\lambda 4000 - 6000$. The spectra have been binned to increase the signal to noise. We have also identified a number of principal stellar and nebular lines (top panel).

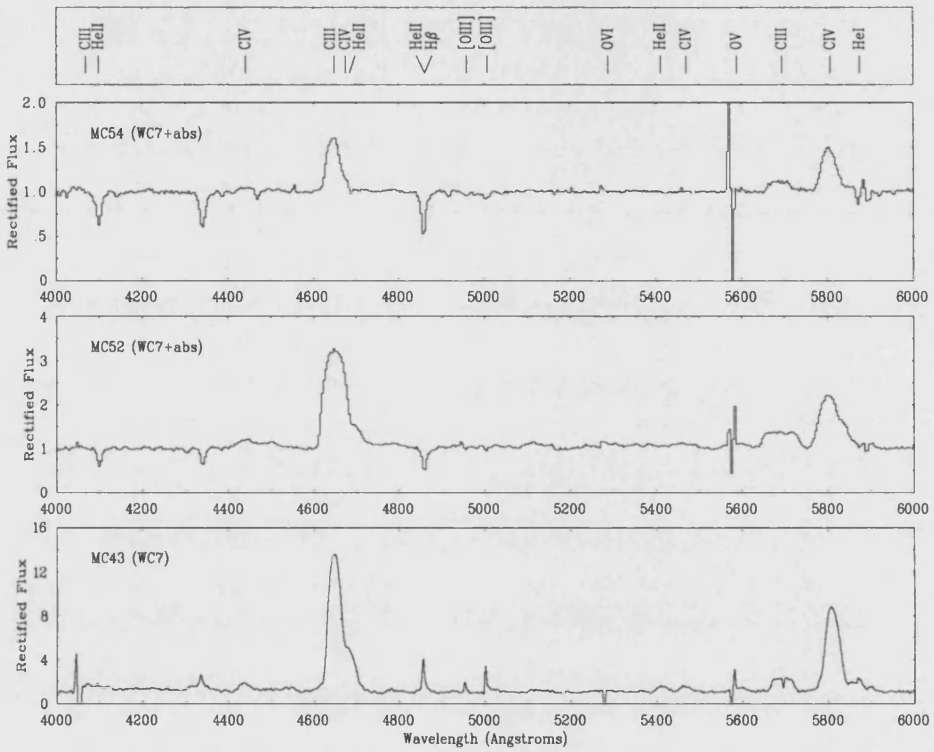

Figure A.7: Plot showing the rectified spectra for the WC stars taken from our sample, covering a spectral range $\lambda\lambda 4000 - 6000$. The spectra have been binned to increase the signal to noise. We have also identified a number of principal stellar and nebular lines (top panel).

APPENDIX B

Observations of WR stars in M 31

The flux calibrated optical spectra for WC stars in M 31 taken with the ISIS double-armed spectrograph on the the 4.2-metre William Herschel Telescope. The observational setup (discussed in Chapter 2) gave a spectral resolution of 3Å. Emission lines are identified at the top of each page.

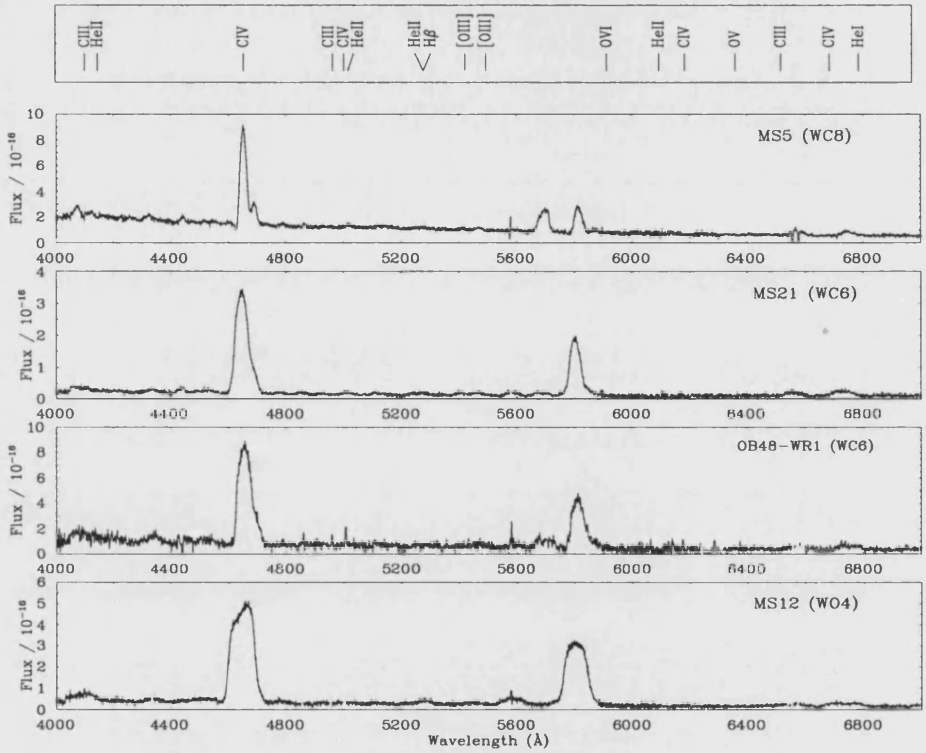

Figure B.1: Plot showing the flux calibrated spectra for the WC stars in M 31, covering a spectral range $\lambda\lambda 4000 - 7000$. We have also identified a number of principal stellar and nebular lines (top panel).

APPENDIX C

Observations of WR stars in IC 10

C.1 Finding Charts

Finding charts for WR stars in IC 10 are shown using data from WHT narrow-band He II and HST WFPC2 F555W imaging. Stars labelled M# are candidates from Massey, Armandroff & Conti (1992) and stars labelled R# are the WR candidates identified by Royer *et al.* (2001). In some cases point sources are resolved into multiple components, with the brighter (and bluer) object presummably the WR star. Except for M24 for which the He II emission line star is still rather uncertain.

C.2 Spectroscopy of WR Stars in IC 10

The flux calibrated optical spectra for WR stars in IC 10 taken with the Gemini Multi-Object Spectrograph (GMOS) on the 8-metre Gemini-North telescope. The observational setup (discussed in Chapter 2) gave a spectral resolution of 7Å. Emission lines are identified at the top of each page.

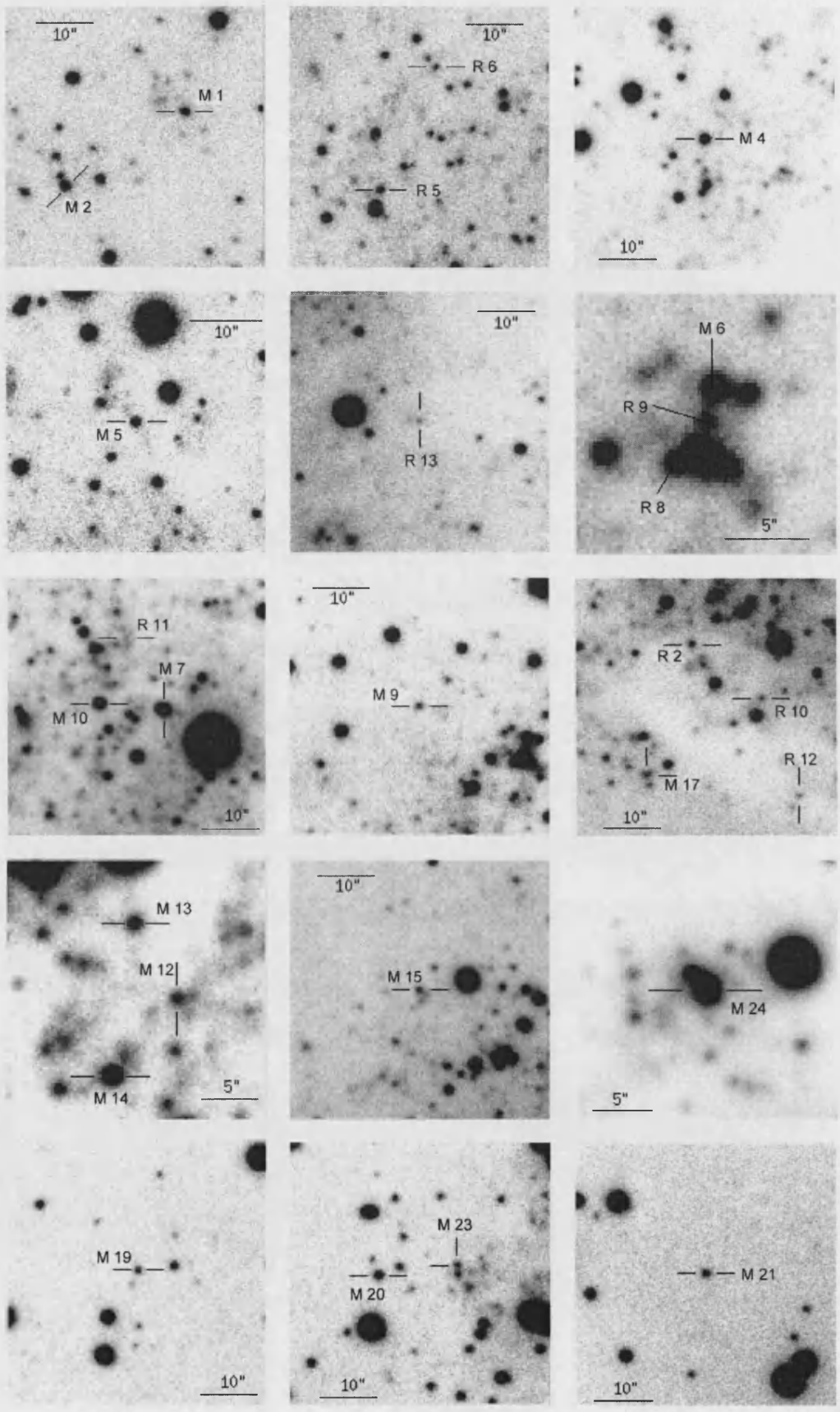

Figure C.1: Finding chart for known WR stars/candidates in the H II region Deh 77/79. The horizontal bars represent 10". North to the top, East to the left.

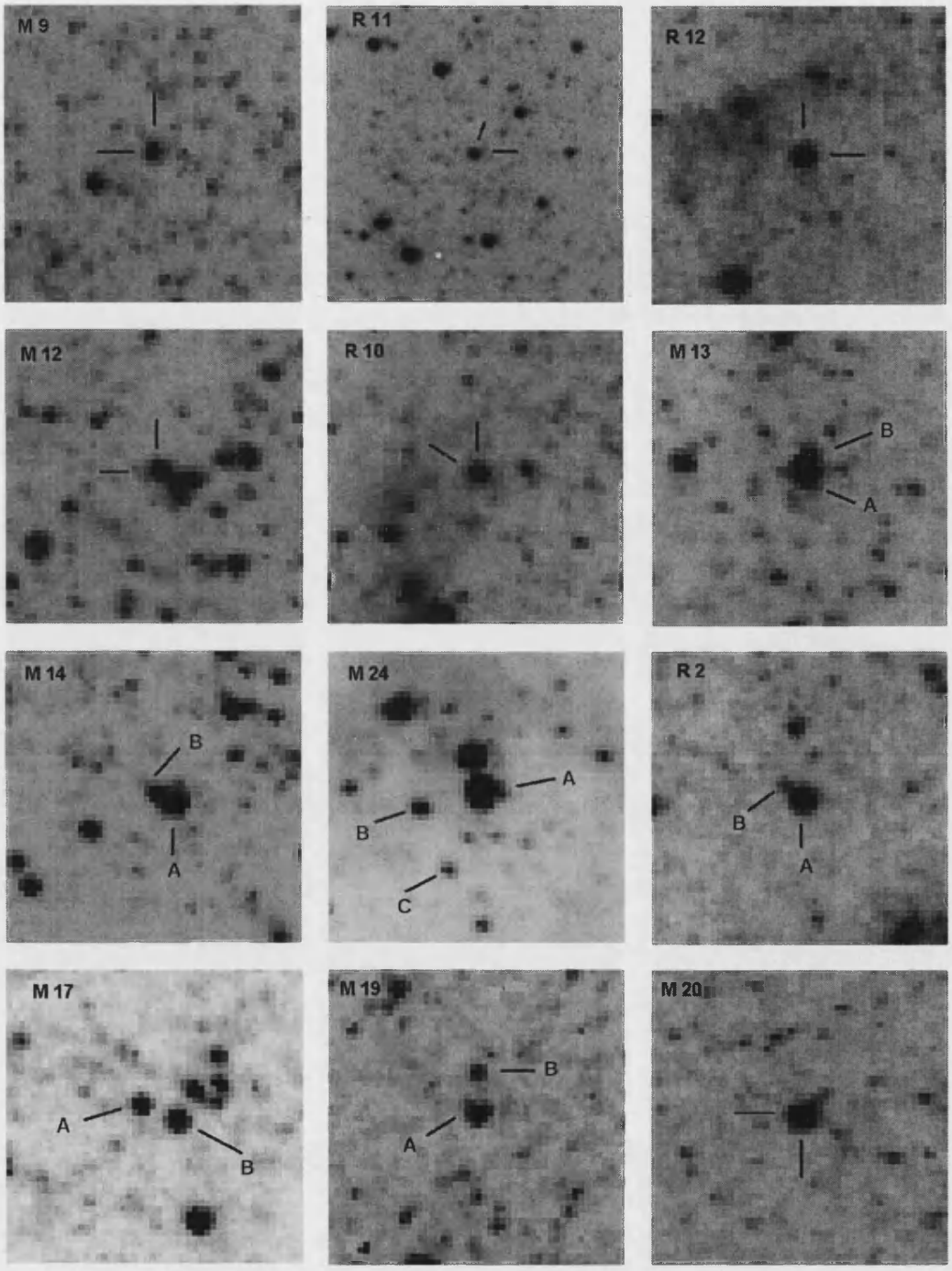

Figure C.2: Finding chart for knwon WR stars/candidates in the H II region Deh 77/79. The horizontal bars represent 10". North to the top, East to the left.

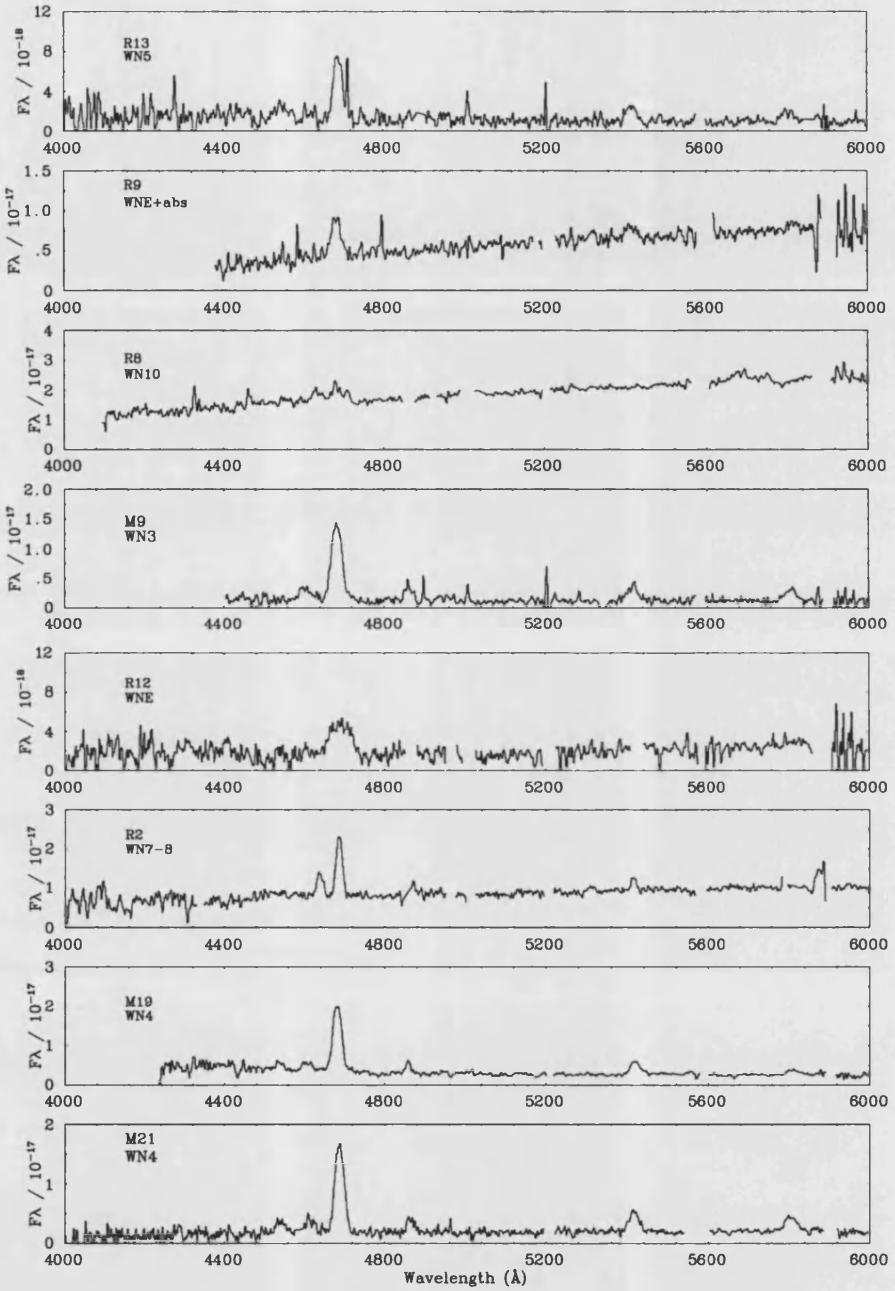

Figure C.3: Flux calibrated optical spectra of WN stars in IC 10 observed with Gemini-GMOS.

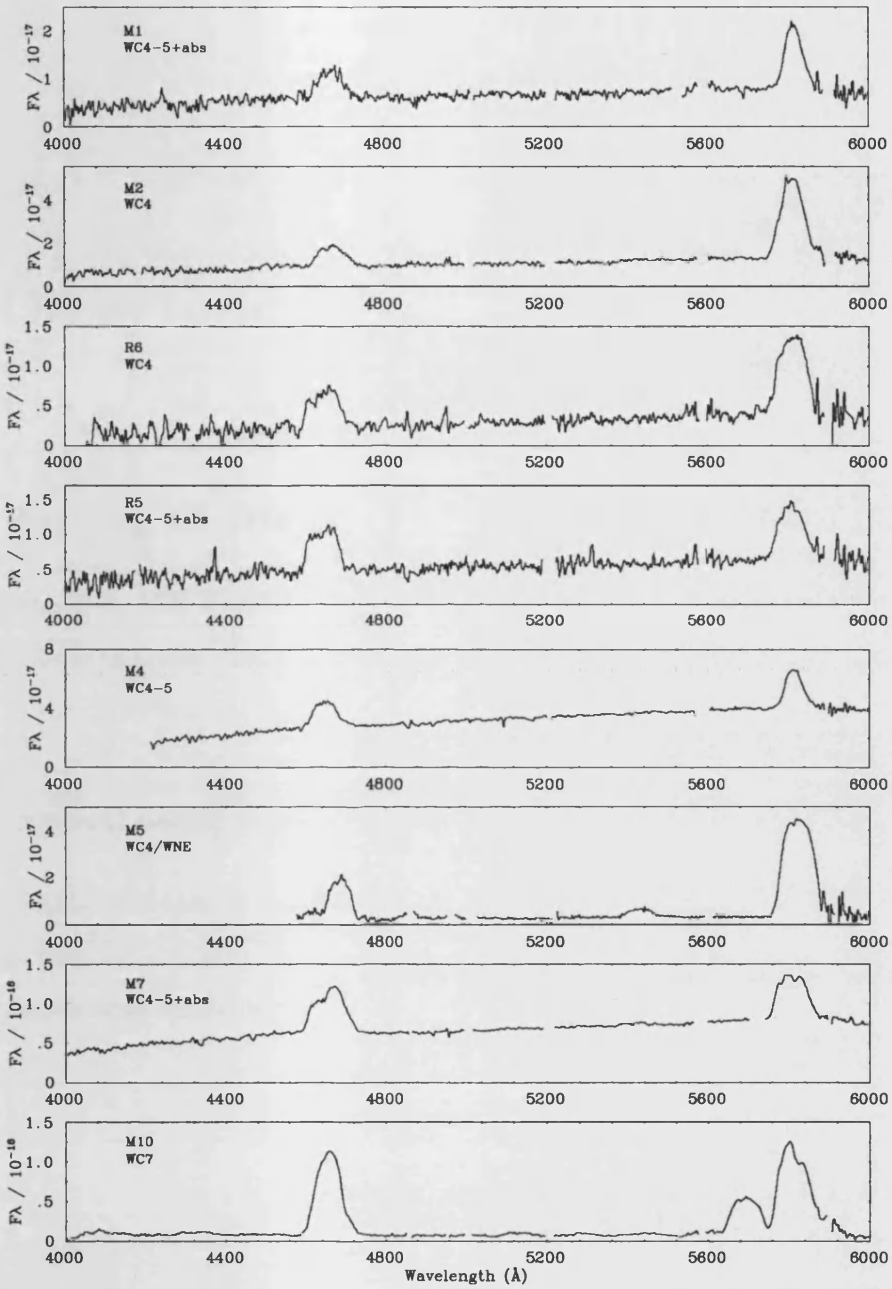

Figure C.4: Flux calibrated optical spectra of WC stars in IC 10 observed with Gemini-GMOS.

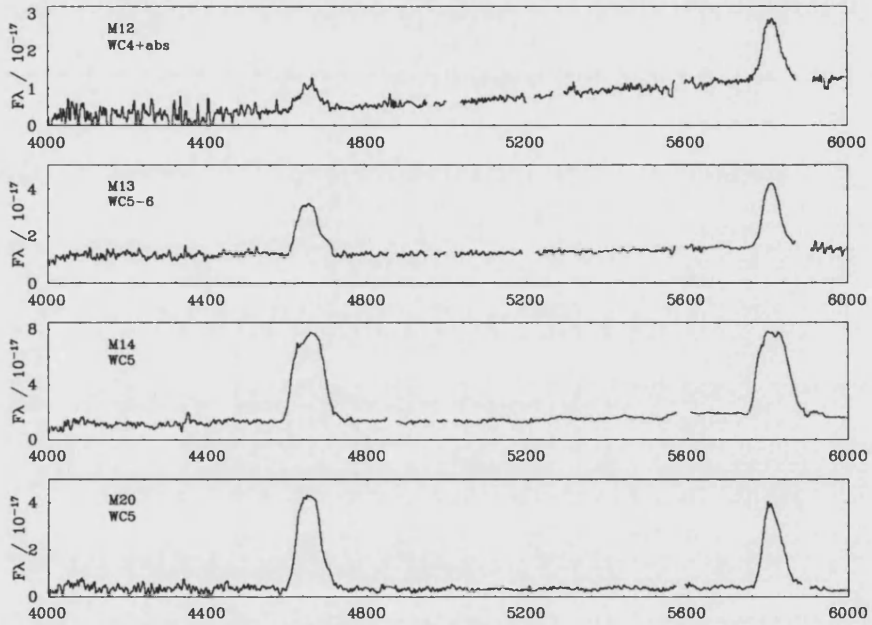

Figure C.5: Flux calibrated optical spectra of WC stars in IC 10 observed with Gemini-GMOS.

APPENDIX D

Observations of WR stars in NGC 300

D.1 Finding Charts

Finding charts for WR stars in NGC 300 are shown using data from taken with the VLT-FORS2 in imaging mode. Stars are numbered according to the WR catalogue in Table 2.11. Details of the observational setup are described in Chapter 2.

D.2 Spectroscopy of WR Stars in NGC 300

The flux calibrated optical spectra for WR stars in NGC 300 taken with with the VLT-FORS2 in long-slit mode (LSS). Two observational setups we used providing a different dispersions, further details are given in Chapter 2.

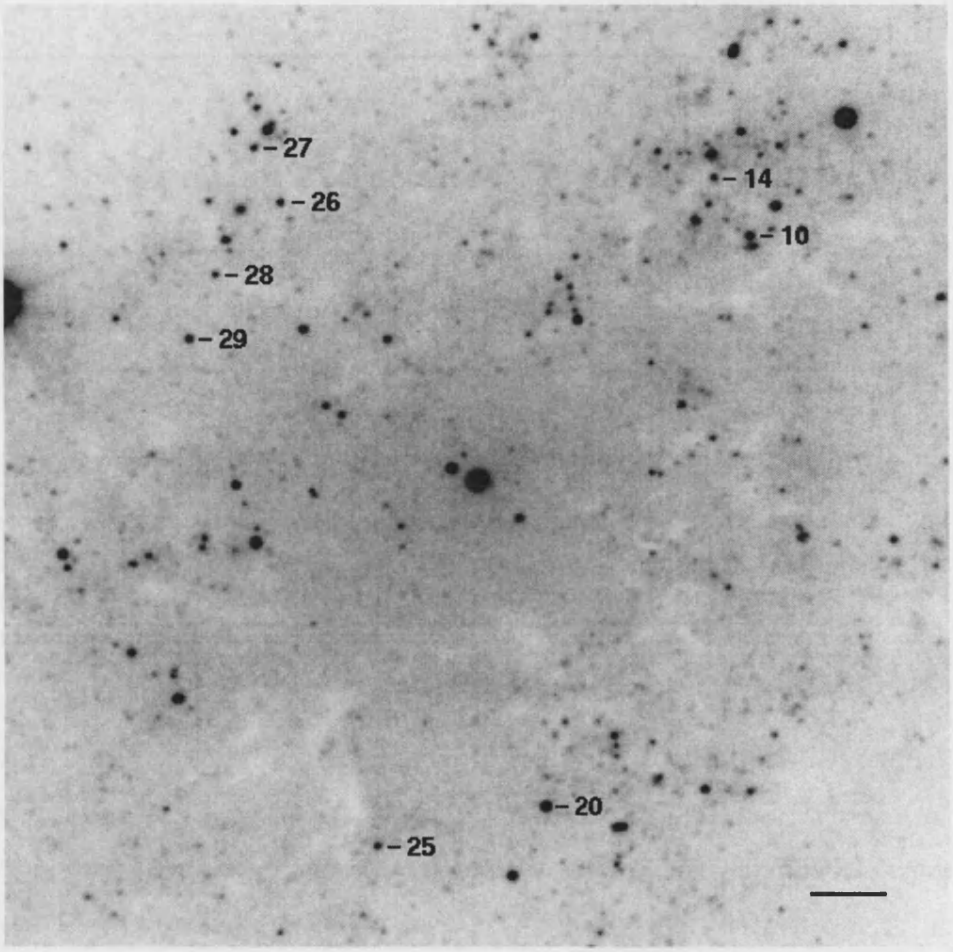

Figure D.1: Finding chart for known WR stars/candidates in NGC 300. This field shows the nuclear region of NGC 300. The horizontal bar represents 10". North to the top, East to the left.

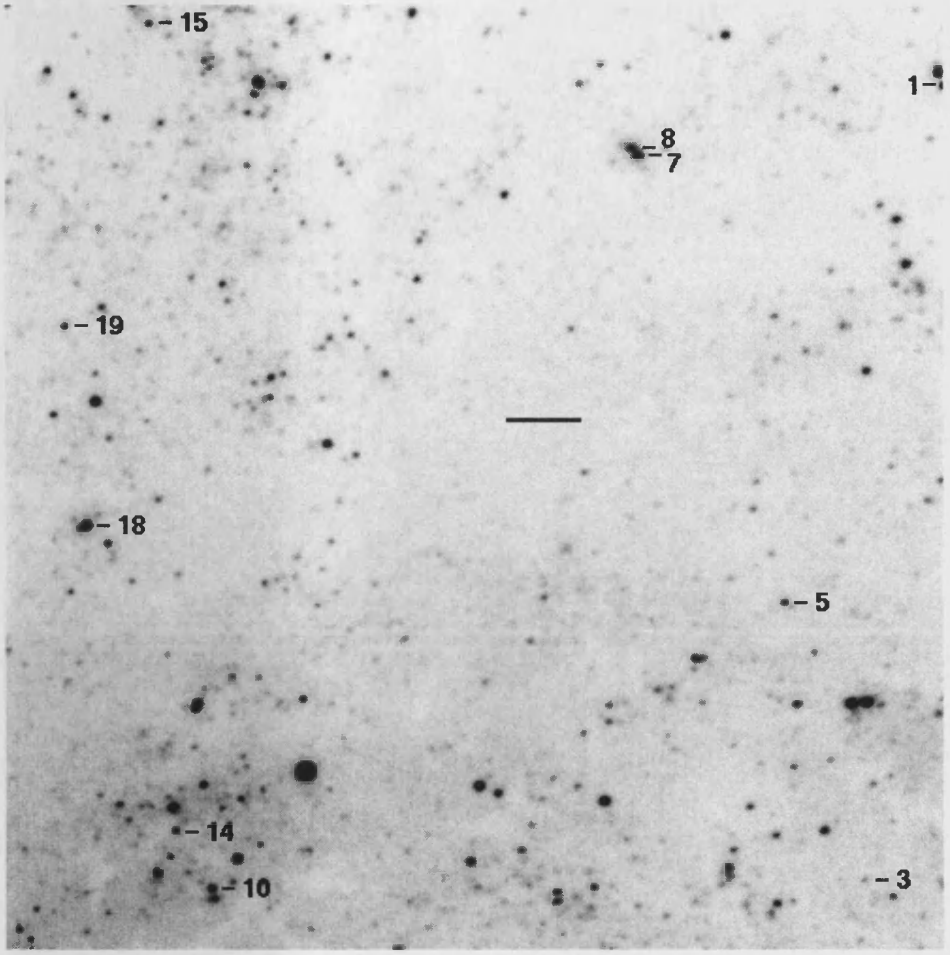

Figure D.2: Finding chart for known WR stars/candidates in NGC300, showing the area northwest of the galactic nucleus. The horizontal bar represents 10". North to the top, East to the left.

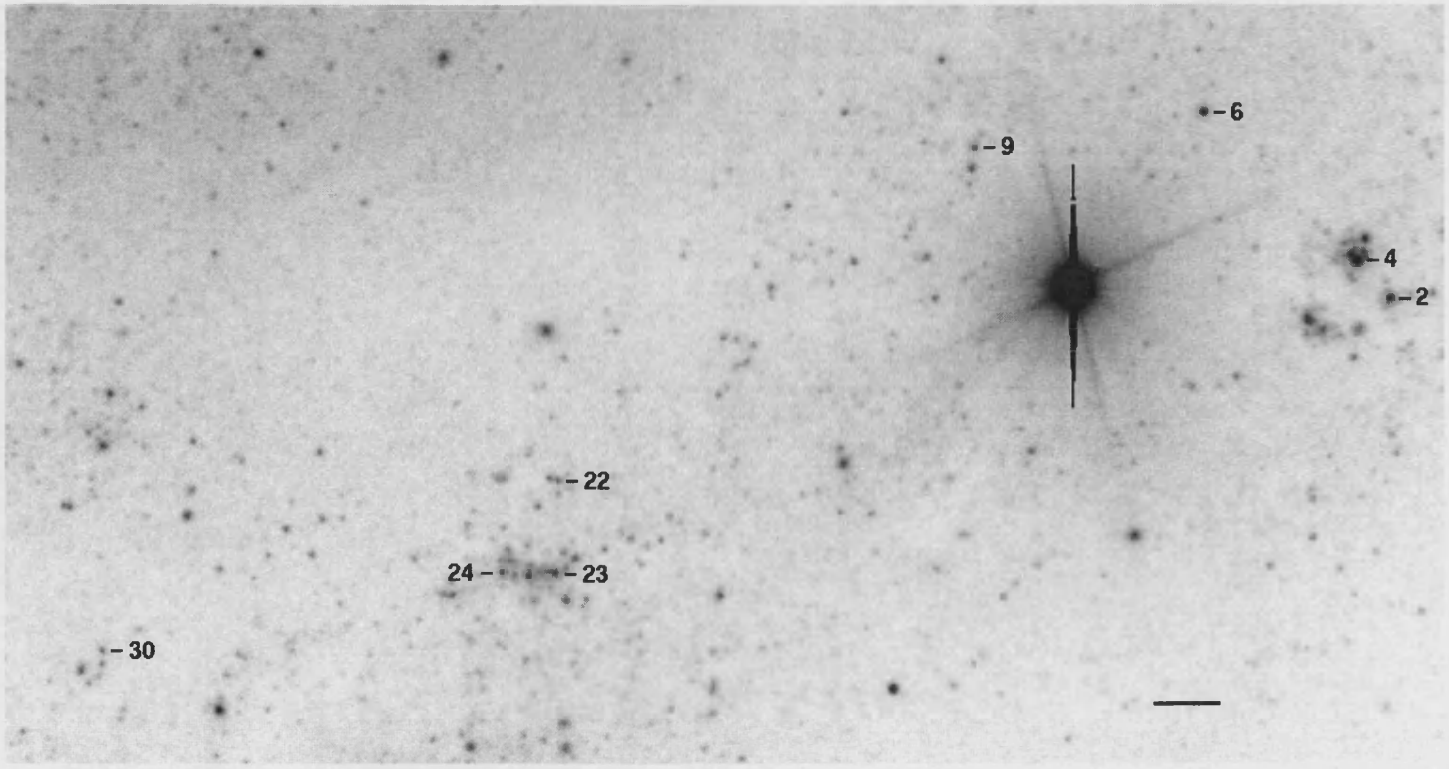

Figure D.3: Finding chart for known WR stars/candidates in the southern spiral arm. The saturated object is the galactic foreground star CD−38° 301. The horizontal bar represents 10". North to the top, East to the left.

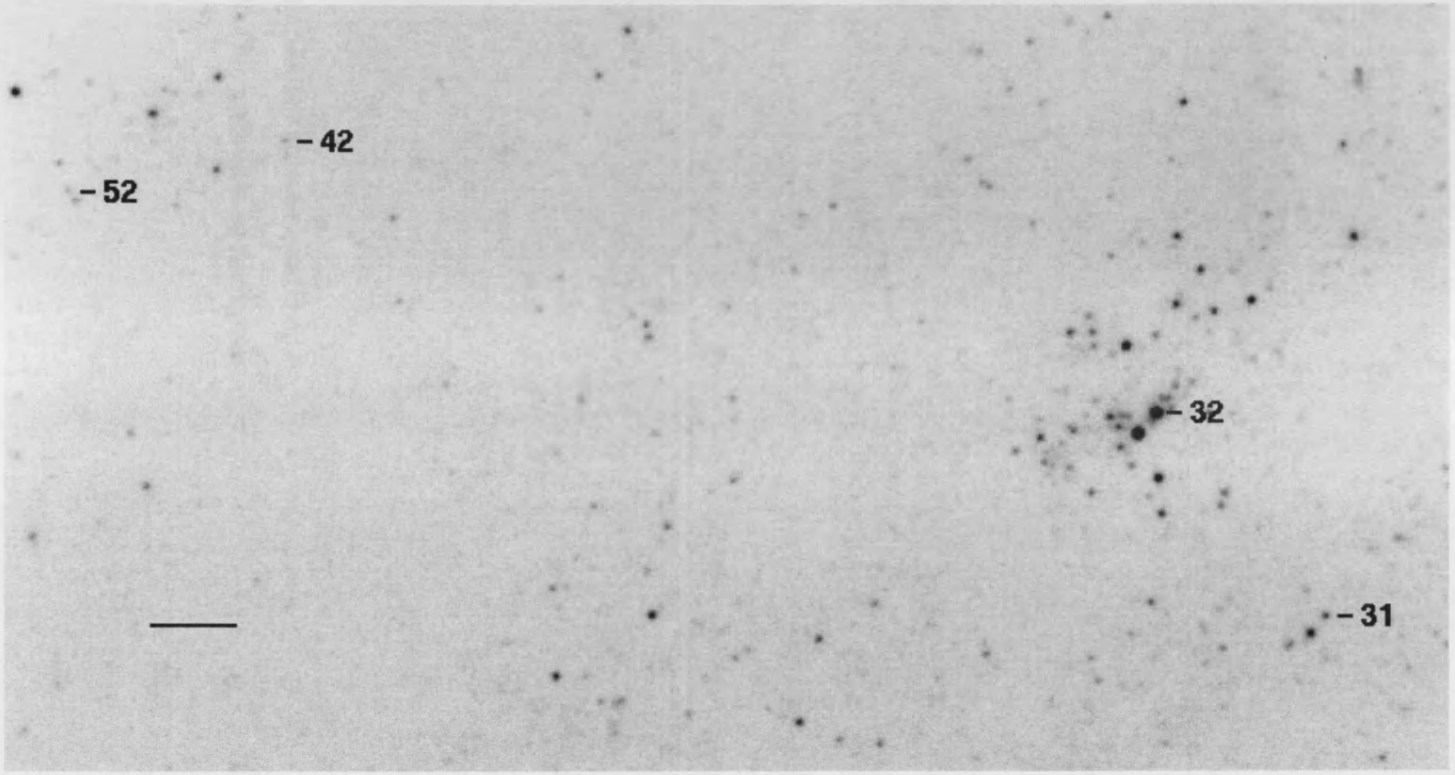

Figure D.4: Finding chart for known WR stars/candidates in the northeast of the nucleus. Some vignetting occurred in the upper left corner (northeast) of our images. The horizontal bar represents 10". North to the top, East to the left.

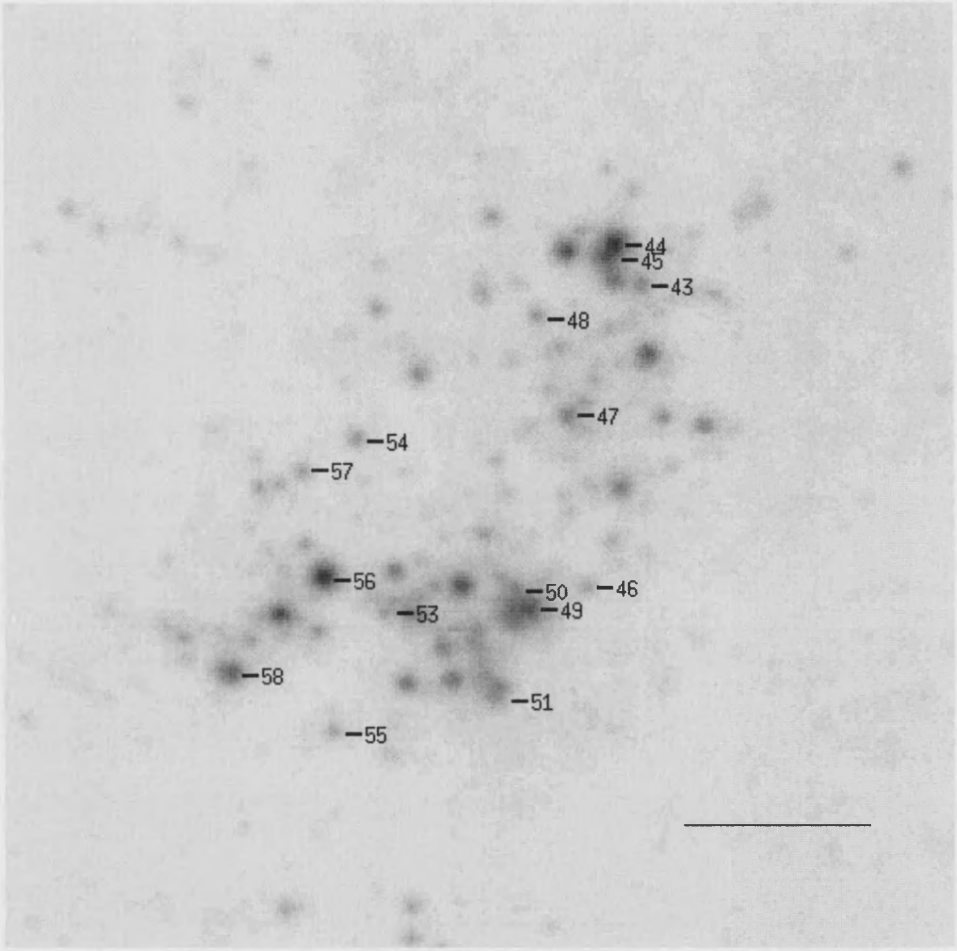

Figure D.5: Finding chart for WR known stars/candidates east of the nucleus. The horizontal bars represent 10". North to the top, East to the left.

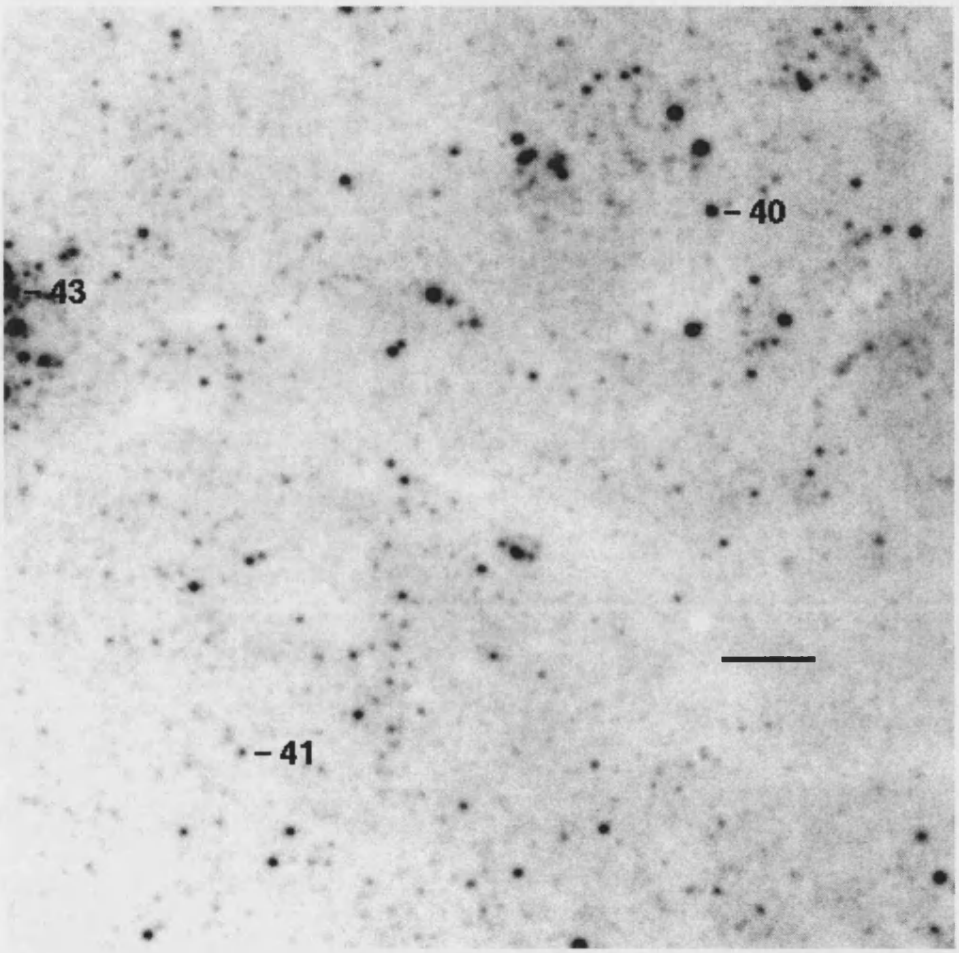

Figure D.6: Finding chart for known WR stars/candidates in the H II region Deh 137. The horizontal bars represent 10". North to the top, East to the left.

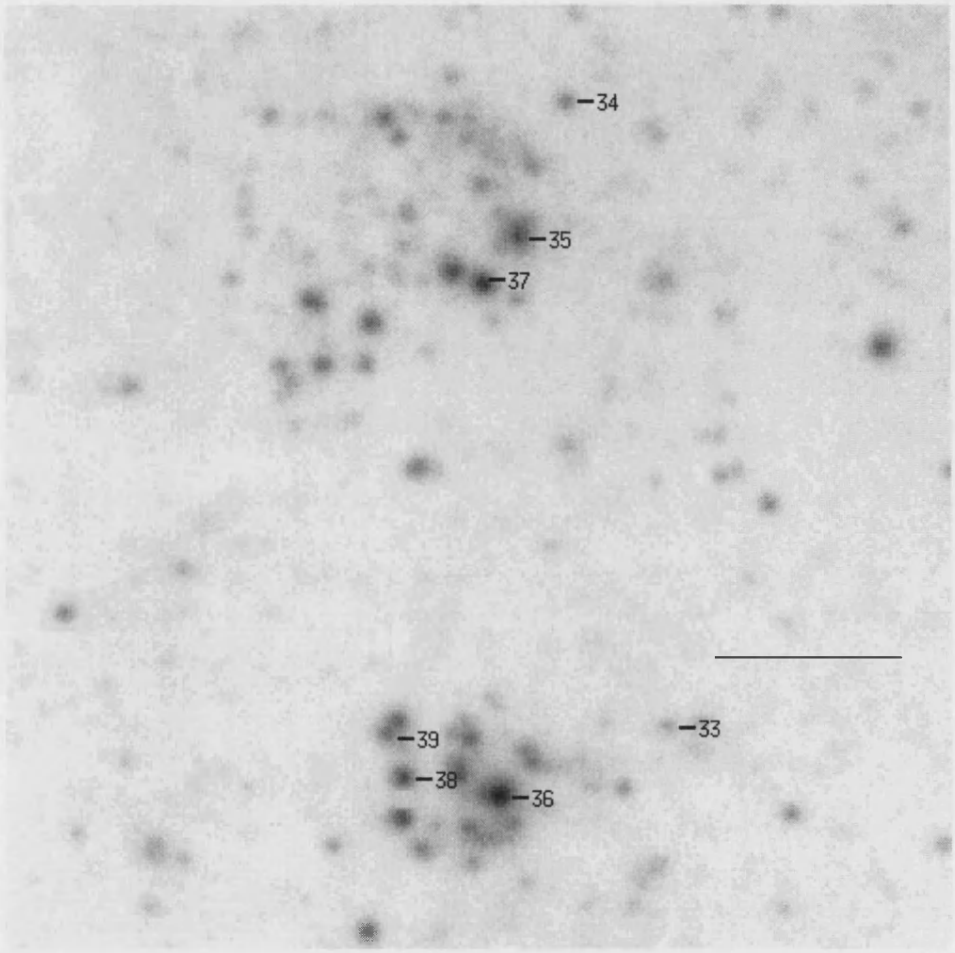

Figure D.7: Finding chart for known WR stars/candidates in the H II region Deh 118/119. The horizontal bars represent 10". North to the top, East to the left.

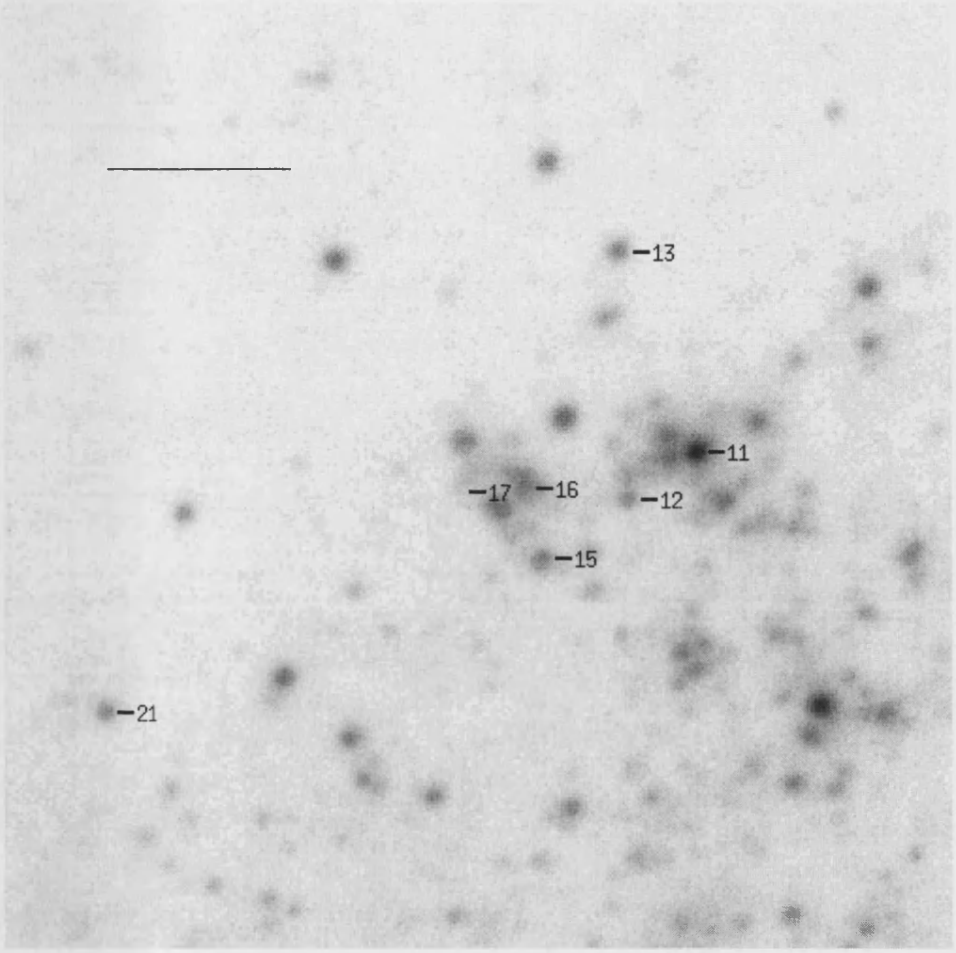

Figure D.8: Finding chart for knwon WR stars/candidates in the H II region Deh 77/79. The horizontal bars represent 10". North to the top, East to the left.

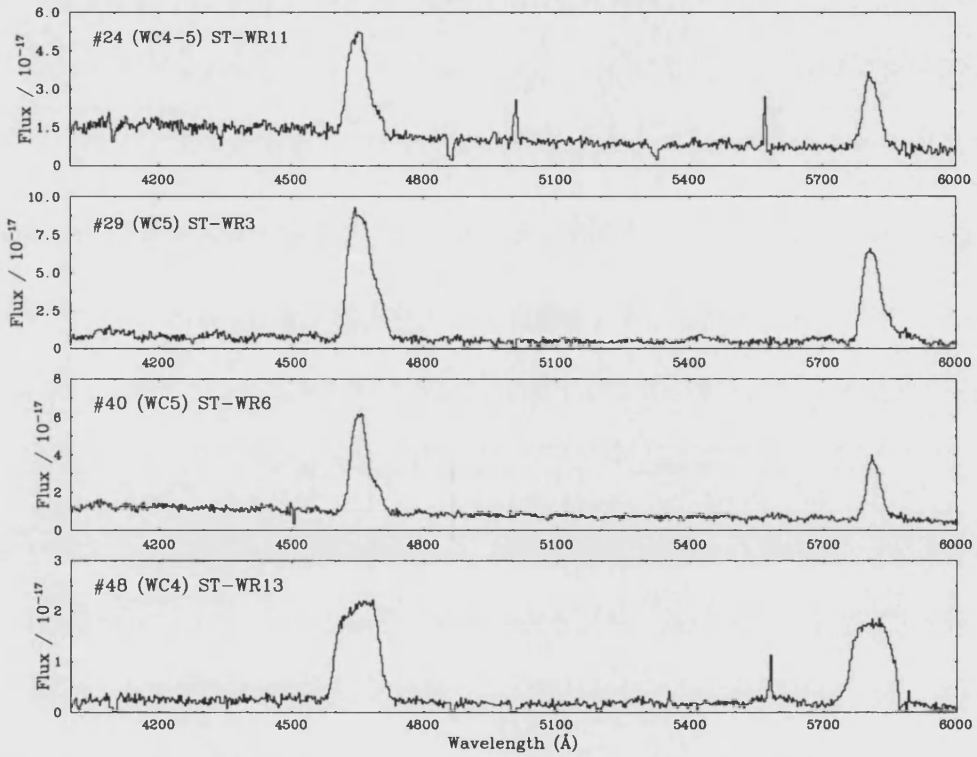

Figure D.9: Low dispersion FORS2 spectroscopy of four WC stars in NGC 300, previously identified by Schild & Testor (1992) and Schild & Testor (1991).

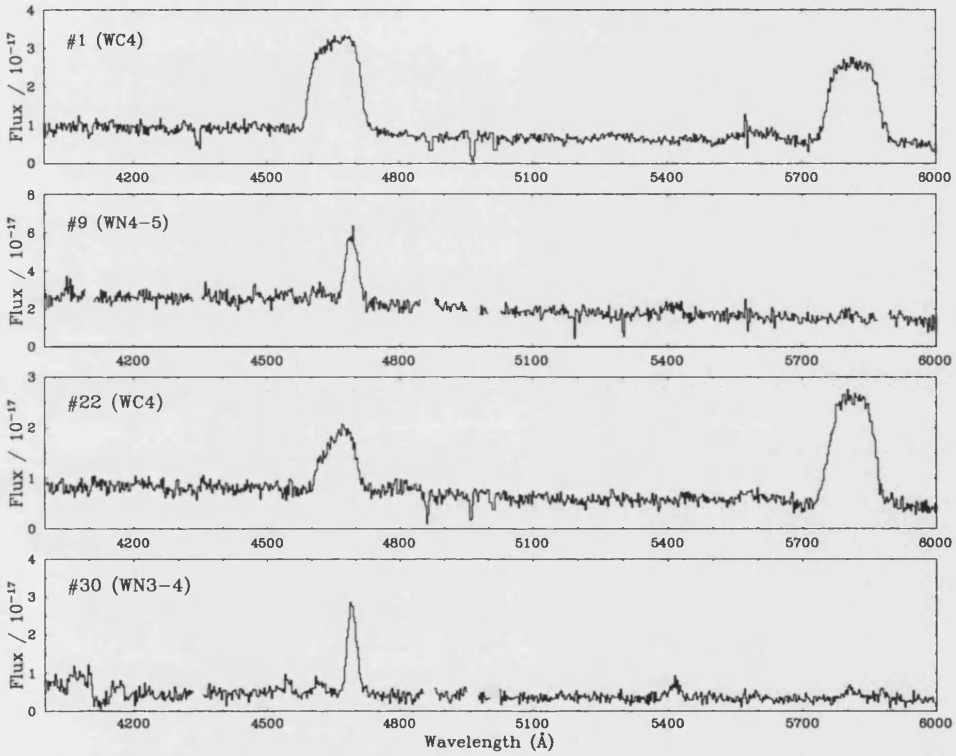

Figure D.10: Low dispersion FORS2 spectroscopy of four newly indentified WR stars in NGC 300.

Appendix E

Observations of WR stars in M 83

E.1 Catalogue of Wolf-Rayet Candidates in M 83

Catalogue of Wolf-Rayet candidates in M 83, made from narrow-band images taken with the VLT-FORS2. Stars are numbered according to the Field (A,B,C and D) and chip (1 and 2) in which they are located. Details of the observational setup are described in Chapter 2.

Table E.1: List of WR candidates in M 83 identified by our narrow-band surveys.

#	Field/Chip	α (2000)	δ (2000)	Hα Assoc.	He II	He II - Cont.
01	A1	13:36:55.15	-29:49:50.5	no	800	500
02	A1	13:36:55.31	-29:48:10.0	diffuse	700	300
03	A1	13:36:55.35	-29:49:47.6	no	500	730
04	A1	13:36:55.85	-29:47:47.5	no	400	250
05	A1	13:36:56.00	-29:49:53.8	strongH II	3500	1900
06	A1	13:36:56.22	-29:49:33.1	no	800	900
07	A1	13:36:58.55	-29:48:12.0	no	1200	700
08	A1	13:36:58.74	-29:48:06.3	strongH II	7000	2200
09	A1	13:37:00.28	-29:48:04.2	strongH II	2600	900
10	A1	13:37:02.49	-29:48:27.4		600	700
11	A1	13:37:02.68	-29:49:40.9	v. strong	21000	5400
12	A1	13:37:02.84	-29:49:15.3	no	900	1100
13	A1	13:37:04.39	-29:48:26.9	weak	2200	700
14	A1	13:37:04.56	-29:49:21.8	no	1200	900
15	A1	13:37:05.34	-29:48:20.4	strong	4000	1500
16	A1	13:37:05.53	-29:48:19.9	diffuse	1200	800

Continued on next page .....

#	Field/Chip	α (2000)	δ (2000)	Hα Assoc.	He II	He II - Cont.
17	A1	13:37:06.36	-29:49:03.7	weak	2300	1100
18	A1	13:37:07.35	-29:49:39.2	yes-CH II	1500	900
19	A1	13:37:07.68	-29:49:13.9	v. strong	16000	3600
20	A1	13:37:07.76	-29:49:18.1	no	1000	1200
21	A1	13:37:08.55	-29:49:06.5	diffuse	6000	3000
22	A1	13:37:09.15	-29:49:20.6	diffuse	1000	500
23	A1	13:37:09.63	-29:49:56.4	no	200	535
24	A1	13:37:09.67	-29:49:01.7	diffuse	500	400
25	A1	13:37:09.75	-29:49:08.0	v. strong	48000	11000
26	A1	13:37:10.02	-29:49:13.4	v. strong	10500	3800
27	A1	13:37:10.88	-29:49:54.7	v. strong	23000	5700
28	A1	13:37:11.03	-29:49:49.1	yes-CH II	1000	1140
29	A1	13:37:11.11	-29:48:24.1	yes-H II	600	539
30	A1	13:37:11.24	-29:49:42.0	no	2000	500
31	A1	13:37:11.46	-29:49:52.9	v. strong	31000	9500
32	A1	13:37:11.67	-29:49:18.1	no	500	500
33	A1	13:37:12.64	-29:49:50.1	weak	500	500
34	A1	13:37:18.08	-29:48:04.5	yes-H II	500	350
35	A1	13:37:22.11	-29:48:43.8	strong	1450	330
36	A1	13:37:23.66	-29:48:53.8	strong	660	257
37	A1	13:37:24.08	-29:48:52.6	diffuse	270	200
01	A2	13:36:55.81	-29:50:17.8	yes	2200	1300
02	A2	13:36:56.78	-29:52:13.3	weak	600	800
03	A2	13:36:56.96	-29:52:49.1	strongH II	7000	2400
04	A2	13:36:57.07	-29:50:20.2	yes	700	1200
05	A2	13:36:58.88	-29:50:12.8	diffuse	2300	1200
06	A2	13:36:59.03	-29:51:26.6	strong	13000	3000
07	A2	13:37:00.41	-29:52:54.1	weak	2400	900
08	A2	13:37:02.52	-29:52:38.1	diffuse	500	800
09	A2	13:37:02.59	-29:50:38.2	no	1000	1000
10	A2	13:37:03.09	-29:50:50.6	strongH II	21000	5000
11	A2	13:37:03.99	-29:52:47.9	strong	6000	3700
12	A2	13:37:05.07	-29:50:59.0		1700	1400
13	A2	13:37:06.62	-29:50:51.4	bright	7500	2000
14	A2	13:37:07.10	-29:50:25.2	diffuse	1200	1000
15	A2	13:37:07.55	-29:51:06.3	v. strong	12000	2300
16	A2	13:37:07.62	-29:52:51.4	strongH II	37000	8000
17	A2	13:37:07.96	-29:52:07.9	yes	1400	800
18	A2	13:37:07.96	-29:50:57.8	weak	28000	5300
19	A2	13:37:08.42	-29:52:54.9	strongH II	11000	5200
20	A2	13:37:08.55	-29:52:12.2	strongH II	20000	6500
21	A2	13:37:08.73	-29:52:28.9	strongH II	45000	11000
22	A2	13:37:08.94	-29:52:05.6	diffuse	2100	1750
23	A2	13:37:09.01	-29:50:07.6	v. strong	15000	2400

Continued on next page .....

#	Field/Chip	α (2000)	δ (2000)	Hα Assoc.	He II	He II - Cont.
24	A2	13:37:09.31	-29:51:50.6	v. strong	30000	8300
25	A2	13:37:09.38	-29:52:20.0	strong	12000	2200
26	A2	13:37:09.48	-29:52:38.1	no	1600	900
27	A2	13:37:09.48	-29:52:22.2	no	3300	1800
28	A2	13:37:09.80	-29:52:36.2	strong	3500	2200
29	A2	13:37:09.87	-29:50:10.5	v. strong	3500	1500
30	A2	13:37:10.77	-29:50:56.6	no	600	900
31	A2	13:37:12.02	-29:51:42.9	difuse	700	700
32	A2	13:37:12.25	-29:51:03.5	v. strong	16000	3900
33	A2	13:37:12.37	-29:50:21.6	v. strong	9000	6700
34	A2	13:37:12.46	-29:52:03.4	yes	2400	1500
35	A2	13:37:12.59	-29:51:06.5	diffuse	1600	1400
36	A2	13:37:13.05	-29:51:37.7	strong	3300	1350
37	A2	13:37:14.89	-29:50:36.0	strong	26000	4500
38	A2	13:37:15.51	-29:52:26.6	yes	1800	1300
39	A2	13:37:16.07	-29:50:56.4	v. strong	1200	1600
40	A2	13:37:16.33	-29:50:56.4	diffuse	800	1500
41	A2	13:37:16.37	-29:50:59.2	strongH II	4000	2500
42	A2	13:37:16.69	-29:50:54.5	strong	3400	1250
43	A2	13:37:16.93	-29:50:43.5	no	600	700
44	A2	13:37:17.18	-29:51:28.0	no	1800	1200
45	A2	13:37:17.52	-29:51:25.2	weak	7000	3200
46	A2	13:37:18.63	-29:51:41.3	no	1000	1400
47	A2	13:37:18.67	-29:52:23.7	no	500	700
48	A2	13:37:22.54	-29:51:59.8	weak	500	700
49	A2	13:37:23.33	-29:51:05.9	no	200	440
01	B1	13:36:41.64	-29:48:24.6	no	300	240
02	B1	13:36:45.98	-29:49:17.1	no	300	350
03	B1	13:36:53.31	-29:49:55.9	no	700	600
04	B1	13:36:53.92	-29:48:49.6	strong H II	17000	3800
05	B1	13:36:55.06	-29:48:49.0	no	300	450
06	B1	13:36:55.32	-29:49:47.8	no	300	600
07	B1	13:36:55.43	-29:48:05.7	diffuse	600	450
08	B1	13:36:55.97	-29:49:53.9	strong	2500	1600
09	B1	13:36:56.20	-29:49:33.3	no	600	700
10	B1	13:36:56.29	-29:48:46.4	no	500	400
11	B1	13:36:58.24	-29:48:16.4	diffuse	2400	1200
12	B1	13:36:58.72	-29:48:06.1	strong H II	5000	1700
13	B1	13:36:59.95	-29:48:42.6	strong	10000	2800
14	B1	13:37:00.27	-29:48:04.0	ring neb	1900	800
15	B1	13:37:02.38	-29:48:27.3	no	300	500
16	B1	13:37:02.64	-29:49:40.8	strong H II	17000	4300
17	B1	13:37:03.00	-29:49:44.4	strong H II	7000	2100
18	B1	13:37:03.01	-29:48:38.8	no	1600	1000

Continued on next page .....

#	Field/Chip	α (2000)	δ (2000)	Hα Assoc.	He II	He II - Cont.
19	B1	13:37:04.81	-29:49:24.8	strong H II	41000	8000
01	B2	13:36:40.32	-29:51:21.1	strong H II	10000	2000
02	B2	13:36:41.33	-29:52:24.2	strong H II	5000	2100
03	B2	13:36:42.57	-29:52:09.3	v. strong	66000	37000
04	B2	13:36:43.44	-29:52:24.2	brightHII	22000	6000
05	B2	13:36:44.01	-29:51:47.1	no	300	300
06	B2	13:36:44.36	-29:52:37.3	v. strong	60000	21000
07	B2	13:36:44.55	-29:52:10.0	no	300	400
08	B2	13:36:45.24	-29:51:05.3	weak	300	500
09	B2	13:36:45.95	-29:52:37.7	strong H II	5000	1900
10	B2	13:36:47.78	-29:51:25.9	strong H II	10000	2100
11	B2	13:36:47.98	-29:51:29.8	no	700	1100
12	B2	13:36:48.56	-29:51:52.2	no	500	600
13	B2	13:36:48.97	-29:51:43.8	no	600	600
14	B2	13:36:49.22	-29:50:56.4	strong H II	10000	2900
15	B2	13:36:49.28	-29:50:52.8	no	1500	850
16	B2	13:36:49.74	-29:50:15.9	no	500	500
17	B2	13:36:49.82	-29:51:19.2	strong H II	5300	2800
18	B2	13:36:49.92	-29:52:09.6	strong	4000	1200
19	B2	13:36:50.42	-29:52:13.1	diffuse	1000	1200
20	B2	13:36:50.87	-29:50:33.1	strong H II	15000	4800
21	B2	13:36:50.88	-29:50:07.4	diffuse	1300	1200
22	B2	13:36:51.06	-29:50:39.4	strong H II	50000	6000
23	B2	13:36:51.11	-29:52:36.8	strong H II	3000	1000
24	B2	13:36:51.19	-29:50:11.2	no	800	1200
25	B2	13:36:51.19	-29:50:07.9	strong H II	17000	4700
26	B2	13:36:51.34	-29:50:10.2	strong H II	10000	2700
27	B2	13:36:52.17	-29:51:17.2	strong H II	8000	1500
28	B2	13:36:52.33	-29:51:20.5	strong H II	26000	6600
29	B2	13:36:52.59	-29:51:08.5	strong	2000	1300
30	B2	13:36:52.64	-29:51:47.5	strong H II	60000	11000
31	B2	13:36:52.89	-29:51:15.2	strong H II	1600	1200
32	B2	13:36:52.92	-29:52:49.7	strong H II	18000	6500
33	B2	13:36:53.42	-29:51:52.5	no	600	600
34	B2	13:36:53.60	-29:52:52.8	strong	1700	1100
35	B2	13:36:53.80	-29:51:30.7	no	700	700
36	B2	13:36:53.89	-29:50:29.8	yes	300	600
37	B2	13:36:53.91	-29:51:02.6	weak	1700	1500
38	B2	13:36:54.06	-29:51:04.8	strong H II	7000	2000
39	B2	13:36:54.25	-29:50:42.4	strong H II	9000	4200
40	B2	13:36:54.36	-29:50:30.3	strong H II	20000	7200
41	B2	13:36:56.95	-29:52:48.0	strong H II	2300	1300
42	B2	13:36:57.06	-29:50:19.2	yes	1200	900
43	B2	13:36:58.86	-29:50:11.9	strong H II	1400	900

Continued on next page .....

#	Field/Chip	α (2000)	δ (2000)	Hα Assoc.	He II	He II - Cont.
44	B2	13:37:01.25	-29:52:52.8	weak	4000	2500
45	B2	13:37:01.47	-29:51:24.8	strong H II	30000	7000
46	B2	13:37:02.56	-29:50:37.4	no	500	500
47	B2	13:37:02.90	-29:50:50.8	no	12000	4300
48	B2	13:37:03.06	-29:50:49.5	strong H II	13000	5000
49	B2	13:37:03.41	-29:50:59.6	strong H II	6000	2400
50	B2	13:37:03.99	-29:52:47.2	strong H II	3000	2100
51	B2	13:37:04.66	-29:50:57.7	strong H II	60000	16000
01	C1	13:36:56.32	-29:54:55.6	no	900	530
02	C1	13:36:56.75	-29:52:12.7	no	1600	1200
03	C1	13:37:00.46	-29:54:13.1	weak	1000	1200
04	C1	13:37:00.64	-29:54:23.0	diffuse	1200	850
05	C1	13:37:01.49	-29:51:25.7	strong H II	50000	1200
06	C1	13:37:01.91	-29:52:13.2	weak	55000	14000
07	C1	13:37:02.84	-29:54:05.5	weak	1000	800
08	C1	13:37:03.10	-29:54:26.2	weak	1100	900
09	C1	13:37:03.52	-29:54:00.7	strong H II	14000	2500
10	C1	13:37:03.79	-29:54:14.3	no	900	1000
11	C1	13:37:03.97	-29:52:47.5	weak	4700	3000
12	C1	13:37:04.58	-29:54:17.1	no	1000	900
13	C1	13:37:06.10	-29:53:43.5	strong H II	16000	4800
14	C1	13:37:06.13	-29:53:30.9	no	600	650
15	C1	13:37:06.60	-29:54:51.6	diffuse	1400	1700
16	C1	13:37:07.19	-29:51:28.1	strong H II	26000	3000
17	C1	13:37:07.58	-29:54:11.2	diffuse	7000	2200
18	C1	13:37:07.71	-29:51:14.9	strong H II	7000	2500
19	C1	13:37:08.25	-29:53:30.5	no	400	750
20	C1	13:37:08.25	-29:51:13.6	weak	3000	1400
21	C1	13:37:08.26	-29:54:01.7	no	600	750
22	C1	13:37:08.53	-29:52:12.0	strong H II	16000	3000
23	C1	13:37:08.70	-29:52:28.9	strong H II	40000	7000
24	C1	13:37:09.18	-29:51:10.1	diffuse	2000	1300
25	C1	13:37:09.56	-29:51:31.3	strong H II	60000	13000
26	C1	13:37:10.42	-29:51:28.0	weak	1800	2700
27	C1	13:37:10.87	-29:54:22.2	diffuse	4200	1200
28	C1	13:37:11.77	-29:51:49.8	no	1100	800
29	C1	13:37:12.01	-29:51:48.3	no	600	530
30	C1	13:37:12.45	-29:52:03.7	weak	2200	1000
31	C1	13:37:12.58	-29:51:07.0	diffuse	1300	1600
32	C1	13:37:12.68	-29:54:47.4		3000	2700
33	C1	13:37:15.50	-29:52:26.7	diffuse	1300	1000
34	C1	13:37:16.38	-29:50:59.5	yes	4500	1700
35	C1	13:37:17.16	-29:51:37.1	no	800	660
36	C1	13:37:18.48	-29:51:42.1	no	500	550

Continued on next page .....

#	Field/Chip	α (2000)	δ (2000)	Hα Assoc.	He II	He II - Cont.
37	C1	13:37:18.63	-29:51:41.7	no	800	1200
01	C2	13:36:55.71	-29:55:40.3	no	500	400
02	C2	13:36:58.58	-29:55:20.6		1700	1250
03	C2	13:37:03.83	-29:55:29.8	no	1400	1000
04	C2	13:37:06.62	-29:56:48.2	no	400	500
05	C2	13:37:11.03	-29:55:43.7	no	1100	1500
06	C2	13:37:12.60	-29:55:37.9	no	700	1100
01	D1	13:36:33.10	-29:51:37.5	no	3000	950
02	D1	13:36:36.00	-29:54:05.2	no	6000	1700
03	D1	13:36:40.28	-29:51:21.1	strong H II	10000	2700
04	D1	13:36:40.40	-29:54:00.9	no	3000	1100
05	D1	13:36:41.04	-29:51:55.9	strong	23000	5500
06	D1	13:36:41.14	-29:51:48.8	no	600	600
07	D1	13:36:41.16	-29:52:21.7	no	1700	800
08	D1	13:36:41.28	-29:52:24.4	diffuse	7000	2700
09	D1	13:36:42.17	-29:52:31.3	weak	7000	1200
10	D1	13:36:43.40	-29:52:24.1	strong H II	30000	7600
11	D1	13:36:43.46	-29:52:08.3	no	800	650
12	D1	13:36:43.86	-29:52:36.4	no	2600	1100
13	D1	13:36:44.02	-29:52:26.5	no	1000	700
14	D1	13:36:44.06	-29:52:32.8	no	5000	1200
15	D1	13:36:44.17	-29:52:26.8	no	1000	900
16	D1	13:36:44.48	-29:52:10.5	no	700	550
17	D1	13:36:44.51	-29:53:22.1	weak	7000	1500
18	D1	13:36:45.21	-29:51:05.5	weak	800	950
19	D1	13:36:45.33	-29:53:25.6	no	4000	1100
20	D1	13:36:45.58	-29:54:55.9	no	6000	2200
21	D1	13:36:45.85	-29:53:35.0	no	800	800
22	D1	13:36:45.86	-29:53:35.0	no	800	800
23	D1	13:36:45.88	-29:52:37.8	strong	6500	3000
24	D1	13:36:45.87	-29:52:37.8	strong H II	6000	3000
25	D1	13:36:46.05	-29:52:49.7	weak	5500	1200
26	D1	13:36:46.06	-29:53:40.3	weak	3000	1500
27	D1	13:36:47.15	-29:51:09.7	no	2500	700
28	D1	13:36:47.53	-29:53:47.3	no	1200	1050
29	D1	13:36:47.79	-29:51:26.3	strong H II	15000	2600
30	D1	13:36:47.92	-29:51:30.3	no	1000	1300
31	D1	13:36:48.07	-29:53:11.3	no	10000	1600
32	D1	13:36:48.08	-29:51:32.4	diffuse	800	700
33	D1	13:36:48.29	-29:52:44.9	weak	5500	1100
34	D1	13:36:48.50	-29:51:52.4	no	900	750
35	D1	13:36:48.54	-29:51:11.4	no	1000	600
36	D1	13:36:48.90	-29:51:44.2	no	1000	1000
37	D1	13:36:49.55	-29:52:34.9	weak	3500	1400

Continued on next page .....

#	Field/Chip	α (2000)	δ (2000)	Hα Assoc.	He II	He II - Cont.
38	D1	13:36:49.63	-29:51:19.5	weak	1500	850
39	D1	13:36:49.77	-29:51:19.8	strong	7500	3500
40	D1	13:36:49.86	-29:52:10.0	yes	6000	1300
41	D1	13:36:50.05	-29:52:14.6	strong H II	33000	6200
42	D1	13:36:50.34	-29:52:13.6	no	1800	1600
43	D1	13:36:50.41	-29:52:19.1	weak	5000	1700
44	D1	13:36:50.57	-29:52:58.6	weak	2500	900
45	D1	13:36:50.72	-29:51:58.9	weak	8000	1100
46	D1	13:36:50.72	-29:54:05.1	strong H II	20000	4500
47	D1	13:36:50.78	-29:54:46.4	no	500	800
48	D1	13:36:50.95	-29:53:01.1	weak	4000	1000
49	D1	13:36:51.05	-29:52:37.0	strong	4900	1100
50	D1	13:36:51.18	-29:54:53.1	weak	5000	950
51	D1	13:36:51.45	-29:53:12.9	weak	2500	1300
52	D1	13:36:51.51	-29:53:13.3	yes	3000	1400
53	D1	13:36:52.11	-29:52:35.2	strong H II	55000	8300
54	D1	13:36:52.14	-29:51:20.4	no	5000	2200
55	D1	13:36:52.20	-29:51:22.1	no	3000	2000
56	D1	13:36:52.35	-29:53:15.2	strong H II	25000	3800
57	D1	13:36:52.46	-29:52:48.7	diffuse	3000	2500
58	D1	13:36:52.53	-29:52:43.9	no	1800	1100
59	D1	13:36:52.54	-29:51:09.5		3200	1600
60	D1	13:36:52.61	-29:53:03.1	diffuse	5000	2700
61	D1	13:36:52.61	-29:51:47.4	strong H II	60000	10000
62	D1	13:36:52.82	-29:51:15.8	weak	3000	1500
63	D1	13:36:52.84	-29:51:11.1	strong H II	27000	4700
64	D1	13:36:52.86	-29:52:50.0	strong H II	24000	4300
65	D1	13:36:53.02	-29:52:28.6	weak	6000	1400
66	D1	13:36:53.21	-29:52:58.5	strong H II	35000	7400
67	D1	13:36:53.21	-29:51:30.7	strong H II	10000	1800
68	D1	13:36:53.34	-29:53:25.8	no	9000	1400
69	D1	13:36:53.34	-29:51:30.0	strong H II	24000	7500
70	D1	13:36:53.36	-29:51:52.9	no	2100	770
71	D1	13:36:53.72	-29:51:31.2	no	1000	1000
72	D1	13:36:53.87	-29:51:03.0	weak	3000	2000
73	D1	13:36:53.87	-29:53:40.9	no	8000	950
74	D1	13:36:53.98	-29:51:05.3	strong	10000	2000
75	D1	13:36:54.90	-29:53:09.4	strong H II	60000	13000
76	D1	13:36:54.94	-29:52:16.3	strong H II	27000	5000
77	D1	13:36:55.20	-29:52:13.6	no	10000	1900
78	D1	13:36:55.61	-29:54:15.5	weak	35000	8400
79	D1	13:36:56.06	-29:52:52.5	weak	10000	2800
80	D1	13:36:56.87	-29:52:48.7	strong	5000	1600
81	D1	13:36:57.14	-29:54:49.2	strong H II	7000	1400

Continued on next page .....

#	Field/Chip	α (2000)	δ (2000)	Hα Assoc.	He II	He II - Cont.
82	D1	13:36:57.23	-29:51:26.3	no	8000	1600
83	D1	13:36:57.95	-29:52:55.0	no	14000	3900
84	D1	13:36:58.95	-29:51:26.5	strong H II	12000	2700
85	D1	13:36:59.17	-29:54:27.0	strong H II	42000	15000
86	D1	13:36:59.41	-29:54:23.1	no	1500	1600
87	D1	13:36:59.72	-29:53:17.3	no	6000	1200
88	D1	13:36:59.76	-29:52:22.6	diffuse	9000	1700
89	D1	13:37:00.40	-29:54:13.2	no	1200	1100
90	D1	13:37:00.81	-29:54:35.4	no	2100	800
91	D1	13:37:01.18	-29:52:53.9	diffuse	8000	2600
92	D1	13:37:01.19	-29:52:52.3	diffuse	6000	1500
93	D1	13:37:01.42	-29:51:25.8	strong H II	40000	9000
94	D1	13:37:02.46	-29:53:07.0	strong	8000	1900
95	D1	13:37:03.38	-29:51:00.3	strong H II	8000	3000
96	D1	13:37:03.44	-29:54:00.9	strong H II	14000	3100
97	D1	13:37:03.44	-29:51:02.9	strong H II	35000	7000
98	D1	13:37:03.88	-29:54:31.1	no	1500	1200
99	D1	13:37:04.08	-29:53:54.7	no	15000	2800
100	D1	13:37:04.36	-29:54:11.8	no	12000	2700
101	D1	13:37:04.65	-29:50:58.4	strong H II	60000	7200
01	D2	13:36:33.69	-29:56:37.2	no	1100	500
02	D2	13:36:34.05	-29:56:17.6	no	1700	300
03	D2	13:36:36.44	-29:57:47.4	no	2100	500
04	D2	13:36:44.27	-29:55:07.3	weak	5000/p/k	1000
05	D2	13:36:44.42	-29:57:49.3	no	2300	900
06	D2	13:36:49.35	-29:55:28.4	no	2000	700
07	D2	13:36:50.12	-29:55:49.0	weak	3400	1200
08	D2	13:36:50.74	-29:57:04.0	no	1500	600
09	D2	13:36:51.27	-29:57:31.1	no	3600	1100
10	D2	13:36:53.08	-29:55:48.8	diffuse	3200	1500
11	D2	13:36:54.93	-29:55:35.1	weak	1300	800
12	D2	13:36:54.94	-29:55:54.7	no	800	1050
13	D2	13:36:56.17	-29:57:58.4	no	2500	900
14	D2	13:36:58.51	-29:55:19.9	weak	1100	1200
15	D2	13:37:00.18	-29:55:39.9	no	500	600
16	D2	13:37:00.94	-29:57:06.4	no	5800	2300
17	D2	13:37:02.04	-29:55:30.2	strong H II	30000	9000
18	D2	13:37:02.19	-29:57:20.2	no	2800	800
19	D2	13:37:02.24	-29:55:33.8	weak	3300	1200
20	D2	13:37:03.20	-29:55:23.5	weak	8500	1500
21	D2	13:37:03.76	-29:55:29.2	diffuse	1600	1200
22	D2	13:37:04.20	-29:55:29.1	weak	6500	1800

BIBLIOGRAPHY

Abbott, D. C., 1982, *ApJ*, **259**, 282

Abbott, D. C. & Lucy, L. B., 1985, *ApJ*, **288**, 679

Ahmad, A. & Jeffery, C. S., 2003, *A&A*, **402**, 335

Anderson, L. S., 1985, *ApJ*, **298**, 848

Anderson, L. S., 1989, *ApJ*, **339**, 558

Armandroff, T. E. & Massey, P., 1985, *ApJ*, **291**, 685

Armandroff, T. E. & Massey, P., 1991, *AJ*, **102**, 927

Asplund, M., 2003, in C. Charbonnel, D. Schaerer & G. Meynet (eds.), *CNO in the Universe* (ASP: San Francisco:)

Auer, L. H. & Koenigsberger, G., 1994, *ApJ*, **436**, 859

Azzopardi, M. & Breysacher, J., 1979, *A&A*, **75**, 120

Barlow, M. J., Roche, P. F. & Aitken, D. K., 1988, *MNRAS*, **232**, 821

Barmby, P., Huchra, J. P., Brodie, J. P., Forbes, D. A., Schroder, L. L. & Grillmair, C. J., 2000, *AJ*, **119**, 727

Beals, C. S., 1930, *Publication Dominion Astrophysical Observatory*, **4**, 271

Bessell, M. S., Castelli, F. & Plez, B., 1998, *A&A*, **333**, 231

Bianchi, L., Catanzaro, G., Scuderi, S. & Hutchings, J. B., 2001*a*, *PASP*, **113**, 697

Bianchi, L., Scuderi, S., Massey, P. & Romaniello, M., 2001*b*, *AJ*, **121**, 2020

Blair, W. P. & Kirshner, R. P., 1985, *ApJ*, **289**, 582

Blair, W. P., Kirshner, R. P. & Chevalier, R. A., 1982*a*, *ApJ*, **254**, 50

Blair, W. P., Kirshner, R. P. & Chevalier, R. A., 1982*b*, *ApJ*, **254**, 50

Boksenberg, A., Willis, A. J. & Searle, L., 1977, *MNRAS*, **180**, 15

Borissova, J., Georgiev, L., Rosado, M., Kurtev, R., Bullejos, A. & Valdez-Gutirrez, M., 2000, *A&A*, **363**, 130

Bransford, M. A., Thilker, D. A., Walterbos, R. A. M. & King, N. L., 1999, *AJ*, **118**, 1727

Bresolin, F. & Kennicutt, R. C., 2002, *ApJ*, **572**, 838

Bresolin, F., Kudritzki, R., Najarro, F., Gieren, W. & Pietrzyński, G., 2002, *ApJ*, **577**, 107

Breysacher, J., 1981, *A&AS*, **43**, 203

Breysacher, J., 1986, *A&A*, **160**, 185

Breysacher, J., Azzopardi, M. & Testor, G., 1999, *A&AS*, **137**, 117

Breysacher, J., Azzopardi, M., Testor, G. & Muratorio, G., 1997, *A&A*, **326**, 976

Calzetti, D., 2001, *PASP*, **113**, 1449

Castor, J. I., 1970, *MNRAS*, **149**, 111

Castor, J. I., Abbott, D. C. & Klein, R. I., 1975, *ApJ*, **195**, 157

Chandar, R., Bianchi, L. & Ford, H. C., 1999, *ApJS*, **122**, 431

Christensen, T., Petersen, L. & Gammelgaard, P., 1997, *A&A*, **322**, 41

Chu, Y. H., Weis, K. & Garnett, D. R., 1999, *AJ*, **117**, 1433

Conti, P. S., 1976, volume 9, p. 193

Conti, P. S., 1984, in A. Maeder & A. Renzini (eds.), *Observational Tests of the Stellar Evolutionary Theory* (Dordrecht: Reidel), volume 105, p. 233

Conti, P. S. & Massey, P., 1981, *ApJ*, **249**, 471

Crowther, P. A., 2000, *A&A*, **356**, 191

Crowther, P. A. & Bohannan, B., 1997, *A&A*, **317**, 532

Crowther, P. A., de Marco, O. & Barlow, M. J., 1998, *MNRAS*, **296**, 367

Crowther, P. A. & Dessart, L., 1998, *MNRAS*, **296**, 622

Crowther, P. A., Dessart, L., Hillier, D. J., Abbott, J. B. & Fullerton, A. W., 2002, *A&A*, **392**, 653

Crowther, P. A., Drissen, L., Abbott, J. B., Royer, P. & Smartt, S. J., 2003, *A&A*, **404**, 483

Crowther, P. A., Fullerton, A. W., Hillier, D. J., Brownsberger, K., Dessart, L., Willis, A. J., De Marco, O., Barlow, M. J., Hutchings, J. B., Massa, D. L., Morton, D. C. & Sonneborn, G., 2000, *ApJ*, **538**, 51

Crowther, P. A., Hillier, D. J. & Smith, L. J., 1995, *A&A*, **293**, 172

Crowther, P. A. & Smith, L. J., 1997, *A&A*, **320**, 500

Crowther, P. A., Szeifert, T., Stahl, O. & Zickgraf, F.-J., 1997, *A&A*, **318**, 543

Davies, R. D., Elliott, K. H. & Meaburn, J., 1976, *MNRAS*, **81**, 89

de Koter, A., Heap, S. R. & Hubeny, I., 1997, *ApJ*, **477**, 792

De Marco, O. & Schmutz, W., 1999, *A&A*, **354**, 163

De Marco, O., Schmutz, W., Crowther, P., Hillier, D. J., Dessart, L., de Koter, A. & Schweickhardt, J., 2000, *A & A*, **358**, 187

de Mello, D. F., Leitherer, C. & Heckman, T. M., 2000, *ApJ*, **530**, 251

Deharveng, L., Caplan, J., Lequeux, J., Azzopardi, M., Breysacher, J., Tarenghi, M. & Westerlund, B., 1988, *A&AS*, **73**, 407

Deharveng, L., Peña, M., Caplan, J. & Costero, R., 2000, *MNRAS*, **311**, 329

Demers, H., Moffat, A. F. J., Marchenko, S. V., Gayley, K. G. & Morel, T., 2002, *ApJ*, **577**, 409

Dennefeld, M. & Kunth, D., 1981, *AJ*, **86**, 989

Dessart, L., 1999, *The Wolf-Rayet phenomenon in massive stars.*, Ph.D. thesis, University College London

Dessart, L., Crowther, P. A., Hillier, D. J., Willis, A. J., Morris, P. W. & van der Hucht, K. A., 2000, *MNRAS*, **315**, 407

Dessart, L. & Owocki, S. P., 2002, *A&A*, **383**, 1113

D'Odorico, S., Rosa, M. & Wampler, E. J., 1983, *A&AS*, **53**, 97

Dolphin, A. E., 2000, *PASP*, **112**, 1383

Dopita, M. A., Bell, J. F., Chu, Y.-H. & Lozinskaya, T., 1994, *ApJS*, **93**, 455

Dopita, M. A., Binette, L., Dodorico, S. & Benvenuti, P., 1984, *ApJ*, **276**, 653

Dopita, M. A., D'Odorico, S. & Benvenuti, P., 1980, *ApJ*, **236**, 628

Dopita, M. A. & Evans, I. N., 1986, *ApJ*, **307**, 431

Dray, L. M., Tout, C. A., Karakas, A. I. & Lattanzio, J. C., 2003, *MNRAS*, **338**, 973

Drissen, L., Moffat, A. F. J. & Shara, M. M., 1990, *AJ*, **105**, 1400

Dufour, R. J., Talbot, R. J., Jensen, E. B. & Shields, G. A., 1980, *ApJ*, **236**, 119

Edmunds, M. G., 1989, in J. E. Beckman & B. E. J. Pagel (eds.), *Evolutionary phenomena in galaxies* (Cambridge: Cambridge Univ. Press), p. 356

Edmunds, M. G. & Pagel, B. E. J., 1984, *MNRAS*, **211**, 507

Eenens, P. R. J. & Williams, P. M., 1994, *MNRAS*, **269**, 1082

Elias, J. H., Frogel, J. A. & Humphreys, R. M., 1985, *ApJS*, **57**, 91

Esteban, C. & Peimbert, M., 1995, in *Revista Mexicana de Astronomia y Astrofisica Conference Series*, p. 133

Filippenko, A. V., 1997, *ARA&A*, **35**, 309

Fitzpatrick, E. L. & Garmany, C. D., 1990, *ApJ*, **363**, 119

Foellmi, C., Moffat, A. F. J. & Guerrero, M. A., 2003*a*, *MNRAS*, **338**, 360

Foellmi, C., Moffat, A. F. J. & Guerrero, M. A., 2003*b*, *MNRAS*, **338**, 1025

Freedman, W. L., Madore, B. F., Gibson, B. K., Ferrarese, L., Kelson, D. D., Sakai, S., Mould, J. R., Kennicutt, R. C., J., Ford, H. C., Graham, J. A., Huchra, J. P., Hughes, S. M. G., Illingworth, G. D., Macri, L. M. & Stetson, P. B., 2001, *ApJ*, **553**, 47

Freedman, W. L., Wilson, C. D. & Madore, B. F., 1991, *ApJ*, **372**, 455

Galarza, V. C., Walterbos, R. A. M. & Braun, R., 1999, *AJ*, **118**, 2775

Garay, G., Brooks, K. J., Mardones, D., Norris, R. P. & Burton, M. G., 2002, *ApJ*, **579**, 678

Garmany, C. D. & Conti, P. S., 1985, *ApJ*, **293**, 407

Garnett, D. & Chu, Y.-H., 1994, *PASP*, **106**, 626

Garnett, D. R., Odewahn, S. C. & Skillman, E. D., 1992, *AJ*, **104**, 1714

Gayley, K. G. & Owocki, S. P., 1995, *ApJ*, **446**, 801

Gayley, K. G., Owocki, S. P. & Cranmer, S. R., 1995, *ApJ*, **442**, 296

Graham, J. A., 1984, *AJ*, **89**, 1332

Grebel, E. K., 1999, in P. Whitelock & R. Cannon (eds.), *Proceedings of 192nd symposium of the International Astronomical Union* (Astronomical Society of the Pacific), p. 17

Gräfener, G., Koesterke, L. & Hamann, W.-R., 2002, *A&A*, **387**, 244

Gummersbach, C. A., Kaufer, A., Schaefer, D. R., Szeifert, T. & Wolf, B., 1998, *A&A*, **338**, 881

Hamann, W.-R., Gräfener, G. & Koesterke, L., 2003, in K. A. van der Hucht, A. Herrero & C. Esteban (eds.), *IAU Symp. 212: A Massive Star Odyssey, from Main Sequence to Supernova* (Astronomical Society of the Pacific), p. 198

Hamann, W.-R. & Koesterke, L., 1998, *A&A*, **335**, 1003

Hamann, W.-R. & Koesterke, L., 2000, *A&A*, **360**, 647

Hamann, W.-R., Koesterke, L. & Wessolowski, U., 1995, *A&A*, **299**, 151

Hamann, W. R. & Schmutz, W., 1987, *A&A*, **174**, 173

Hauschildt, P. H. & Wehrse, R., 1991, *JQSRT*, **46**, 81

Heger, A., Fryer, C. L., Woosley, S. E., Langer, N. & Hartmann, D. H., 2003, *ApJ*, **591**, 288

Heger, A. & Langer, N., 1996, *A&A*, **315**, 421

Henry, R. B. C. & Howard, J. W., 1995, *ApJ*, **438**, 170

Herald, J. E., Hillier, D. J. & Schulte-Ladbeck, R. E., 2001, *ApJ*, **548**, 932

Hillier, D. J., 1987*a*, *ApJS*, **63**, 965

Hillier, D. J., 1987*b*, *ApJS*, **63**, 947

Hillier, D. J., 1989, *AJ*, **347**, 392

Hillier, D. J., 1991, *A&A*, **247**, 455

Hillier, D. J., Crowther, P. A., Najarro, F. & Fullerton, A. W., 1998, *A&A*, **340**, 483

Hillier, D. J. & Miller, D. L., 1998, *ApJ*, **496**, 407

Hodge, P. & Lee, M. G., 1990, *PASP*, **102**, 26

Holland, S., 1998, *AJ*, **115**, 1916

Howarth, I. D. & Schmutz, W., 1992, *A&A*, **261**, 503

Hubble, E. & Sandage, A., 1953, *ApJ*, **118**, 353

Hubble, E. P., 1936, *The Realm of the Nebulae* (New Haven: Yale University Press)

Hubeny, I., 1999, in *Encyclopedia of Astronomy and Astrophysic* (-), pp. 10–11

Hubeny, I., Hummer, D. G. & Lanz, T., 1994, *A&A*, **282**, 151

Hubeny, I. & Lanz, T., 1995, *ApJ*, **439**, 875

Hummer, D. G., Berrington, K. A., Eissner, W., Pradhan, A. K., Saraph, H. E. & Tully, J. A., 1993, *A&A*, **279**, 298

Humphreys, R. M., 1980, *ApJ*, **241**, 587

Humphreys, R. M. & Davidson, K., 1979, *ApJ*, **232**, 409

Humphreys, R. M. & Davidson, K., 1984, *Science*, **223**, 243

Humphreys, R. M. & Davidson, K., 1994, *PASP*, **106**, 1025

Humphreys, R. M. & Sandage, A., 1980, *ApJS*, **44**, 319

Ignace, R., Cassinelli, J. P., Quigley, M. & Babler, B., 2001, *ApJ*, **558**, 771

Ignace, R., Oskinova, L. M. & Brown, J. C., 2003, *A&A*, **408**, 353

Israel, F. P. & Baas, F., 2001, *A&A*, **371**, 433

Jerjen, H., Freeman, K. C. & Binggeli, B., 2000, *AJ*, **119**, 166

Johnson, H. M. & Hogg, D. E., 1965, *ApJ*, **142**, 1033

Johnson, S. B. & Joner, M. D., 1987, *AJ*, **94**, 324

Karachentsev, I. D., Grebel, E. K., Sharina, M. E., Dolphin, A. E., Geisler, D., Guhathakurta, P., Hodge, P. W., Karachentseva, V. E., Sarajedini, A. & Seitzer, P., 2003, *A&A*, **404**, 93

Karachentsev, I. D., Sharina, M. E., Dolphin, A. E., Grebel, E. K., Geisler, D., Guhathakurta, P., Hodge, P. W., Karachentseva, V. E., Sarajedini, A. & Seitzer, P., 2002, *A&A*, **385**, 21

Kennicutt, R. C., Stetson, P. B., Saha, A., Kelson, D., Rawson, D. M., Sakai, S., Madore, B. F., Mould, J. R., Freedman, W. L., Bresolin, F., Ferrarese, L., Ford, H., Gibson, B. K., Graham, J. A., Han, M., Harding, P., Hoessel, J. G., Huchra, J. P., Hughes, S. M. G., Illingworth, G. D., Macri, L. M., Phelps, R. L., Silbermann, N. A., Turner, A. M. & Wood, P. R., 1998, *ApJ*, **498**, 181

Kobulnicky, H. A., Kennicutt, R. C. J. & Pizagno, J. L., 1999, *ApJ*, **514**, 544

Koenigsberger, G., 1990, *A&A*, **235**, 282

Koesterke, L. & Hamann, W.-R., 1995, *A&A*, **299**, 503

Koesterke, L., Hamann, W.-R., Wessolowski, U. & Schmutz, W., 1991, *A&A*, **248**, 166

Korn, A. J., Keller, S. C., Kaufer, A., Langer, N., Przybilla, N., Stahl, O. & Wolf, B., 2002, *A&A*, **385**, 143

Kucinskas, A., Vansevicius, V., Sauvage, M. & Tanabé, T., 2000, *A&A*, **353**, 21

Kudritzki, R., Pauldrach, A. W. A. & Puls, J., 1987, *A&A*, **173**, 293

Kudritzki, R. & Puls, J., 2000, *ARAA*, **38**, 613

Kudritzki, R. P., Pauldrach, A. W. A., Puls, J. & Abbott, D. C., 1989, *AAP*, **219**, 205

Kurucz, R. L., 1979, *ApJSS*, **40**, 1

Kwitter, K. B. & Aller, L. H., 1981, *MNRAS*, **195**, 939

Lamers, H. J. G. L. M. & Cassinelli, J. P., 1999, *Introduction to Stellar Winds* (Cambridge University Press), chapter 8, p. 187

Langer, N., 1989, *A&A*, **220**, 135

Langer, N. & Maeder, A., 1995, *A&A*, **295**, 685

Lanz, T. & Hubeny, I., 2003, *ApJS*, **146**, 417

Lee, H., McCall, M. L., Kingsburgh, R. L., Ross, R. & Stevenson, C. C., 2003, *AJ*, **125**, 146

Leitherer, C., Robert, C. & Drissen, L., 1992, *ApJ*, **401**, 596

Lequeux, J., Rayo, J. F., Serrano, A., Peimbert, M. & Torres-Peimbert, S., 1979, *A&A*, **80**, 155

Lucy, L. B. & Abbott, D. C., 1993, *ApJ*, **405**, 738

Macri, L. M., Stanek, K. Z., Sasselov, D. D., Krockenberger, M. & Kaluzny, J., 2001, *AJ*, **121**, 861

Maeder, A., 1983, *A&A*, **120**, 113

Maeder, A. & Meynet, G., 1987, *A&A*, **182**, 243

Maeder, A. & Meynet, G., 1994, *A&A*, **287**, 803

Maeder, A. & Meynet, G., 2001, *A&A*, **373**, 555

Massey, P., 1998*a*, *ApJ*, **264**, 153

Massey, P., 1998*b*, in G. Gilmore & D. Howell (eds.), *The Stellar Initial Mass Function, 38th Herstmonceux Conference* (ASP), volume 142, p. 17

Massey, P., 2002, *ApJS*, **141**, 81

Massey, P., 2003, *ARAA*, **41**, 15

Massey, P. & Armandroff, T. E., 1995, *AJ*, **109**, 2470

Massey, P., Armandroff, T. E. & Conti, P. S., 1986, *AJ*, **92**, 1303

Massey, P., Armandroff, T. E. & Conti, P. S., 1992, *AJ*, **103**, 1159

Massey, P., Armandroff, T. E., Pyke, R., Patel, K. & Wilson, C. D., 1995, *AJ*, **110**, 2715

Massey, P., Bianchi, L., Hutchings, J. B. & Stecher, T. P., 1996, *ApJ*, **469**, 629

Massey, P. & Conti, P. S., 1983, *ApJ*, **264**, 166

Massey, P., Conti, P. S. & Armandroff, T. E., 1987*a*, *AJ*, **94**, 1538

Massey, P., Conti, P. S., Moffat, A. F. J. & Shara, M. M., 1987*b*, *PASP*, **99**, 816

Massey, P. & Duffy, A. S., 2001, *ApJ*, **550**, 713

Massey, P. & Holmes, S., 2002, *ApJ*, **580**, 35

Massey, P. & Johnson, O., 1998, *ApJ*, **505**, 793

Massey, P., Olsen, K. A. G. & Parker, J. W., 2003

Massey, P., Waterhouse, E. & DeGioia-Eastwood, K., 2000, *AJ*, **119**, 2214

Matsushita, S., Kawabe, R., Matsumoto, H., Tsuru, T. G., Kohno, K., Morita, K.-I., Okumura, S. K. & Vila-Vilar, B., 2000, *ApJ*, **545**, 107

Mayall, N. U. & Aller, L. H., 1942, *ApJ*, **95**, 5

McCall, M. L., Rybski, P. M. & Shields, G. A., 1985, *ApJS*, **57**, 1

McGaugh, S., 1991, *ApJ*, **380**, 140

Melisse, J. P. M. & Israel, F. P., 1994, *A&AS*, **103**, 391

Meynet, G. & Maeder, A., 2000, *A&A*, **361**, 101

Meynet, G. & Maeder, A., 2003, *A&A*, **100**, 10

Meynet, G., Maeder, A., Schaller, G., Schaerer, D. & Charbonnel, C., 1994, *A&AS*, **103**, 97

Mihalas, D., Kunasz, P. B. & Hummer, D. G., 1975, *ApJ*, **202**, 92

Mihalas, D., Kunasz, P. B. & Hummer, D. G., 1976, *ApJ*, **206**, 515

Milne, E. A., 1926, *MNRAS*, **86**, 459

Moffat, A. F. J., 1988, *ApJ*, **330**, 766

Moffat, A. F. J., 1989, *ApJ*, **347**, 373

Moffat, A. F. J., 1999, in K. A. van der Hucht, G. Koenigsberger & P. R. J. Eenens (eds.), *IAU Symp. 193, Wolf-Rayet Phenomena in Massive Stars and Starburst Galaxies* (Astronimcal Society of the Pacific), p. 278

Moffat, A. F. J. & Shara, M. M., 1983, *ApJ*, **273**, 544

Moffat, A. F. J. & Shara, M. M., 1987, *ApJ*, **320**, 266

Monteverde, M. I., Herrero, A., Lennon, D. J. & Kudritzki, R.-P., 1997, *ApJ*, **474**, 107

Moran, J. P., Davis, R. J., Spencer, R. E., Bode, M. F. & Taylor, A. R., 1989, *Nature*, **340**, 449

Morgan, D. H., Vassiliadis, E. & Dopita, M. A., 1991, *MNRAS*, **251**, 51

Morton, D. C., 1967, *ApJ*, **147**, 1017

Nazé, Y., Rauw, G., Manfroid, J., Chu, Y.-H. & Vreux, J.-M., 2003, *A&A*, **401**, 13

Nugis, T., 1989, *SvA Lett.*, **15**, 19

Nugis, T., Crowther, P. A. & Willis, A. J., 1998, *A&A*, **333**, 956

Nugis, T. & Lamers, H. J. G. L. M., 2000, *A&A*, **360**, 227

Owocki, S. P., Castor, J. I. & Rybicki, G. B., 1988, *ApJ*, **335**, 914

Owocki, S. P. & Gayley, K. G., 1999, in *IAU Symp. 193: Wolf-Rayet Phenomena in Massive Stars and Starburst Galaxies*, p. 157

Owocki, S. P. & Puls, J., 2002, *ApJ*, **568**, 9650

Pagel, B. E. J., Edmunds, M. G., Blackwell, D. E., Chun, M. S. & Smith, G., 1979, *MNRAS*, **189**, 95

Pagel, B. E. J., Edmunds, M. G. & Smith, G., 1980, *MNRAS*, **193**, 219

Pakull, M. W., 1991, in *IAU Symp. 143: Wolf-Rayet Stars and Interrelations with Other Massive Stars in Galaxies*, p. 391

Palla, F. & Stahler, S. W., 1993, *ApJ*, **418**, 414

Parker, E. N., 1960, *ApJ*, **132**, 821

Pauldrach, A. W. A., Hoffmann, T. L. & Lennon, M., 2001, *A&A*, **375**, 161

Paunzen, E., Andrievsky, S. M., Chernyshova, I. V., Klochkova, V. G., Panchuk, V. E. & Handler, G., 1999, *A&A*, **351**, 981

Pietrzyński, G., Gieren, W. & Udalski, A., 2002, *PASP*, **114**, 298

Pilyugin, L. S., 2000, *A&A*, **362**, 325

Pilyugin, L. S., 2001, *A&A*, **369**, 594

Pilyugin, L. S., 2003, *A&A*, **397**, 109

Pilyugin, L. S., Ferrini, F. & Shkvarun, V., 2003, *A&A*, **401**, 557

Pottasch, S. R., 1984, *Planetary nebulae (Dordrecht: Reidel)*, **107**

Prinja, R., 1987, *MNRAS*, **228**, 173

Prinja, R. K., Barlow, M. J. & Howarth, I. D., 1990, *ApJ*, **361**, 607

Puls, J. & Hummer, D. G., 1988, *A&A*, **191**, 87

Puls, J., Kudritzki, R.-P., Herrero, A., Pauldrach, A. W. A., Haser, S. M., Lennon, D. J., Gabler, R., Voels, S. A., Vilchez, J. M., Wachter, S. & Feldmeier, A., 1996, *A&A*, **305**, 171

Reynolds, R. J., 1984, *ApJ*, **282**, 191

Richer, H. B., Pritchet, C. J. & Crabtree, D. R., 1985, *ApJ*, **298**, 240

Richer, M. G., Bullejos, A., Borissova, J., McCall, M. L., Lee, H., Kurtev, R., Georgiev, L., Kingsburgh, R. L., Ross, R. & Rosado, M., 2001, *A&A*, **370**, 34

Robert, C., 1994, *Ap&SS*, **221**, 137

Rochowicz, K. & Niedzielski, A., 1995, *AcA*, **45**, 307

Rolleston, W. R. J., Smartt, S. J., Dufton, P. L. & Ryans, R. S. I., 2000, *A&A*, **363**, 537

Rolleston, W. R. J., Venn, K., Tolstoy, E. & Dufton, P. L., 2003, *A&A*, **400**, 21

Rosa, M. & D'Odorico, S., 1986, in C. W. H. de Loore, A. J. Willis & P. Laskarides (eds.), *IAU Symp. 116: Luminous Stars and Associations in Galaxies* (Dordrecht: Reidel), p. 355

Rosa, M. & Richter, O. G., 1988, *A&A*, **192**, 57

Rountree, J. & Sonneborn, G., 1991, *ApJ*, **369**, 515

Royer, P., Smartt, S. J., Manfroid, J. & Vreux, J.-M., 2001, *A&A*, **366**, 1

Royer, P., Vreux, J.-M. & Manfroid, J., 1998, *A&AS*, **130**, 407

Runacres, M. C. & Owocki, S. P., 2003, in K. A. van der Hucht, A. Herrero & C. Esteban (eds.), *IAU Symp. 212: A Massive Star Odyssey, from Main Sequence to Supernova* (Astronomical Society of the Pacific), p. 226

Russell, S. C. & Dopita, M. A., 1990, *ApJS*, **74**, 93

Sakai, S., Madore, B. F. & Freedman, W. L., 1999, *ApJ*, **511**, 671

Salpeter, E. E., 1955, *ApJ*, **121**, 161

Sandage, A. & Johnson, H. L., 1974, *ApJ*, **191**, 63

Santolaya-Rey, A. E., Puls, J. & Herrero, A., 1997, *A&A*, (323)

Schaerer, D. & Maeder, A., 1992, *A&A*, **263**, 129

Schild, H., P.A.Crowther, P. A., Abbott, J. B. & Schmutz, W., 2003, *A&A*, **397**, 859

Schild, H., Smith, L. J. & Willis, A. J., 1990, *A&A*, **237**, 169

Schild, H. & Testor, G., 1991, *A&A*, **243**, 115

Schild, H. & Testor, G., 1992, *A&A*, **266**, 145

Schmidt, B. P., Kirshner, R. P., Eastman, R. G., Phillips, M. M., Suntzeff, N. B., Hamuy, M., Maza, J. & Aviles, R., 1994, *ApJ*, **432**, 42

Schmutz, D. S., 1997, *A&A*, **321**, 268

Schmutz, W., Hamann, W. R. & Wessolowski, U., 1989, *A&A*, **210**, 236

Schulte-Ladbeck, R. E., 1995, in K. A. van der Hucht & P. M. Williams (eds.), *IAU Symp. 163, Wolf-Rayet Stars, Binaries* (Dordrecht: Kluwer), p. 176

Searle, L., 1971, *ApJ*, **168**, 327

Seaton, M. J., 1987, *J. Phys. B.*, **20**, 6363

Seaton, M. J., 1995, *The Opacity Project*, volume 1 (Bristol UK: Institute of Physics Publishing)

Shaver, P. A., McGee, R. X., Newton, L. M., Danks, A. C. & Pottasch, S. R., 1983, *MNRAS*, **204**, 53

Shortridge, K., Meyerdierks, H., Currie, M. & et al., 1999, Technical Report SUN 86.17, Rutherford Appleton Laboratory

Skillman, E. D., Terlevich, R. & Melnick, J., 1989, *MNRAS*, **240**, 563

Smartt, S. J., Crowther, P. A., Dufton, P. L., Lennon, D. J., Kudritzki, R. P., Herrero, A., McCarthy, J. K. & Bresolin, F., 2001*a*, *MNRAS*, **325**, 257

Smartt, S. J., Dufton, P. L. & Lennon, D. J., 1997, *A&A*, **326**, 763

Smartt, S. J. & Rolleston, W. R. J., 1997, *ApJ*, **481**, 47

Smartt, S. J., Venn, K. A., Dufton, P. L., Lennon, D. J., Rolleston, W. R. J. & Keenan, F. P., 2001*b*, *A&A*, **367**, 86

Smith, H. E., 1975, *ApJ*, **199**, 591

Smith, L. F., 1968, *MNRAS*, **138**, 109

Smith, L. F. & Maeder, A., 1991, *A&A*, **241**, 77

Smith, L. F., Shara, M. M. & Moffat, A. F. J., 1990, *ApJ*, **358**, 229

Smith, L. F., Shara, M. M. & Moffat, A. F. J., 1996, *MNRAS*, **281**, 163

Smith, L. J., Crowther, P. A. & Prinja, R. K., 1994, *A&A*, **281**, 833

Smith, L. J., Crowther, P. A. & Willis, A. J., 1995, *A&A*, **302**, 830

Smith, L. J., Norris, R. P. F. & Crowther, P. A., 2002, *MNRAS*, **337**, 1309

Smith, R. C., Kirshner, R. P. & Blair, W. P., 1993, *ApJ*, **407**, 564

Smith Neubig, M. M. S. & Bruhweiler, F. C., 1997, *AJ*, **114**, 1951

Sobolev, V. V., 1960, *Moving envelopes of stars* (Cambridge MA: Harvard University Press,)

Soria, R. & Wu, K., 2002, *A&A*, **384**, 99

Springmann, U., 1994, *A&A*, **289**, 505

Stahl, O., Wolf, B., Klare, G., Cassatella, A., Krautter, J., Persi, P. & Ferrari-Toniolo, M., 1983, *A&A*, **127**, 49

Taylor, M., Nordsieck, K. H., Schulte-Ladbeck, R. E. & Bjorkman, K. S., 1991, *AJ*, **102**, 1197

Thim, F., Tammann, G. A., Saha, A., Dolphin, A., Sandage, A., Tolstoy, E. & Labhardt, L., 2003, *ApJ*, **590**, 256

Torres, A. V., Conti, P. S. & Massey, P., 1986, *ApJ*, **300**, 379

Torres-Dodgen, A. V. & Massey, P., 1988, *AJ*, **96**, 1076

Trundle, C., Dufton, P. L., Lennon, D. J., Smartt, S. J. & Urbaneja, M. A., 2002, *A&A*, **395**, 519

van den Bergh, S., 1964, *ApJS*, **9**, 65

van den Bergh, S., 2000, *IrAJ*, **27**, 233

van der Hucht, K. A., 2001, *NewA Rev.*, **45**, 135

van Zee, L., Salzer, J. J., Haynes, M. P., O'Donoghue, A. A. & Balonek, T. J., 1998, *AJ*, **116**, 2805

Vanbeveren, D., de Loore, C. & van Rensbergen, W., 1998, *A&A Rev.*, **9**, 63

Venn, K. A., Lennon, D. J., Kaufer, A., McCarthy, J. K., Przybilla, N., Kudritzki, R. P., Lemke, M., Skillman, E. D. & Smartt, S. J., 2001, *ApJ*, **547**, 765

Venn, K. A., McCarthy, J. K., Lennon, D. J., Przybilla, N., Kudritzki, R. P. & Lemke, M., 2000, *ApJ*, **541**, 610

Vila-Costas, M. B. & Edmunds, M. G., 1992, *MNRAS*, **259**, 121

Vilchez, J. M., Pagel, B. E. J., Diaz, A. I., Terlevich, E. & Edmunds, M. G., 1988, *MNRAS*, **235**, 633

Vink, J. S., de Koter, A. & Lamers, H. J. G. L. M., 2001, *A&A*, **369**, 574

Walborn, N. R., 1977, *ApJ*, **215**, 53

Walborn, N. R., 1982, *ApJ*, **256**, 452

Walborn, N. R., 1986, in C. W. H. De Loore, A. J. Willis & P. Laskarides (eds.), *Proc. IAU Symp.* (Dordrecht: Reidel), volume 116, p. 185

Walborn, N. R. & Fitzpatrick, E. L., 1990, *PASP*, **102**, 379

Walborn, N. R., Howarth, I. D., Lennon, D. J., Massey, P., Oey, M. S., Moffat, A. F. J., Skalkowski, G., Morrell, N. I., Drissen, L. & Parker, J. W., 2002, *AJ*, **123**, 2754

Walborn, N. R., Nichols-Bohlin, J. & Panek, R. J., 1985, *International Ultraviolet Explorer Atlas of O-typespectra from 1200 to 1900 angstroms*, (NASA RP-1155)

Wampler, E. J., 1982, *A&A*, **114**, 165

Webster, L. B. & Smith, M. G., 1983, *MNRAS*, **204**, 743

Westerlund, B. E., Azzopardi, M., Breysacher, J. & Lequeux, J., 1983, *A&A*, **123**, 159

Williams, B. F., 2003, *MNRAS*, **340**, 143

Willis, A., 1998, in *ESA SP-413: Ultraviolet Astrophysics Beyond the IUE Final Archive*, p. 165

Willis, A. J., Schild, H. & Smith, L. J., 1992, *A&A*, **261**, 419

Woosley, S. E. & Weaver, T. A., 1995, *ApJS*, **101**, 181

Wray, J. D. & Corso, G. J., 1972, *ApJ*, **172**, 577

Yang, H. & Skillman, E. D., 1993, *AJ*, **106**, 1448

Zaritsky, D., Harris, J., Thompson, I. B., Grebel, E. K. & Massey, P., 2002, *AJ*, **123**, 855

Zaritsky, D., Kennicutt, R. C. & Huchra, J. P., 1994, *ApJ*, **420**, 87